Hesselø Offshore Wind Farm

Site Metocean Conditions Assessment for FEED

Report

24 March 2022

Prepared for Energinet Eltransmission A/S

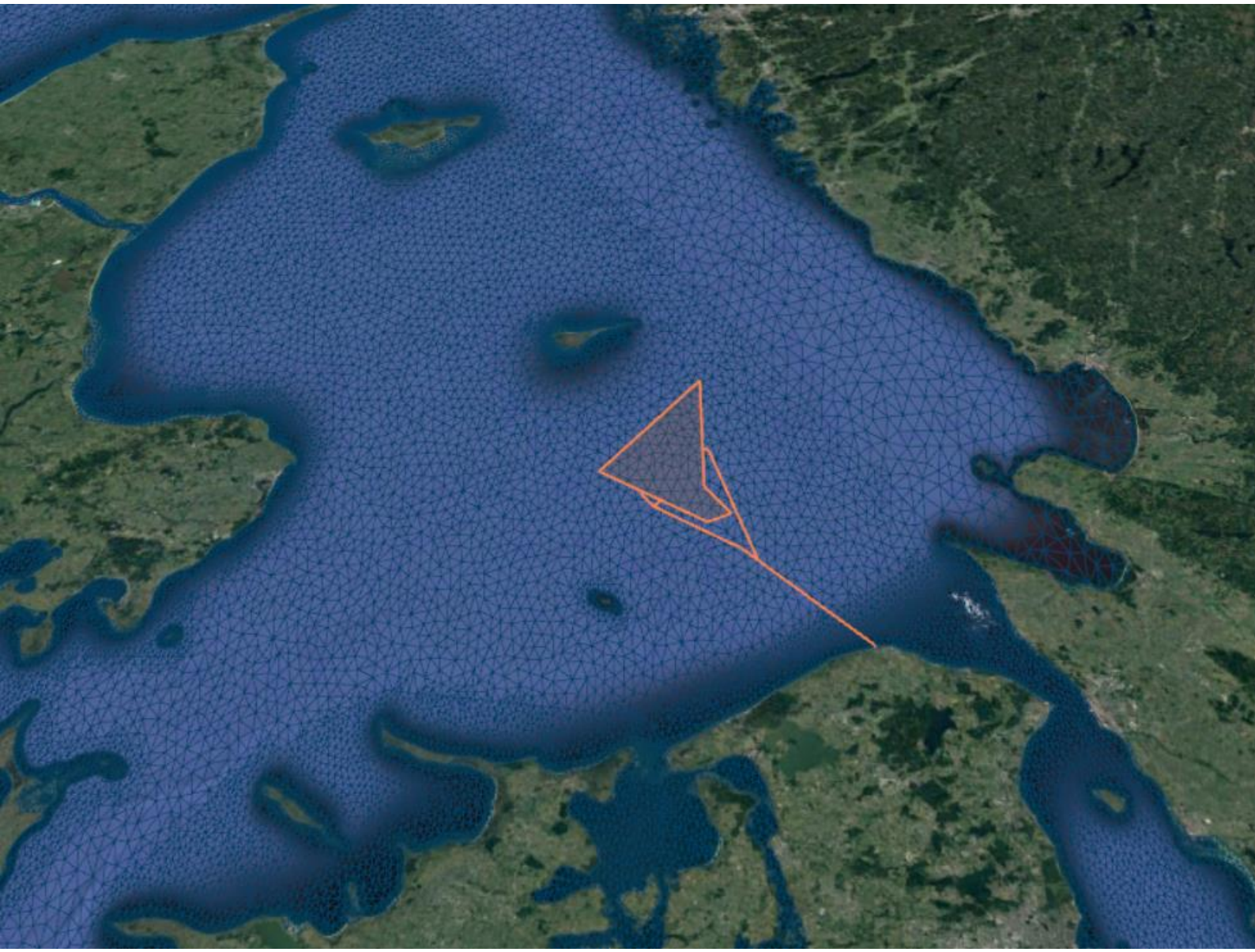

The expert in **WATER ENVIRONMENTS**

Hesselø Offshore Wind Farm

Site Metocean Conditions Assessment

Report
Project No 11826722

Prepared for: Energinet Eltransmission A/S
Represented by Mr Kim Parsberg Jakobsen

Project Manager:	Matthew Easton
Quality Supervisor:	Maziar Golestani
Author:	Simone de Lemos, Adam Leonard Williams, Matthew Easton
Project No.:	11826722
Approved by:	Jesper Fuchs
Approval date:	24 March 2022
Revision:	Final 1.0
Classification:	**Open**
File name:	11826722_ENDK_Hesselø_Metocean_RPT.docx

DHI A/S • Agern Allé 5 • • DK-2970 Hørsholm • Denmark
Telephone: +45 4516 9200 • dhi@dhigroup.com • www.dhigroup.com • Company Reg. No.: 36466871

Contents

Figures

Tables

Appendices

Nomenclature

Abbreviations	
ADCP	Acoustic Doppler Current Profiler
API	Application Programming Interface
BAL MFC	Baltic Monitoring and Forecasting Centre
CMEMS	Copernicus Marine Environment Monitoring Service
CORDEX	Coordinated Regional Climate Downscaling Experiment
COSMO	COnsortium for Small-Scale MOdelling
CREA6	COSMO Reanalysis 6
DEA	Danish Energy Agency
DKW	Danish Waters
DMI	Danish Meteorological Institute
DTM	Digital Terrain Model
DWD	Deutscher Wetterdienst
ECMWF	European Centre for Medium-Range Weather Forecasts
EMODnet	European Marine Observation and Data Network
FEED	Front-End Engineering Design
F-LiDAR	Floating Light Detection and Ranging
HD	Hydrodynamic
LAT	Lowest Astronomical Tide
MSL	Mean Sea Level
MW	Megawatt
NWP	Numerical Weather Prediction
OWF	Offshore wind farm
RANS	Reynolds' averaged Navier-Stokes
SCA	Site Conditions Assessment
SMHI	Swedish Meteorological and Hydrological Institute
SW	Spectral Wave
TEOS	Thermodynamic Equation of Seawater
UTM	Universal Transverse Mercator
WGS	World Geodetic System

Subscripts	
DKW	Danish Waters
NE	North Europe
Residual	Residual component of water level or current
Sea	Wind-sea component of wave spectrum
Surf	Surface current speed or direction
Swell	Swell component of wave spectrum
Tide	Tidal component of water level or current
Total	Total water level or current (i.e., combined tide and residual) Total sea-state (i.e., combined wind-sea and swell)

Definitions	
Time	Times are relative to UTC
Levels	Levels are relative to mean sea level (MSL) or still water level (SWL) as specified
Directions	Wind: °N coming from and positive clockwise Waves: °N coming from and positive clockwise Current: °N going towards and positive clockwise

Symbols	
c	Wave celerity
C	Wave crest elevation
C_{max}	Maximum wave crest elevation
CD	Current direction
CS	Current speed
ED2f	Direction-frequency wave energy spectrum
H_{m0}	Spectral significant wave height
H_{max}	Maximum individual wave height
H	Individual wave height
λ	Number of events per year
MWD	Mean wave direction
PWD	Peak wave direction
θ	Wave propagation direction
T	Individual wave period
T_{01}	Spectral equivalent of the mean wave period
T_{02}	Spectral equivalent of the mean zero-crossing wave period
T_a	Temporal averaging period
T_{Hmax}	Wave period associated with maximum individual wave height
T_R	Return period in years
T_p	Peak wave period
T_{sea}	Temperature of seawater
WS_{10}	Wind speed at 10 mMSL
WD_{10}	Wind direction at 10 mMSL
WD_{140}	Wind Direction at 140 mMSL
WS_{10}	Wind speed at 10 mMSL
WS_{140}	Wind Speed at 140 mMSL
WL	Water level

Executive Summary

The Hesselø offshore wind farm is a project development located within Danish territorial waters, approximately 30 km north of Zealand and 20 km from the island of Hesselø in the Kattegat. This report and its accompanying appendices describe the establishment of meteorological and oceanographic (metocean) data and analysis to serve as the basis for the Front-End Engineering Design of offshore wind turbines and related project infrastructure.

Long-term metocean time-series data at the Hesselø offshore wind farm (OWF) are provided from DHI's Danish Waters hindcast model database. This database includes wind conditions, water levels, depth-averaged currents, and wave conditions at hourly time intervals over a continuous period of 24-years (1995 to 2018, inclusive). Atmospheric conditions are provided from the COSMO-REA6 (CREA6) data set developed by the Hans-Ertel-Centre of the Deutscher Wetterdienst and the University of Bonn in Germany. Water levels, depth-averaged current conditions, and ocean surface waves are provided from state-of-the-art, high-resolution numerical hydrodynamic and spectral wave hindcast models established by DHI.

The Danish Waters model is validated against several measurement stations in the vicinity of the Hesselø OWF to establish the quality of the model predictions. Wind conditions, water levels, and waves are very well predicted by the hindcast models. However, the depth-averaged representation of the hydrodynamic conditions provided by the two-dimensional flow model does not describe the possible stratification of the water column. Hence, further analyses of the current conditions based on a three-dimensional flow model should be considered if the currents and seasonal stratification are critical for structural design.

Time series metocean data from the DHI's Danish Waters hindcast database are provided for three (3) locations within the Hesselø OWF site, denoted OWF-1, OWF-2, and OWF-3. Details of the model database, the data extraction points, and a description of the metocean parameters are included in this report.

The time series of data have been analysed to describe the variation in metocean conditions within the Hesselø OWF area. The analysis includes assessment of the annual and monthly statistics of metocean parameters and extreme value analysis of omnidirectional conditions for return periods of up to 50-years. A summary of the extreme value results is given in Table 0.1 for the three metocean analysis points.

Table 0.1 Summary of extreme metocean conditions at Hesselø OWF

Omnidirectional, all-year extreme wave, depth-averaged current speed and residual water levels at analysis points OWF-1, OWF-2, and OWF-3

Analysis point	OWF-1				OWF-2				OWF-3			
Return period, T_R [years]	1	5	10	50	1	5	10	50	1	5	10	50
Spectral significant wave height, 3-hour sea-state, H_{m0} [m]	3.6	4.1	4.3	5.0	3.6	4.2	4.4	5.0	3.4	3.9	4.1	4.7
Peak wave period associated with extreme H_{m0}, T_p [s]	7.3	7.6	7.8	8.2	7.2	7.7	7.8	8.2	7.0	7.3	7.4	7.8
Maximum individual wave height, H_{max} [m]	6.5	7.6	8.0	9.1	6.6	7.8	8.2	9.3	6.3	7.3	7.7	8.7
Wave period associated with extreme H_{max}, $T_{Hmax,50\%}$ [s]	6.4	6.9	7.1	7.5	6.5	7.0	7.2	7.6	6.3	6.8	7.0	7.4
Wave crest elevation above to mean sea- level, $C_{max,MSL}$ [mMSL]	4.7	5.6	6.1	7.1	4.8	5.7	6.1	7.1	4.5	5.4	5.8	6.7
Depth-averaged total current speed, CS_{Total} [m/s]	0.6	0.8	0.9	1.1	0.4	0.5	0.5	0.6	0.50	0.7	0.7	0.8
Positive residual water level, $WL_{Resid,High}$ [m]	0.9	1.2	1.3	1.5	0.9	1.2	1.3	1.6	1.0	1.2	1.3	1.5
Negative residual water level, $WL_{Resid,Low}$ [m]	-0.6	-0.8	-0.8	-0.9	-0.6	-0.8	-0.8	-0.9	-0.6	-0.8	-0.8	-0.9

1 Introduction

This document has been prepared for **Energinet Eltransmission A/S (Energinet)** by DHI A/S (DHI), in relation to the site metocean conditions assessment for the **Hesselø Offshore Wind Farm**.

1.1 Background to the project

The Energy Agreement of June 2018 sets out long-term energy policy for Denmark [1]. Among the aims of this agreement is to transform Denmark to a low carbon society that is independent of fossil fuels. Funding has been allocated to achieve a target of a 100% contribution of renewable energy to Denmark's electricity consumption by the year 2030. To achieve these targets, the energy agreement commits to the construction of three offshore wind farms. Each offshore wind farm (OWF) will have a capacity of at least 800 megawatts (MW).

In June 2020, the Danish Climate Agreement for Energy and Industry identified the Hesselø offshore wind farm as the second project to be developed under the Energy Agreement [2]. The wind farm is to be located within Hesselø Bugt in the Kattegat, approximately 30 km north of Zealand and around 20 km from the island of Hesselø (Figure 1.1). The wind farm will have a total capacity of between 800 MW and 1,200 MW and cover an area of approximately 247 km^2. Power will be exported to land and connected to the electricity network at the Hovegård high-voltage electricity substation, west of the town of Ballerup. The wind farm must be completed by the end of 2027.

In July 2020, the Danish Energy Agency (DEA) instructed Energinet to initiate site investigations for the Hesselø OWF and to undertake supplementary studies and analyses. This includes the establishment of meteorological and oceanographic (metocean) data and documentation to support the tendering process and enable bidders to submit qualified economic bids.

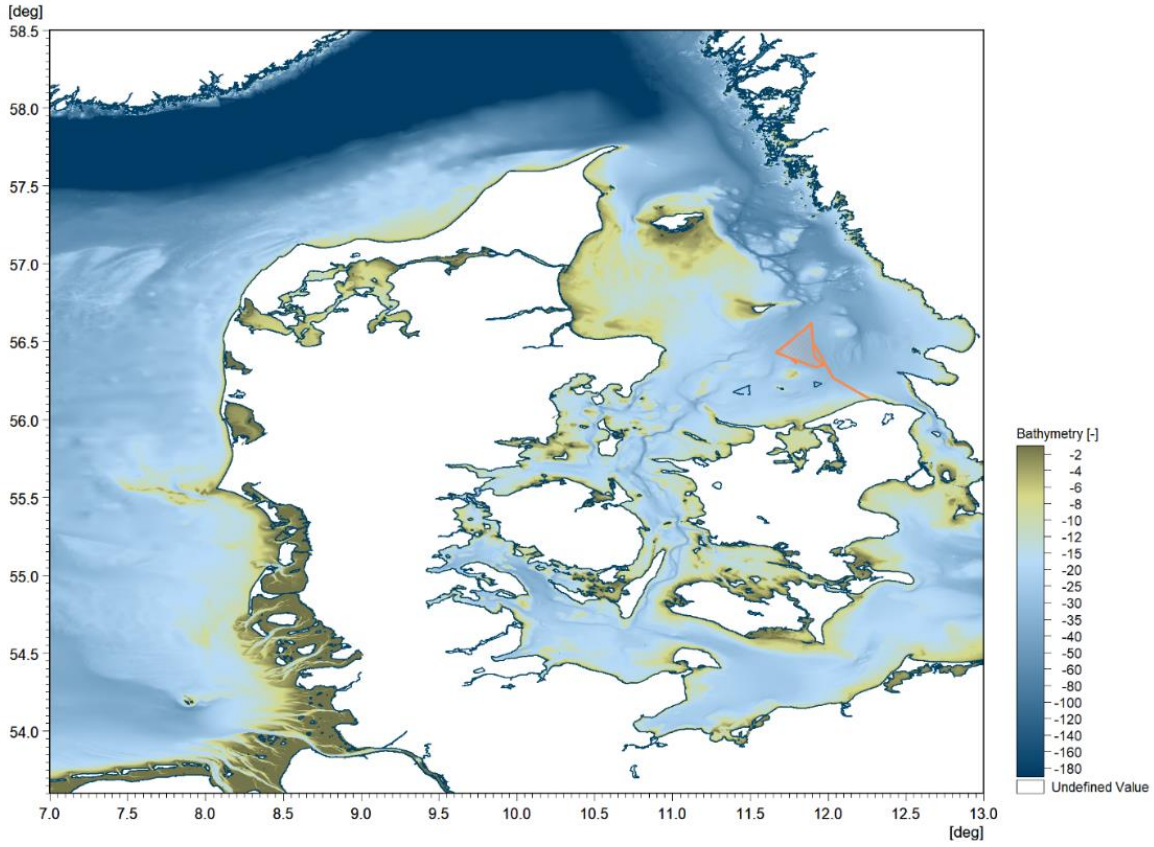

Figure 1.1 Map showing the location of the Hesselø offshore wind farm site
The Hesselø OWF and its export cable corridor are shown by the orange polygon. The coloured shading shows the bathymetry in metres relative to lowest astronomical tide (LAT) from EMODnet 2018 (see Section 2.1.2)

1.2 Aims and objectives

The aim of this report is to provide metocean data and analysis that will form part of the overall site conditions assessment (SCA) to serve as the basis for the Front-End Engineering Design (FEED) of offshore wind turbines and related project infrastructure.

In working towards this overall aim, the objectives of this site metocean conditions assessment report is to:

1. Provide a long-term hindcast model database of winds, waves, currents, and water levels, with a suitable temporal and a spatial resolution to adequately resolve the meteorological and oceanographical processes at the Hesselø OWF and the surrounding area
2. Validate the metocean hindcast models against *in situ* measurements to establish the quality and validity of the model data base
3. Perform metocean analyses to establish operational and extreme metocean conditions at three locations within the Hesselø OWF site

It must be noted by the reader that the wind and other meteorological conditions presented in this site metocean conditions report are provided for information only. The recommended meteorological and atmospheric design values for FEED are contained in the **Site Wind Condition Assessment** for the Hesselø offshore wind farm [3]

1.3 Layout of this report

The remaining sections of this report are organised as follows:

- Section 2 describes the data basis for the site metocean conditions assessment. This includes details of the site bathymetry, the available measurement data, and details of the DHI's Danish Waters metocean hindcast model database
- Section 3 presents the results of the validation of the atmospheric, hydrodynamic, and spectral wave models against measured data
- Section 4 describes the three data extraction and analysis points for the site metocean conditions assessment at Hesselø OWF. The time-series data provided alongside this report are also described
- Section 5 presents the results of the operational (i.e., normal) metocean conditions at three metocean analysis points
- Section 6 summarised the results of the extreme metocean conditions at three metocean analysis points
- Section 7 presents information on the properties of air, seawater, and information on marine growth

2 Study Data Basis

This section describes the data basis, both measurements and model data sets, used as input to the site metocean conditions assessment at the Hesselø OWF.

The information below includes an overview of the site bathymetry data (Section 2.1) and the available measurement stations (Section 2.2). DHI's Danish Waters metocean hindcast model database utilised during the project is also described (Section 2.3) as is the Baltic Sea physical reanalysis model (Section 2.4).

2.1 Bathymetry

The bathymetric data sets that were used for the site metocean conditions assessment are described below.

2.1.1 Hesselø site bathymetry

A geophysical survey of the Hesselø site to map the bathymetry and characterise the nature of the seafloor and sub-seafloor geology was performed between October and December 2020 [4]. The bathymetry data were provided by Energinet in a .xyz file format at a horizontal resolution of 5 m, referenced to Universal Transverse Mercator (UTM) Northern Hemisphere Zone 32 N, and vertically referenced to mean sea level (MSL).

- F172145_Hesselo_WPA_MBES_Bathymetry_5pt0m_MSL.xyz

Figure 2.1 shows a map of the bathymetry of the Hesselø OWF site with water depths range from 24.7 m to 33.5 m relative to MSL. The site is characterised by gentle seafloor slopes, on average ranging between approximately 0˚ and 3˚ (see Section 4.2 of [4]).

The detailed bathymetry data are used in this report to verify the model seafloor elevation at the metocean analysis points within the offshore wind farm.

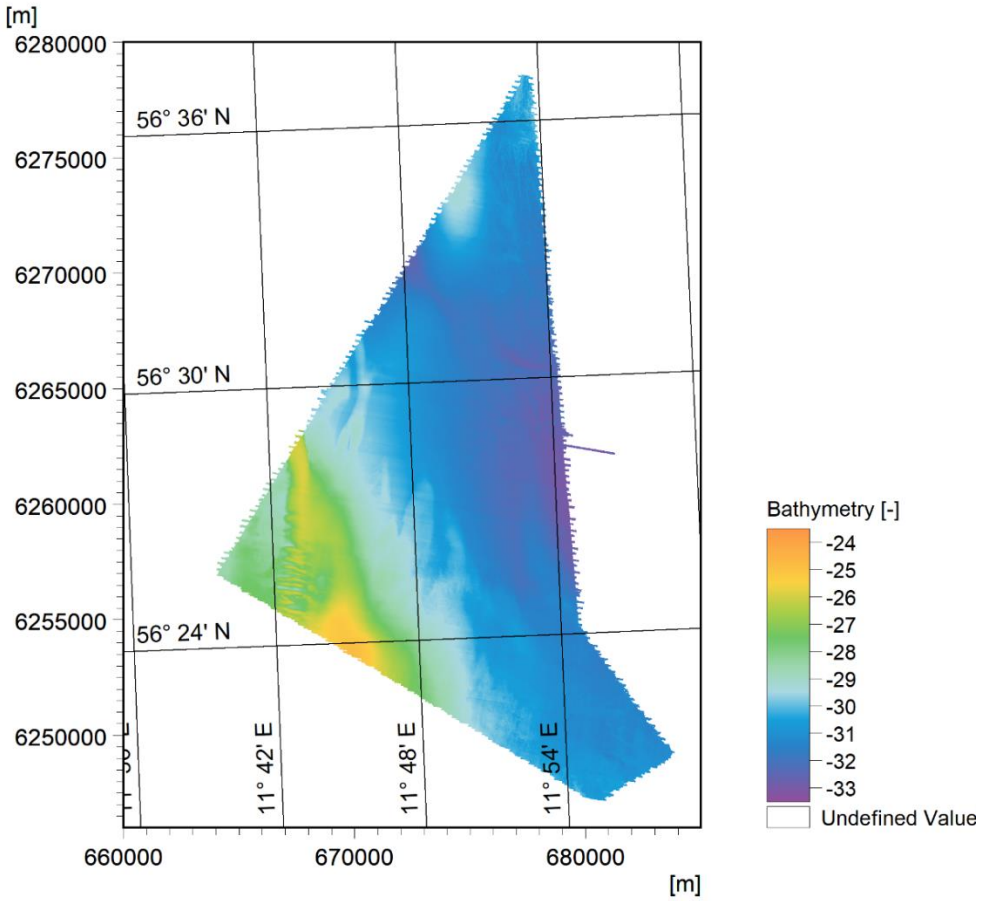

Figure 2.1 Hesselø site bathymetry
The seafloor elevation is given in metres relative to mean sea level

2.1.2 EMODnet

Additional information on the seafloor elevation in the area around the Hesselø OWF, including the export cable corridor, was obtained from the Digital Terrain Model (DTM) product of the European Marine Observation and Data Network (EMODnet)[1]. This portal was initiated by the European Commission and includes a digital bathymetric product produced from aggregated bathymetry data sets collated from public and private organisations. The data is provided processed, and quality controlled at a grid resolution of 1/16 x 1/16 arc minutes (approximately 115 m latitude x 63 m longitude at the project site). The average water depth in LAT for each cell is provided (see Figure 1.1).

EMODnet 2018 was used as the primary bathymetry data source in the establishment of DHI's Danish Waters metocean hindcast database (see Section 2.3).

It is noted that the horizontal resolution of the underlying bathymetry data may be somewhat coarser than the EMODnet grid. The original bathymetry data source at the Hesselø OWF is the Danish waters 500m grid DTM (D500M), produced by the Danish Geodata Agency at the Danish Hydrographic Office. The D500M was most recently revised in 2018 and is a combination of data that has been collected with different techniques from late 19th century up to the year 2017.

[1] EMODnet Bathymetry (emodnet-bathymetry.eu) – accessed March 2022

2.2 Measurement data

Measurement data were used for validating the metocean hindcast models that form the basis of the site metocean conditions assessment. The measurement data was also used for assessing site conditions (e.g., the normal wind profile and vertical current speed profile).

The following sub-sections briefly summarise the characteristics of the measurement stations, including the quality checks and processing that were applied to the data.

In this study, data for the period 1995 to 2018 (inclusive) were prioritised as this is aligned with the period of the hindcast models database. Any data recorded before 1995 were not considered.

2.2.1 Wind measurement stations

Table 2.1 summarises the data from the wind measurement stations that were available for the site metocean conditions assessment. This includes the data provider, geographic position, station and measurement height, averaging period, and the reporting time interval. The location of the stations is shown on the map in Figure 2.2.

DMI Measurement Stations

Time-series of wind speed and wind direction at three coastal measurement stations (Anholt Havn, Gniben, and Nakkehoved Fyr) were accessed via the Danish Meteorological Institute (DMI) Open Data Application Programming Interface (API)[2]. These data were recorded for a measurement height of 10 m above ground level, and the station height above MSL is also reported (see Table 2.1). The 10-minute averaged wind speed and wind direction were available at an output time interval of either 1-hour or 10-minutes (depending on the station and date of collection).

According to DMI the meteorological data are provided as raw files that are neither quality controlled nor processed in any way [5]; hence, errors in these measurements may sometimes occur. DHI therefore carefully inspected the data to check for consistency over time, and to detect and remove anomalies or spikes in the data record.

SMHI Measurement Stations

Time-series of wind speed and wind direction for the coastal measuring stations at Hallands Väderö and the offshore buoy at Läsö Ost A were obtained from the Swedish Meteorological and Hydrological Institute (SMHI) national archive.

The SMHI measurement station at Halmstad Flygplats was also identified as a relevant wind data set in study scope of work (see Table 1-1 of [6]). However, on inspecting these data, DHI identified that there were no valid measurements during the period of interest (i.e., from 1995 to 2018, inclusive).

M1 Met. Mast (Læsø Syd)

Wind speed and direction data from the M1 Meteorological Mast, 12 km south of the island of Læsø, were provided by Energinet. This data set included

[2] Danish Meteorological Institute - Open Data - DMI Open Data - Confluence (govcloud.dk) – accessed March 2022

measured wind speed at heights of 15 m, 45 m and 62 m above sea level, and measured wind direction at heights of 28 m and 43 m above sea level. Data were collected for the c. 18-month period between November 1999 and April 2001 and were provided as a 10-minute average values at 10-minute intervals. Quality flags as well as time series and scatter plots of wind speed and direction were used to identify and remove any period of invalid data. For more information on the measurement system and quality control procedure please see [7].

Wind speed measurements at 15 m and 45 m were recorded by boom mounted anemometers oriented in a NE and SW direction. Wind speed data were filtered to account for mast shadow. At each timestep the data was chosen from the anemometer that was not in the lee of the mast, based on the wind direction. This results in a single dataset at each height.

Hesselø F-LiDAR

Energinet provided measured wind speed data from a EOLOS FLS200 E01 Floating Light Detection and Ranging (F-LiDAR) unit installed within the Hesselø project site. The dataset included wind speed and wind direction at various heights form 12 m to 240 m above sea level and were provided in a processed and quality-controlled format by the data provider [8].

The data were collected over a c. 7-month period between February and September 2021. This period was outside of the available period of the hindcast model database (see Section 2.3), meaning that the Hesselø F-LiDAR data could not be used for validating the wind conditions at the site. However, these data were adopted for the purposes of assessing the vertical wind speed profile during normal wind conditions.

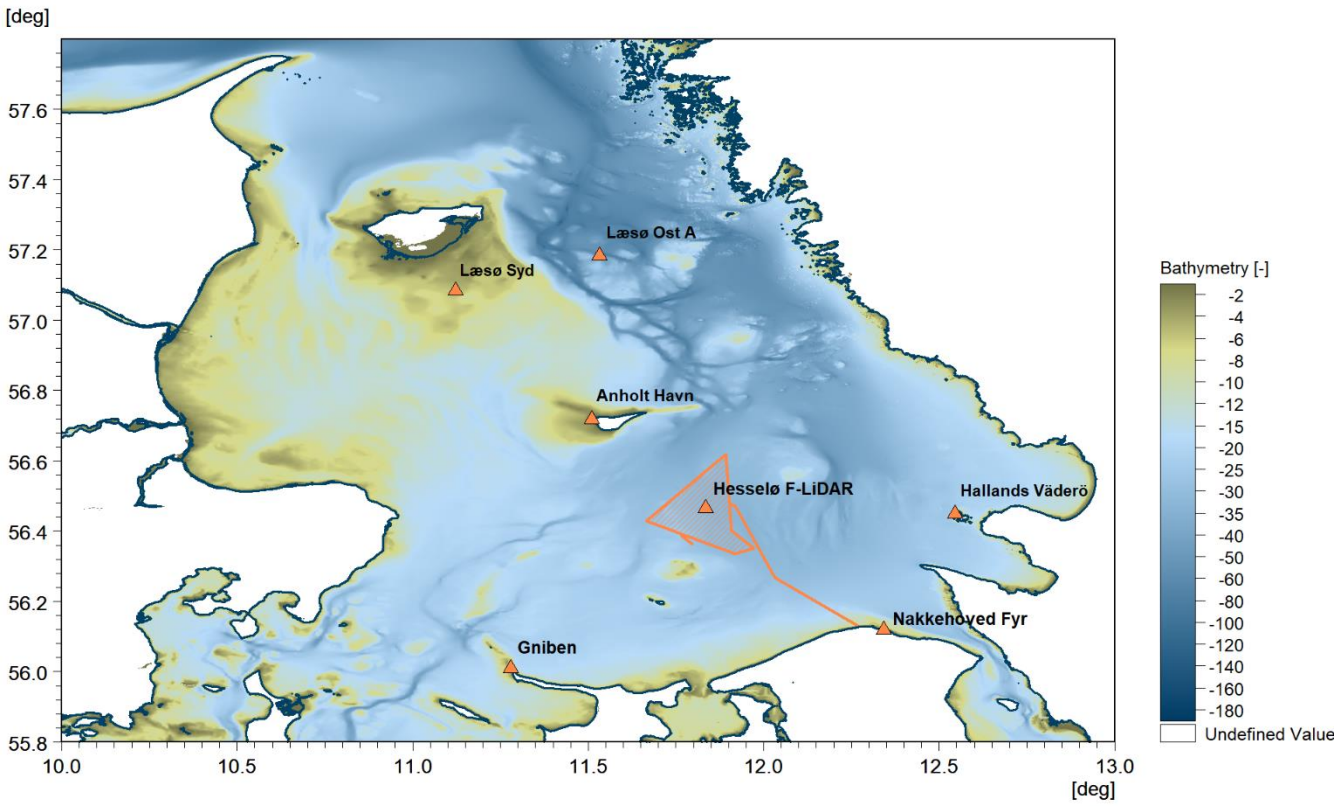

Figure 2.2 Map showing location of the wind measurement stations
The coloured shading shows the bathymetry in metres relative to lowest astronomical tide (LAT) from the EMODnet 2018 (see Section 2.1.2)

Table 2.1 Wind measurement stations available for the site metocean conditions assessment

Station Name (data provider)	Position [WGS 84]		Station height [mMSL]	Measurement height [m]	Start Date	End Date	Averaging period [minutes]	Reporting time interval [minutes]
	Lon. [°E]	Lat. [°N]						
Anholt Havn (DMI)	11.5098	56.7169	2.36	10	1995-01-01	2018-12-31	10	60 (Jan. 1995 – Sept. 1999) 10 (Sept. 1999 – Dec. 2018)
Gniben (DMI)	11.2787	56.0083	14.39	10	1995-01-01	2018-12-31	10	60 (Jan. 1995 – Aug. 2002) 10 (Aug. 2002 – Dec. 2018)
Nakkehoved Fyr (DMI)	12.3429	56.1193	37.00	10	1995-01-01	2018-12-31	10	60 (Jan. 1995 – Sept. 1999) 10 (Sept. 1999 – Dec. 2018)
Hallands Väderö (SMHI)	12.5453	56.4496	9.17	10	1995-08-01	2018-12-31	10	60
Läsö Ost A (SMHI)	11.5332	57.1834	0	4	2004-09-01	2008-09-04	10	60
Læsø Syd (Energinet)	11.1233	57.0842	0	15, 45, 62 (speed) 28, 43 (direction)	1999-11-01	2001-04-23	10	10
Hesselø F-LiDAR (Energinet)	11.8351	56.4642	0	238, 198, 178, 158, 138, 118, 98, 68, 38, 10	2021-03-01	2021-09-27	10	10

2.2.2 Water level measurement stations

Table 2.2 summarises the water level measurement stations available for the site metocean conditions assessment. This includes the data provider, geographic position, period of measurement, and the reporting time interval. The location of the stations is shown on the map in Figure 2.3.

The water level measurements were visually inspected to ensure consistency over time. Outlier detection and spike removal was performed following the procedure as outlined by the Sea Level Station Monitoring Facility[3]

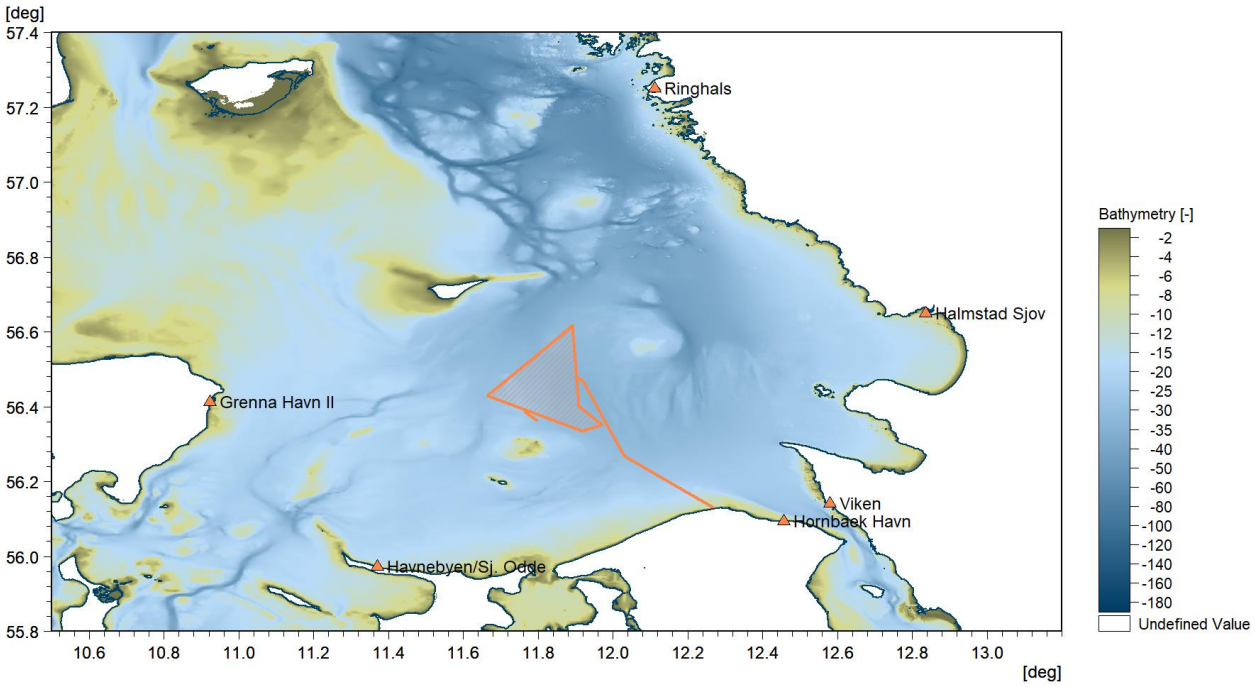

Figure 2.3 Map showing location of the water level measurement stations
The coloured shading shows the bathymetry in metres relative to lowest astronomical tide (LAT) from the EMODnet 2018 (see Section 2.1.2)

[3] http://ioc-sealevelmonitoring.org/service.php - accessed March 2022

Table 2.2 Water level measurement stations for the site metocean conditions assessment

Station Name (data provider)	Position [WGS 84]		Start Date	End Date	Reporting time interval [minutes]
	Lon. [°E]	Lat. [°N]			
Grenaa Havn II (DMI)	10.922	56.4121	2014-04-15	2020-12-31	10
Havnebyen Sjællands Odde (DMI)	11.3694	55.9728	2012-01-01	2019-01-01	15 (Jan. 2012 - May 2001) 10 (May 2001 – Jan. 2012)
Hornbæk Havn (DMI)	12.4571	56.0934	1995-01-01	2018-12-31	10
Viken (SMHI)	12.5792	56.1422	1995-01-01	2019-01-01	60
Halmstad Sjöv (SMHI)	12.8358	56.6488	2009-04-28	2018-12-31	60
Ringhals (SMHI)	12.1125	57.2497	1995-01-01	2019-01-01	60

2.2.3 Current measurement stations

Table 2.3 summarises the current measurements stations available for the site metocean conditions assessment. This includes the data provider, geographic position, period of measurement, seafloor elevation, as well as the sampling and reporting time interval. The location of the stations is shown on the map in Figure 2.4.

Anholt OWF

The currents at the Anholt OWF (approximately 40 km northwest of the Hesselø OWF site) were recorded by an acoustic Doppler current Profiler (ADCP) mounted on a frame placed on the seafloor [9]. The survey covered a period of approximately 2-months during the spring of 2010. Velocity components were recorded at 10-minute intervals within vertical bins of 0.5 m, starting from 1.89 m above the seafloor. Near surface bins were removed as these data are often contaminated by reflections of the water surface, so-called 'side-lobe' interference (see Section 11 of [10]).

Hesselø F-LiDAR

Current speeds were also provided from a current profiler mounted on the floating unit (EOLOS FLS200 E01) within the Hesselø OWF project site [8]. The data included velocity components sampled over a 3-minute period and reported at intervals of 30-minutes between February and September 2021. These data were outside of the available period of the hindcast model database (see Section 2.3), meaning that the Hesselø F-LiDAR ADCP data could not be used for direct validation of the current speeds at the site. However, these data were adopted for the purposes of assessing the vertical current profile.

The Hesselø F-LiDAR ADCP provided current velocities at 22 depth intervals through the water column:

- 2021-03-01 to 2021-07-14, at 1.6 m intervals from 6.0 m to 39.6 m below sea surface

- 2021-07-17 to 2021-09-27, at 1.6 m intervals from 3.6 m to 37.2 m below sea surface

According to the data provider the current sensor data are corrected with respect to tidal variation. However, given the nominal water depth at the site is 31.5 mMSL[4], the last few levels are likely to be erroneous being either below the seafloor or impacted by reflections off the seafloor. Thus, any data associated with vertical levels below 90% of the nominal water depth were discarded.

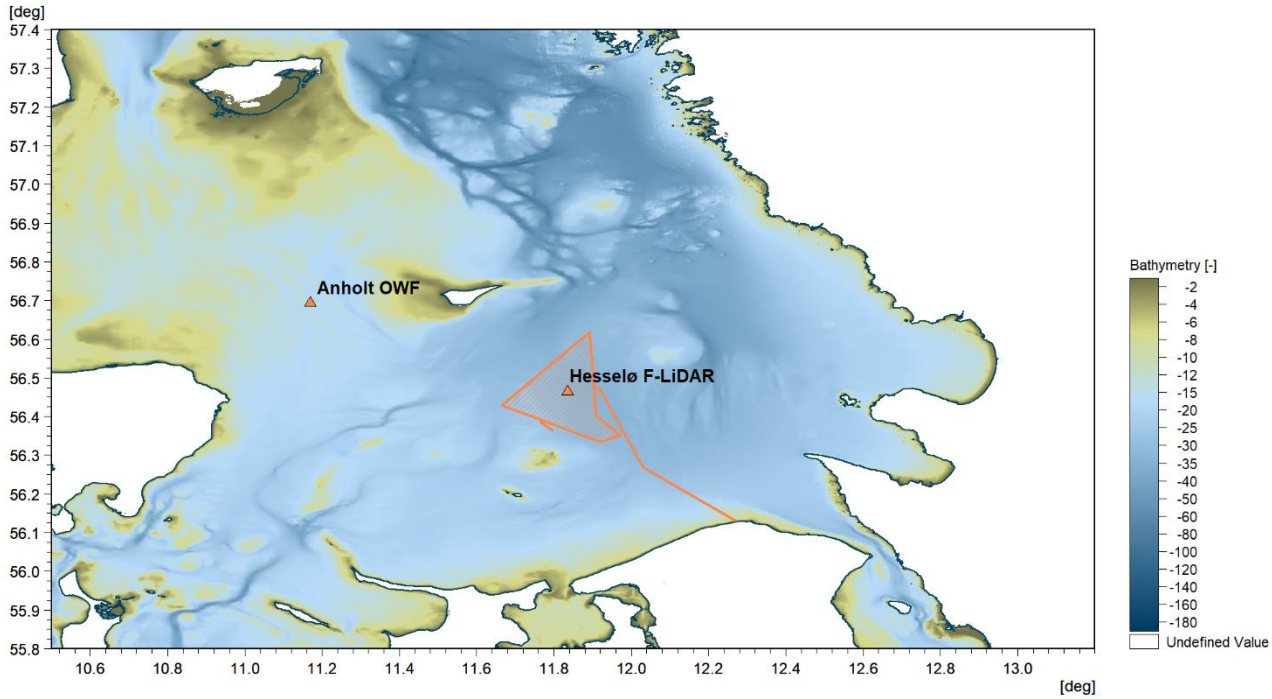

Figure 2.4 Map showing location of the current measurement stations
The coloured shading shows the bathymetry in metres relative to lowest astronomical tide (LAT) from the EMODnet 2018 (see Section 2.1.2)

[4] obtained from the detailed site bathymetry, see Section 2.1.1

Table 2.3 Current measurement stations for the site metocean conditions assessment

Station Name (data provider)	Position [WGS 84]		Start Date	End Date	Averaging time [minutes]	Reporting time interval [minutes]	Recorded seafloor elevation [mMSL]	Model seafloor elevation [mMSL]
	Lon. [°E]	Lat. [°N]						
Anholt OWF (Energinet)	11.1695	56.6935	2010-03-17	2010-05-20	10	10	-15.2	-16.0
Hesselø F-LiDAR (Energinet)	11.8351	56.4642	2021-03-01	2021-09-27	3	30	-31.5	-31.5

2.2.4 Wave measurement stations

Figure 2.5 shows the locations of the wave measurement stations that were available for the site metocean conditions assessment. Table 2.4 provides further details of these stations, summarising the data provider, geographic position, water depth, averaging period, and reporting time interval.

Anholt OWF

Wave measurements at the Anholt OWF site (~40 km northwest of the Hesselø OWF site) were recorded by an ADCP mounted on a frame placed on the seafloor [9]. The survey covered period of approximately 2-months between March and May of 2010. The wave data were recorded over a 20-minute sampling interval at 1-hour intervals. The wave parameters include significant wave height (H_{m0}), peak wave period (T_p), mean wave period (T_{02}), and mean wave direction (MWD).

Sejero Bugt

Wave measurements at the Sejero Bugt (~75 km southwest of Hesselø OWF) were available for a period of approximately 6 months between November 2013 and March 2014. The data were recorded using a 600 kHz ADCP manufactured by RDI Systems, mounted in a bottom frame looking upwards. Wave parameters including significant wave height (H_{m0}), peak wave period (T_p), mean wave period (T_{02}), and mean wave direction (MWD), were available at hourly time intervals based on a 20-minute sampling period. More information on the survey campaign, including instrumentation setup, calibration, and pre-deployment tests can be found in [11].

Time series of significant wave height, mean wave direction, peak wave period, and mean zero-crossing period were analysed with several spikes removed before use in the spectral wave model validation.

Fladen Boj

Time series of wave parameters at the Fladen Boj (~65 km north of the Hesselø OWF) were obtained from SMHI[5] . Observations were available at hourly time intervals based on a 30-minute sampling period and included significant wave height (H_{m0}) and mean wave period (T_{02}) between 1995 and 1999.

Time series plots of each parameter were used to identify and remove periods of invalid data, such as spikes and repeated values (i.e., flat lining) before use in the spectral wave model validation.

Læsø Ost A

Wave parameters were available from SMHI, recorded from a SeaWatch buoy located east of the island of Læsø in the Skagerrak. This consisted of quality-controlled wave parameters (H_{m0}, T_{02}, and PWD) between May 2001 and February 2009.

Læsø Syd

Waves data were measured between June 1999 to July 2000 at Læsø Syd using an S4 wave and current meter (see Section 5 of [7]). The data were recorded hourly with a 10-minute sampling period. This data set was collected on behalf of Elsam (now Ørsted), who have permitted its use in this report.

[5] Download oceanographic observations | SMHI – accessed March 2022

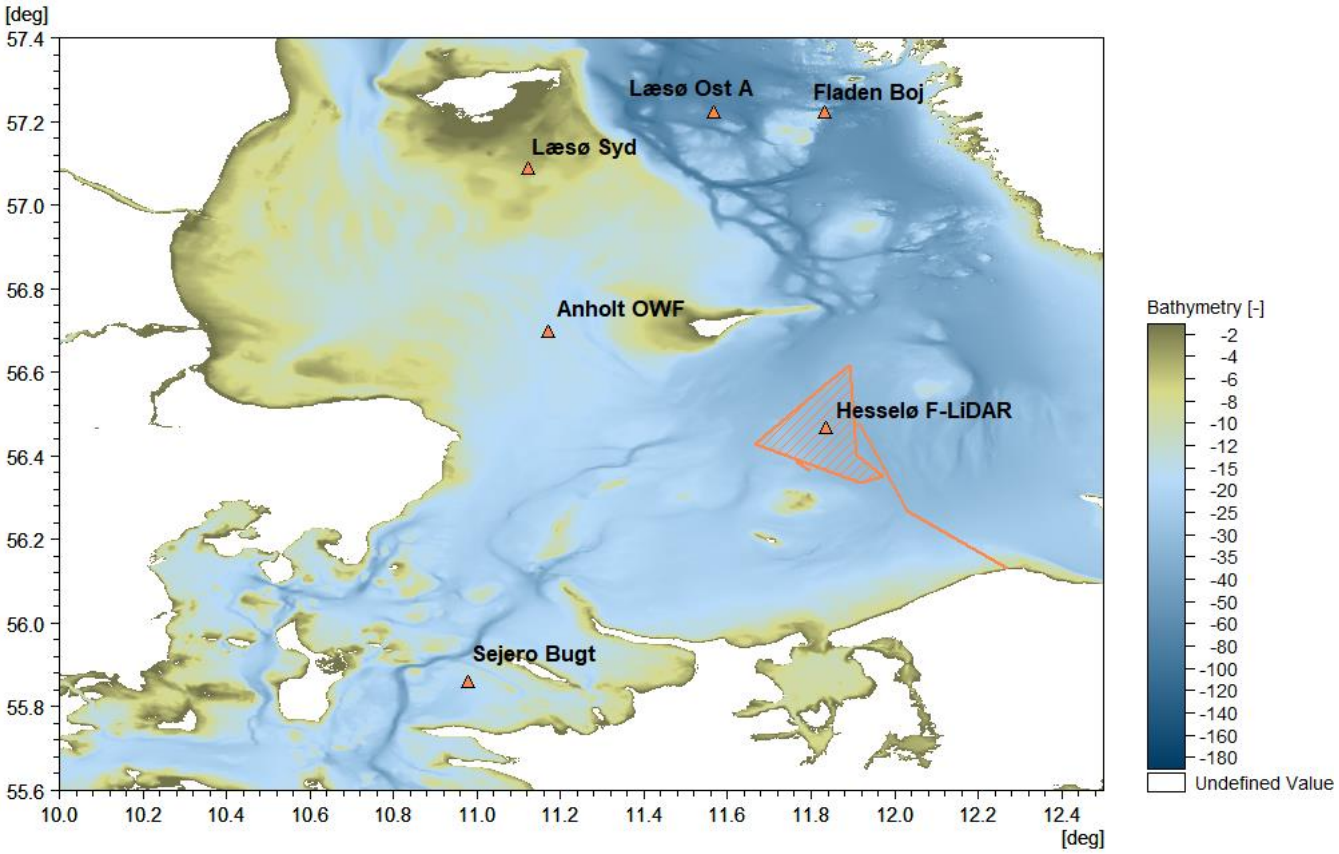

Figure 2.5 Map showing location of the wave stations used in the validation of the model database
The coloured shading shows the bathymetry in metres relative to lowest astronomical tide (LAT) from the EMODnet 2018 (see Section 2.1.2)

Table 2.4 Wave measurement stations available for the site metocean conditions assessment

Station Name (data provider)	Position [WGS 84]		Start Date	End Date	Averaging time [minutes]	Reporting time interval [minutes]	Recorded seafloor elevation [mMSL]	Model seafloor elevation [mMSL]	Parameters available
	Lon. [°E]	Lat. [°N]							
Anholt OWF (Energinet)	11.1695	56.6935	2010-03-16	2010-05-20	20	60	-15.2	-15.9	H_{m0}, MWD, T_p, T_{02}.
Sejero Bugt (DHI)	10.9781	55.8651	2013-10-27	2014-03-06	20	60	-21.8	-20.0	H_{m0}, MWD, T_p, T_{02}.
Fladen Boj (SMHI)	11.8308	57.2164	1995-01-01	1999-08-31	30	60	-14.1	-43.0	H_{m0}, T_{02}
Læsø Ost A (SMHI)	11.5666	57.2166	2001-05-08	2009-02-14	Not known	60	-70.0	-55.0	H_{m0}, T_{02}, PWD
Læsø Syd (Ørsted)	11.3694	55.9728	1999-06-25	2000-07-26	10	60	-5.4	-5.4	H_{m0}, MWD, T_p, T_{02}.

2.3 DHI Danish Waters hindcast database

DHI have established a regional hindcast model database of Danish Waters. The database provides a long-term repository of data to support marine projects and metocean studies in the seas around Denmark, including: the North Sea, Skagerrak, Kattegat, Northern Belt, Great Belt, Little Belt, Southern Belt, Øresund, and the Baltic Sea (Figure 2.6).

The hindcast model database spans a continuous period of 24-years (January 1995 to December 2018, inclusive), and consists of the following model components:

- Wind conditions from the COSMO-REA6 (**CREA6**) atmospheric model (see Section 2.3.1)
- A 2-dimensional hydrodynamic model, **HD_{DKW}** (see Section 2.3.2)
- A spectral wave model, **SW_{DKW}** (see Section 2.3.3)

The following sections provide a brief description of each of these models. For more information, the reader is referred to the model setup, calibration, and validation report [12].

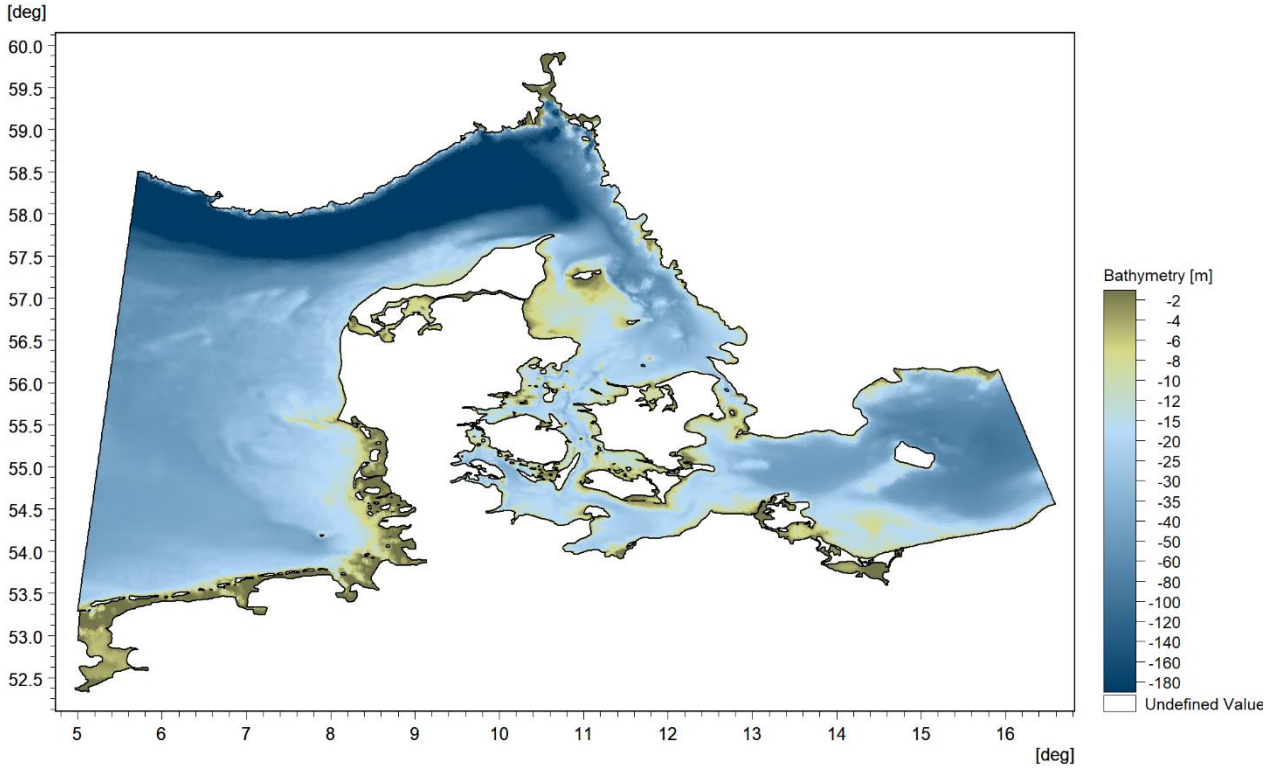

Figure 2.6 The domain of the DHI's Danish Waters hindcast model database
The model domain includes the sea areas around Denmark. The coloured shading shows the model bathymetry in metres relative to mean sea level

2.3.1 Atmospheric model (COSMO-REA6)

The Danish waters hindcast database was established using the high-resolution atmospheric model reanalysis system COSMO-REA6 (henceforth, CREA6). This product has been developed by the German Meteorological Service, Deutscher Wetterdienst (DWD) by the Hans-Ertel Centre for Weather Research at the University of Bonn [13]. CREA6 employs the numerical weather prediction (NWP) model from the **CO**nsortium for **S**mall-**S**cale **MO**delling (**COSMO**)[6].

The CREA6 grid covers the CORDEX (Coordinated Regional Climate Downscaling Experiment) EUR-11 domain (Figure 2.7). The models initial and boundary data are provided the global reanalysis ERA-Interim from European Centre for Medium-Range Weather Forecasts (ECMWF) [14], with assimilation of observational data. The atmospheric parameters of the reanalysis are provided at a high-resolution of 0.055°, which is approximately 6.1 km latitude × 3.3 km longitude at the Hesselø OWF site (Figure 2.8).

Land-sea mask

The land-sea mask defines where the surface of the earth in the atmospheric model is interpreted as either land or as water. Whether an element is interpreted as land or water affects e.g., the estimated roughness of the surface, which in turn affects the wind velocity profile. The roughness over land is generally higher than the roughness over sea; hence, the wind speed over land is generally lower than the wind speed over sea. The land sea mask of the CREA6 model is shown in Figure 2.8 and denotes the proportion of land, as opposed to water in each model grid cell. This dimensionless parameter ranges from a value of 1 (100% land in the cell) to a value of 0 (100% water in the cell).

CREA6 outputs

The outputs from CREA6 are available at 40 vertical levels, but the nine lowermost levels are of the most relevance for establishing site metocean conditions: 10, 40, 60, 80, 100, 125, 150, 175, and 200 m above sea/ground level. These data are provided at 1-hour output time intervals for a continuous period between January 1995 and August 2019.

The following parameters were used in this metocean site conditions assessment (units in brackets):

- Wind speed at various vertical levels [m/s]
- Wind direction at various vertical levels [°N – coming from]
- Air pressure at mean sea level, PMSL [Pa]
- Air temperature at 2 mMSL, $T_{air,2m}$ [°C]
- Relative humidity [%]

Temporal scale

The modelled wind conditions are essentially instantaneous 'snapshots' of the wind field that are saved at 1-hour time intervals from the model. The time scales resolved in the numerical model behind the reanalysis data are affected by the spatial resolution, and hence the delivered CREA6 data with a sampling time of 1-hour represent wind speeds that are implicitly averaged over some

[6] Consortium (cosmo-model.org) – accessed March 2022

time averaging period T_a. For practical applications, such as extreme value assessment or load calculations (e.g., wind associated with extreme sea-states), appropriate accounting for the smoothed nature of the model data must be considered.

A simple approach of assessing the representative temporal scale (or smoothing) of the CREA6 wind model is by comparing the power spectra of modelled wind speeds with the power spectra of observations that have been smoothed using various averaging windows. Figure 2.9 presents such an analysis for the 10 mMSL wind speeds at the DMI Anholt Havn measurement station (see Section 2.2.1) where the measured wind speeds have been assessed for a 10-minute, 30-minute, 60-minute, and 120-minute averaging window. Although some aliasing is observed for the highest frequencies in the spectrum of CREA6, the spectrum follows the 10-minutes and 30-minutes lines closely. This is consistent with previous analysis, e.g., in section 2.5.1 of [15]. For the purposes of this study, we have adopted 30-minutes as the representative temporal averaging period of the CREA6 model, i.e., T_a = 30 minutes.

For normal conditions, the long-term wind speed statistics are considered to be independent of the averaging period within the range 10-minutes to 3-hours (see Section 6.4.3.1 of [16]). However, for extreme wind conditions, conversion factors need to be applied to determine the extreme wind speeds for the different temporal averaging periods (see Section 6.2.1).

A validation of the CREA6 wind model in the area around the Hesselø OWF is presented in Section 3.1.

Table 2.5 Characteristics of COSMO-REA6 wind and air-pressure data

Dataset	Availability	Output time interval	Horizontal Spatial resolution	Vertical levels
COSMO-REA6	Jan. 1995 – Aug. 2019	1 hour	0.055°	40 levels

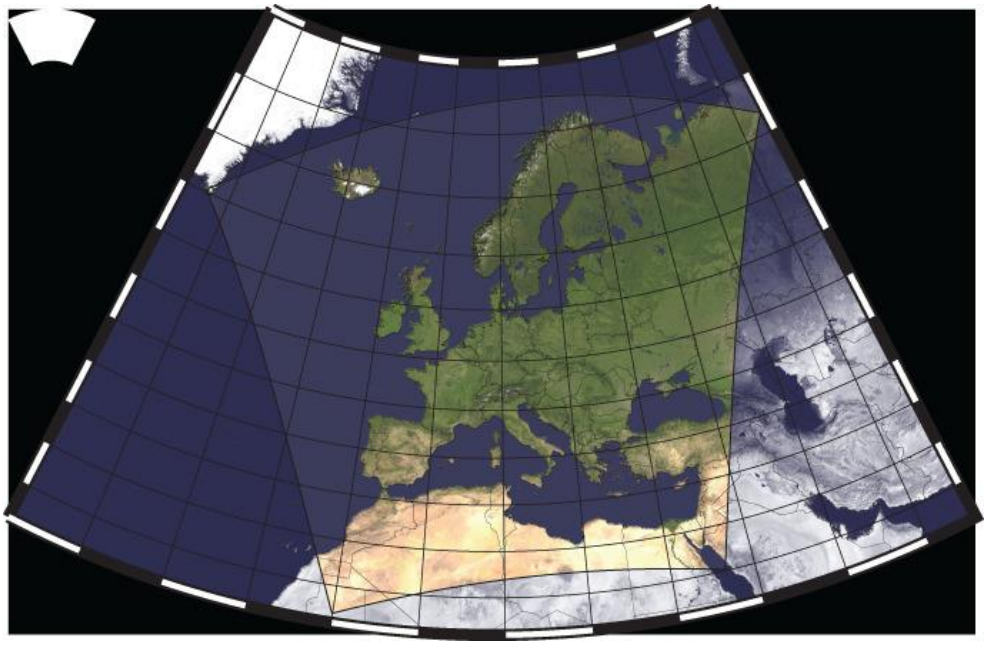

Figure 2.7 Model domain of COSMO-REA6 (CORDEX EUR-11)
Image reproduced from Figure 1 of [13]

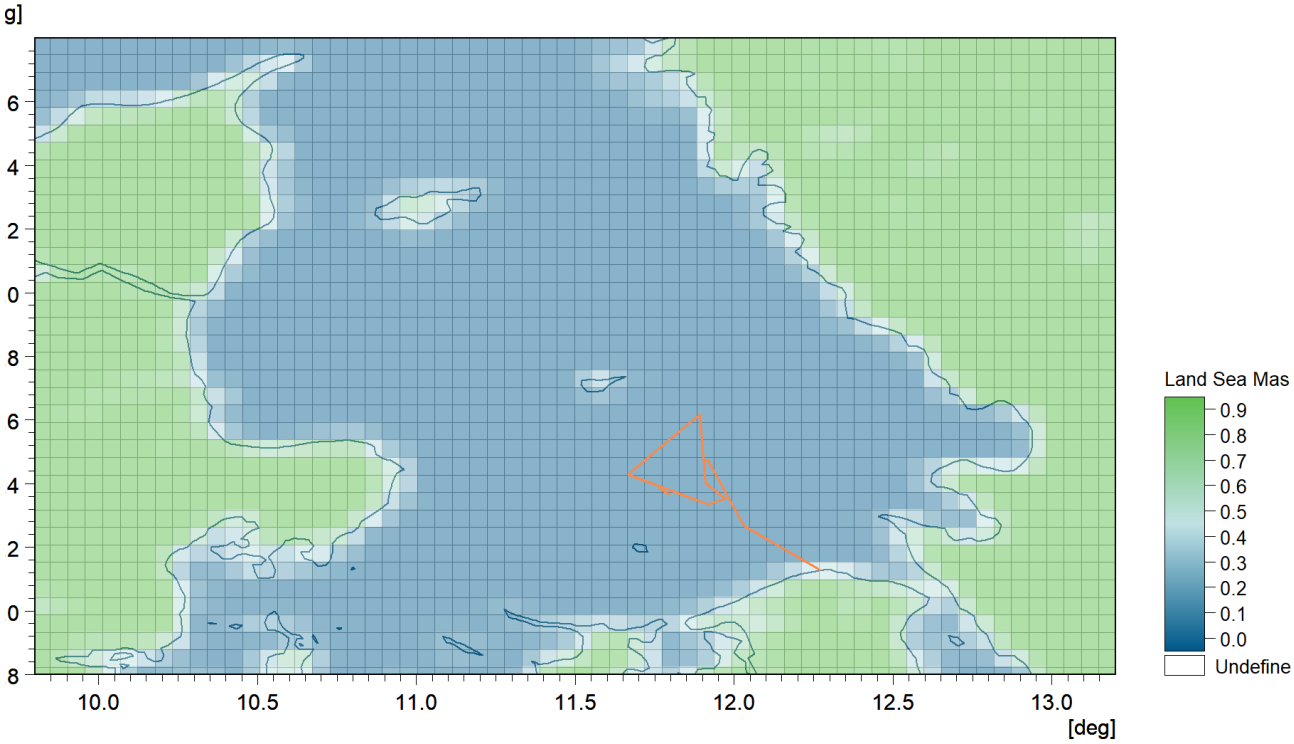

Figure 2.8 Numerical grid and land-sea mask of the COSMO-CREA6 model
The CREA6 model mesh is shown by the grey gridlines and the Hesselø OWF wind farm and export cable route is shown by the orange polygon. The coloured shading designates the CREA6 land sea mask, a dimensionless parameter which denotes the proportion of land as opposed water in each cell (1 = 100% land, 0 = 100% water)

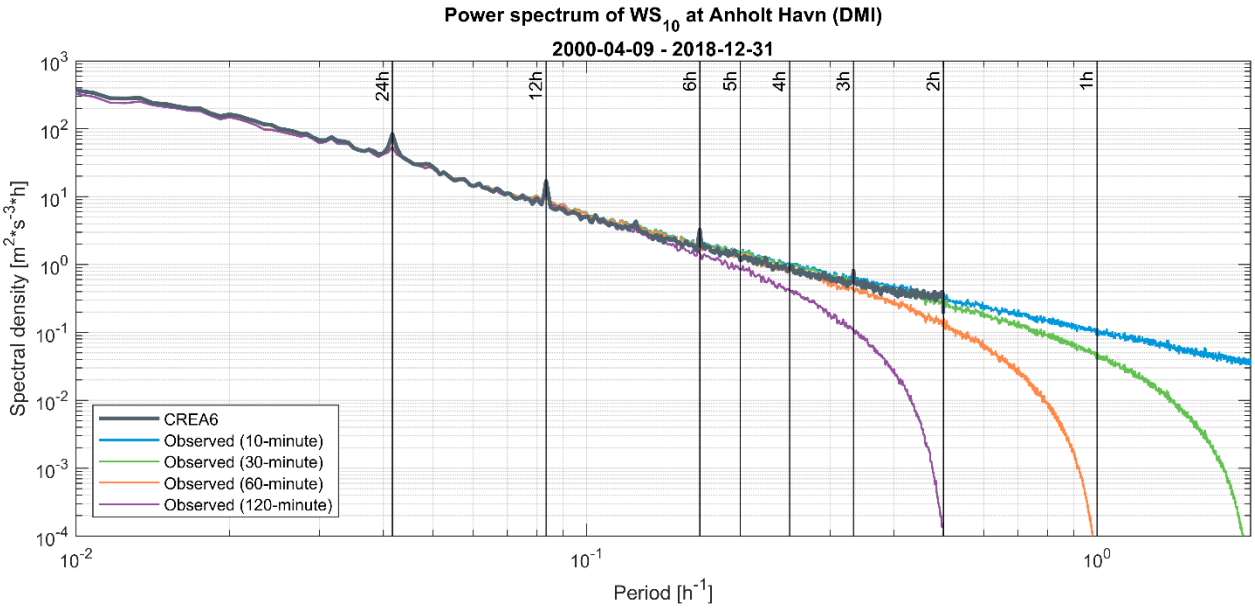

Figure 2.9 Spectral density of CREA6 and observed wind speeds for various averaging windows
The comparison is based on the 10 mMSL (WS_{10}) at the DMI Anholt Havn measurement station

2.3.2 Danish waters hydrodynamic model

DHI's Danish waters hydrodynamic model (**HD_{DKW}**) provides information on water levels and depth-averaged currents established through numerical modelling using the MIKE 21 Flow Model FM [17]. The general settings of HD_{DKW} are summarised in Table 2.6.

The MIKE 21 Flow Model is based on the numerical solution of the two-dimensional (2D) incompressible Reynolds-averaged Navier-Stokes (RANS) equations, subject to the assumptions of Boussinesq and hydrostatic pressure. The model is applicable for the simulation of hydraulic and environmental phenomena in lakes, estuaries, bays, coastal areas, and seas where stratification is negligible. The model can be used to simulate a wide range of hydraulic and related items, including tidal exchange, currents, and storm surges.

The HD_{DKW} model domain includes all Danish nearshore waters, plus areas offshore of Norway, Sweden, Poland, Germany, and the Netherlands (Figure 2.10). The model domain covers a total area of approximately 220,0000 km^2 and has three open ('sea') boundaries: 1) an eastern boundary in the Baltic Sea between Poland and Sweden, 2) a western boundary in the North Sea between Norway and the Frisian Islands (Netherlands), and 3) a short boundary from the Frisian Islands to the mainland of the Netherlands.

HD_{DKW} is based on an unstructured flexible mesh with refined resolution in shallow areas. The resolution of the model is 3 to 4 km in offshore areas, decreasing to around 2 km in Danish nearshore waters. Near to the Danish coastline, the resolution varies from 1 km to around 500 m. At the Hesselø offshore wind farm site, the resolution of the HD_{DKW} mesh is around 2 km (see left-hand panel of Figure 2.11.). Bathymetry data in the Kattegat was provided from the EMODnet DTM (see Section 2.1.2 of this report, as well as Section 2.1 of [12]).

The Danish waters hydrodynamic model is forced across its open (sea) boundaries by spatially and temporally varying water levels and depth-averaged currents extracted from DHI's regional North Europe Hydrodynamic model (HD_{NE}). These open boundaries include the effects of both tide and surge (see Section 3.2 of [12] for further details). HD_{DKW} also includes locally generated surge driven by the wind and air pressure fields from the CREA6 atmospheric model (see Section 2.3.1).

The HD_{DKW} model also includes tidal potential, i.e., forcing directly generated by the variations in gravity due to the relative motion of the earth, the moon, and the sun. The forcing acts through-out the computational domain, calculated as the sum of 11 harmonic terms, each representing a specific constituent (see Section 4.6 of [17]).

Calibration and validation of HD_{DKW} has been performed based on eight water level stations in the model domain: seven stations in Denmark and one in Norway (see Section 3.5 and 3.6 of [12]). Further validation of modelled water levels for stations in the area around the Hesselø OWF is presented in Section 3.3.1 of this report. An additional assessment of depth-averaged currents is also included in Section 3.3.2.

The outputs from HD_{DKW} include water level relative to mean-sea-level (WL), depth-averaged current speed (CS), and depth-averaged current direction (CD), which are saved for each model mesh element at an output time interval of 0.5-hours.

The hydrodynamic setting of the Kattegat

The Hesselø OWF is located within the Kattegat, the major hydrographic transition zone between the brackish waters of the Baltic Sea (to the South) and the saline waters of the North Sea (to the North, via the Skagerrak). The waters of the Kattegat are generally described as two-layered consisting of:

- The northwards flow of the low salinity Baltic Current at the surface, with seasonally varying salinity and temperature
- An underlying counter-current of oceanic waters from North Sea

The density gradients between the different water masses plays an important role in setting the circulation in the Kattegat. Strong wind-generated flows also modify the conditions over relatively short time periods. These 3-dimensional phenomena will not be replicated by a 2-dimensional hydrodynamic model such as HD_{DKW}, which is suited to describing barotropic flows where stratification is negligible.

If the currents and a possible stratification are critical for structural design, an analysis based on a three-dimensional hydrodynamic model should be considered. Such an analysis is not part of the scope of work for this site metocean conditions assessment

Table 2.6 General settings of DHI's Danish Waters hydrodynamic model (HD_{DKW})

Setting	HD_{DKW}
Simulation period	1995-01-01 to 2018-12-31 (24 years)
Basic equations	2D incompressible Reynolds averaged Navier-Stokes (RANS) equations
Horizontal mesh	Variable resolution unstructured grid, 3 – 4 km in offshore areas, 2 km in Danish waters (including area around the Hesselø OWF development area), and 1 km to 500 m at Danish Coastline (see Figure 2.10 and Figure 2.11)
Density	Barotropic
Model time step (adaptive)	0.01 to 300 seconds
Model output time interval	0.5 hours
Atmospheric forcing	Wind and air pressure from the CREA6 atmospheric model (see Section 2.3.1)
Tidal potential	11 constitutes (see Section 4.6 of [17])
Boundary conditions	Spatially and temporally varying water levels (tide + surge) extracted from DHI's North Europe hydrodynamic model (HD_{NE})
Output parameters	• Water level relative to mean sea level (WL) • Depth-averaged current speed (CS) • Depth-averaged current direction (CD)

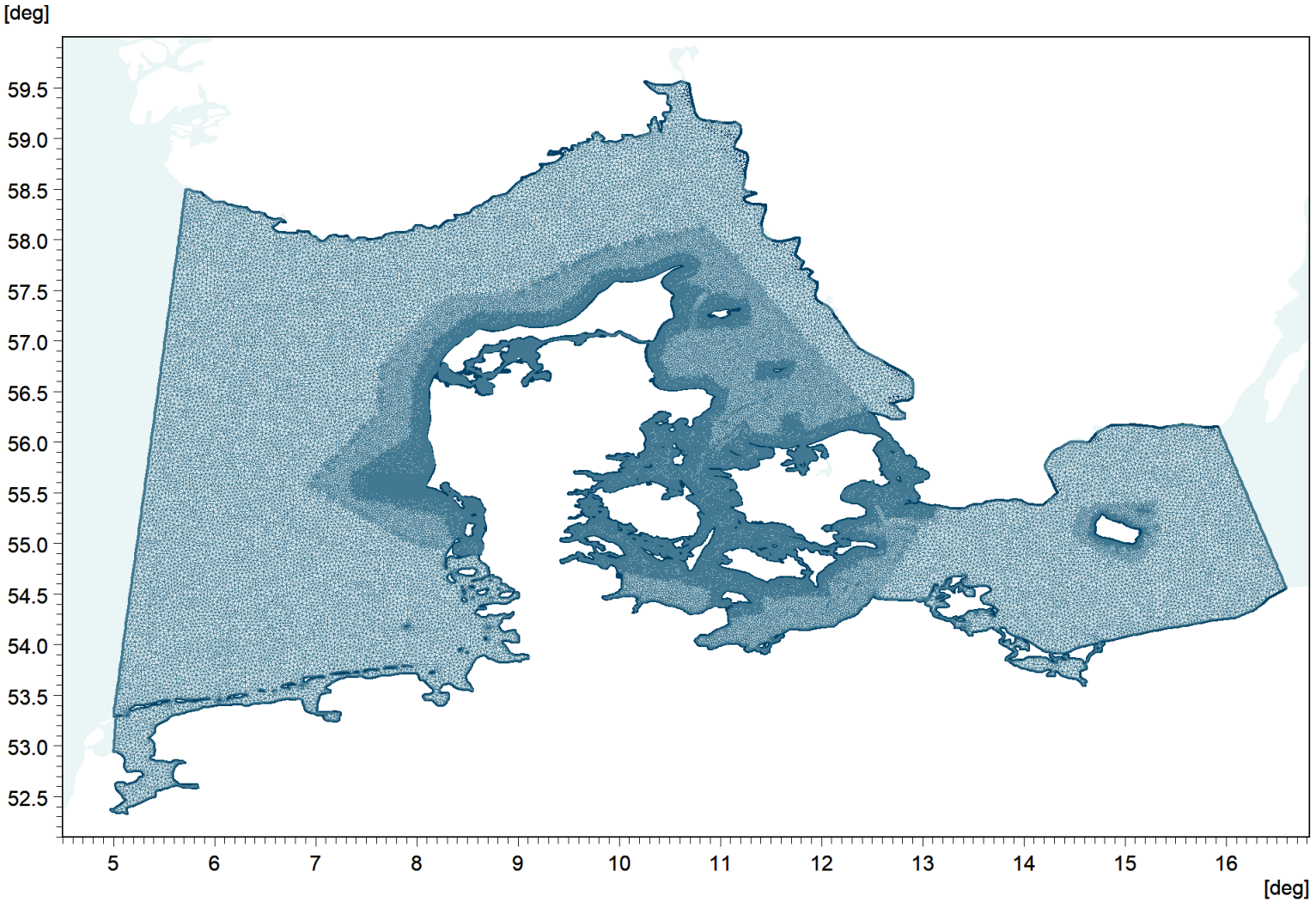

Figure 2.10 Domain and mesh of the DHI Danish waters hydrodynamic model

The hydrodynamic model mesh based on unstructured flexible elements, with refined resolution around the coastline of Denmark

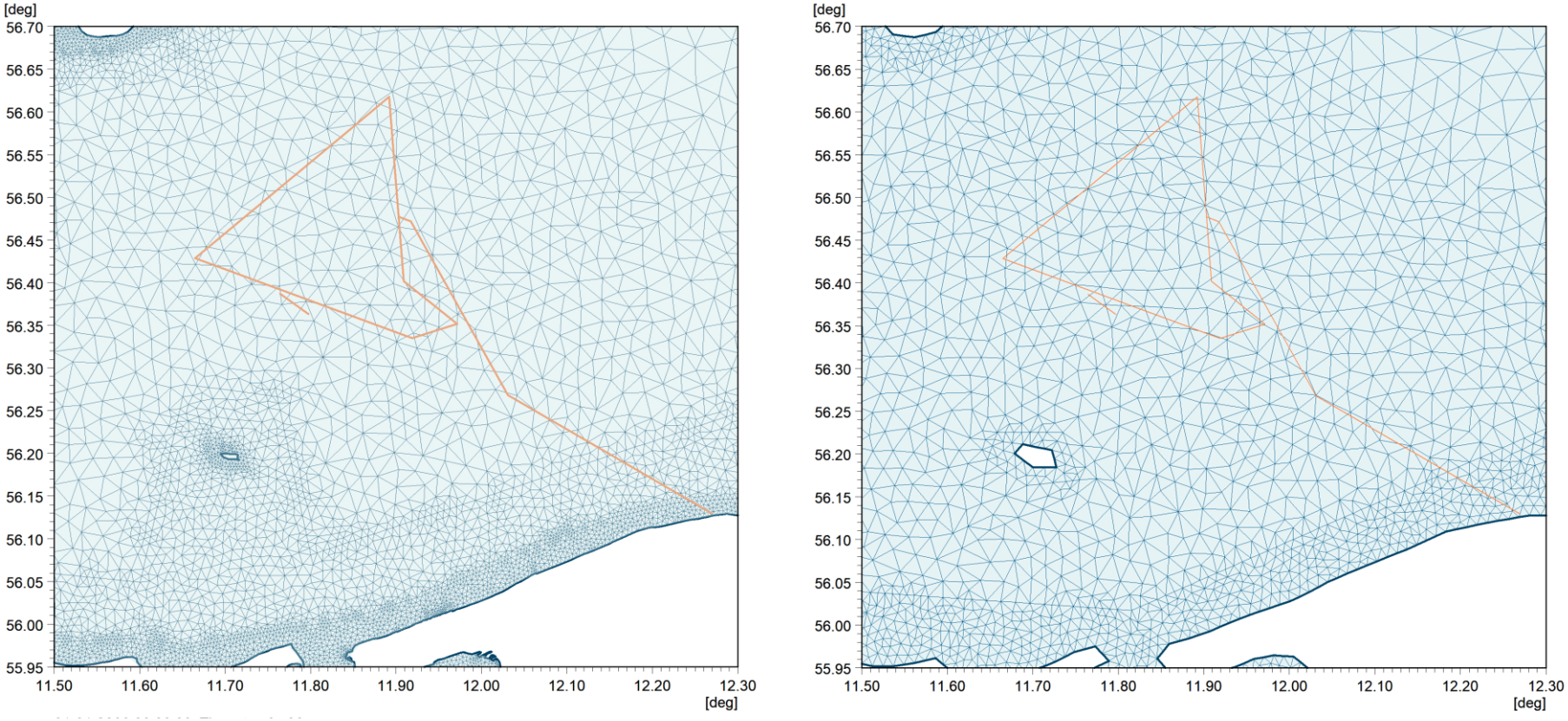

Figure 2.11 Numerical mesh of the Danish Waters metocean hindcast model around the Hesselø OWF

The unstructured flexible mesh is shown by the blue triangles for the hydrodynamic model HD_{DKW} (left panel) and spectral wave model SW_{DKW} (right panel). The Hesselø OWF development area and export cable corridor is designated by the orange outline

2.3.3 Danish waters spectral wave model

DHI's Danish waters spectral wave model (**SW_{DKW}**) provides information on surface wave parameters and wave energy spectra. The model database was established through state-of-the-art numerical wave modelling software, MIKE 21 SW by DHI [18, 19]. MIKE 21 SW is a third-generation spectral wind-wave model based on unstructured meshes. The model simulates the growth, decay, and transformation of wind-waves and swell waves in offshore and coastal areas. The general settings of SW_{DKW} are summarised in Table 2.7.

The wave model domain was the same as the Danish Waters hydrodynamic model described in Section 2.3.2 (see Figure 2.6 and Figure 2.10). As for the hydrodynamic model, the spatial discretisation of waves was based on an unstructured flexible mesh with resolution of around 2 km at the Hesselø OWF (see right-hand panel of Figure 2.11). However, it should be noted that the numerical mesh of SW_{DKW} was not identical to HD_{DKW}, as the latter contained additional refinement in shallow areas and within deep-water channels that were not considered relevant for the former.

As for Danish Waters hydrodynamic model, the EMODnet DTM was used as input bathymetry data source for the spectral wave model (see Section 2.1.2 of this report, as well as Section 2.1 of [12]).

The spectral resolution includes 32 directions (11.25° bins), and 30 frequencies, geometrically distributed between 0.033 Hz to 1.005 Hz (i.e., wave periods ~1 to 30.3 seconds).

SW_{DKW} was set up with the fully spectral, in-stationary formulation, suitable for wave studies involving time-dependent wave events, and rapidly varying wind conditions (in space and time). The model is forced by 10 mMSL wind fields from the CREA6 atmospheric model (see Section 2.3.1). Wave conditions across the model open boundaries were provided by spatially and temporally varying wave energy spectral data from DHI's regional North Europe Hydrodynamic model (SW_{NE}). This regional wave model was also forced by CREA6 wind fields, thus ensuring consistency in the model boundary forcing (for more information on SW_{NE} please see Section 4.2 of [12]).

SW_{DKW} also includes the effects of varying water levels and current speeds that are provided from the outputs of the Danish Waters hydrodynamic model, HD_{DKW} (see Section 2.3.2).

During the model build, detailed sensitivity and calibration studies of wind input, bottom friction, and white capping were performed based on the largest storms at measurement stations throughout the model domain (see Section 4.5 of [12]). The model was then validated based on a 1-year simulation to confirm the suitability of the final model setup. Further validation of SW_{DKW} at measurement stations in the area around the Hesselø OWF is presented in Section 3.4 of this report.

The spectral wave model data represents an area and duration determined by a combination of the resolution (temporal and spatial), the resolution of the applied forcing (i.e., the wind field), and the model mesh, whereas observed wave conditions commonly measure sea-state over a period of 0.5 - 1 hour at a single point. One may expect that observations will exhibit more variability compared to the model data. Therefore, the model data may be regarded as "smoothed" (in space and time) compared to observed wave conditions.

Previous analysis presented in Section 4.4 of [12] has concluded that modelled sea-states have an implicit averaging time of T_a=3 hours.

Outputs from the SW_{DKW} include integral wave parameters at 1-hour intervals in each model mesh element. The integral wave parameters are provided for the total spectrum, and for wind sea and swell components. Swell conditions are defined as the wave components fulfilling the following wave-age criterion:

$$\frac{WS_{10}}{c}\cos(\theta - WD_{10}) < 0.83 \qquad 2.1$$

where WS_{10} is the wind speed at 10m above MSL, c is the phase speed, and θ and WD_{10} are, respectively, the wave direction and wind direction.

Table 2.7 General settings of DHI's Danish Waters spectral wave model (SW_{DKW})

Setting	SW_{DKW}
Simulation period	1995-01-01 to 2018-12-31 (24 years)
Basic equations	Full spectral, in-stationary formulation
Solution technique	Lower order geographical space discretisation
Horizontal mesh	Variable resolution unstructured grid, 3 – 4 km in offshore areas, 2 km in Danish waters (including area around the Hesselø OWF development area), and 1 km to 500 m at Danish Coastline (see Figure 2.10 and Figure 2.11)
Model output time interval	1-hour
Spectral resolution	30 frequencies (0.033 Hz to 1.005 Hz), 32 directions (11.25° intervals)
Wind forcing	Wind from the CREA6 atmospheric model (see Section 2.3.1)
Water level and current conditions	From the Danish Waters hydrodynamic model, HD_{DKW} (see Section 2.3.2)
Open boundary conditions	Wave action spectra varying in time and along boundaries from DHI's North Europe metocean hindcast model forced by CREA6 winds (SW_{NE})
Output parameters	Integral wave parameters in each model mesh element (total, wind-sea, and swell) Direction-frequency wave energy spectra at selected locations on a 0.1° grid across Danish waters

2.4 Baltic Sea physical reanalysis model

Long-term information on the properties on seawater (temperature and salinity) were obtained from the Baltic Sea physical reanalysis product[7] produced by the Copernicus Marine Environment Monitoring Service's (CMEMS) Baltic Monitoring and Forecasting Centre (BAL MFC) [20]. The model provides information on the daily mean water temperature and salinity from January 1993 to December 2018. The model data are discretised on a horizontal grid of resolution 0.05556° latitude x 0.03333° (approx. 3.5 km x 3.5 km, Figure 2.12) and up to 56 vertical layers.

Quality information on the Baltic Sea physical reanalysis model, including validation of temperature and salinity predictions, can be found in [21].

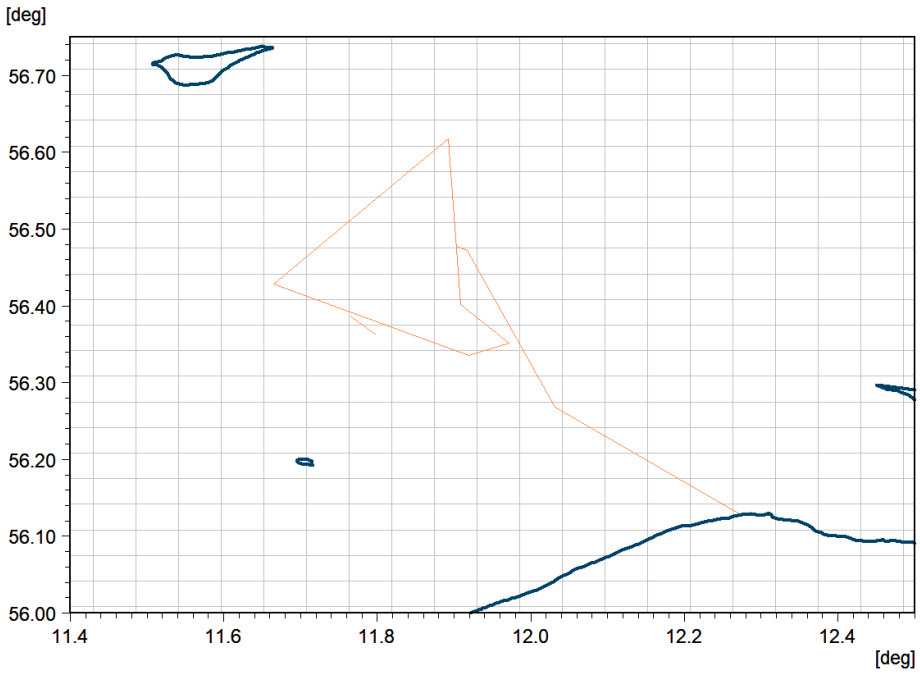

Figure 2.12 Spatial resolution of the Baltic Sea physical reanalysis model
The Hesselø OWF development area and export cable corridor is designated by the orange outline

[7] BALTICSEA_REANALYSIS_PHY_003_011 – accessed March 2022

3 Validation of the Model Database

This section presents the results of the validation exercise to establish the quality and validity of DHI's Danish Waters hindcast models. This includes comparison of the model bathymetry and statistical comparison of the atmospheric, hydrodynamic, and spectral wave models against measured data in and around the Hesselø OWF.

The validation results in this section are presented as time series, histogram, and scatter plots. Throughout this section, reference is made to model quality indices (QI's) that are used to assess performance. Please see Appendix A for a more detailed description of the model quality indices.

3.1 Atmospheric model CREA6

Validation of CREA6 wind model was performed at the wind measurement stations detailed in Section 2.2.1.

For the DMI stations and the Læsø Syd measurements station, observations were available as 10-minute average values with an output interval of 10-minutes[8]. These data were temporally averaged ('smoothed') to 30-minutes to match the representative temporal averaging period of the CREA6 model (see Section 2.3.1). The average was calculated on the u (west-to-east) and v (north-to-south) components of the wind velocity, which were subsequently converted to wind speed and wind direction. For the SMHI measurement stations 10-minute average observations were available at an output reporting interval of 1-hour; hence, no additional smoothing was possible, and the 10-minute average measured winds were directly compared to the 30-minute averaged model winds.

The wind model validation was performed at the measurement station height. For measurement heights that were not at model output levels, the CREA6 wind speeds were sheared up/down from the closest available model level. The CREA6 wind direction was adopted from the model level closest to the measurement height.

3.1.1 Validation at Anholt Havn

Figure 3.9 shows validation of 10m wind speeds at Anholt Havn, the closest measurement station to the Hesselø OWF. The CREA6 model provided a good replication of the measured wind speeds, with a small positive bias of +0.04 m/s. However, there was a noticeably large scatter (SI = 0.23), particularly for measured wind speeds < 12 m/s. The histogram comparison shows that CREA6 slightly underestimates the frequency of wind speeds in the range 2 m/s to 8 m/s, and slightly overestimates the frequency of measured wind speeds above 8 m/s.

Anholt Havn is located on the north-west of Anholt Island, where the DMI station is positioned on the northern edge of the harbour (Figure 3.2). While the station is exposed to winds coming off the sea (i.e., winds from south to north-east directions), winds from the east and south-east directions will be influenced by the presence of land. For example, the aerial image in the lower

[8] after Sept. 1999 at Anholt Havn and Nakkehoved Fyr, and after Aug 2001 at Gniben, see Table 2.1

panel of Figure 3.2 reveals several buildings within 100 m of the measurement station. At these length scales, the buildings will impart a local roughness that is not resolved by the model. Furthermore, the horizontal spatial resolution of CREA6 means that Anholt is only approximated as a partial land cell (Figure 2.8).

Figure 3.3 shows validation of 10 m wind speeds at Anholt Havn for 'open sea' directions only (i.e., the wind speeds associated with 30° directional sectors centred at 60°N to 150°N have been removed). Compared to the validation based on all wind directions, the results reveal a larger mean wind speed, a small negative bias (-0.36 m/s), lower AME and RMSE, a reduction in the scatter index (SI = 0.16), and a Q-Q fit line that is closer to the 1:1 line. The peak ratio (PR = 1.0) indicates that the wind speed events are very well captured by the CREA6 model (based on an average of 2 peak events per year).

Figure 3.4 shows validation of 10 m wind direction at Anholt Havn. The results are conditioned on wind speeds above 4 m/s. The results show very good agreement in the distribution of wind direction between the measurements and CREA6.

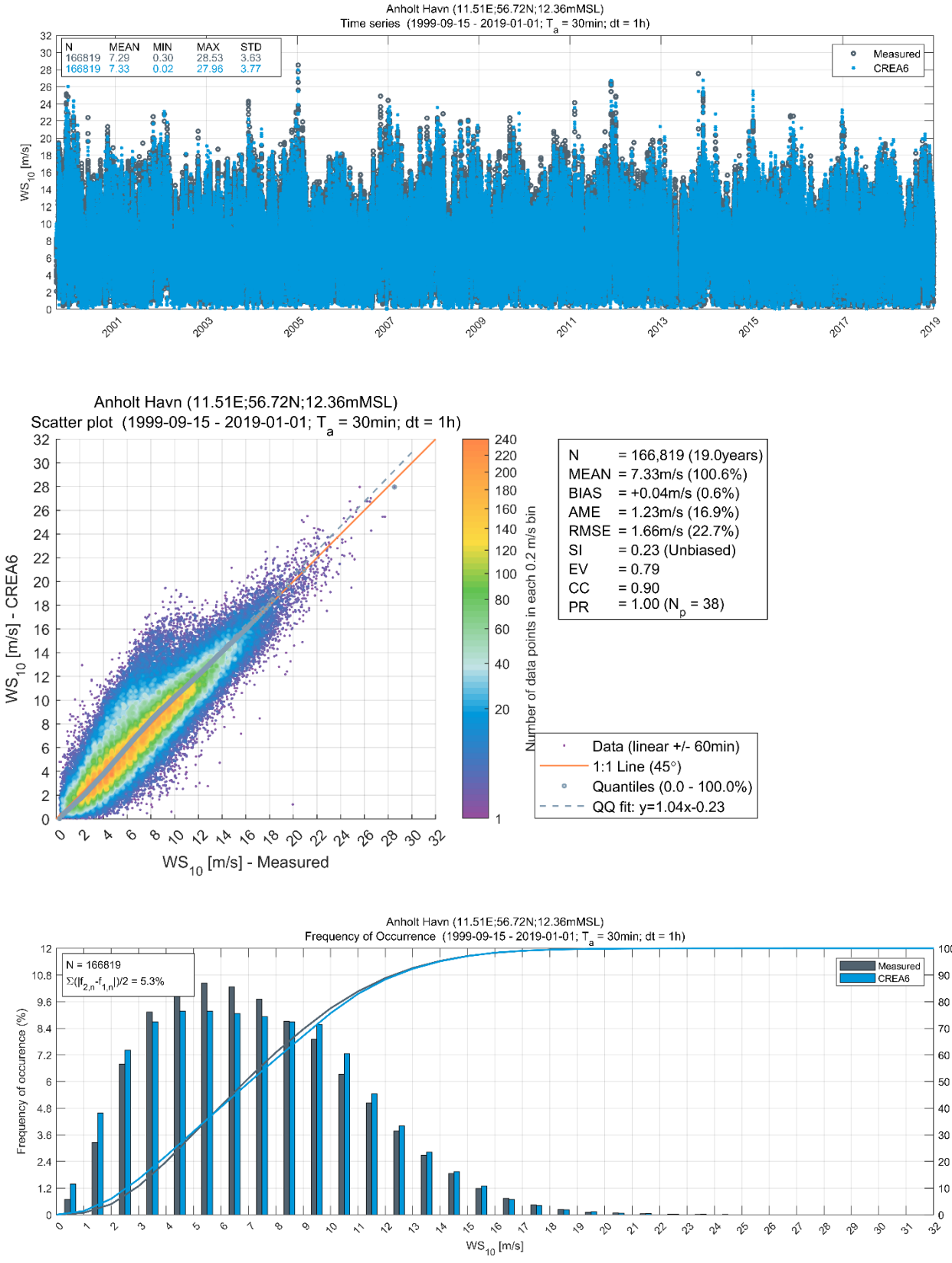

Figure 3.1 Validation of CREA6 wind speeds at Anholt Havn

Time series (upper panel), scatter plot (central panel), and histogram (lower panel) comparison of modelled and measured 10 m wind speed (omnidirectional)

Figure 3.2 The position of the DMI Anholt Havn measurement station
The measurement station is located on the Northwest of Anholt island (upper panel), at the northern end of Anholt Havn (lower panel).

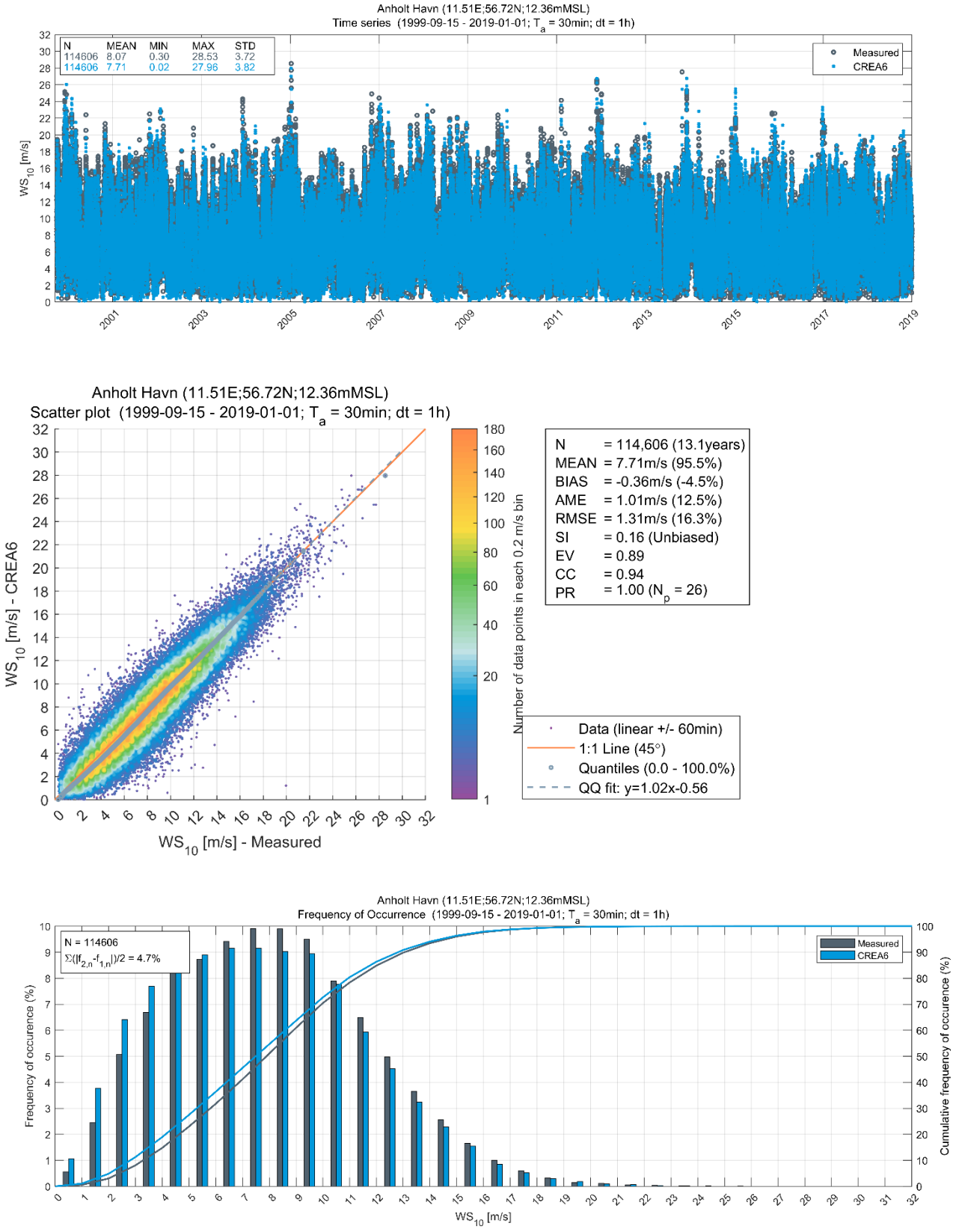

Figure 3.3 Validation of CREA6 wind speeds at Anholt Havn for 'open sea' directions only
Time series (upper panel), scatter plot (central panel), and histogram (lower panel) comparison of modelled and measured wind speed at 10 m. Wind speeds from directional sectors 60°N to 150°N are omitted from the comparison

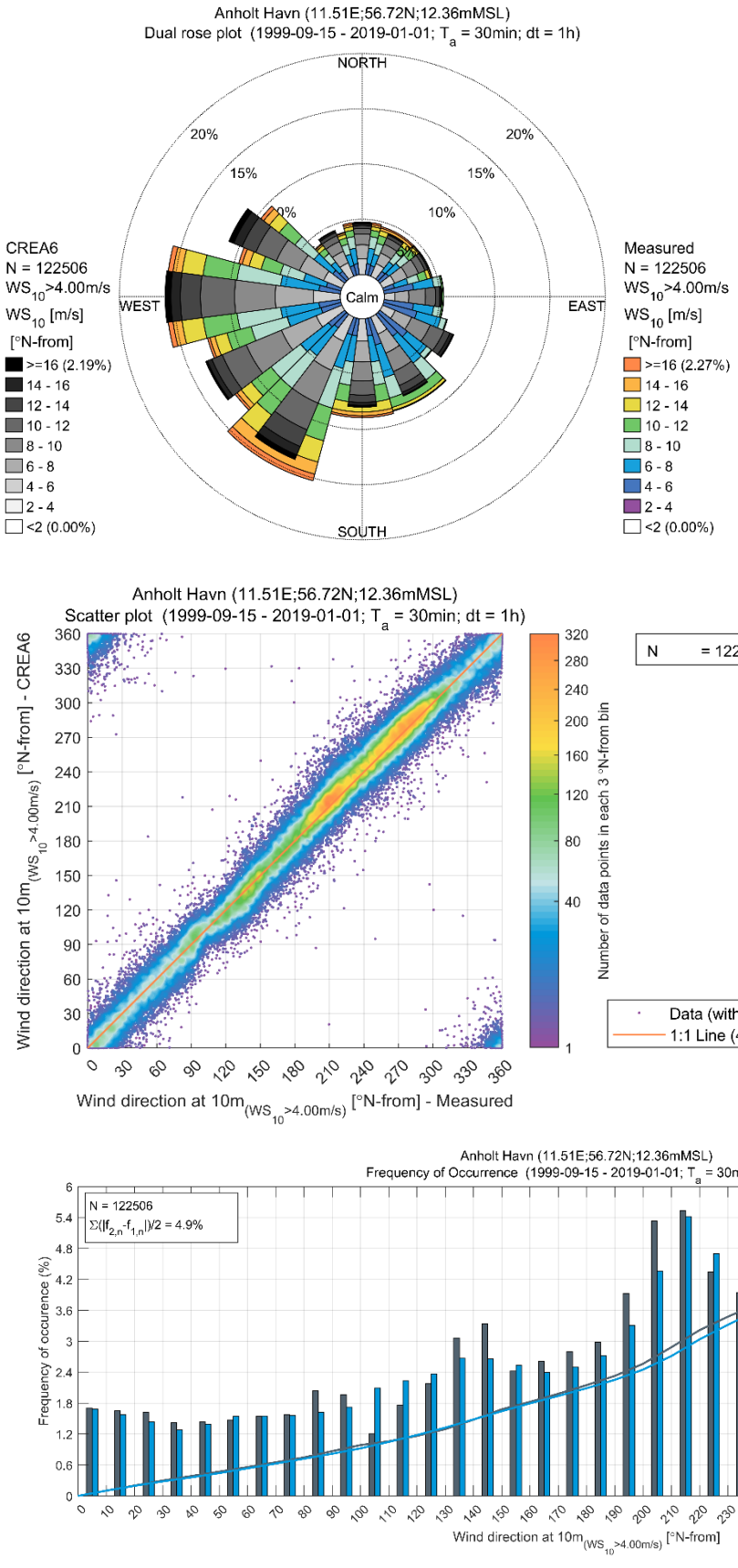

Figure 3.4 Validation of CREA6 wind direction at Anholt Havn

Rose plot (upper panel), scatter plot (central panel), and histogram (lower panel) comparison of modelled and measured wind direction at 10 mMSL. The results are conditions on WS_{10} > 4 m/s

3.1.2 Validation at other stations

Figure 3.7 shows scatter plot comparisons of wind speed for wind measurement stations at Læsø Ost A, Hallands Väderö, Nakkehoved Fyr, and Gniben. The results at Hallands Väderö and Gniben show that CREA6 provides a very good comparison to the measurements for both normal conditions (small bias) and extreme conditions (PR ~ 1).

At Læsø Ost A, the CREA6 model tends to overestimate the largest measurement wind speeds (> 10 m/s). This may be related to the movement of the moored buoy on which the measurement data were collected during high sea-state conditions.

The validation of CREA6 at Nakkehoved Fyr is very poor with respect to all model quality indices compared with the other wind measurement. The station height is reported as 37 m above mean sea level (Table 2.1), and examining the location of this station more closely, reveals that it is located atop of a steep cliff (Figure 3.6), a topographical feature that will not be resolved in a regional scale wind model like CREA6.

Figure 3.7 shows scatter plot comparisons of wind speed for wind measurement stations at Læsø Syd at 15 mMSL, 45 mMSL, and 62 mMSL. The CREA6 model provides a good replication of the measured wind speeds at all heights with low bias. The model overestimates the magnitude of the largest wind events by up to 8% at 62 mMSL (PR > 1.08).

Time series, histogram, and rose plots comparison of wind speed and wind direction at all wind stations are included within Appendix B.

3.1.3 Summary of wind validation

Table 3.1 summarises the wind speed validation statistics for all measurement stations. In general, the performance of the CREA6 wind model is very good in the area around the Hesselø OWF; hence, CREA6 provides a suitable long-term dataset for performing an analysis of normal and extreme wind conditions at the project site.

Table 3.1 Summary of model quality indices for wind speed

Station	Height [m]	Mean [m/s]	Bias [m/s]	AME [m/s]	RMSE [m/s]	SI	EV	CC	PR
Anholt Havn	10	7.71	-0.36	1.01	1.31	0.16	0.89	0.94	1.00
Gniben	10	7.17	0.11	1.11	1.47	0.21	0.84	0.92	0.96
Nakkehoved Fyr	10	5.33	0.96	1.72	2.23	0.46	0.43	0.78	0.88
Hallands Väderö	10	6.40	0.23	1.11	1.45	0.23	0.81	0.91	1.02
Laesø Ost A	4	6.82	0.25	1.11	1.48	0.22	0.81	0.92	1.09
Laesø Syd	62	9.31	-0.01	1.34	1.78	0.19	0.83	0.92	1.08
	45	8.85	-0.10	1.29	1.70	0.19	0.83	0.92	1.03
	15	7.61	-0.04	1.18	1.58	0.21	0.80	0.91	1.01

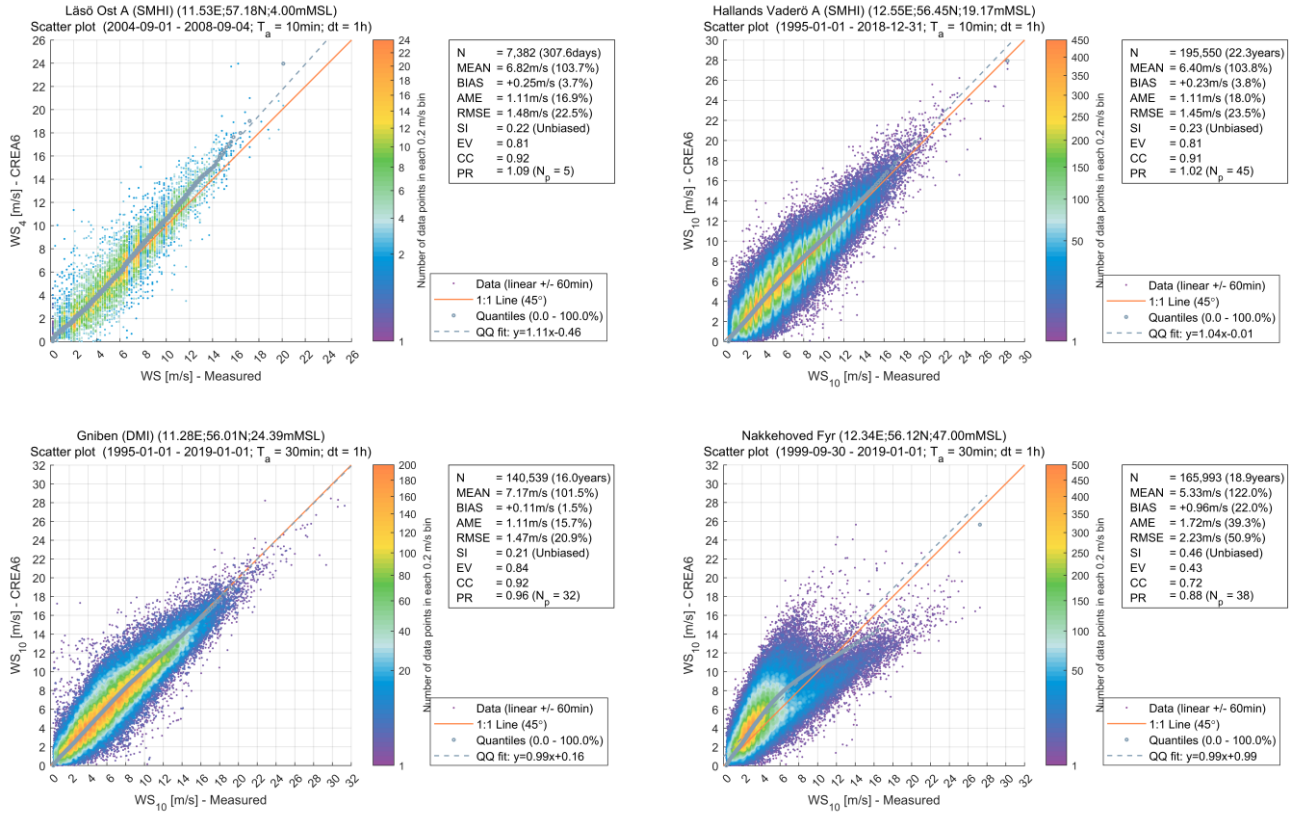

Figure 3.5 Scatter plot comparisons of CREA6 wind speed at wind measurement stations
Scatter plot comparison of measured and modelled wind speeds, clockwise from top left: Laesø Ost A (4 m), Hallands Väderö (10 m), Nakkehoved Fyr (10 m), and Gniben (10 m)

Figure 3.6 The DMI measurement station at Nakkehoved Fyr
Images are reproduced by permission of Museum Nordsjælland

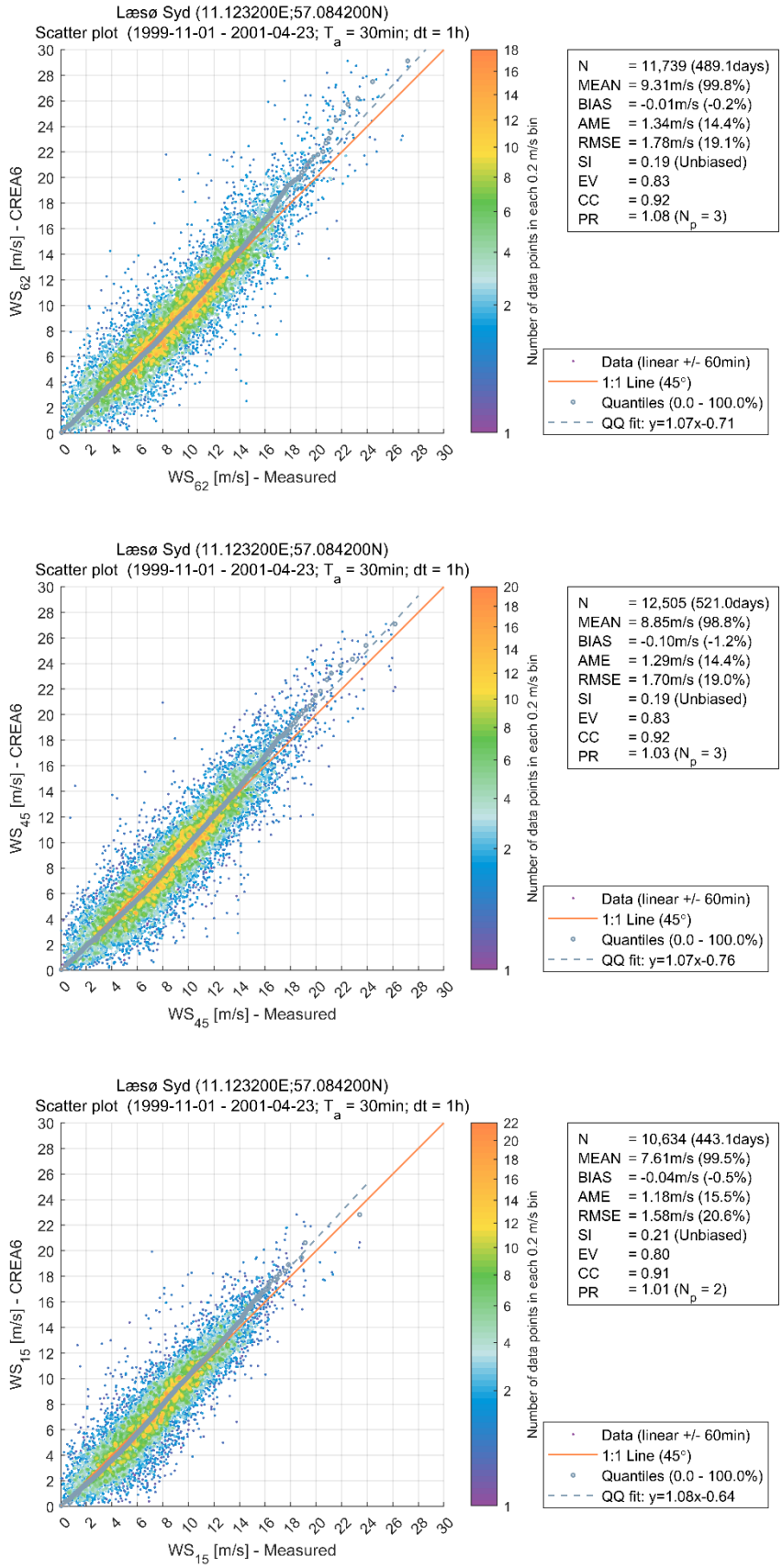

Figure 3.7 Scatter plot comparisons of CREA6 wind speed at Læsø Syd

Scatter plot comparison of measured and modelled wind speed at Læsø Syd: at height of 62 m (upper panel), 45 m (central panel), and 15 m (lower panel)

3.2 Model bathymetry

The local Hesselø bathymetry data (see Section 2.1.1) was interpolated onto the SW_{DKW} numerical mesh. The resulting mesh was then compared with the mesh used in the generation of DHI's Danish Waters hindcast database based on the EMODnet 2018 DTM (see Section 2.1.2). In both cases the underlying bathymetry data were vertically referenced to MSL.

Figure 3.8 shows a map of the difference in the bathymetry for the mesh elements within the Hesselø OWF (i.e., the mesh generated with the local bathymetry minus the mesh generated with the EMODnet DTM). In general, the bathymetry generated with the local measurements was slightly deeper (larger water depths) than the Danish Waters model bathymetry (average absolute difference of -0.22 m). Considering that the water depth across the site ranges from 24.7 m to 33.5 m relative to MSL with gentle seafloor slopes, the noted difference in the bathymetry is considered negligible in terms of the hydrodynamic and wave conditions of the regional model database.

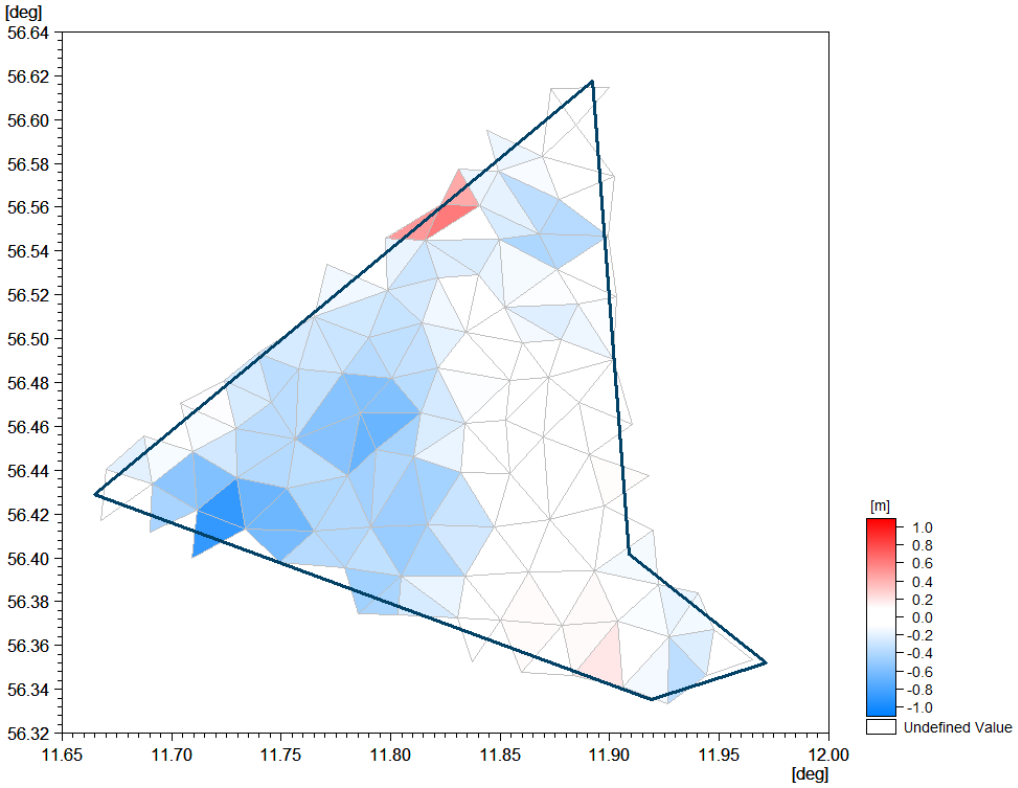

Figure 3.8 Validation of model bathymetry at Hesselø OWF
Map shows the difference in metres of the seafloor elevation (relative to mean-sea-level) within the Hesselø OWF site (black polygon) of the SW_{DKW} mesh interpolated with the local site bathymetry and the EMODnet DTM. Red colours show the model mesh elements where the local site bathymetry is shallower than the EMODnet DTM. Blue shading shows model mesh elements where the local site bathymetry is deeper than the EMODnet DTM

3.3 Hydrodynamic model

3.3.1 Water levels

Validation of HD_{DKW} modelled water levels was performed at the six water level measurement stations as detailed in Section 2.2.2. As the tidal variation is very small in the area, the validation was based on the non-tidal (i.e., residual/surge) component of the water level. Both the modelled and measured water levels were subjected to a harmonic tidal analysis to separate the tidal and non-tidal components. The "de-tiding" was conducted using the U-tide package [22], a method which builds upon the tidal analysis approach defined by the Institute of Oceanographic Sciences (IOS) as described by [23].

Figure 3.9 shows model validation results at Hornbæk Havn, which is the closest measurement station to the Hesselø OWF and its export cable corridor. The HD_{DKW} model provides a very good replication of the measured residual water levels at this station.

Scatter plot comparisons at all six water level measurement stations are shown in Figure 3.10 (for DMI stations) and Figure 3.11 (for SMHI stations). The model QI's are summarised in Table 3.2 (time series and histogram comparison at all stations are also provided within Appendix B). The performance of HD_{DKW} is very consistent between the measurement stations.

Table 3.2 Summary of model quality indices for residual water levels

Measurement station	Mean [m]	Bias [m]	AME [m]	RMSE [m]	SI	EV	CC	PR
Grenaa Havn II (DMI)	0.00	0.00	0.07	0.09	0.57	0.82	0.91	0.86
Havnebyen Sjællands Odde (DMI)	0.00	0.00	0.05	0.07	0.54	0.85	0.92	0.87
Hornbæk Havn (DMI)	0.00	0.00	0.06	0.07	0.48	0.88	0.94	0.94
Viken (SMHI)	0.00	0.00	0.05	0.06	0.46	0.89	0.94	0.94
Halmstad Sjöv (SMHI)	0.00	0.00	0.05	0.07	0.48	0.88	0.94	0.86
Ringhals (SMHI)	0.00	0.00	0.05	0.06	0.45	0.89	0.94	0.93

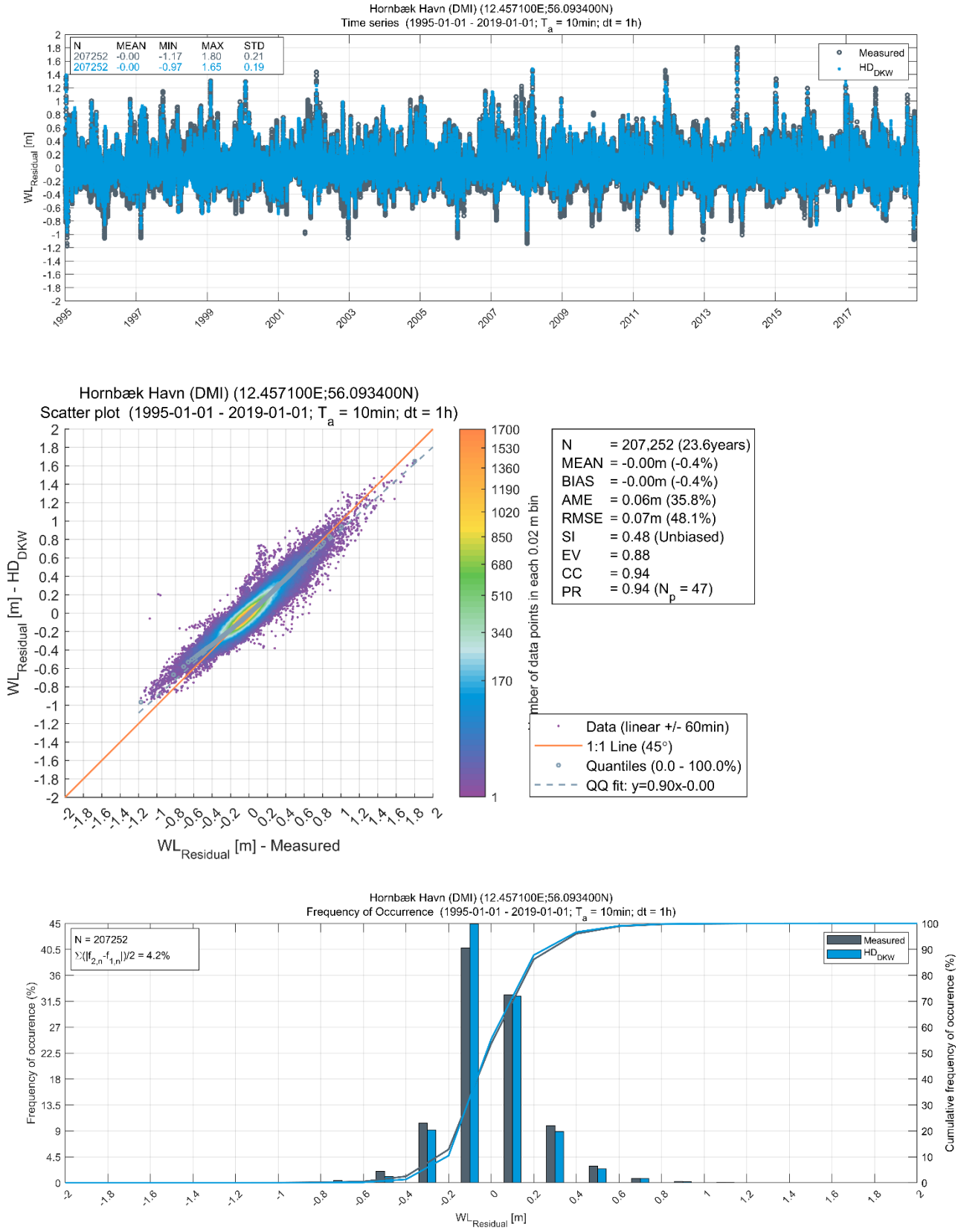

Figure 3.9 Validation of HD_{DKW} residual water level at Hornbæk Havn
Time series (upper panel), scatter plot (central panel), and histogram (lower panel) comparison of modelled and measured residual water level

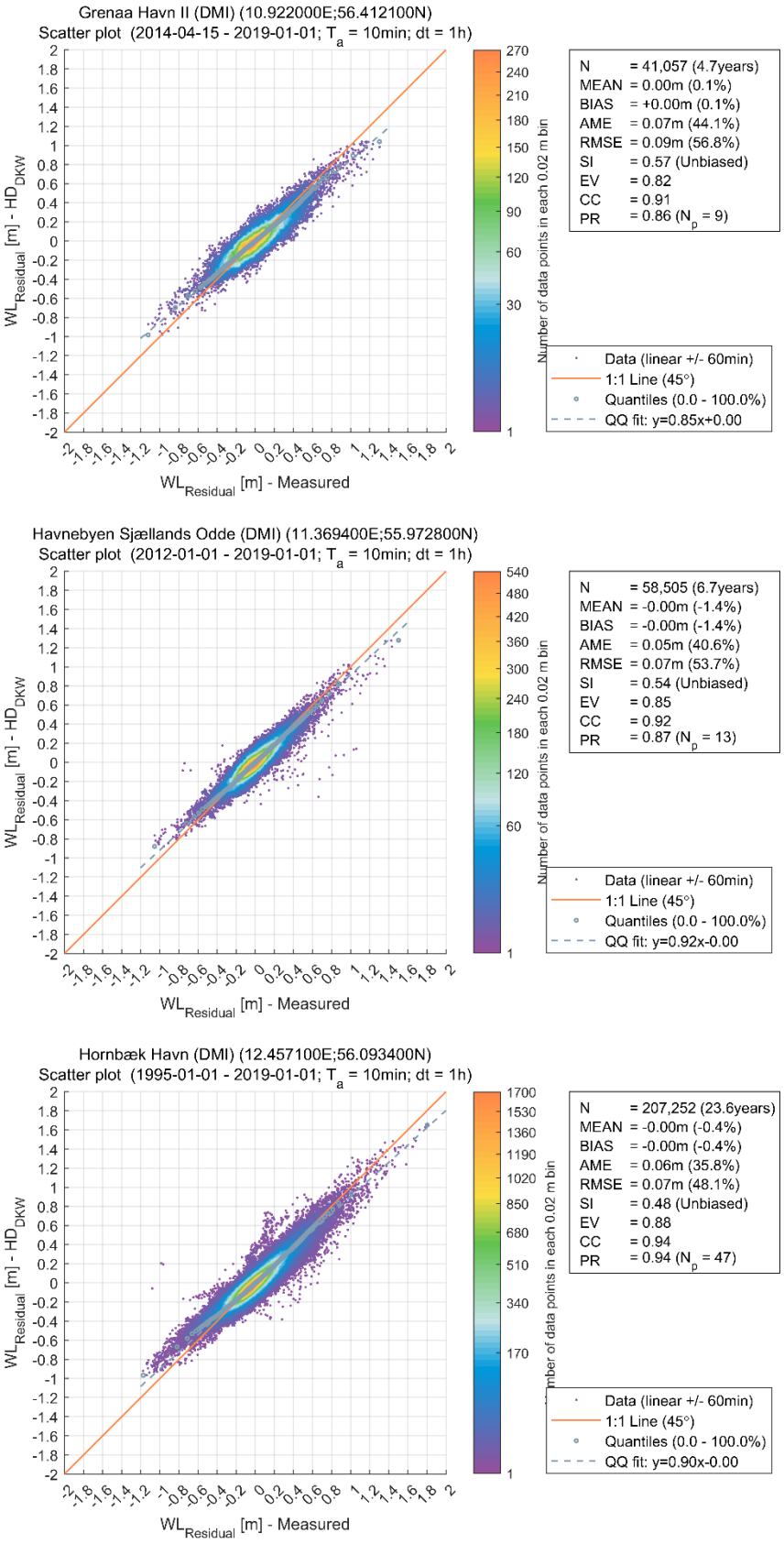

Figure 3.10 Validation of HD_{DKW} residual water level at DMI measurement stations
Scatter plot comparison of measured and modelled residual water levels at Grenaa Havn (upper panel), Havnebyen Sjællands Odde (central panel) and Hornbæk Havn (lower panel)

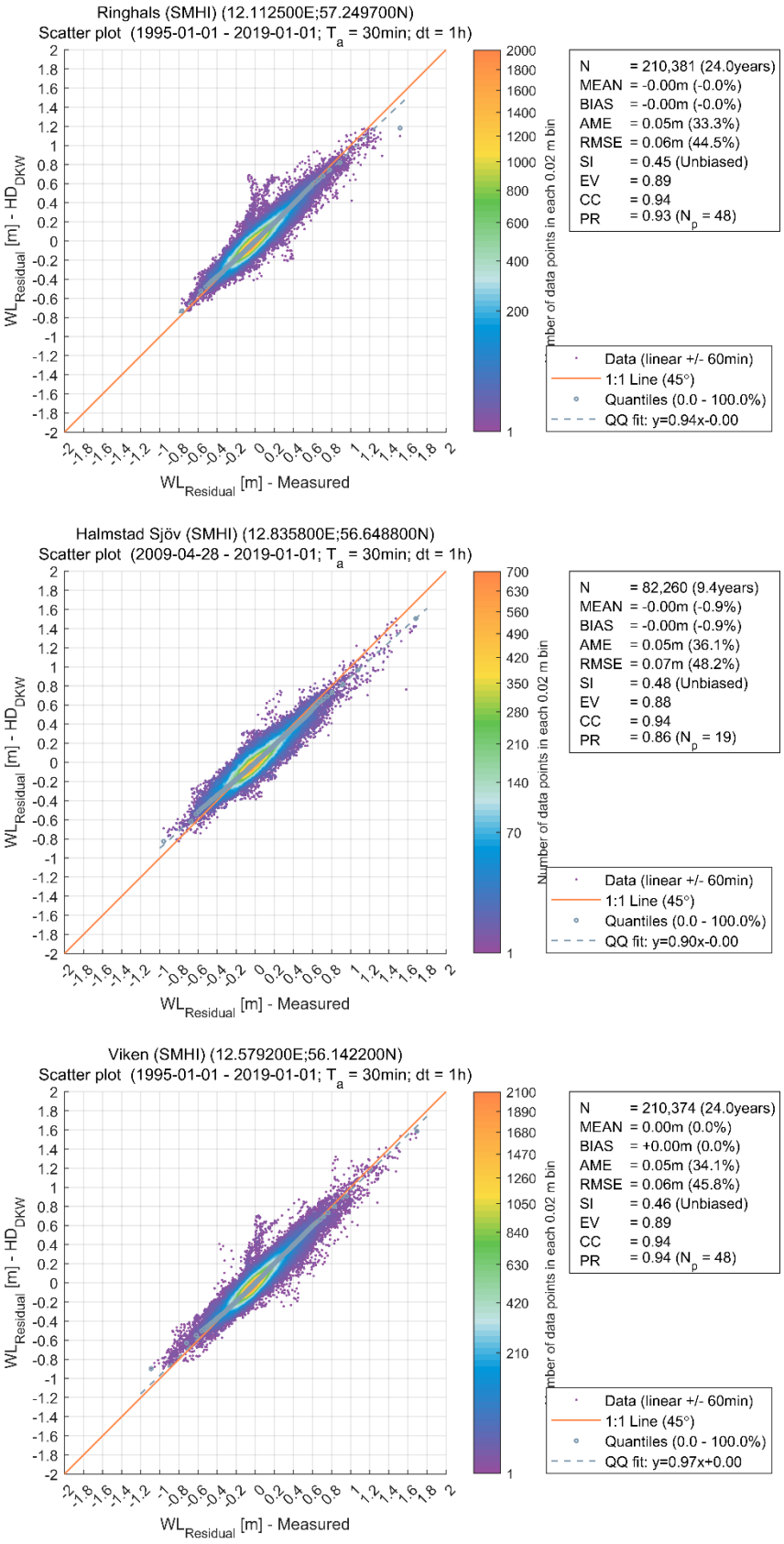

Figure 3.11 Validation of HD_{DKW} residual water level at SMHI measurement stations
Scatter plot comparison of measured and modelled residual water levels at RInghals (upper panel), Halmstad Sjöv (central panel) and Viken (lower panel)

3.3.2 Current conditions

Figure 3.12 shows validation plots of measured and HD_{DKW} modelled depth-averaged current speeds (CS) at Anholt OWF. The model underestimates the depth-averaged current speeds, with the mean value during the observation period being approximately 50% lower than the measured mean value.

As explained previously (see box on page 23), the flow in the Kattegat is governed by three-dimensional flow phenomena[9]. In this context, it is often more informative to compare the distribution of CS as opposed to the time-domain comparisons. The upper panel of Figure 3.13 shows a histogram comparison of measured and HD_{DKW} modelled CS at Anholt OWF. The model overpredicts the frequency of the lower current speed (i.e., CS ≤ 0.15 m/s), and underpredicts the frequency of higher current speeds (i.e., CS > 0.15 m/s).

The lower panel of Figure 3.13 shows a histogram comparison of CS at Anholt OWF with a multiplication factor of 1.5 applied to the HD_{DKW} modelled values. The result is that the cumulative frequency of occurrence of CS more closely matches that of the measurements.

To verify this approach, Figure 3.14 shows a histogram comparison of depth-averaged current speeds at the Hesselø F-LiDAR. In this plot, the measured data are for the period 01 March to 27 September 2021, while the model results are based on the same date interval for the years 1995 to 2018. Mirroring the results at Anholt, the upper panel of Figure 3.14 shows that HD_{DKW} overpredicts the frequency of the lower current speed (i.e., CS ≤ 0.06 m/s), and underpredicts the frequency of higher currents speeds (i.e., CS ≥ 0.08 m/s). However, after applying a multiplication factor of 1.5 to the modelled values, the cumulative frequency of occurrence of CS more closely matches that of the measurements (lower panel of Figure 3.14).

The correction to the depth-averaged current speeds as described above is a rather crude one, and DHI consider that the current predictions from a two-dimensional model are not a suitable basis for the detailed design of structures at the Hesselø OWF. It is a strong recommendation of this report to make use of a validated three-dimensional flow model data and/or long-term measurements of current profiles establish current conditions representative of the wind farm site.

[9] See section 5.3.7 for a detailed analysis of the vertical current profile at the Hesselø F-LiDAR

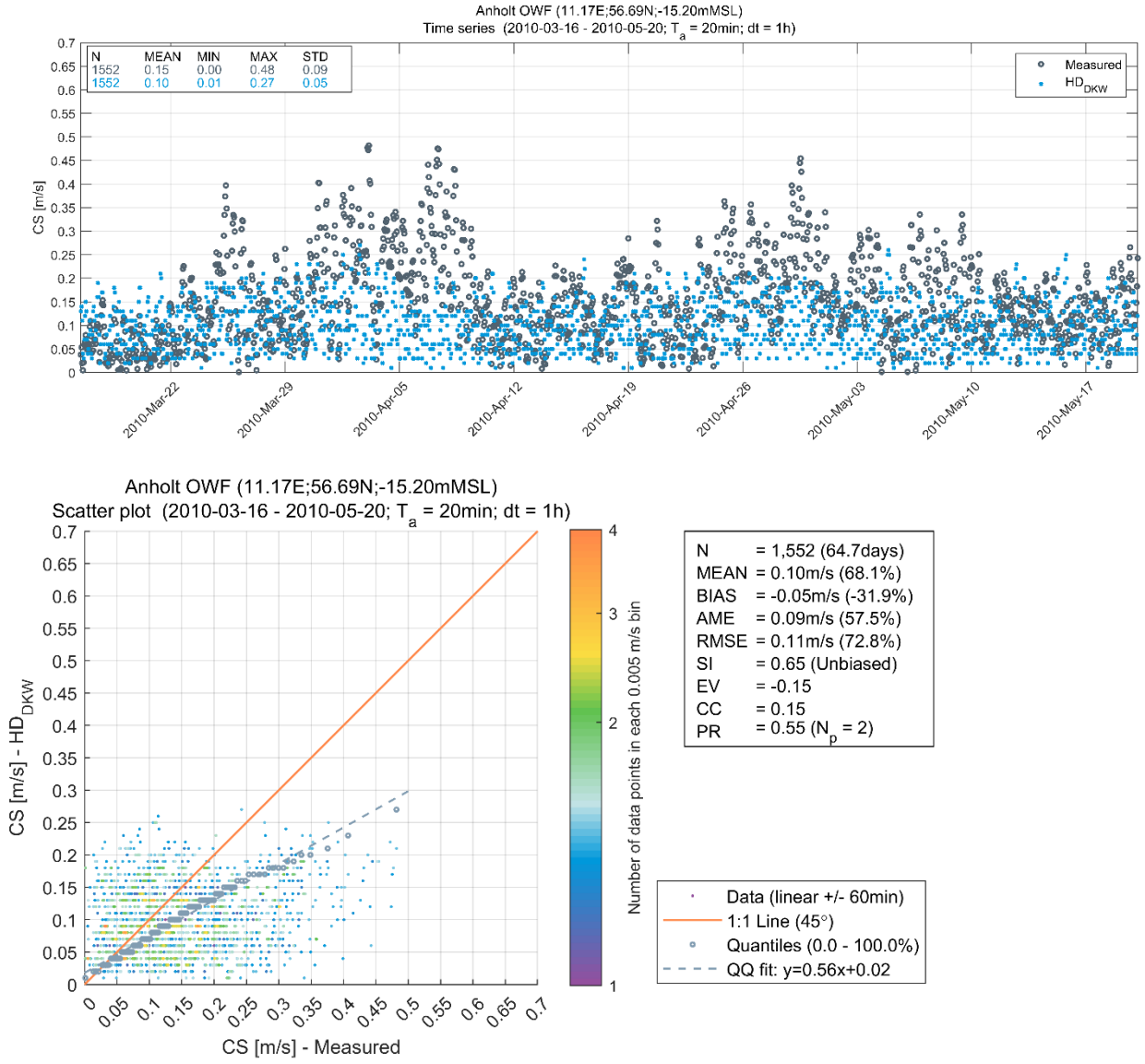

Figure 3.12 Validation of HD_{DKW} total depth-averaged current speed at Anholt
Time series (upper panel), scatter plot (lower panel) comparison

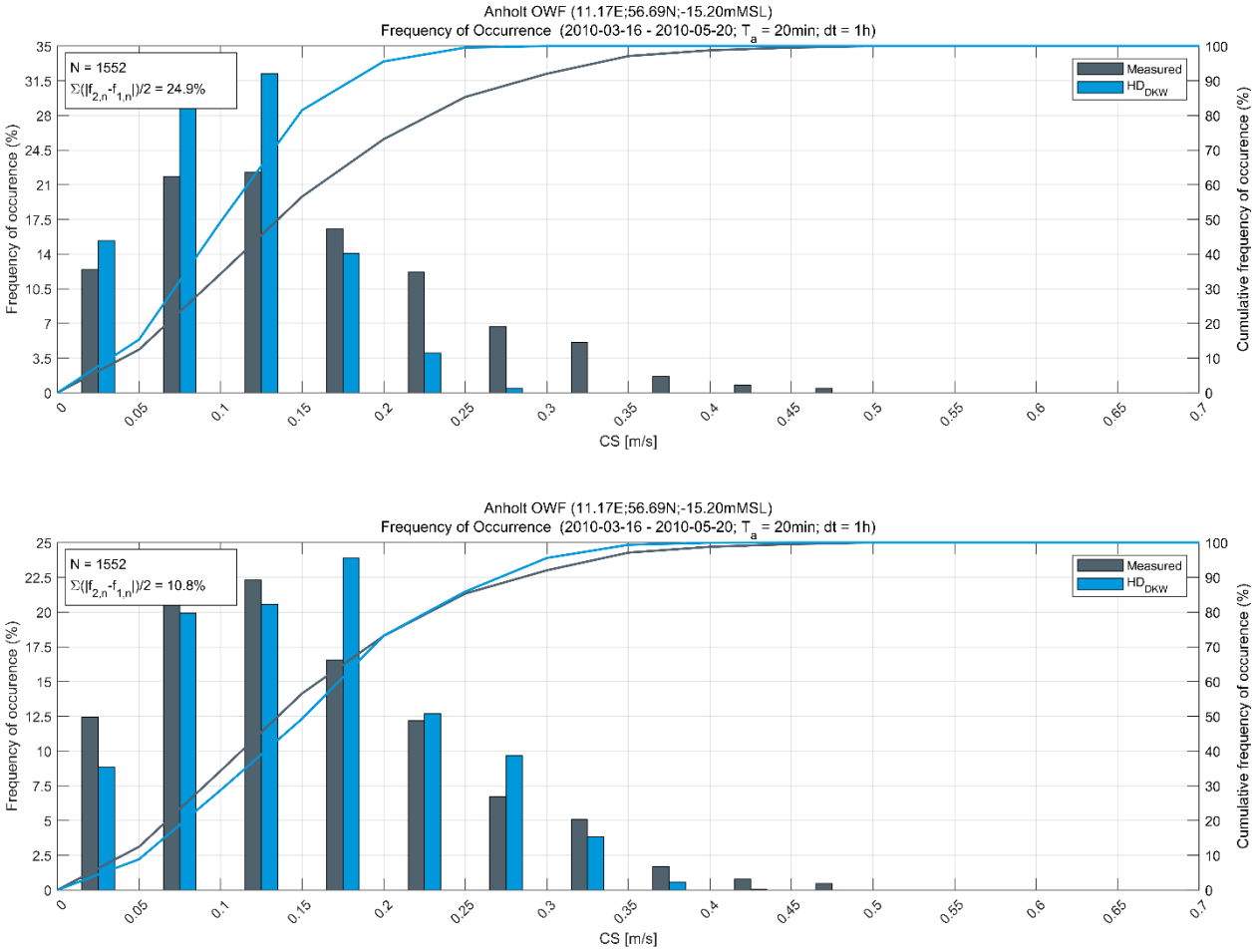

Figure 3.13 Histogram comparison depth-averaged current speed at Anholt OWF
The comparison is based on the HD_{DKW} modelled depth-averaged current speeds (upper panel), and with a multiplication factor of 1.5 applied to the HD_{DKW} modelled depth-averaged current speeds plot (lower panel)

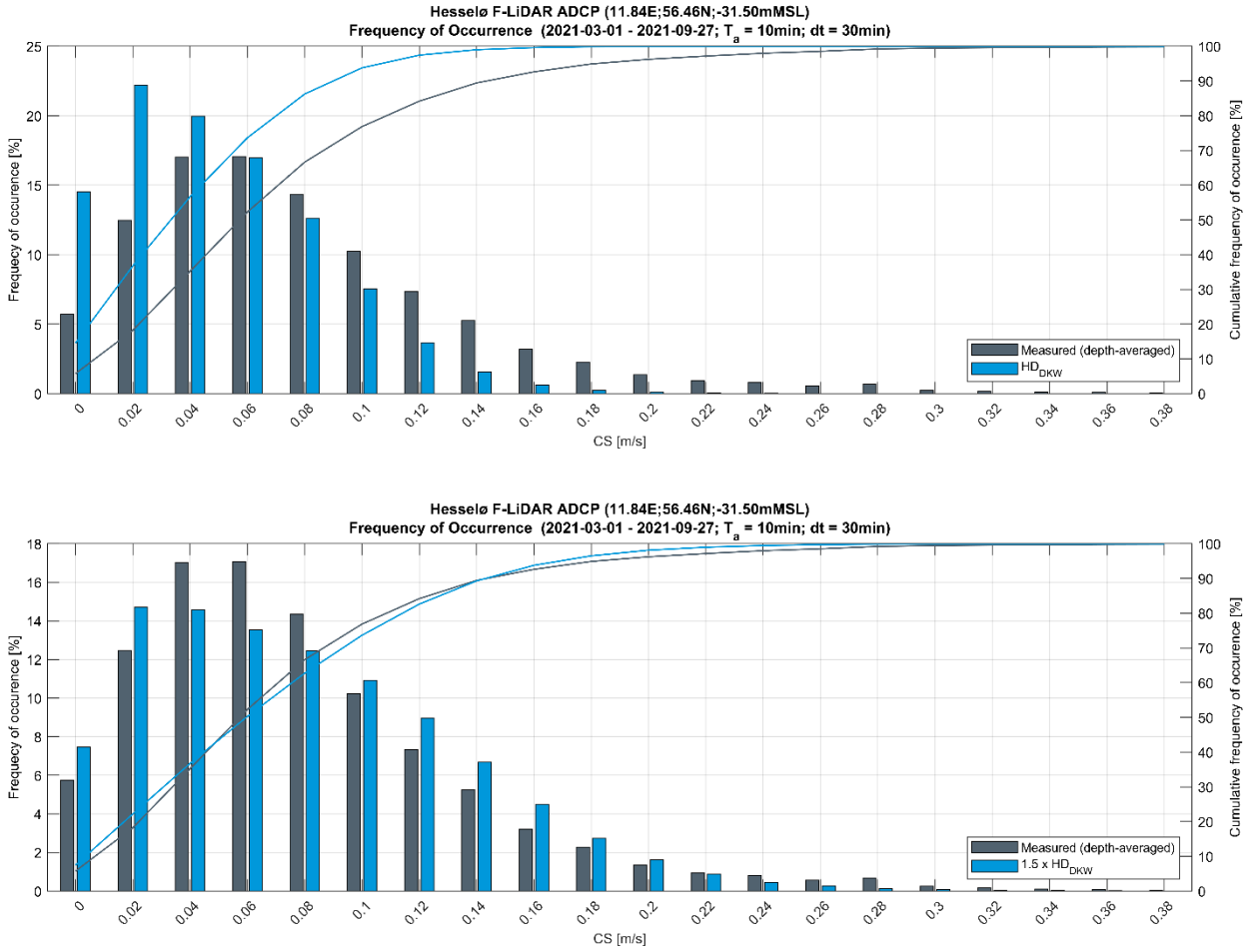

Figure 3.14 Histogram comparison total depth-averaged current speed at Hesselø F-LiDAR
The measurements were recorded at the Hesselø between 01 March and 27 September 2021. The model values are calculated based on 24-years of HD_{DKW} depth-averaged current speeds between from 01 March and 27 September (1995 to 2018). In the lower panel a multiplication factor of 1.5 has been applied to the HD_{DKW} modelled depth-averaged current speeds

3.4 Spectral wave model

Validation of SW_{DKW} modelled wave heights, directions and periods was performed at the five wave measurement stations as described in Section 2.2.4.

It was mentioned in Section 2.3.3 that the model outputs are considered to represent sea-states with an averaging period of 3-hours. This means that for a fair comparison the measurements should also be averaged over 3-hours. Thus, a running 3-hour smoothing was conducted on all observations of integral parameters, except for peak wave period and peak wave direction. Peak wave period and peak wave direction were not averaged since this requires a spectral average which was not performed. The main impact was that the observed peak values were reduced (because the energy is averaged using a 3-hour window) and that the scatter between observations and model data was also reduced.

The validation results for H_{m0} at the Anholt OWF, the closest wave measurement station to the Hesselø OWF, are shown in Figure 3.15. SW_{DKW} represents the measured significant wave height very well, with low bias (-0.02 m) and scatter (SI = 0.18). The peak ratio shows that the largest measured waves heights are slightly underestimated (PR = 0.98); however, as the Anholt measurement cover only a relatively short duration (~2 months during spring), a robust assessment of model performance during extreme sea-states was not possible.

Validation results for MWD and T_p and Anholt are shown in Figure 3.16 and Figure 3.17, respectively. The model predicts the measured wave conditions very well.

Figure 3.18 shows the model validation results for H_{m0} and MWD at Læsø Ost A, which is located approximately 65 km north of Hesselø OWF. This station provides a useful for assessing the wave conditions in the north of the Kattegat. In addition, Læsø Ost is also a relatively long-term measurement data set (3.8 years). The smaller and more frequent waves (H_{m0} < 1.2 m) are generally underestimated by the SW_{DKW}, however the larger sea-states tend to be overpredicted. At this location the PR indicates that the largest wave events are overestimated by 5%.

Figure 3.19 shows scatter plot comparisons of H_{m0} at the remaining wave measurement stations (Fladen Boj, Læsø Syd and Sejero Bugt). Figure 3.20 provides rose plot comparisons of H_{m0} and MWD at Læsø Syd and Sejero Bugt (directional information was not available at Fladen Boj).

The model QI's in terms of H_{m0} are summarised in Table 3.3 and full validation plots for the remaining stations are provided within Appendix B.3.

Table 3.3 Summary of model quality indices for significant wave height

Measurement station	Mean [m]	Bias [m]	AME [m]	RMSE [m]	SI	EV	CC	PR
Anholt OWF	0.58	-0.02	0.09	0.11	0.18	0.90	0.95	0.98
Sejero Bugt	0.77	0.00	0.12	0.15	0.19	0.81	0.92	1.18
Fladen Boj	0.82	0.06	0.16	0.23	0.29	0.80	0.95	1.12
Laesø Ost	0.74	-0.08	0.15	0.19	0.21	0.88	0.96	1.02
Læsø Syd	0.59	-0.03	0.09	0.13	0.20	0.91	0.96	0.98

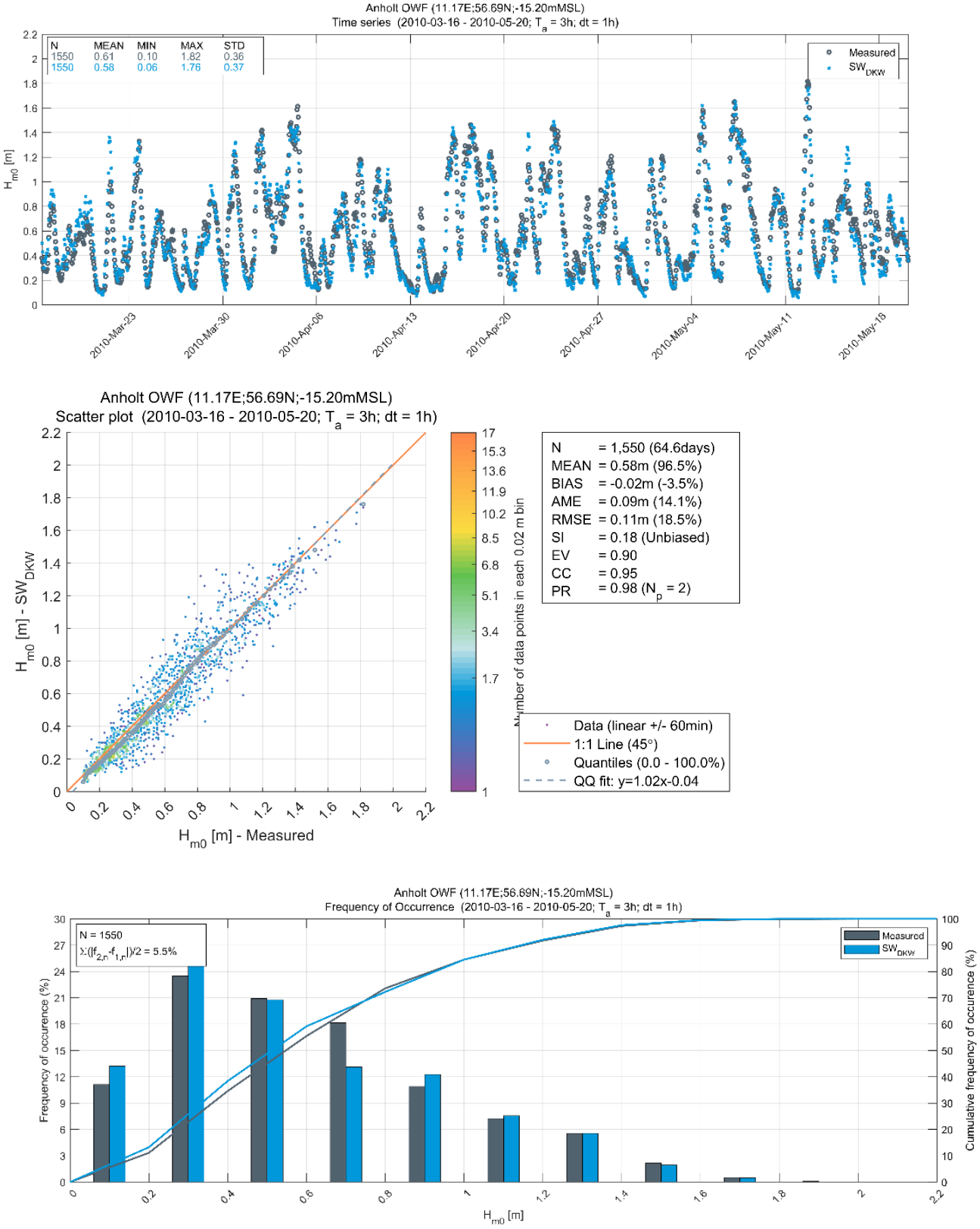

Figure 3.15 Validation of SW_{DKW} significant wave height data at Anholt
Time series (upper panel), scatter plot (central panel), and histogram (lower panel) comparison of modelled and measured significant wave height

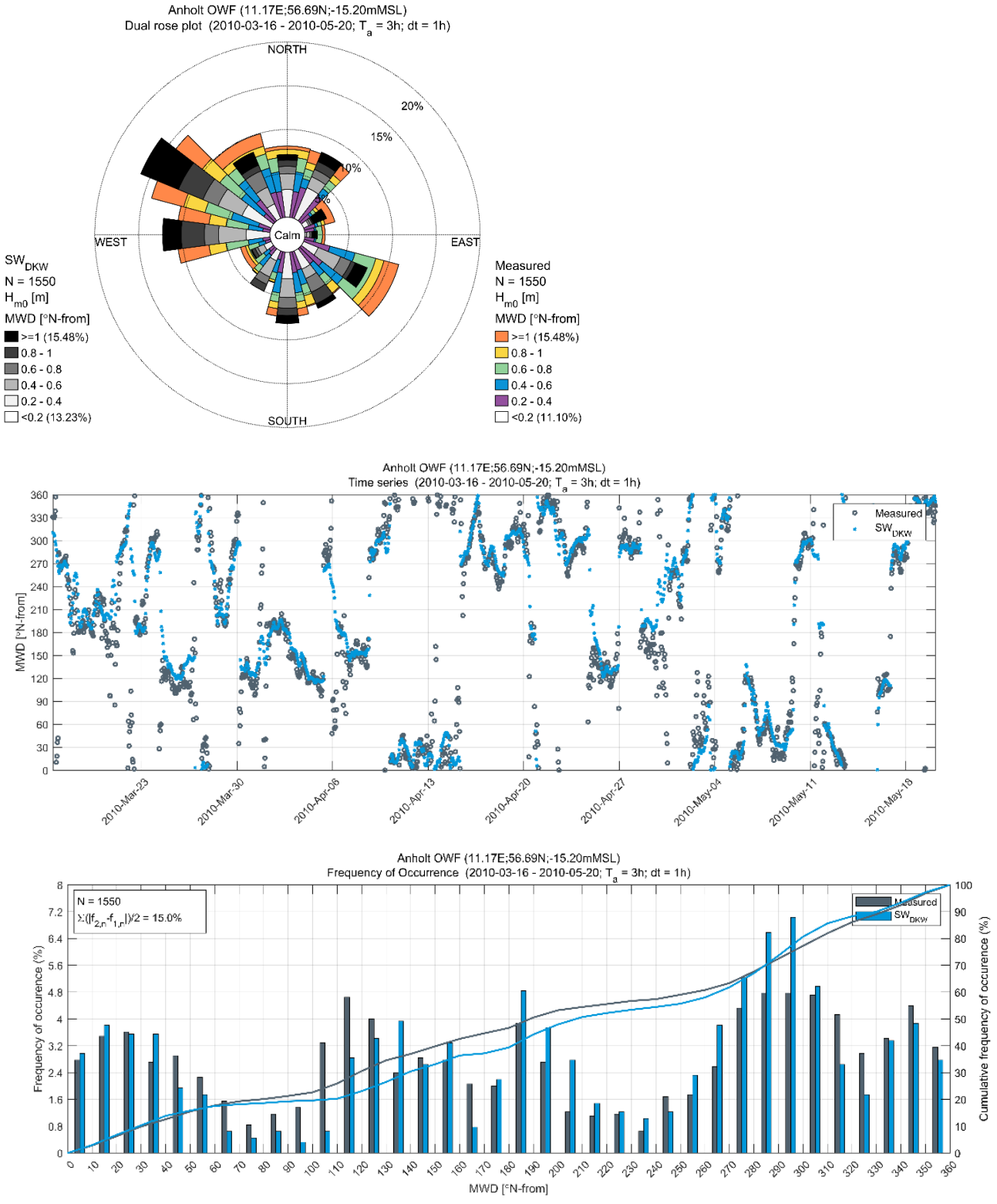

Figure 3.16 Validation of SW_{DKW} mean wave direction data at Anholt

Overlaid rose plot of H_{m0} and MWD (upper panel), Time series of MWD (central panel), and histogram of MWD (lower panel)

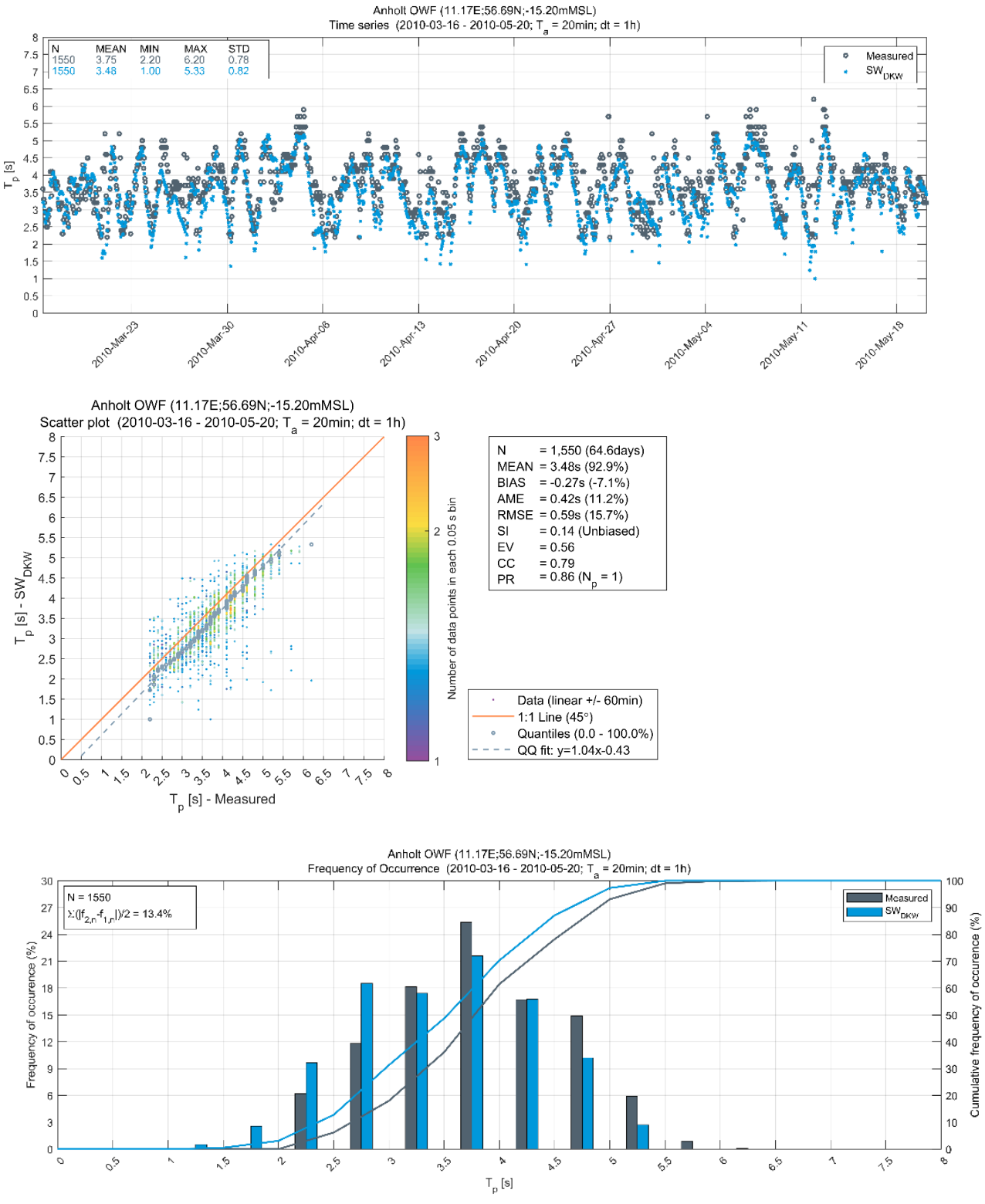

Figure 3.17 Validation of SW_{DKW} peak wave period data at Anholt

Time series (upper panel), scatter plot (central panel), and histogram (lower panel) comparison of modelled and measured peak wave period

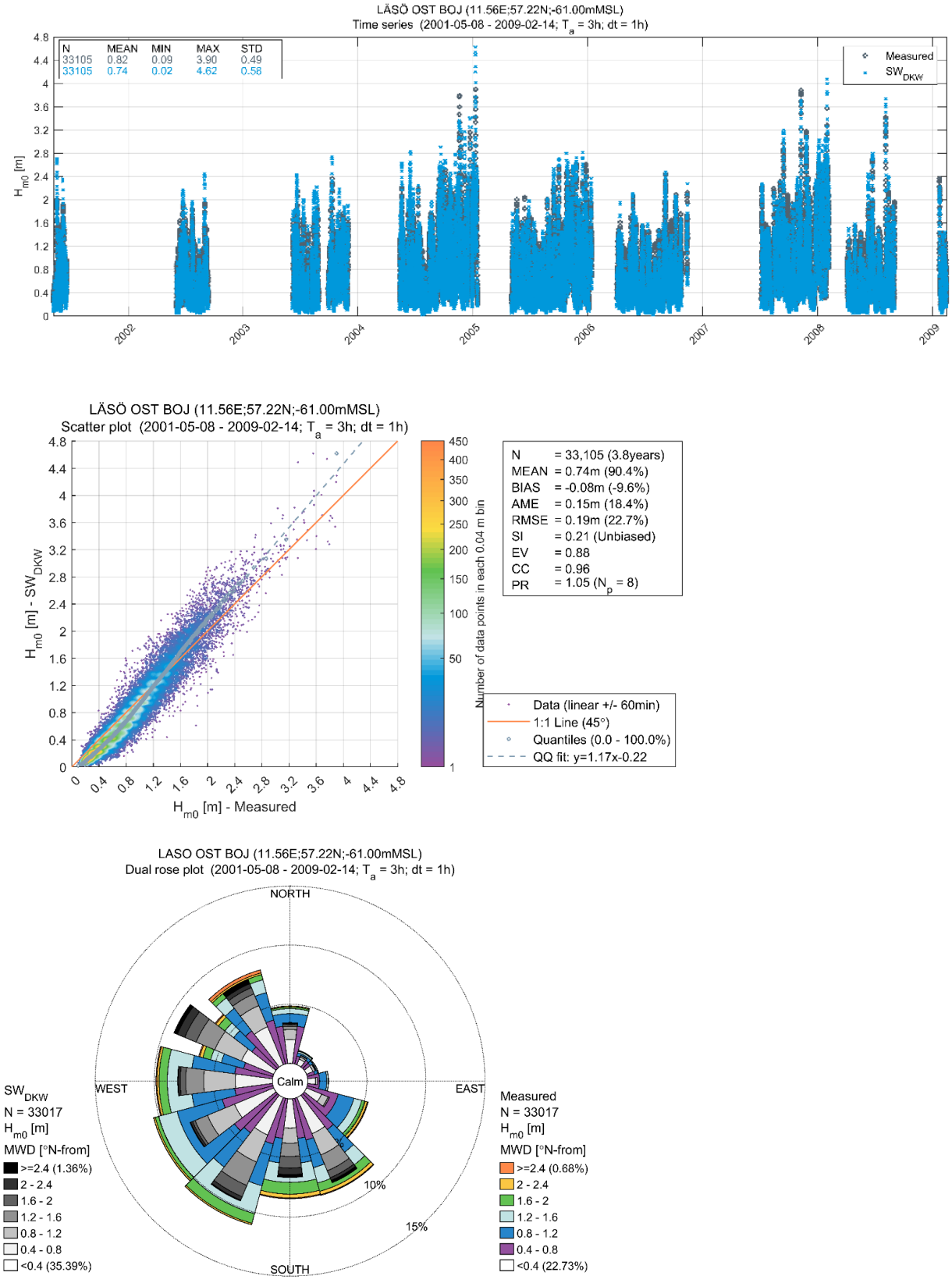

Figure 3.18 Validation of SW_{DKW} at Laesø Ost A

Time series comparison of H_{m0} (upper panel), scatter plot comparison of H_{m0} (central panel), and rose plot of H_{m0} and MWD (lower panel)

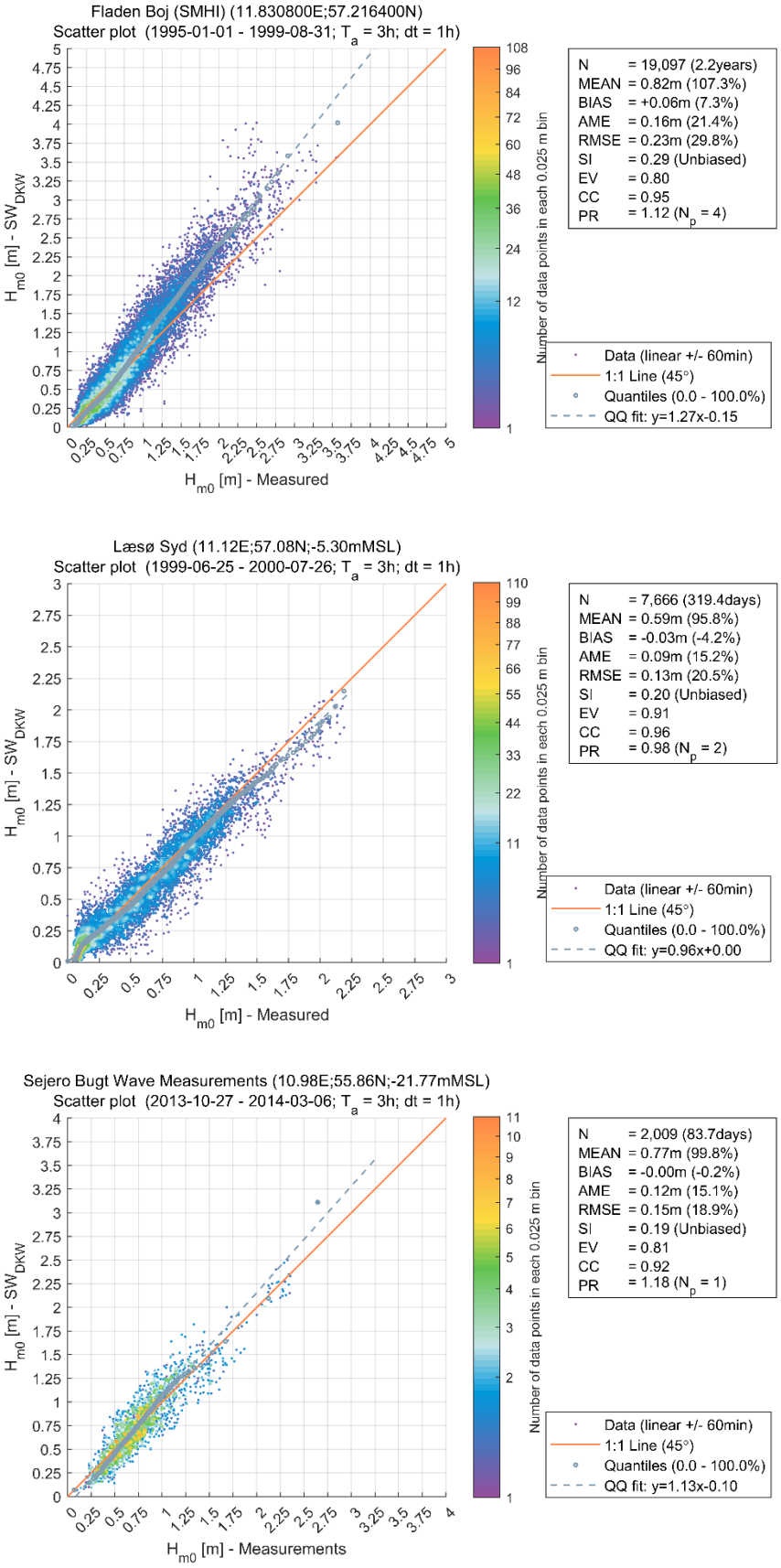

Figure 3.19 Validation of SW_{DKW} significant wave height at Fladen Boj, Læsø Syd, and Sejero Bugt
Scatter plots of measured and modelled H_{m0} at Fladen Boj (top panel), Læsø Syd (central panel) and Sejero Bugt (lower panel)

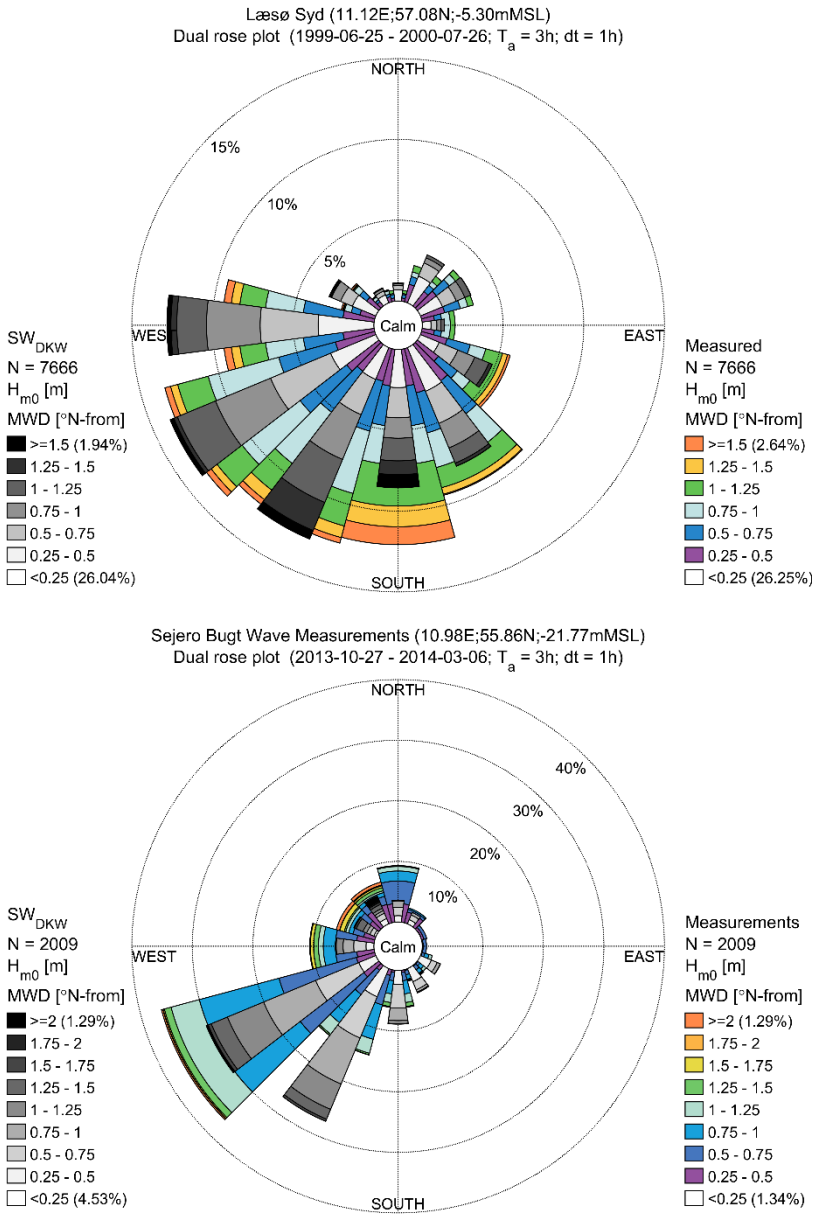

Figure 3.20 Validation of wave roses at Læsø Syd, and Sejero Bugt
Comparison of the measured and modelled distributions of significant wave height and mean wave direction

4 Extraction of Metocean Data

This section describes the metocean data that were extracted from the DHI Danish Waters hindcast model database and provided to Energinet as part of the scope of service. This included wind conditions, water levels, depth-averaged current conditions, integral wave parameters, and direction-frequency wave energy spectra time series data. These data are used as the basis for the metocean analysis presented in Sections 5 and 6 of this report.

The data extraction locations are described in Section 4.1, and details on the metocean time series data are summarised in Section 4.2.

4.1 Selection of data extraction and analysis points

The model data extraction points were chosen in collaboration with Energinet and were selected to represent the spatial variation in conditions across the Hesselø OWF site. Table 4.1 summarises the selected data extraction points, which are also displayed on the maps showing the CREA6 mesh (Figure 4.1) and the mesh and bathymetry from DHI's Danish Waters hindcast database: HD_{DKW} (Figure 4.2) and SW_{DKW} (Figure 4.3).

Directional wave energy spectra data were output from the SW_{DKW} on a regular grid of 0.1° (Figure 4.3); hence, the closest available spectral output point to each data extraction point were extracted: OWF-1 (11.90°E, 56.60°N), OWF-2: (11.90°E, 56.40°N), OWF-3: (11.70°E, 56.40°N).

Table 4.1 Data extraction and analysis points for the Hesselø OWF site metocean conditions assessment

Analysis Point	Position [WGS 84]		Position [UTM 32V]		Recorded seafloor elevation [mMSL]	HD_{DKW} seafloor elevation [mMSL]	SW_{DKW} seafloor elevation [mMSL]	Description
	Lon. [°W]	Lat. [°N]	Easting [m]	Northing [m]				
OWF-1	11.882	56.590	676,967	6,275,464	-30.70	-30.60	-30.81	Northern corner of the Hesselø OWF site
OWF-2	11.940	56.360	681,622	6,250,028	-31.25	-31.26	-30.99	South-east corner of the Hesselø OWF site
OWF-3	11.704	56.440	666,698	6,258,330	-26.27	-26.83	-27.35	Western corner of the Hesselø OWF site

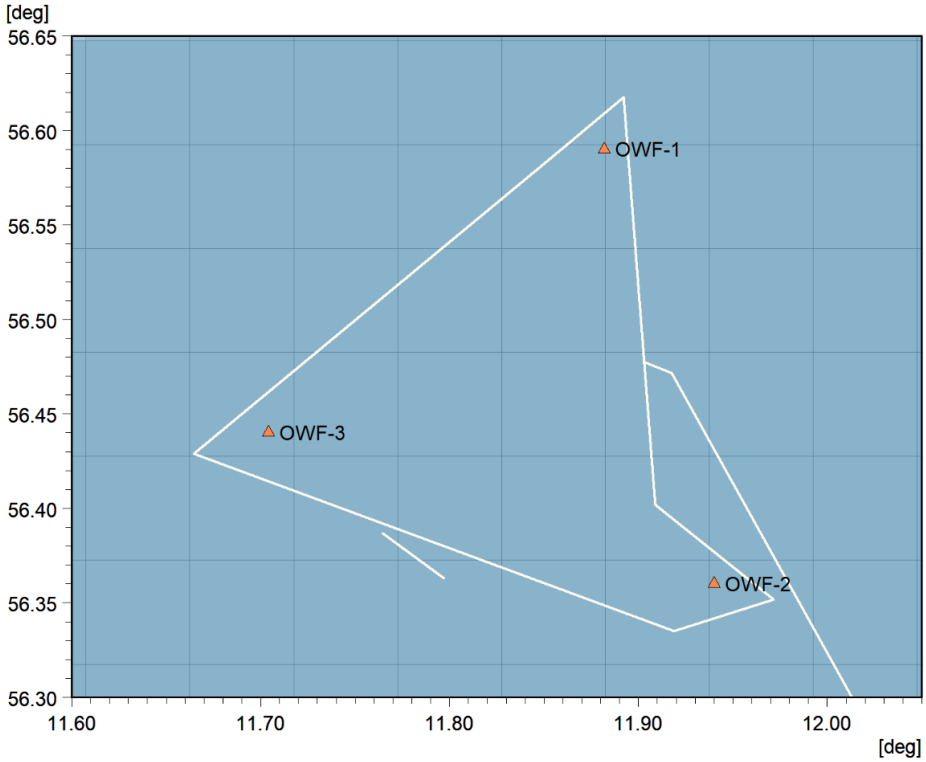

Figure 4.1 Data extraction and analysis points in relation to CREA6 model mesh
The three data extraction and analysis points (OWF-1, OWF-2, and OWF-3) are shown by the orange triangle markers. The Hesselø OWF is designated by the white outline. The background shows the CREA6 numerical mesh

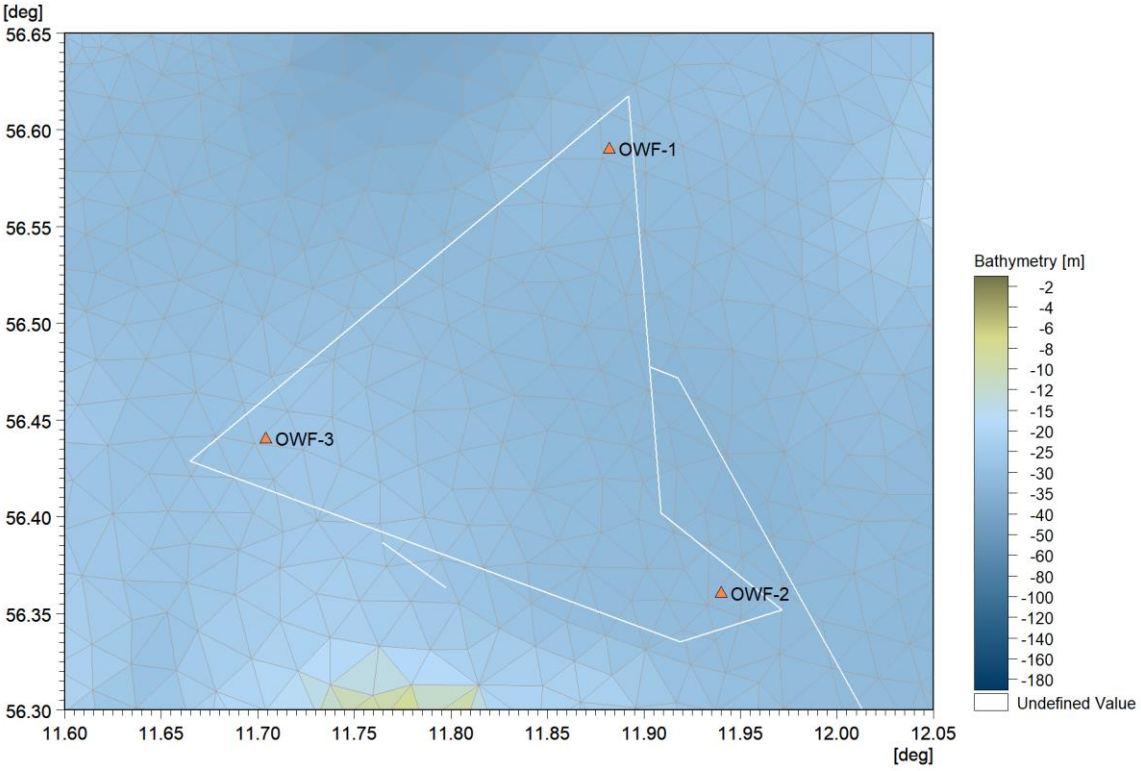

Figure 4.2 Data extraction and analysis points in relation to HD_{DKW} model mesh and bathymetry
The three data extraction and analysis points (OWF-1, OWF-2, and OWF-3) are shown by the orange triangle markers. The Hesselø OWF is designated by the white outline. The background shows the HD_{DKW} model numerical mesh and bathymetry in metres relative to MSL

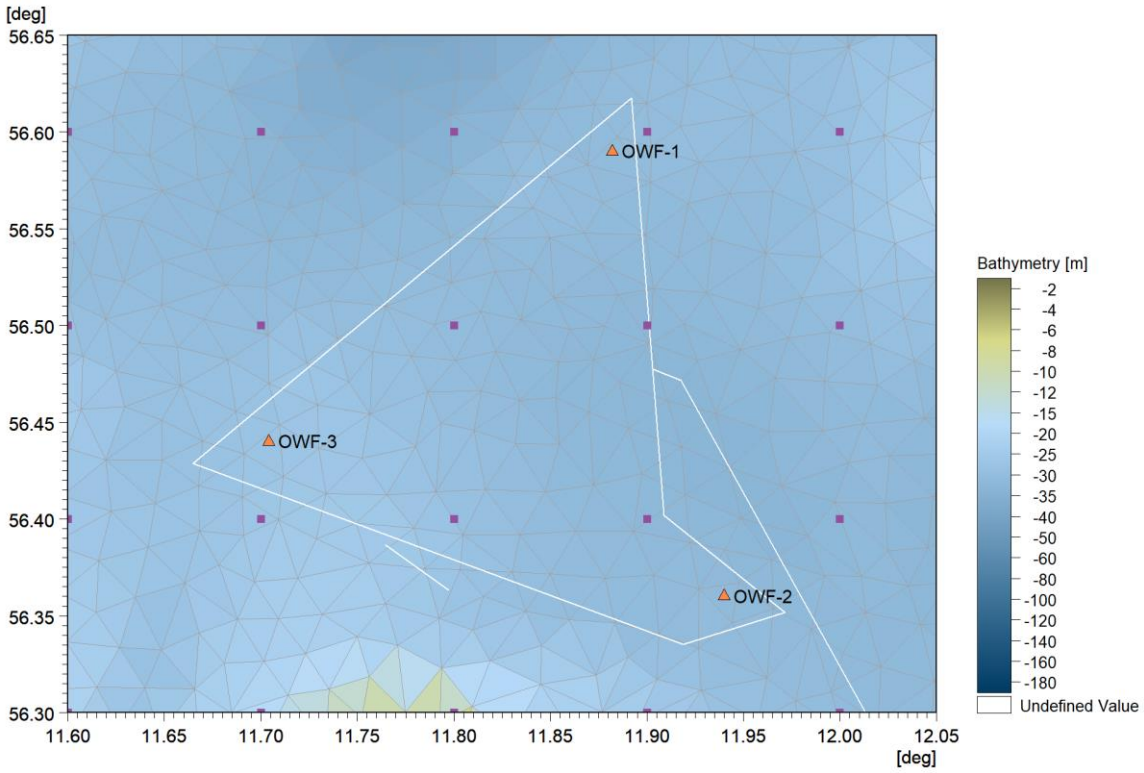

Figure 4.3 Data extraction and analysis points in relation to SW_{DKW} model mesh and bathymetry
The three data extraction and analysis points (OWF-1, OWF-2, and OWF-3) are shown by the orange triangle markers. The Hesselø OWF is designated by the white outline. The background shows the SW_{DKW} model numerical mesh and bathymetry in metres relative to MSL. The SW_{DKW} spectral output points are shown by the purple square markers

4.2 Output specifications

Modelled time series metocean data, including wind, water levels, currents, and integral wave parameters, were provided to Energinet as plain text files that contain records of data with comma separated values (csv).

Directional wave-energy spectra data were provided in the binary data container format that is standard to the MATLAB[10] program.

The names, symbols, and units of the metocean parameters are summarised in Table 4.2 and the filenames of the supplied time-series data are summarised in Table 4.3.

Integral wave parameters were provided for the total, wind-sea, and swell part of the wave spectrum. Wind-sea and swell partitions were based on the wave-age criterion as described in Section 2.3.3. The modelled sea-states are considered to have an implicit averaging period of 3-hours.

The multiplication factor of 1.5 has been already applied to the total current speeds (see Section 3.3.2).

Water level, depth-averaged current speed, and depth-averaged current direction data are provided for the total conditions (i.e., combined tidal and residual). Depth-averaged current speed and current direction were also provided for separated tidal and residual components. The “de-tiding” was conducted using the U-tide package [22], a method that builds upon the tidal

[10] MAT-File Versions - MATLAB & Simulink accessed March 2022

analysis approach defined by the Institute of Oceanographic Sciences (IOS) as described by [23].

The wind speed and wind direction are provided for two heights: 10 mMSL and 140 mMSL. The 10 mMSL were extracted from the CREA6 model at that level directly. The wind speed at 140 mMSL were calculated from the wind speeds at 150 mMSL, sheared down to 140 mMSL:

$$WS_{140} = WS_{150} \cdot \left(\frac{140}{150}\right)^{\alpha} \quad 4.1$$

Where the shear exponent (α) was a time-dependent value calculated for each model output time-step from wind speeds at 125 mMSL and 150 mMSL. The wind direction at 140 mMSL was assumed to be the same as the wind speed at 150 mMSL. From the analysis presented in Section 2.3.1 , the CREA6 wind data are considered to have an implicit averaging period of T_a = 30 minutes.

All data are provided for a 24-year period (1995 to 2018, inclusive), at an output time interval of 1-hour. All times are referenced to Coordinated Universal Time (UTC).

The values in the csv time-series data listed as NaN are “Not a Number”. Such instances occur when there is a gap in the CREA6 model time-series, or when the wave heights are so small that a wave period or wave direction cannot be reasonable defined.

Table 4.2 Parameters, symbols, and units for metocean time series data extraction points

Parameter name	Symbol	Unit	Model
Spectral significant wave height	H_{m0}	m	SW_{DKW}
Peak wave period	T_p	s	
Spectral equivalent of mean wave period	T_{01}	s	
Spectral equivalent of mean zero-crossing wave period	T_{02}	s	
Peak wave direction	PWD	°N (coming from)	
Mean wave direction	MWD	°N (coming from)	
Directional standard deviation	DSD	°	
Direction-frequency wave energy spectra	ED2f	m^2s/deg.	
Total water level relative to mean sea level	WL_{Total}	mMSL	HD_{DKW}
Total depth-averaged current speed	CS_{Total}	m/s	
Total depth-averaged current direction	CD_{Total}	°N (going towards)	
Tidal depth-averaged current speed	CS_{Tide}	m/s	
Tidal depth-averaged current direction	CD_{Tide}	°N (going towards)	
Residual depth-averaged current speed	$CS_{Residual}$	m/s	
Residual depth-averaged current direction	$CD_{Residual}$	°N (going towards)	
Wind speed at 10 mMSL	WS_{10}	m/s	CREA6
Wind direction at 10 mMSL	WD_{10}	°N (coming from)	
Wind speed at 140 mMSL	WS_{140}	m/s	
Wind direction at 140 mMSL	WD_{140}	°N (coming from)	
Air temperature at 2 mMSL	$T_{air,2m}$	°C	
Relative humidity	ϕ	%	

Table 4.3 Time series data files for the Hesselø OWF site metocean conditions assessment

Filename	Description
DKW_Hesselø_OWF1_11.882E56.590N_1995-01-01_2018-12-31.csv	Integral wave parameters, hydrodynamic conditions, and wind conditions at OWF-1
DKW_Hesselø_OWF1_Spectra_1995-01-01_2018-12-31.mat	Direction-frequency wave energy spectra at OWF-1
DKW_Hesselø_OWF2_11.940E56.360N_1995-01-01_2018-12-31.csv	Integral wave parameters, hydrodynamic conditions, and wind conditions at OWF-2
DKW_Hesselø_OWF2_Spectra_1995-01-01_2018-12-31.mat	Direction-frequency wave energy spectra at OWF-2
DKW_Hesselø_OWF3_11.704E56.440N_1995-01-01_2018-12-31.csv	Integral wave parameters, hydrodynamic conditions, and wind conditions at OWF-3
DKW_Hesselø_OWF3_Spectra_1995-01-01_2018-12-31.mat	Direction-frequency wave energy spectra at OWF-3

5 Operational Metocean Conditions

This section describes the results of analyses performed to establish operational metocean conditions analysis at three (3) analysis points within the Hesselø OWF.

The analysis of operational metocean conditions was based on metocean time-series data extracted from DHI's Danish Waters hindcast model database covering a period of 24-years (1995 – 2018, inclusive) as described in Section 2.3. It should be noted that during the first year of the model database, the initial propagation of the model boundaries can result in spurious predictions within the domain (the so-called model spin-up period). As such, a period of several days was excluded from the analysis presented in this section. In this case the model data set spanned the period 1995-01-14 to 2020-12-31 (~24-years).

- Section 5.1: operational wind conditions
- Section 5.2: operational wave conditions
- Section 5.3: operational current conditions
- Section 5.4: operational water level conditions

The results presented in each section presents the all-year metocean statistics. The monthly distributions of these statistics are provided in the excel files that accompany this report (see Appendix C).

5.1 Wind conditions

Operational wind conditions are presented in this section for heights of 10 mMSL and 140 mMSL based on the CREA6 atmospheric model. According to Section 6.4.3.1 of [16], the long-term probability distribution of wind speed is independent of averaging periods between 10-minutes and 3-hours (except in the tail where the extremes are defined); hence, normal conditions are presented here for 30-minute average values equal to the output from the model.

Directional statistics are presented for 12 x 30° directional sectors (centred on 0°N, 30°N, 60°N, etc.).

The normal wind conditions presented in this section relate to the wind model used as input to hydrodynamic and spectral wave models. The recommended meteorological and atmospheric values for FEED are contained in the **Site Wind Condition Assessment** for the Hesselø offshore wind farm [3]

5.1.1 Wind speed statistics at 10 mMSL

Figure 5.1 presents plots of the monthly and directional statistics (mean, minimum, maximum, and standard deviation) of WS_{10} at analysis point OWF-1. The statistics are summarised for all analysis points in Table 5.1 and Table 5.2.

The largest wind speeds are associated with the months of November through to February and the smallest winds occur from May to July. Directional sectors from 210°N to 300°N exhibit the largest wind speeds. The smallest average wind speeds are from 0°N to 60°N, while the smallest maximum wind speeds are from sectors 90°N to 150°N.

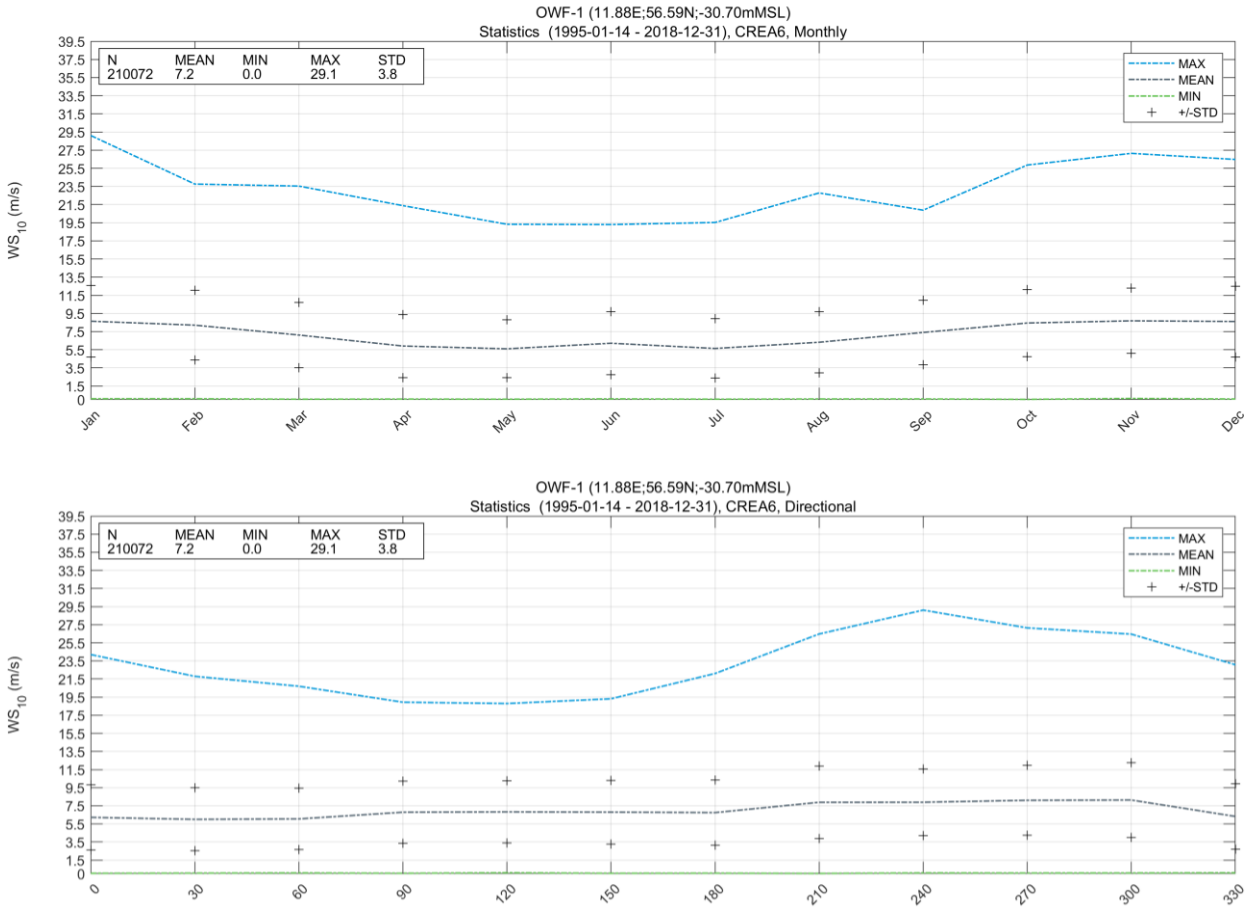

Figure 5.1 Monthly and directional WS_{10} statistics at analysis point OWF-1
Mean, minimum, maximum, and standard deviation of CREA6 model wind speeds at 10 mMSL (1995-01-14 to 2018-12-31)

Table 5.1 All-year and monthly statistics of WS_{10} at the Hesselø OWF

Mean, minimum, maximum, and standard deviation of CREA6 model wind speeds at 10 mMSL (1995-01-14 to 2018-12-31)

Month	OWF-1				OWF-2				OWF-3			
	Mean [m/s]	Min. [m/s]	Max. [m/s]	STD [m/s]	Mean [m/s]	Min. [m/s]	Max. [m/s]	STD [m/s]	Mean [m/s]	Min. [m/s]	Max. [m/s]	STD [m/s]
All-year	7.2	0.0	29.1	3.8	7.1	0.0	30.8	3.7	7.2	0.0	29.0	3.8
Jan	8.6	0.1	29.1	4.0	8.6	0.0	30.8	3.9	8.7	0.1	29.0	3.9
Feb	8.2	0.1	23.8	3.8	8.2	0.1	24.6	3.8	8.2	0.1	23.4	3.8
Mar	7.1	0.0	23.5	3.6	7.1	0.1	23.6	3.6	7.2	0.1	23.6	3.6
Apr	5.9	0.1	21.4	3.5	5.8	0.0	21.6	3.5	5.9	0.0	22.0	3.5
May	5.6	0.0	19.3	3.2	5.5	0.0	18.1	3.1	5.6	0.1	18.6	3.2
Jun	6.2	0.1	19.3	3.5	6.1	0.1	19.1	3.4	6.2	0.0	19.5	3.4
Jul	5.6	0.0	19.5	3.3	5.5	0.1	20.7	3.2	5.6	0.0	20.1	3.2
Aug	6.3	0.1	22.8	3.4	6.2	0.1	24	3.3	6.3	0.1	23.4	3.4
Sep	7.4	0.1	20.9	3.5	7.3	0.1	20.7	3.5	7.4	0.1	20.7	3.5
Oct	8.4	0.0	25.9	3.7	8.3	0.1	26.7	3.6	8.4	0.0	24.8	3.7
Nov	8.7	0.1	27.1	3.6	8.6	0.1	25.1	3.5	8.7	0.1	25.6	3.6
Dec	8.6	0.1	26.5	3.9	8.6	0.1	27.3	3.8	8.6	0.1	27.2	3.9

Table 5.2 Omnidirectional and directional statistics of WS_{10} statistics Hesselø OWF

Mean, minimum, maximum, and standard deviation of CREA6 model wind speeds at 10 mMSL (1995-01-14 to 2018-12-31)

Direction sector (°from)	OWF-1				OWF-2				OWF-3			
	Mean [m/s]	Min. [m/s]	Max. [m/s]	STD [m/s]	Mean [m/s]	Min. [m/s]	Max. [m/s]	STD [m/s]	Mean [m/s]	Min. [m/s]	Max. [m/s]	STD [m/s]
Omnidirectional	7.2	0.0	29.1	3.8	7.1	0.0	30.8	3.7	7.2	0.0	29.0	3.8
[345 – 015[	6.2	0.0	24.2	3.6	6.2	0.1	23.6	3.6	6.3	0.1	24.2	3.6
[015 - 045[	6.0	0.1	21.8	3.5	5.9	0.1	23.4	3.5	6.1	0.1	23.5	3.5
[045 - 075[	6.1	0.1	20.7	3.4	6.1	0.0	20.9	3.5	6.1	0.1	21.1	3.4
[075 – 105[	6.8	0.0	18.9	3.4	6.6	0.1	20.1	3.4	6.8	0.0	20.6	3.5
[105 – 135[	6.8	0.1	18.8	3.4	6.8	0.0	18.9	3.4	7.0	0.1	19.1	3.5
[135 – 165[	6.8	0.0	19.3	3.5	6.5	0.1	17.9	3.3	6.7	0.0	18.2	3.5
[165 – 195[	6.7	0.1	22.1	3.6	6.5	0.1	20.4	3.4	6.7	0.1	21.5	3.6
[195 – 225[	7.9	0.0	26.5	4.0	7.7	0.0	26.5	3.9	7.9	0.1	27.2	4.0
[225 – 255[	7.9	0.1	29.1	3.7	8.1	0.1	30.8	3.8	7.9	0.1	29.0	3.7
[255 – 285[	8.1	0.1	27.1	3.9	8.0	0.0	24.9	3.8	8.0	0.0	25.3	3.7
[285 – 315[	8.1	0.1	26.5	4.1	7.9	0.1	27.3	4.0	8.1	0.0	27.2	4.1
[315 – 345[	6.3	0.1	23.1	3.6	6.4	0.1	23.6	3.7	6.4	0.1	21.6	3.7

5.1.2 Wind speed statistics at 140m MSL

Figure 5.2 presents plots of the monthly and directional statistics (mean, minimum, maximum, and standard deviation) of WS_{10} at analysis point OWF-1. The statistics are summarised for all analysis points in Table 5.3 and Table 5.4.

As for the analysis at 10 mMSL (Section 5.1.1) the largest wind speeds are associated with the months of November through to February and the smallest winds occur from May to July. Directional sectors from 210°N to 300°N exhibit the largest wind speeds. The smallest average wind speeds are from 0°N to 60°N, while the smallest maximum wind speeds are from sectors 90°N to 150°N.

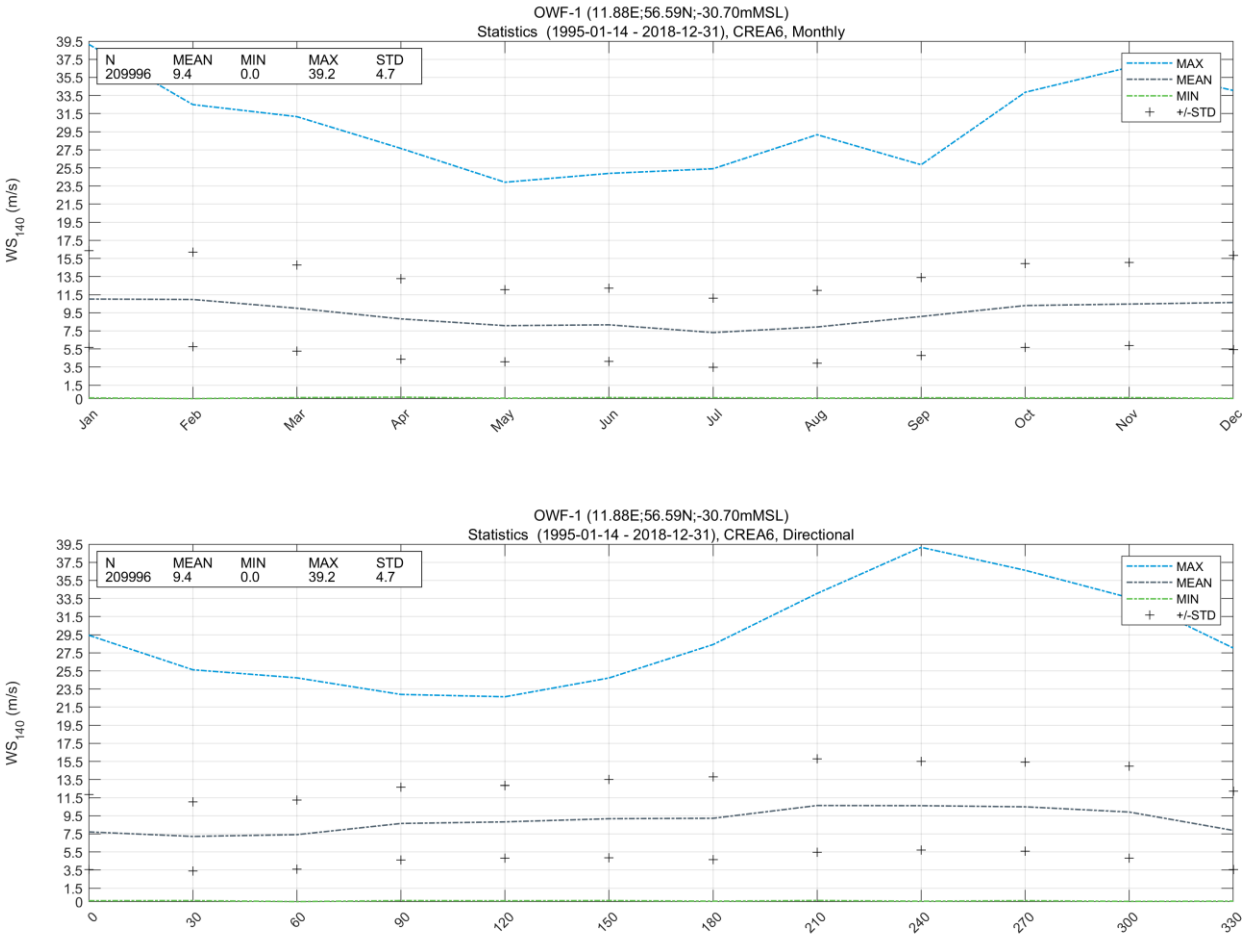

Figure 5.2 Monthly and directional WS_{140} statistics at analysis point OWF-1
Mean, minimum, maximum, and standard deviation of CREA6 model wind speeds at 140 mMSL (1995-01-14 to 2018-12-31)

Table 5.3 All-year and monthly statistics of WS_{140} at the Hesselø OWF

Mean, minimum, maximum, and standard deviation of CREA6 model wind speeds at 140 mMSL (1995-01-14 to 2018-12-31)

Month	OWF-1				OWF-2				OWF-3			
	Mean [m/s]	Min. [m/s]	Max. [m/s]	STD [m/s]	Mean [m/s]	Min. [m/s]	Max. [m/s]	STD [m/s]	Mean [m/s]	Min. [m/s]	Max. [m/s]	STD [m/s]
All-year	9.4	0.0	39.2	4.7	9.3	0.0	41.5	4.7	9.4	0.0	38.9	4.7
Jan	11.0	0.1	39.2	5.4	11.0	0.1	41.5	5.3	11.1	0.1	38.9	5.3
Feb	11.0	0.0	32.5	5.2	11.0	0.1	33.1	5.2	11.1	0.1	32.2	5.2
Mar	10.0	0.1	31.2	4.8	10.0	0.1	31.6	4.7	10.1	0.1	31.4	4.7
Apr	8.8	0.2	27.7	4.4	8.8	0.1	28.7	4.4	8.9	0.1	28.9	4.4
May	8.1	0.1	23.9	4.0	8.0	0.0	22.1	3.9	8.1	0.0	22.1	4.0
Jun	8.2	0.1	24.9	4.1	8.0	0.1	24.2	4.0	8.1	0.1	25.2	4.0
Jul	7.3	0.1	25.4	3.8	7.2	0.1	26.5	3.7	7.3	0.1	26.2	3.8
Aug	7.9	0.1	29.2	4.0	7.9	0.2	30.6	4.0	8.0	0.0	29.3	4.0
Sep	9.1	0.1	25.9	4.3	9.0	0.0	25.3	4.2	9.1	0.1	27.4	4.3
Oct	10.3	0.1	33.9	4.6	10.2	0.1	33.9	4.5	10.3	0.1	32.0	4.6
Nov	10.5	0.1	36.6	4.6	10.4	0.1	33.5	4.5	10.5	0.1	33.9	4.6
Dec	10.6	0.0	34.1	5.2	10.6	0.1	34.6	5.1	10.7	0.1	35.3	5.2

Table 5.4 Omnidirectional and directional statistics of WS_{140} statistics Hesselø OWF

Mean, minimum, maximum, and standard deviation of CREA6 model wind speeds at 140 mMSL (1995-01-14 to 2018-12-31)

Direction sector (°from)	OWF-1				OWF-2				OWF-3			
	Mean [m/s]	Min. [m/s]	Max. [m/s]	STD [m/s]	Mean [m/s]	Min. [m/s]	Max. [m/s]	STD [m/s]	Mean [m/s]	Min. [m/s]	Max. [m/s]	STD [m/s]
Omnidirectional	9.4	0.0	39.2	4.7	9.3	0.0	41.5	4.7	9.4	0.0	38.9	4.7
[345 – 015[	7.7	0.1	29.4	4.2	7.7	0.1	28.3	4.2	7.8	0.0	29.6	4.2
[015 - 045[	7.2	0.1	25.6	3.8	7.2	0.1	28.1	3.9	7.3	0.1	28.2	3.9
[045 - 075[	7.4	0.0	24.7	3.8	7.7	0.1	25.3	4.0	7.6	0.1	25.7	3.9
[075 – 105[	8.6	0.1	22.9	4.0	8.4	0.1	24.5	3.9	8.6	0.1	23.5	4.0
[105 – 135[	8.8	0.1	22.6	4.0	9.0	0.1	22.5	4.0	9.1	0.1	23.1	4.1
[135 – 165[	9.2	0.1	24.7	4.3	8.9	0.1	23.6	4.1	9.1	0.0	24.9	4.2
[165 – 195[	9.2	0.1	28.4	4.6	9.0	0.1	27.7	4.4	9.2	0.1	27.5	4.5
[195 – 225[	10.6	0.1	34.1	5.2	10.5	0.1	34.6	5.0	10.7	0.2	35.3	5.2
[225 – 255[	10.6	0.1	39.2	4.9	10.9	0.1	41.5	5.0	10.7	0.1	38.9	4.9
[255 – 285[	10.5	0.1	36.6	4.9	10.3	0.0	34.3	4.8	10.3	0.2	33.9	4.7
[285 – 315[	9.9	0.0	33.6	5.1	9.8	0.2	34.6	5.0	10.0	0.1	34.8	5.1
[315 – 345[	7.9	0.1	28.0	4.3	7.9	0.0	28.4	4.4	7.9	0.1	27.9	4.4

5.1.3 Rose plot and directional scatter table at 10m MSL

Figure 5.3 and Figure 5.4 present the all-year rose plot and density scatter plots of WS_{10} and WD_{10} at analysis points OWF-1, OWF-2, and OWF-3. The most frequent wind direction at all analysis points is from the south-west (directional sector centred at 240°N).

Tables giving the frequency of occurrence [%] of wind speed and wind direction at all analysis points are provided in digital format (Microsoft Excel, .xlsx) accompanying this report (see Appendix C). The tables are provided for the following intervals:

- WS_{10} intervals of 1 m/s, centred on integer values. Please note that the first bin includes the interval 0.0 m/s ≤ WS_{10} < 1.5 m/s.
- WD_{10} intervals of 30°, centred on 0°N, 30°N, 60°N, etc.
- All-year and for each calendar month

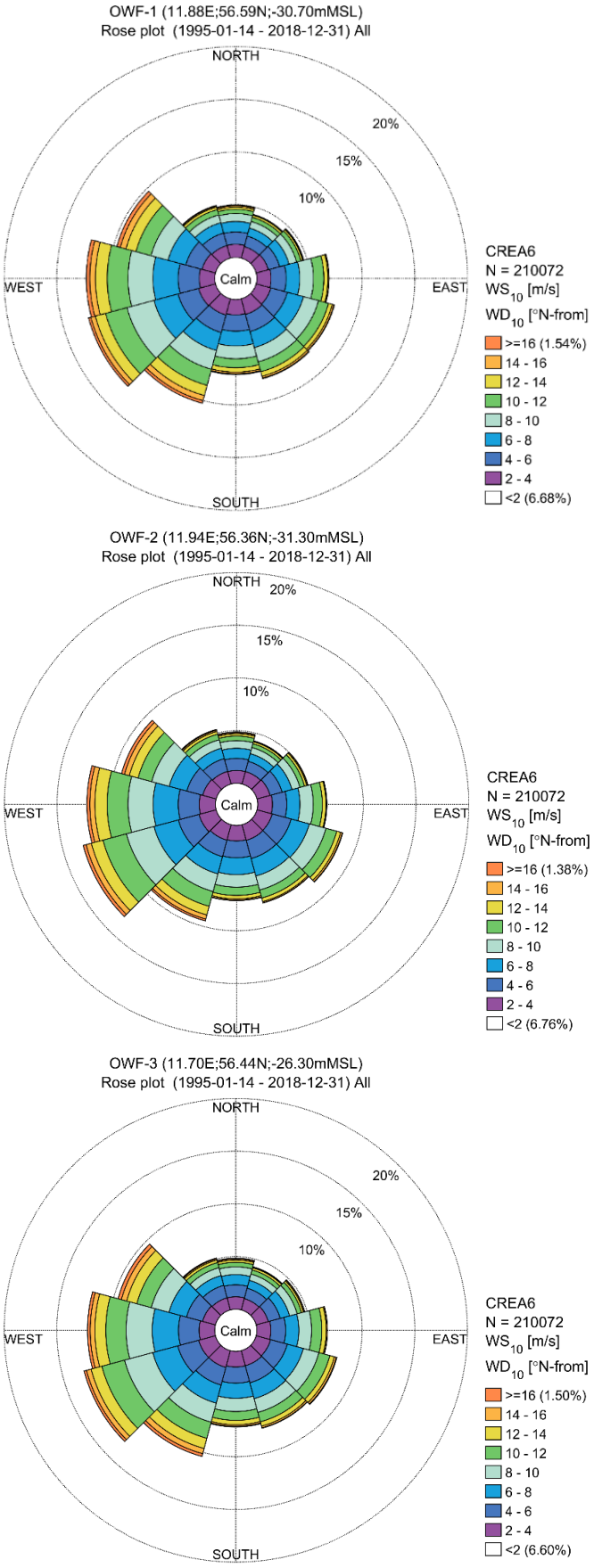

Figure 5.3 Rose plots of all-year WS_{10} and WD_{10} at analysis points OWF-1, OWF-2, and OWF-3
Rose plots show the frequency of occurrence of mean wind speed for each 30° direction bin at 10m MSL, derived from CREA6 model (1995-01-14 to 2018-12-31)

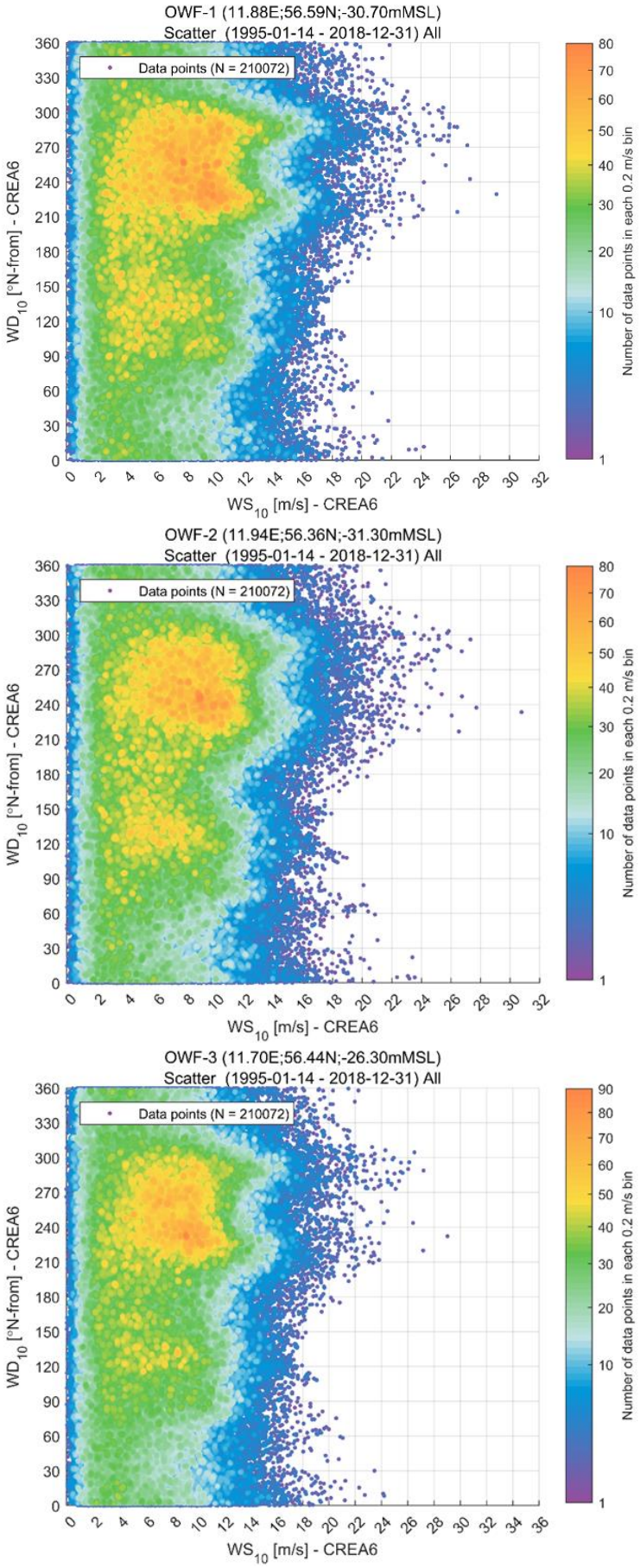

Figure 5.4 Density scatter plot of WS_{10} and WD_{10} at analysis points OWF-1, OWF-2, and OWF-3

5.1.4 Rose plot and directional scatter table at 140 mMSL

Figure 5.3 and Figure 5.4 present the all-year rose plot and density scatter plot of WS_{140} and WD_{140} at analysis points OWF-1, OWF-2, and OWF-3. The most frequent wind direction at 140 mMSL is west at analysis points OWF-1 and OWF-3 (directional sector centred on 270°N), and south-west at analysis point OWF-2 (directional sector centred on 240°N).

Tables giving the frequency of occurrence [%] of wind speed and wind direction at all analysis points are provided in digital format (Microsoft Excel, .xlsx) accompanying this report (see Appendix C). The tables are provided for the following intervals:

- WS_{140} intervals of 1 m/s, centred on integer values. Please note that the first bin includes the interval 0.0 m/s ≤ WS_{140} < 1.5 m/s.
- WD_{140} intervals of 30°, centred on 0°N, 30°N, 60°N, etc.
- All-year and for each calendar month

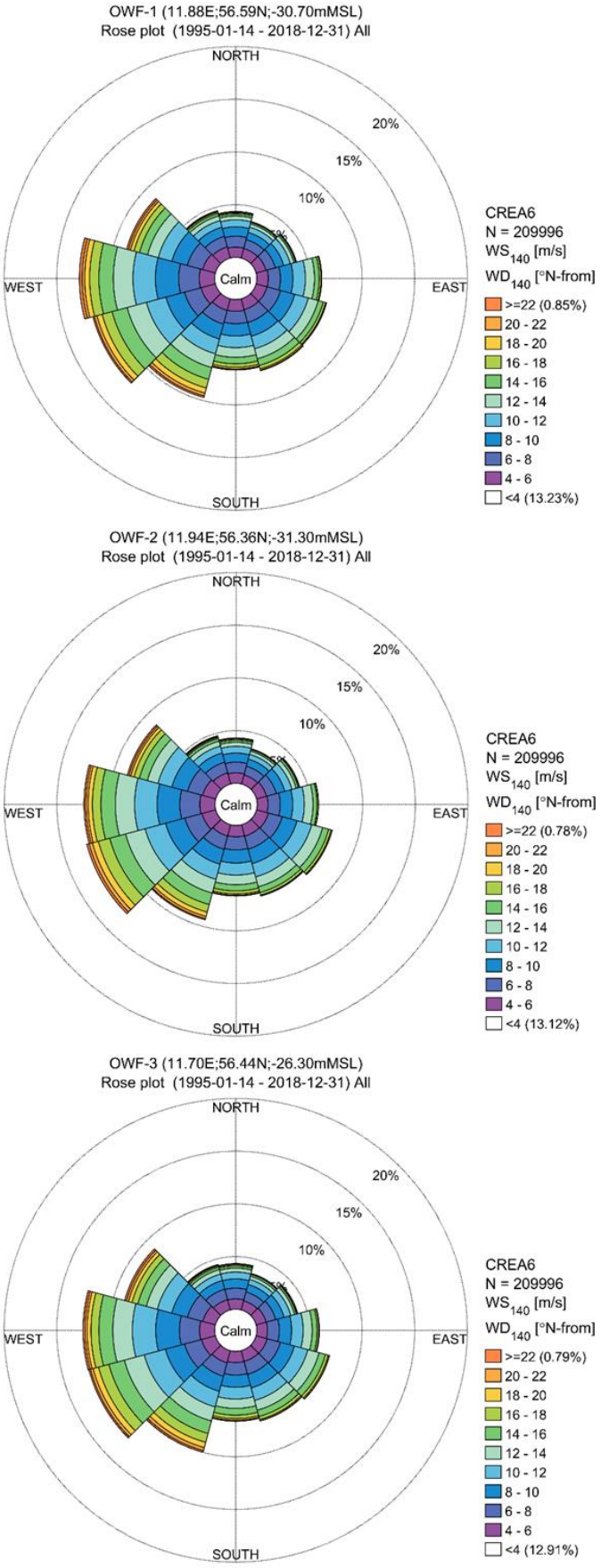

Figure 5.5 Rose plots of all-year WS_{140} and WD_{140} at analysis points OWF-1, OWF-2, and OWF-3
Rose plots show the frequency of occurrence of mean wind speed for each 30° direction bin at 140m MSL, derived from CREA6 model (1995-01-14 to 2018-12-31)

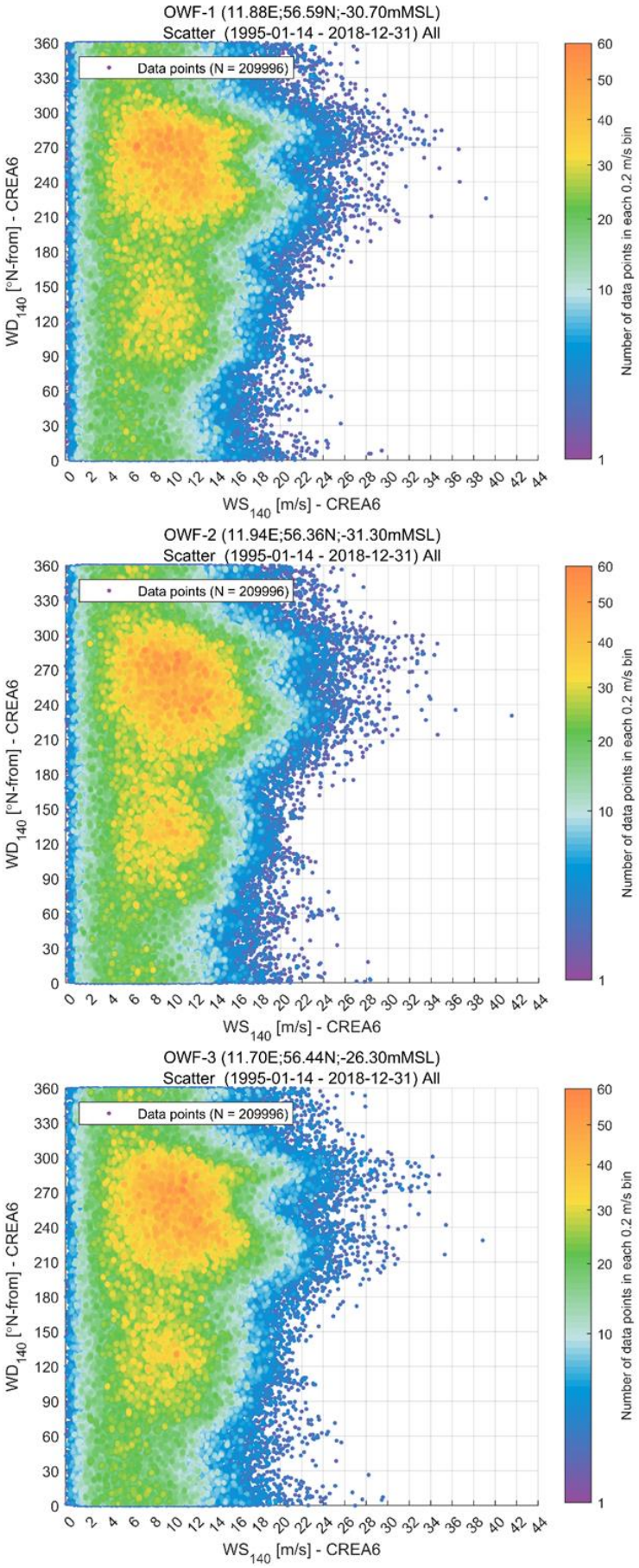

Figure 5.6 Density scatter plot of WS_{140} and WD_{140} at analysis points OWF-1, OWF-2, and OWF-3

5.1.5 Normal wind speed profile

The wind profile describes the average wind speed as a function of height, Z, above the sea level. According to section 6.3.2.2 of [24], the normal wind speed profile is given by a power law of the form:

$$WS_{Z1} = WS_{Z2} \cdot \left(\frac{Z1}{Z2}\right)^{\alpha} \quad 5.1$$

Where WS_{Z1} and WS_{Z2} are the average wind speed at heights $Z1$ and $Z2$, respectively, and α is the wind shear exponent. Rearranging the above equation, the value of α can be derived as:

$$\alpha = \frac{\ln\left(\frac{WS_{Z2}}{WS_{Z1}}\right)}{\ln\left(\frac{Z2}{Z1}\right)} \quad 5.2$$

In general, α is a function of atmospheric stratification; when the sea surface is warmer than the air aloft, the sea is releasing heat and the atmosphere is unstable (convective), and when the sea surface is colder than the air aloft, the sea absorbs heat, and the atmosphere is stably stratified. For zero heat flux between the sea surface and the air aloft, the atmospheric stratification is termed neutral. Unstable atmospheric conditions are associated with low shear, while stable conditions are associated with high shear. Furthermore, the wind shear is a function of height; in general, winds close to the surface have higher shear than wind further aloft.

The normal wind profile at the Hesselø OWF site was investigated using observations from the Hesselø F-LiDAR (see Section 2.2.1). This data set included approximately 29,000 samples of 10-minute average wind speeds, corresponding to around 200 days of measurement (March to September 2021); hence, a spring-summer seasonal bias may be present in the results.

Figure 5.7 shows the distribution of α calculated from 10-minute average wind speeds at the Hesselø F-LiDAR based on two height intervals: 138 mMSL to 158 mMSL, and 10 mMSL to 38 mMSL. The mean and median value of α decrease with height above the sea surface.

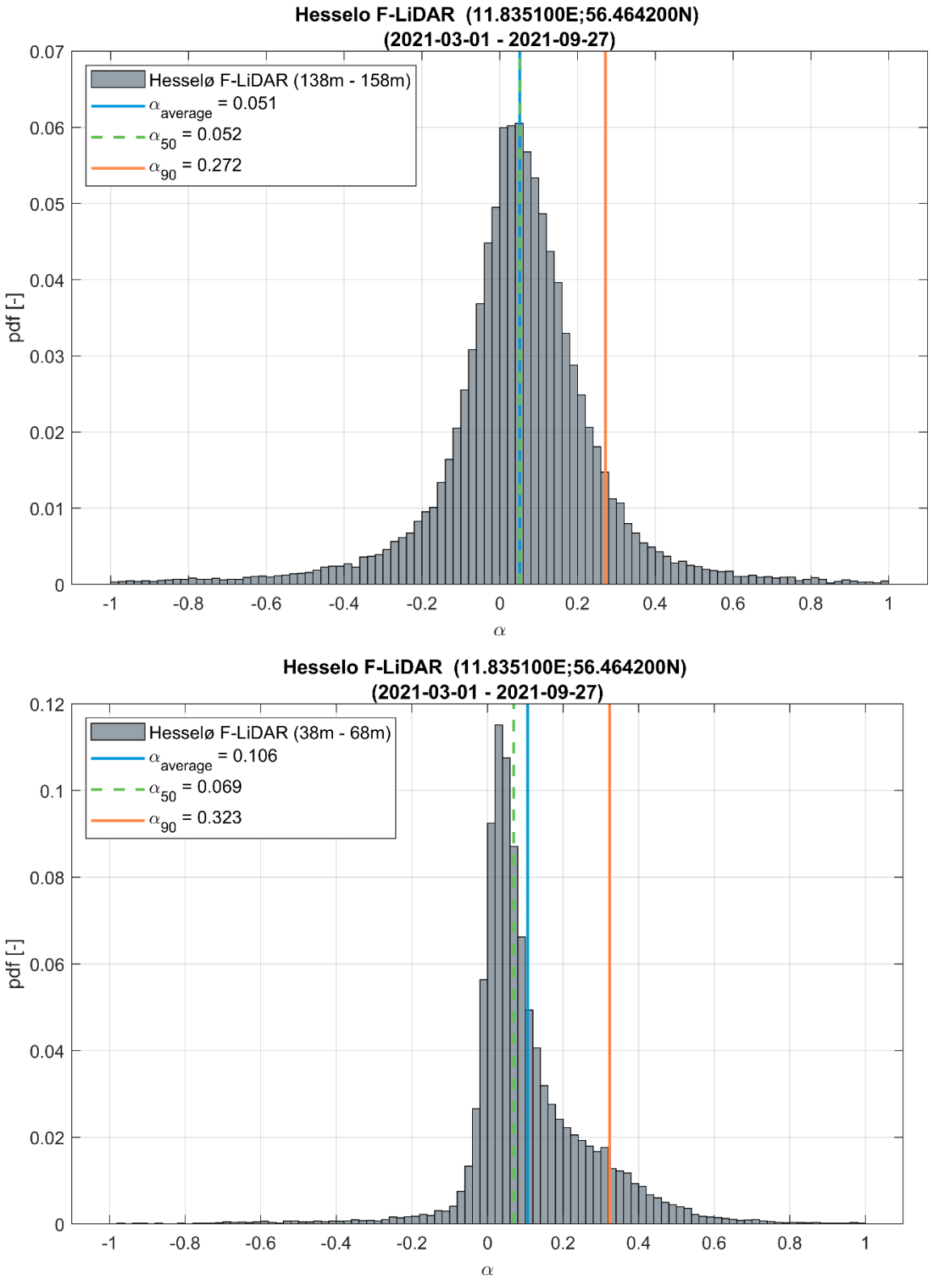

Figure 5.7 Distribution of shear exponents at the Hesselø F-LiDAR
Analysis based on 10-minute averaged measurements at heights 138 mMSL to 158 mMSL (upper panel) and 10 mMSL to 38 mMSL (lower panel). The average ($\alpha_{average}$), median (α_{50}), and 90th percentile (α_{90}) values are shown for all wind speeds and directions

5.2 Wave conditions

Operational wave conditions at the Hesselø OWF are derived from the outputs for SW_{DKW} as described in Section 2.3.3. The representative averaging period of SW_{DKW} modelled wave data should be considered to represent a sea state duration of 3 hours.

The analysis presented in the following sub-sections are for the total part of the wave spectrum (i.e., combined wind-sea and swell). Figure 5.8 presents a scatter plot of $H_{m0,Sea}$ vs. $H_{m0,Total}$ at analysis point OWF-1 and shows the dominance of the wind sea component to the total sea state conditions. A bar plot showing the ratio of wind-sea energy to total sea-state energy and swell energy to total sea-state energy is provided in Figure 5.9 (the energy being proportional to the square of H_{m0}). Only for the very lowest sea state (i.e., H_{m0} < 0.25 m) are swell waves responsible for over 50% of the total wave energy. Wind-sea waves are responsible for over 85% of the total sea-state energy when H_{m0} > 1.0 m.

Directional wave analysis is presented for 12 x 30° sectors conditioned by Mean Wave Direction (MWD).

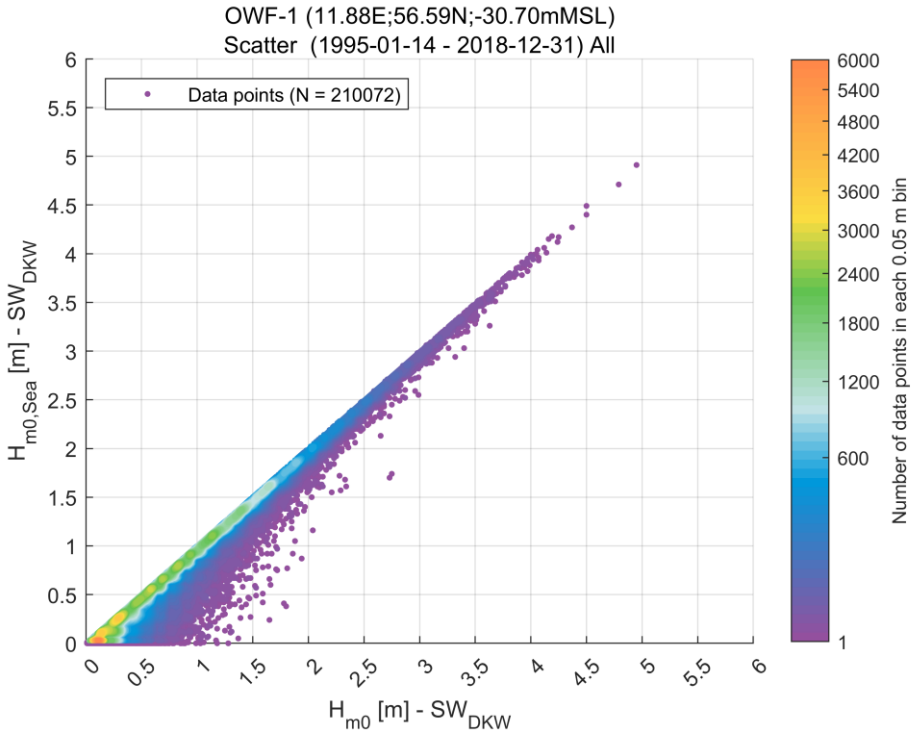

Figure 5.8 Scatter plot of $H_{m0,Sea}$ vs. $H_{m0,Total}$ at analysis point OWF-1

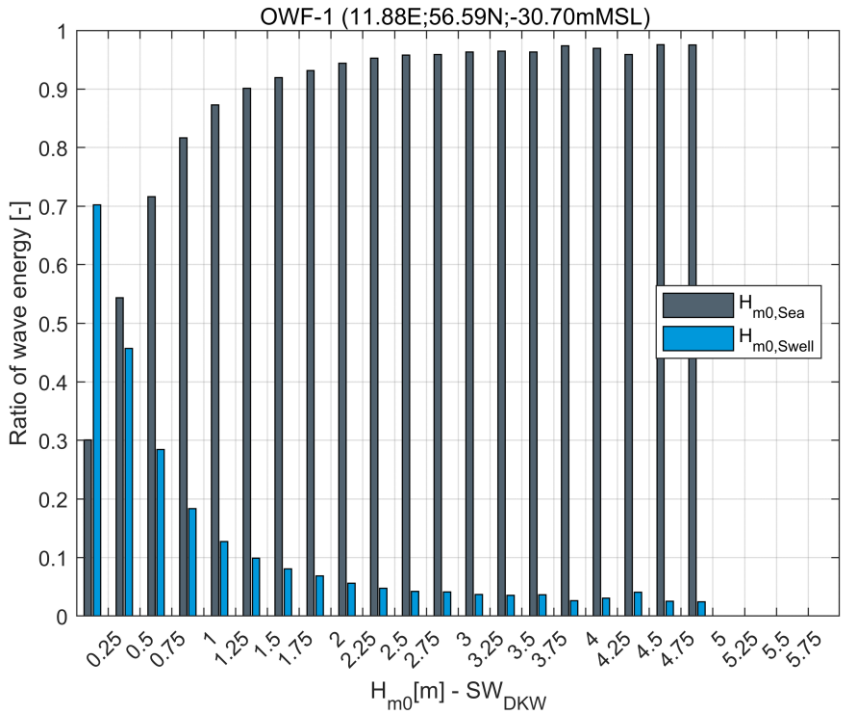

Figure 5.9 The average ratio of wind-sea and swell energy
Average ratio of wind-sea to total sea-state energy (grey bars) and swell to total sea-state energy (blue) against $H_{m0,Total}$ at analysis point OWF-1

5.2.1 H_{m0} statistics

Figure 5.10 presents plots of plots of the monthly and directional statistics (mean, min, max and standard deviation) of H_{m0} at analysis point OWF-1. The statistics are summarised for all analysis points in Table 5.5 and Table 5.6.

The largest wave heights are associated with the months of November to February, while the smallest waves occur from May to July. This is consistent with the monthly statistics of wind speed presented in Sections 5.1.1 and 5.1.2. Directional sectors from 210°N to 0°N exhibit the largest significant wave heights. The smallest average significant wave heights are from 0° to 60° whilst the smallest maximum significant wave heights are from sectors 60°N to 180°N.

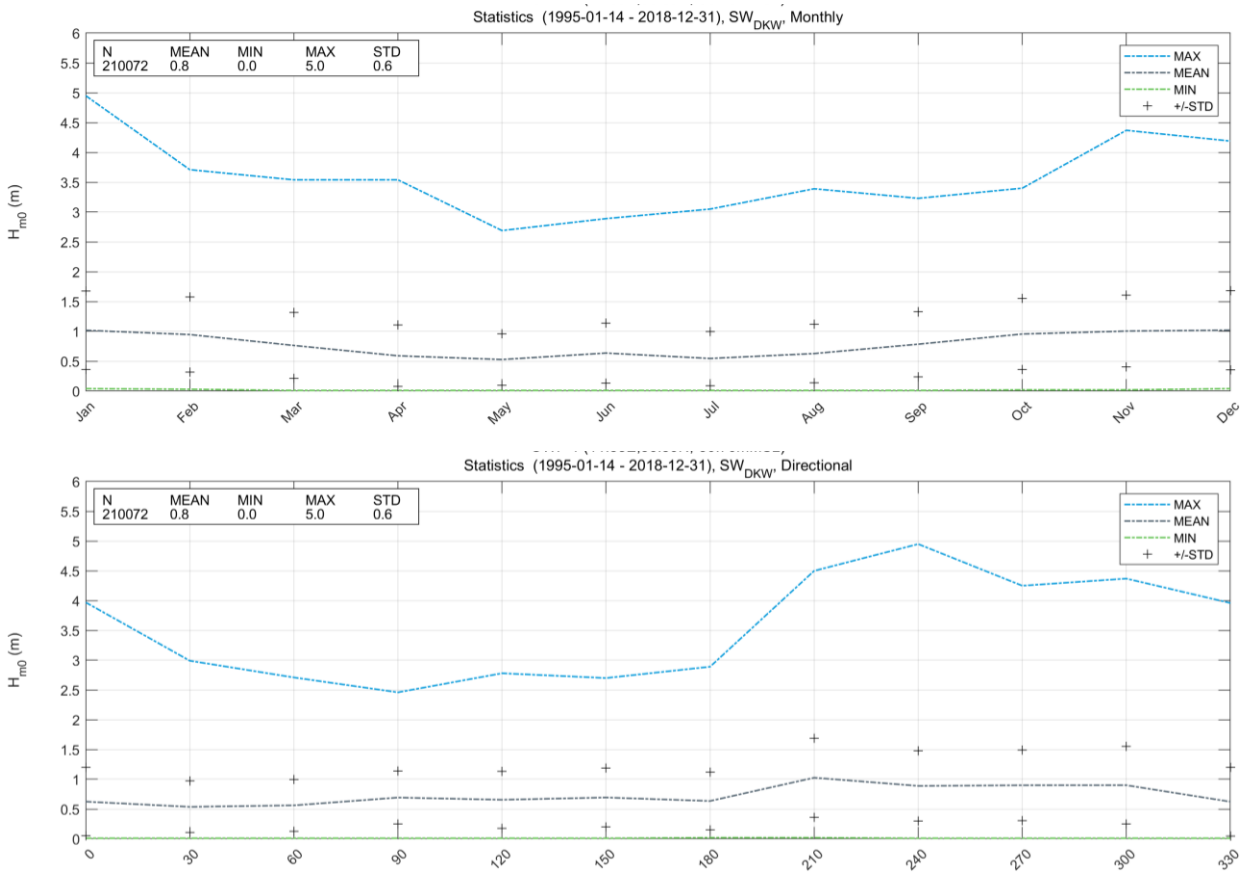

Figure 5.10 Monthly and directional H_{m0} statistics at analysis point OWF-1
Mean, minimum, maximum, and standard deviation of H_{m0} derived from SW_{DKW} model (1995-01-14 to 2018-12-31)

Table 5.5 All-year and monthly statistics of H_{m0} at the Hesselø OWF

Mean, minimum, maximum, and standard deviation of SW_{DKW} model spectral significant wave heights (1995-01-14 to 2018-12-31)

Month	OWF-1				OWF-2				OWF-3			
	Mean [m]	Min. [m]	Max. [m]	STD [m]	Mean [m]	Min. [m]	Max. [m]	STD [m]	Mean [m]	Min. [m]	Max. [m]	STD [m]
All-year	0.8	0.0	5.0	0.6	0.7	0.0	4.6	0.6	0.8	0.0	4.6	0.6
Jan	1.0	0.0	5.0	0.7	0.9	0.0	4.6	0.6	1.0	0.0	4.6	0.6
Feb	0.9	0.0	3.7	0.6	0.9	0.0	3.9	0.6	0.9	0.0	3.7	0.6
Mar	0.8	0.0	3.5	0.6	0.7	0.0	3.9	0.5	0.8	0.0	3.5	0.5
Apr	0.6	0.0	3.5	0.5	0.6	0.0	4.0	0.5	0.6	0.0	3.5	0.5
May	0.5	0.0	2.7	0.4	0.5	0.0	2.8	0.4	0.5	0.0	2.6	0.4
Jun	0.6	0.0	2.9	0.5	0.6	0.0	3.1	0.5	0.6	0.0	2.8	0.5
Jul	0.5	0.0	3.1	0.5	0.5	0.0	2.9	0.5	0.5	0.0	3.0	0.4
Aug	0.6	0.0	3.4	0.5	0.6	0.0	3.7	0.5	0.6	0.0	3.2	0.5
Sep	0.8	0.0	3.2	0.5	0.7	0.0	3.5	0.5	0.8	0.0	3.1	0.5
Oct	1.0	0.0	3.4	0.6	0.9	0.0	4.0	0.6	0.9	0.0	3.5	0.6
Nov	1.0	0.0	4.4	0.6	0.9	0.0	4.5	0.6	1.0	0.0	4.1	0.6
Dec	1.0	0.0	4.2	0.7	1.0	0.0	4.5	0.6	1.0	0.0	4.2	0.6

Table 5.6 Omnidirectional and directional statistics of H_{m0} at the Hesselø OWF

Mean, minimum, maximum, and standard deviation of SW_{DKW} model spectral significant wave heights (1995-01-14 to 2018-12-31)

Direction sector (°from)	OWF-1				OWF-2				OWF-3			
	Mean [m]	Min. [m]	Max. [m]	STD [m]	Mean [m]	Min. [m]	Max. [m]	STD [m]	Mean [m]	Min. [m]	Max. [m]	STD [m]
Omnidirectional	0.8	0.0	5.0	0.6	0.7	0.0	4.6	0.6	0.8	0.0	4.6	0.6
[345 – 015[	0.6	0.0	4.0	0.6	0.6	0.0	4.3	0.6	0.6	0.0	4.0	0.6
[015 - 045[	0.5	0.0	3.0	0.4	0.5	0.0	2.7	0.5	0.6	0.0	3.6	0.5
[045 - 075[	0.6	0.0	2.7	0.4	0.6	0.0	2.9	0.5	0.6	0.0	3.2	0.5
[075 – 105[	0.7	0.0	2.5	0.4	0.6	0.0	2.5	0.4	0.7	0.0	2.9	0.5
[105 – 135[	0.7	0.0	2.8	0.5	0.6	0.0	2.4	0.4	0.7	0.0	2.8	0.5
[135 – 165[	0.7	0.0	2.7	0.5	0.5	0.0	2.1	0.4	0.6	0.0	2.4	0.4
[165 – 195[	0.6	0.0	2.9	0.5	0.5	0.0	2.3	0.4	0.6	0.0	2.7	0.4
[195 – 225[	1.0	0.0	4.5	0.7	0.7	0.0	3.4	0.5	0.9	0.0	3.8	0.6
[225 – 255[	0.9	0.0	5.0	0.6	1.0	0.0	4.6	0.6	0.9	0.0	4.6	0.6
[255 – 285[	0.9	0.0	4.3	0.6	0.8	0.0	4.0	0.6	0.8	0.0	4.0	0.5
[285 – 315[	0.9	0.0	4.4	0.6	1.0	0.0	4.5	0.7	0.9	0.0	4.2	0.6
[315 – 345[	0.6	0.0	4.0	0.6	0.7	0.0	4.3	0.6	0.6	0.0	3.6	0.6

5.2.2 T_p statistics

Figure 5.11 presents plots of the monthly and directional statistics (mean, min, max and standard deviation) of peak wave period (T_p) at analysis point OWF-1. The statistics are summarised for all analysis points in Table 5.7 and Table 5.8.

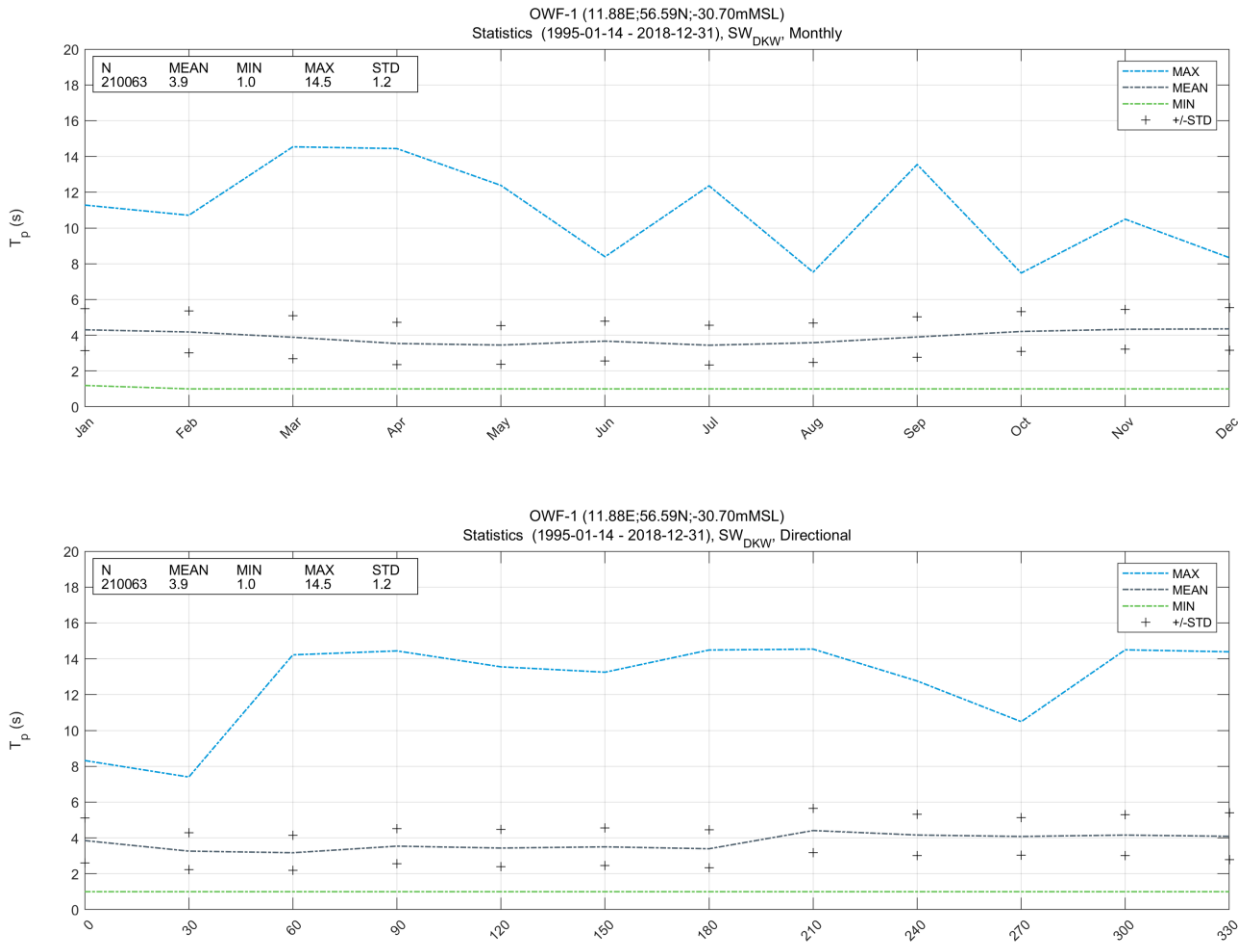

Figure 5.11 Monthly and directional T_p statistics at analysis point OWF-1
Mean, minimum, maximum, and standard deviation of T_p derived from SW_{DKW} model (1995-01-14 to 2018-12-31)

Table 5.7 All-year and monthly statistics of T_p at the Hesselø OWF

Mean, minimum, maximum, and standard deviation of SW_{DKW} model peak wave period (1995-01-14 to 2018-12-31)

Month	OWF-1				OWF-2				OWF-3			
	Mean [s]	Min. [s]	Max. [s]	STD [s]	Mean [s]	Min. [s]	Max. [s]	STD [s]	Mean [s]	Min. [s]	Max. [s]	STD [s]
All-year	3.9	1.0	14.5	1.2	3.8	1.0	14.5	1.2	3.8	1.0	14.6	1.2
Jan	4.3	1.2	11.3	1.2	4.1	1.0	12.0	1.1	4.2	1.0	11.4	1.1
Feb	4.2	1.0	10.7	1.2	4.0	1.0	11.6	1.2	4.1	1.0	7.3	1.1
Mar	3.9	1.0	14.5	1.2	3.8	1.0	14.5	1.2	3.8	1.0	14.6	1.2
Apr	3.5	1.0	14.4	1.2	3.4	1.0	14.3	1.2	3.4	1.0	14.3	1.2
May	3.5	1.0	12.4	1.1	3.4	1.0	12.0	1.1	3.3	1.0	11.8	1.1
Jun	3.7	1.0	8.4	1.1	3.6	1.0	8.9	1.2	3.6	1.0	8.6	1.1
Jul	3.4	1.0	12.4	1.1	3.4	1.0	12.0	1.1	3.3	1.0	11.7	1.1
Aug	3.6	1.0	7.5	1.1	3.5	1.0	8.1	1.1	3.5	1.0	7.6	1.1
Sep	3.9	1.0	13.6	1.1	3.8	1.0	14.0	1.1	3.8	1.0	13.5	1.1
Oct	4.2	1.0	7.5	1.1	4.0	1.0	7.4	1.1	4.1	1.0	7.4	1.1
Nov	4.3	1.0	10.5	1.1	4.1	1.0	11.3	1.1	4.2	1.0	7.6	1.1
Dec	4.4	1.0	8.3	1.2	4.2	1.1	8.2	1.2	4.2	1.2	7.5	1.1

Table 5.8 Omnidirectional and directional statistics of T_p at the Hesselø OWF

Mean, minimum, maximum, and standard deviation of SW_{DKW} model peak wave period (1995-01-14 to 2018-12-31)

Direction sector (°from)	OWF-1				OWF-2				OWF-3			
	Mean [s]	Min. [s]	Max. [s]	STD [s]	Mean [s]	Min. [s]	Max. [s]	STD [s]	Mean [s]	Min. [s]	Max. [s]	STD [s]
Omnidirectional	3.9	1.0	14.5	1.2	3.8	1.0	14.5	1.2	3.8	1.0	14.6	1.2
[345 – 015[	3.9	1.0	8.3	1.3	3.8	1.0	14.5	1.3	3.7	1.0	13.7	1.2
[015 - 045[	3.3	1.0	7.4	1.0	3.3	1.0	14.3	1.1	3.3	1.0	11.8	1.1
[045 - 075[	3.2	1.0	14.2	1.0	3.4	1.0	13.7	1.1	3.3	1.0	14.1	1.1
[075 – 105[	3.5	1.0	14.4	1.0	3.3	1.0	14.0	1.0	3.6	1.0	14.3	1.1
[105 – 135[	3.4	1.0	13.6	1.0	3.2	1.0	11.4	0.9	3.5	1.0	6.8	1.0
[135 – 165[	3.5	1.0	13.3	1.0	3.0	1.0	13.8	0.9	3.2	1.0	14.5	1.0
[165 – 195[	3.4	1.0	14.5	1.1	3.0	1.0	9.0	0.8	3.3	1.0	14.6	1.0
[195 – 225[	4.4	1.0	14.5	1.2	3.5	1.0	11.6	1.0	4.2	1.0	7.4	1.2
[225 – 255[	4.2	1.0	12.8	1.2	4.3	1.0	10.7	1.1	4.1	1.0	8.3	1.1
[255 – 285[	4.1	1.0	10.5	1.1	4.0	1.0	12.9	1.1	3.8	1.0	14.6	1.0
[285 – 315[	4.2	1.0	14.5	1.1	4.3	1.0	12.0	1.2	4.2	1.0	14.5	1.1
[315 – 345[	4.1	1.0	14.4	1.3	4.0	1.0	13.5	1.3	3.7	1.0	14.2	1.2

5.2.3 T_{02} statistics

Figure 5.12 presents plots of the monthly and directional statistics (mean, min, max and standard deviation) of the spectral equivalent of the mean zero-crossing wave period (T_{02}) at analysis point OWF-1. The statistics are summarised for all analysis points in Table 5.9 and Table 5.10.

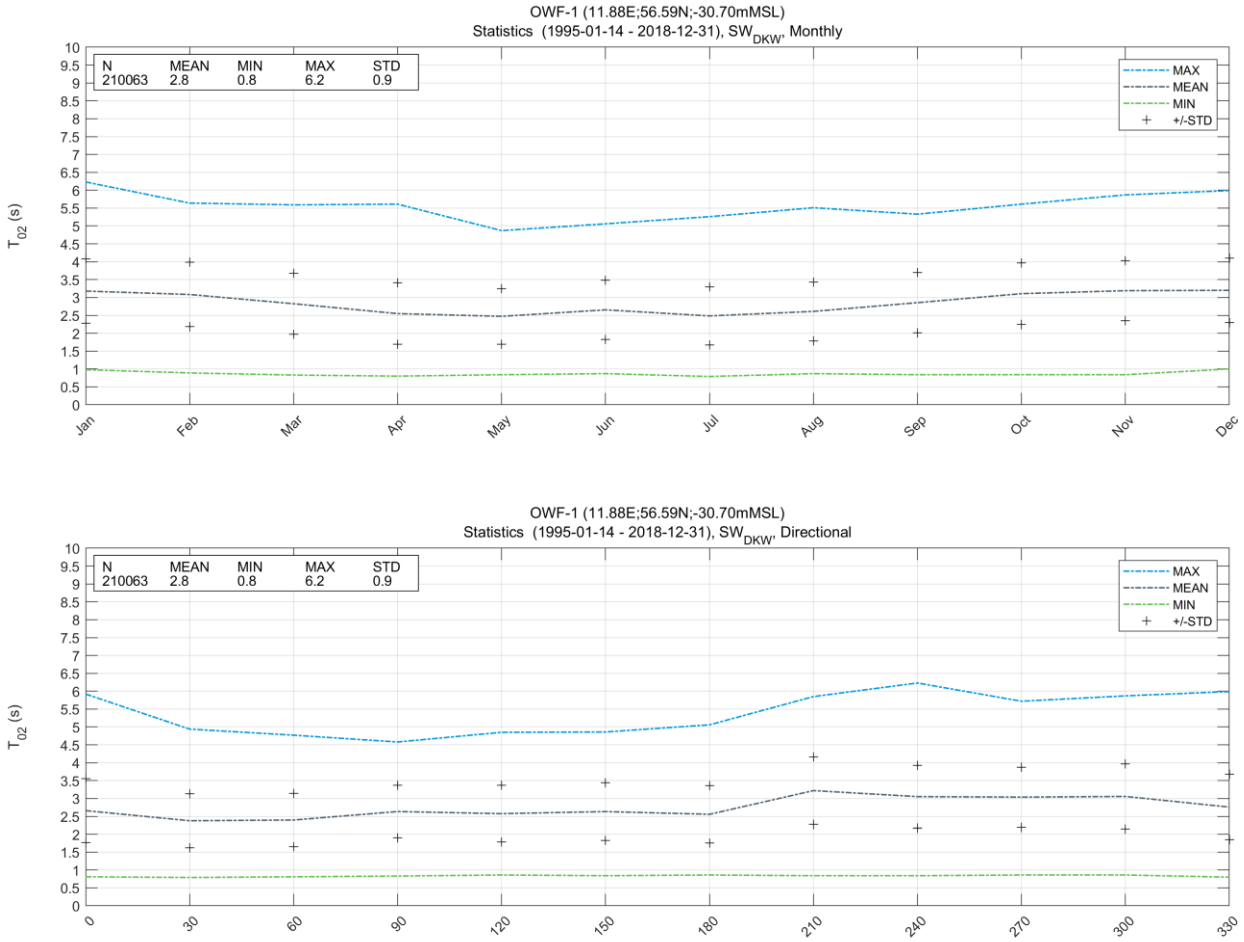

Figure 5.12 Monthly and directional T_{02} statistics at analysis point OWF-1
Mean, minimum, maximum, and standard deviation of T_{02} derived from SW_{DKW} model (1995-01-14 to 2018-12-31)

Table 5.9 All-year and monthly statistics of T_{02} at the Hesselø OWF

Mean, minimum, maximum, and standard deviation of SW_{DKW} model spectral equivalent of the mean zero-crossing period (1995-01-14 to 2018-12-31)

Month	OWF-1				OWF-2				OWF-3			
	Mean [s]	Min. [s]	Max. [s]	STD [s]	Mean [s]	Min. [s]	Max. [s]	STD [s]	Mean [s]	Min. [s]	Max. [s]	STD [s]
All-year	2.8	0.8	6.2	0.9	2.8	0.8	6.2	0.9	2.8	0.8	6.0	0.9
Jan	3.2	1.0	6.2	0.9	3.0	0.8	5.9	0.9	3.1	0.9	6.0	0.9
Feb	3.1	0.9	5.6	0.9	3.0	0.9	5.9	0.9	3.0	0.9	5.5	0.9
Mar	2.8	0.8	5.6	0.9	2.7	0.8	5.9	0.9	2.8	0.8	5.4	0.9
Apr	2.5	0.8	5.6	0.9	2.5	0.8	6.0	0.9	2.5	0.8	5.5	0.9
May	2.5	0.8	4.9	0.8	2.4	0.8	5.1	0.8	2.4	0.8	4.8	0.8
Jun	2.7	0.9	5.1	0.8	2.6	0.8	5.4	0.9	2.6	0.8	5.0	0.8
Jul	2.5	0.8	5.3	0.8	2.5	0.8	5.0	0.8	2.4	0.8	5.1	0.8
Aug	2.6	0.9	5.5	0.8	2.6	0.8	5.7	0.8	2.6	0.9	5.3	0.8
Sep	2.9	0.8	5.3	0.8	2.8	0.9	5.5	0.8	2.8	0.9	5.1	0.8
Oct	3.1	0.8	5.6	0.9	3.0	0.8	5.6	0.8	3.0	0.8	5.6	0.8
Nov	3.2	0.8	5.9	0.8	3.0	0.9	6.1	0.8	3.1	0.9	5.7	0.8
Dec	3.2	1.0	6.0	0.9	3.1	0.9	6.2	0.9	3.1	1.0	5.7	0.9

Table 5.10 Omnidirectional and directional statistics of T_{02} at the Hesselø OWF

Mean, minimum, maximum, and standard deviation of SW_{DKW} model spectral equivalent of the mean zero-crossing period (1995-01-14 to 2018-12-31)

Direction sector (°from)	OWF-1				OWF-2				OWF-3			
	Mean [s]	Min. [s]	Max. [s]	STD [s]	Mean [s]	Min. [s]	Max. [s]	STD [s]	Mean [s]	Min. [s]	Max. [s]	STD [s]
Omnidirectional	2.8	0.8	6.2	0.9	2.8	0.8	6.2	0.9	2.8	0.8	6.0	0.9
[345 – 015[	2.7	0.8	5.9	0.9	2.7	0.8	6.1	0.9	2.6	0.8	5.7	0.9
[015 - 045[	2.4	0.8	4.9	0.8	2.4	0.8	4.9	0.8	2.4	0.8	5.4	0.8
[045 - 075[	2.4	0.8	4.8	0.7	2.5	0.9	5.0	0.8	2.5	0.9	5.2	0.9
[075 – 105[	2.6	0.8	4.6	0.7	2.5	0.9	4.6	0.7	2.7	0.9	5.0	0.8
[105 – 135[	2.6	0.9	4.9	0.8	2.4	0.8	4.5	0.7	2.6	0.8	4.9	0.8
[135 – 165[	2.6	0.8	4.9	0.8	2.3	0.8	4.2	0.6	2.5	0.8	4.6	0.8
[165 – 195[	2.6	0.9	5.1	0.8	2.3	0.8	4.3	0.6	2.5	0.8	4.7	0.7
[195 – 225[	3.2	0.8	5.9	0.9	2.6	0.8	4.9	0.7	3.1	0.9	5.6	0.9
[225 – 255[	3.1	0.8	6.2	0.9	3.1	0.8	5.8	0.8	3.0	0.9	6.0	0.9
[255 – 285[	3.0	0.9	5.7	0.8	2.9	0.9	5.7	0.9	2.9	0.9	5.7	0.8
[285 – 315[	3.1	0.9	5.9	0.9	3.2	0.9	6.1	0.9	3.1	0.8	5.7	0.9
[315 – 345[	2.8	0.8	6.0	0.9	2.7	0.8	6.1	0.9	2.6	0.8	5.6	0.9

5.2.4 Distribution of H_{m0} and MWD

Figure 5.13 and Figure 5.14 present the all-year rose plot and density scatter plots of H_{m0} and MWD at analysis points OWF-1, OWF-2, and OWF-3. Typically, the most frequent wave directions are associated with sectors between 210°N and 300°N across all analysis sites, although at OWF-2 and OWF-3 there are fewer waves from the 270°N sector than at analysis point OWF-1.

Tables giving the frequency of occurrence [%] of spectral significant wave height and mean wave direction at all analysis points are provided in digital format (Microsoft Excel, .xlsx) accompanying this report (see Appendix C). The tables are provided for the following intervals:

- H_{m0} intervals of 0.5 m.
- MWD intervals of 30°, centred on 0°N, 30°N, 60°N, etc.
- All-year and for each calendar month

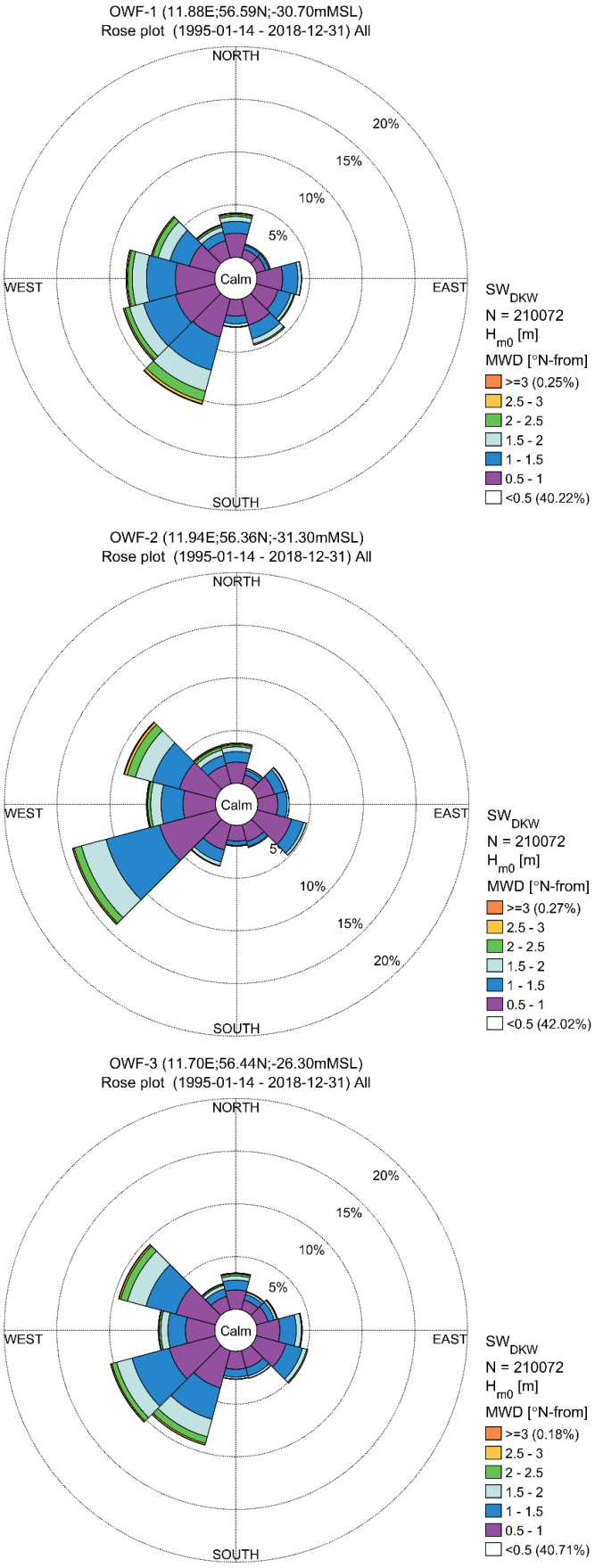

Figure 5.13 Rose plots of all-year H_{m0} and MWD at analysis points OWF-1, OWF-2, and OWF-3
Rose plots show the frequency of occurrence of significant wave height for each 30° direction bin, derived from SW_{DKW} model (1995-01-14 to 2018-12-31)

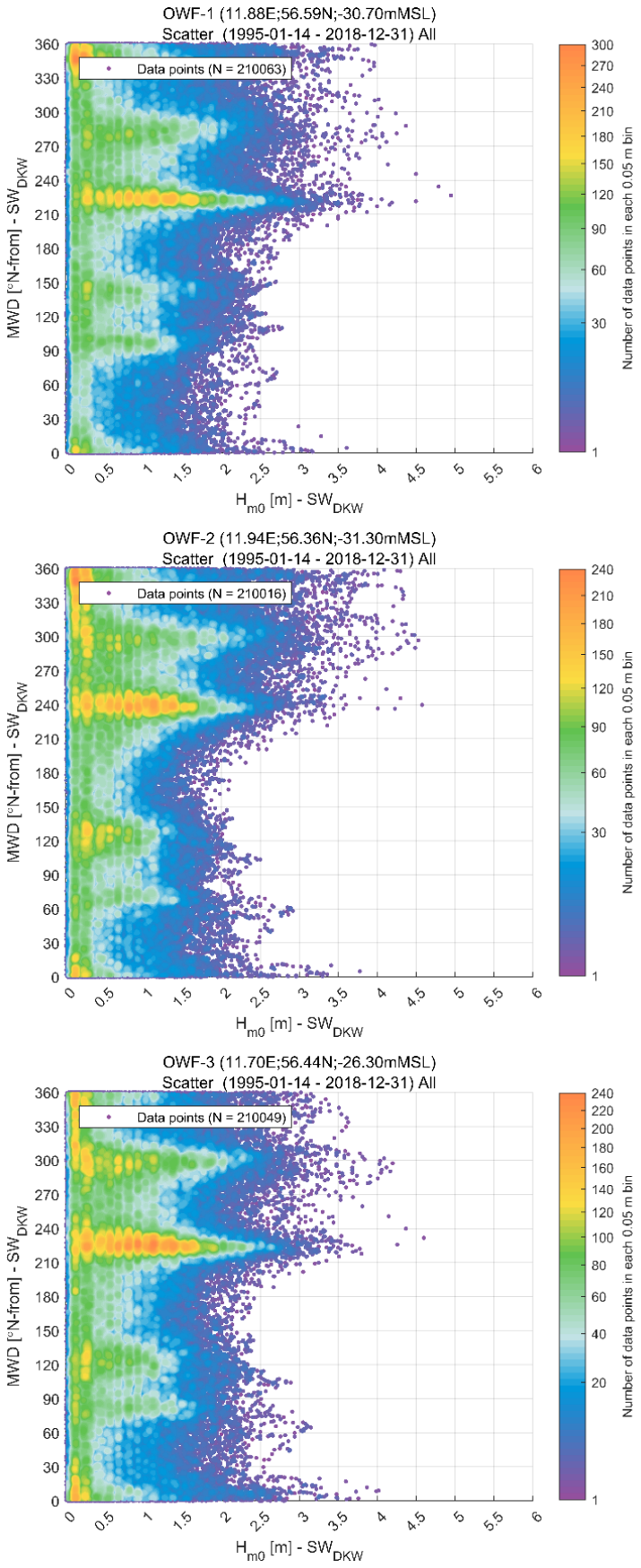

Figure 5.14 Density scatter plots of H_{m0} and MWD at analysis points OWF-1, OWF-2, and OWF-3
All-year density scatter plot showing magnitude of joint occurrence for total sea state conditions

5.2.5 Distributions of H_{m0} and wave periods

Figure 5.15 and Figure 5.16 present the density scatter plots (annual and omnidirectional) of T_p vs. H_{m0} and T_{02} vs. H_{m0}, respectively. A least-squares power function of the form $T = a \cdot {H_{m0}}^b$ was fitted to the 50% quantile of the wave period data for each H_{m0} bin (conditioned on the largest 10% of the H_{m0} data). The resulting fits were used to estimate the values of T_p and T_{02} associated with omnidirectional extreme significant wave heights in Section 6.2.4.

Tables giving the frequency of occurrence [%] of spectral significant wave height and wave period (T_p and T_{02}) at all analysis points are provided in digital format (Microsoft Excel, .xlsx) accompanying this report (see Appendix C). The tables are provided for the following intervals:

- H_{m0} intervals of 0.5 m
- Wave period intervals (T_p and T_{02}) of 0.5 s
- Omnidirectional and for 12 x 30° directional sectors (conditioned on MWD)

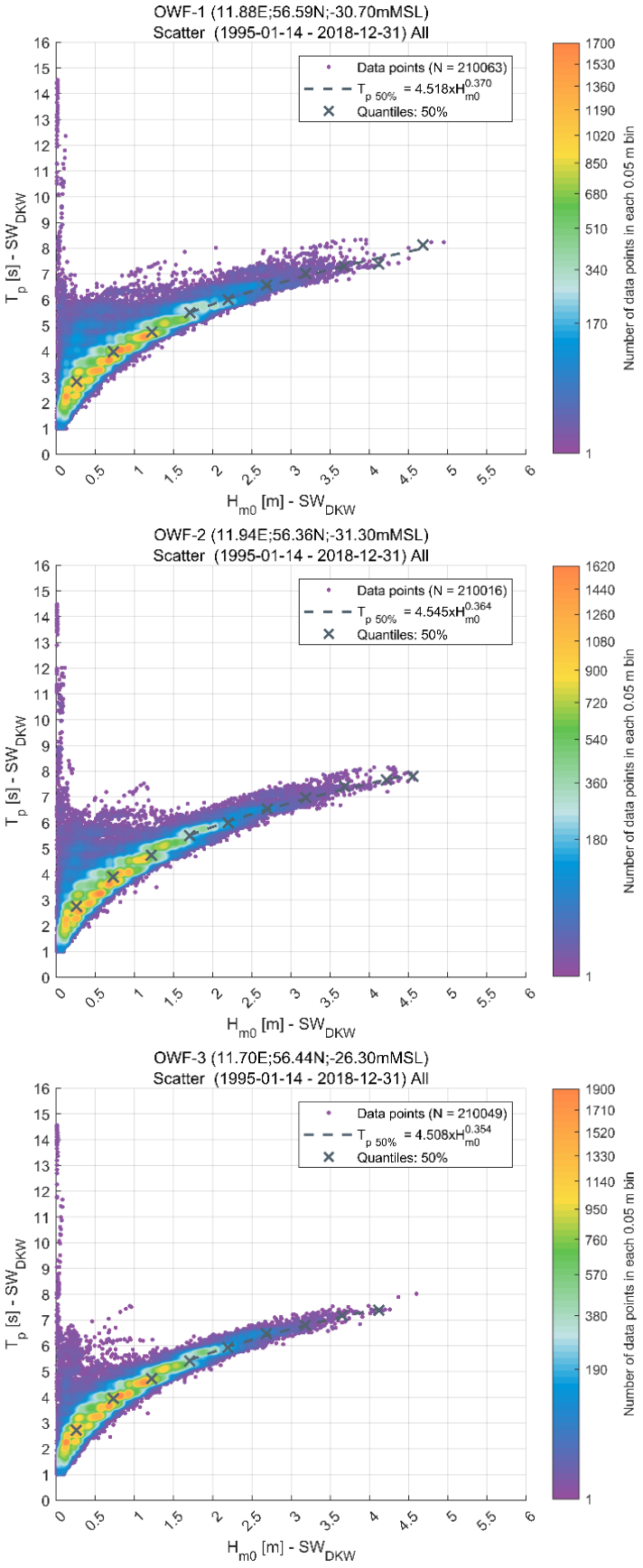

Figure 5.15 Density scatter plots of H_{m0} and T_p at analysis points OWF-1, OWF-2, and OWF-3
Omnidirectional and all-year. The dashed grey line shows a least-squares power function fits to the largest waves (above the 90-percentile value of H_{m0}). The resulting equations are given in the legend, where T_p is given in units of seconds, and H_{m0} is given in units of meters

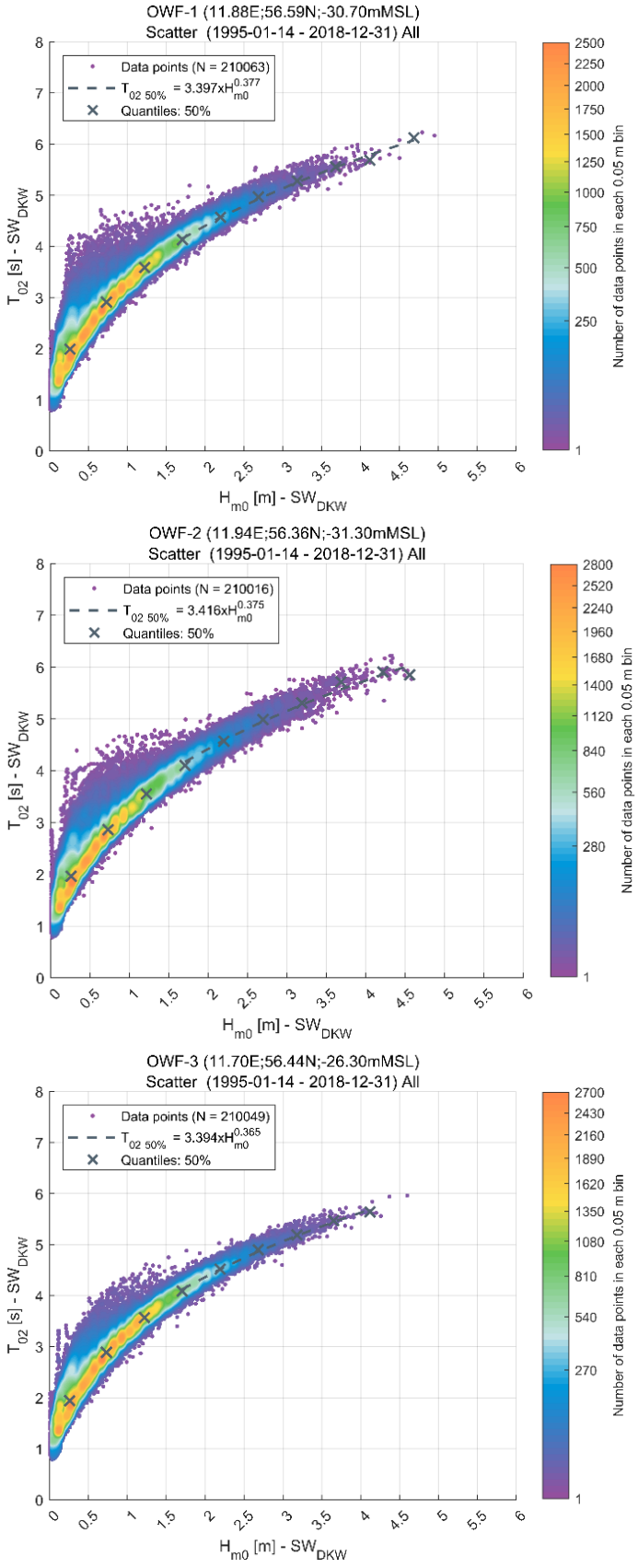

Figure 5.16 Density scatter plot of H_{m0} and T_{02} at analysis points OWF-1, OWF-2, and OWF-3
Omnidirectional and all-year. The dashed grey line shows a least-squares power function fits to the 50% quantiles of the largest waves (above the 90-percentile value of H_{m0}). The resulting equations are given in the legend, where T_{02} is given in units of seconds, and H_{m0} is given in units of meters

5.2.6 Wind – wave misalignment

Wind-wave misalignment was calculated as mean wave direction minus wind direction at 10 mMSL (i.e., MWD – WD_{10}) at each model time-step. For example, if the wind is coming from south (WD_{10} = 180 °N) and the mean wave direction is from the east (MWD = 90 °N), the misalignment is -90°.

Figure 5.17 presents a scatter plot of misalignment angle versus H_{m0} together with the all-year and monthly mean average misalignment for H_{m0} intervals of 0.5 m. Figure 5.18 shows the all-year and monthly probability distribution of misalignment. The misalignment displays high scatter for small sea-states (e.g., H_{m0} < 0.5 m), but for larger sea-state (e.g., H_{m0} > 2.0 m), the misalignment is generally ±30°.

Figure 5.19 shows density scatter plots of MWD and WD_{10} at analysis points OWF-1, OWF-2, and OWF-3. Tables giving the frequency of occurrence [%] of MWD and WD_{10} are provided in digital format (Microsoft Excel, .xlsx) accompanying this report (see Appendix C). The tables are provided for the following intervals:

- MWD and WD_{10} intervals of 30°, centred on 0°N, 30°N, 60°N, etc.
- All-year and for each calendar month

5.2.7 Wave height and water level correlation

Figure 5.19 presents a density scatter plots (all-year and omnidirectional) of H_{m0} and total water level (WL) at analysis points OWF-1, OWF-2, and OWF-3. The largest significant wave heights are, in general, associated with positive water levels at all three analysis points.

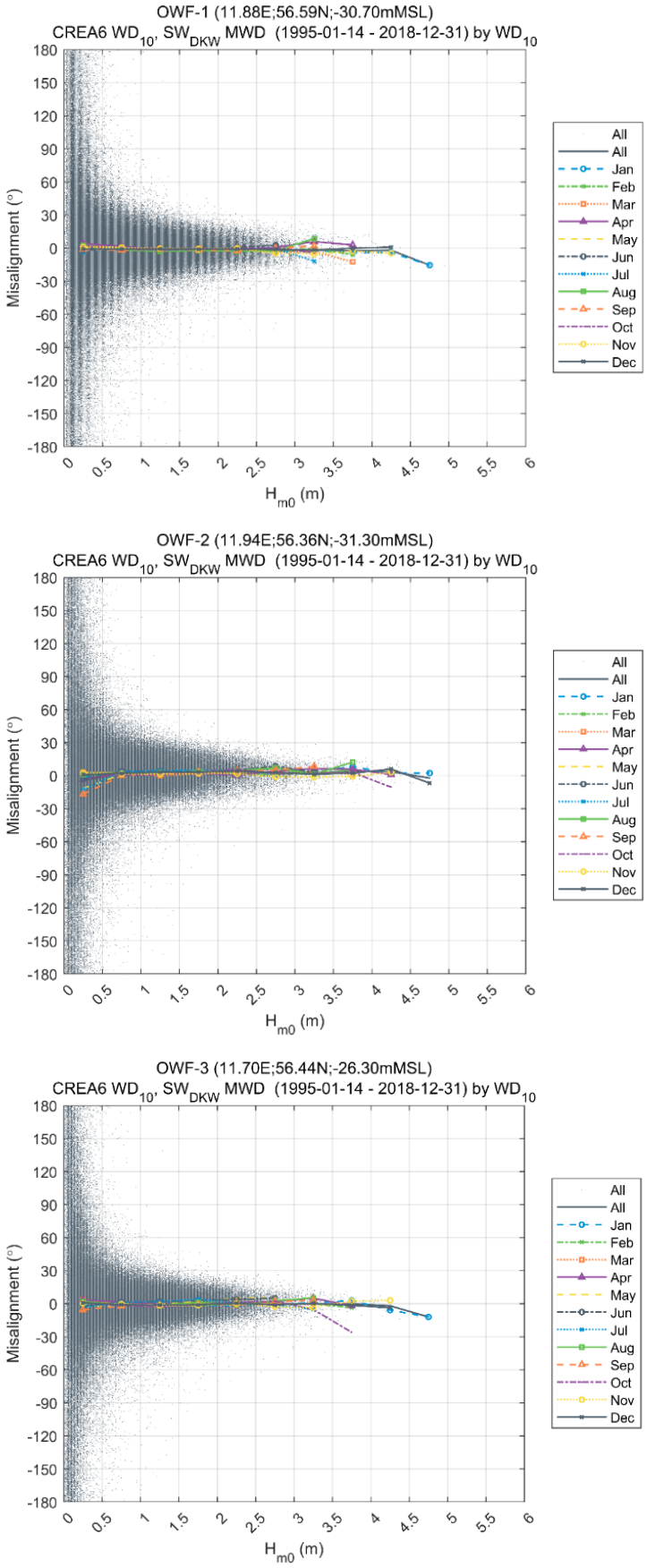

Figure 5.17 Scatter plot of H_{m0} and misalignment angle at analysis point OWF-1, OWF-2, and OWF-3
All-year and monthly mean misalignment angle (MWD – WD_{10}) for total sea-state conditions

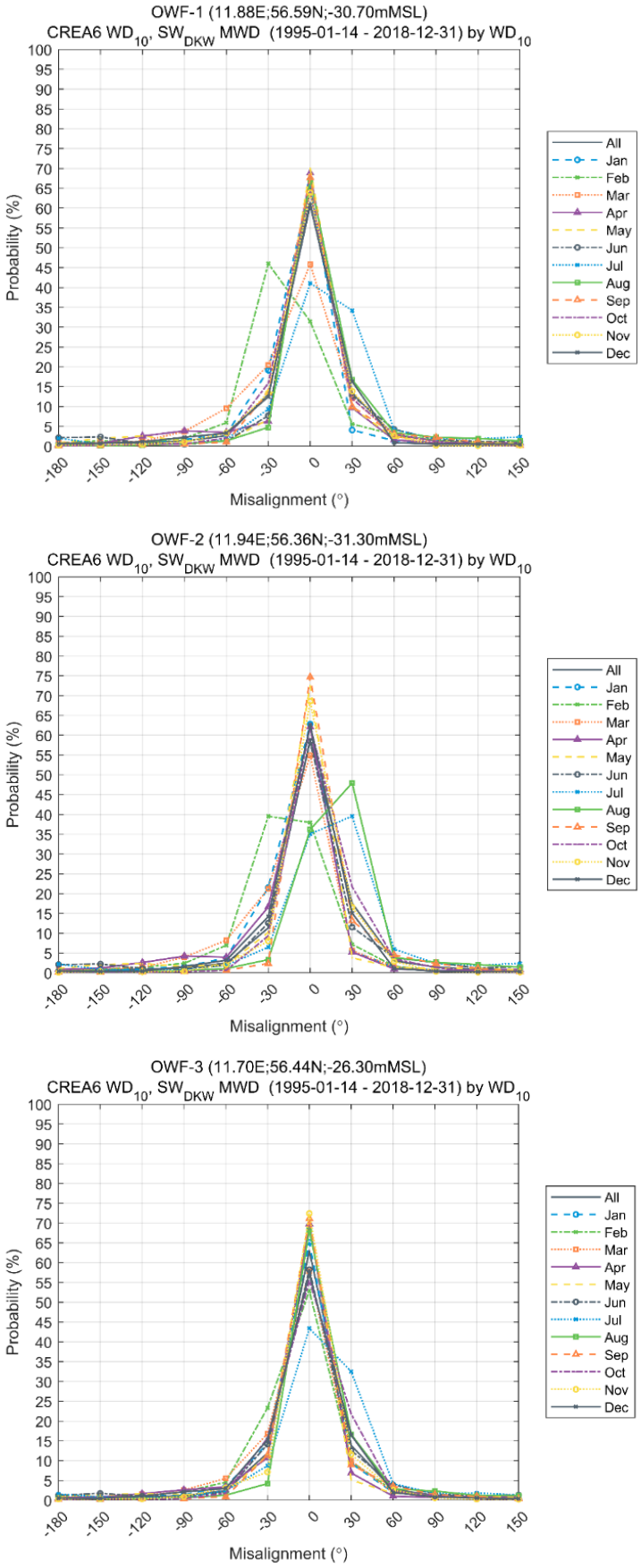

Figure 5.18 Probability of direction misalignment at analysis points OWF-1, OWF-2, and OWF-3
All-year and monthly mean misalignment angle (MWD – WD_{10}) for total sea-state conditions

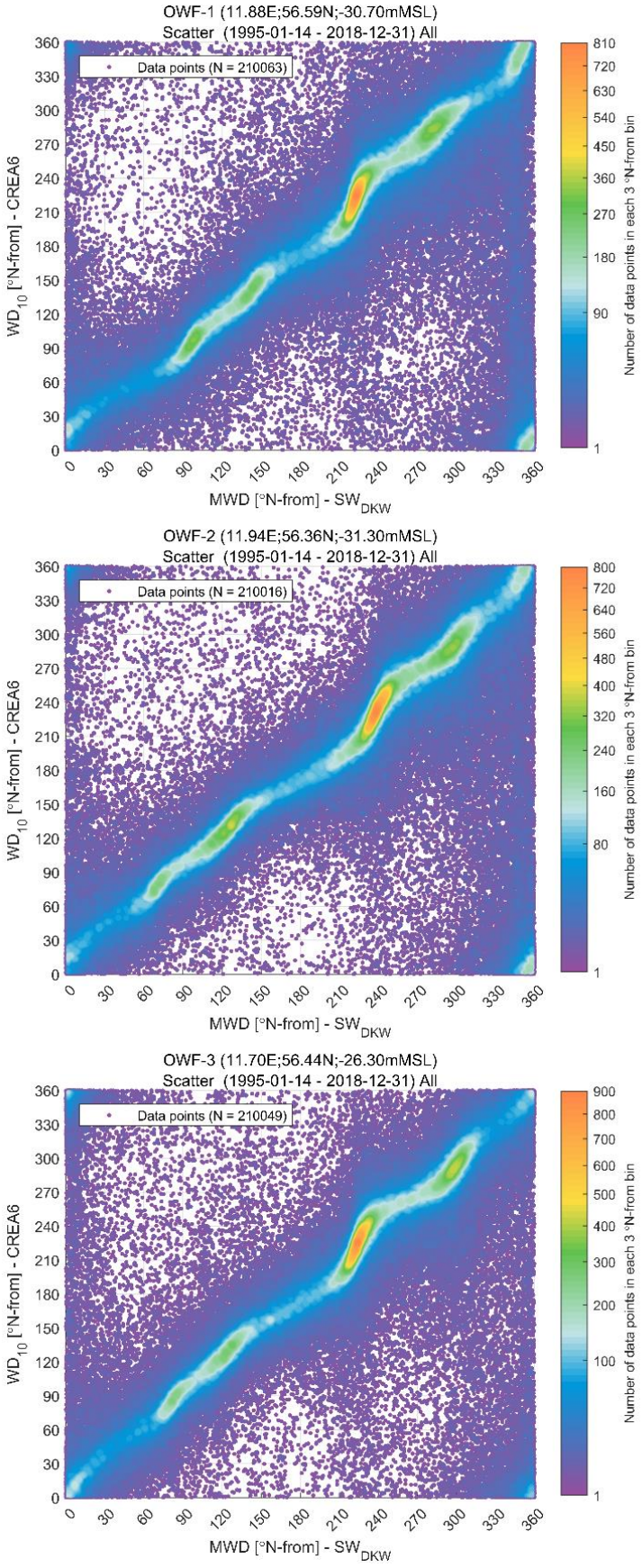

Figure 5.19 Density scatter plots of MWD and WD_{10} at analysis points OWF-1, OWF-2, and OWF-3
All-year density scatter plot showing magnitude of joint occurrence for total sea state conditions

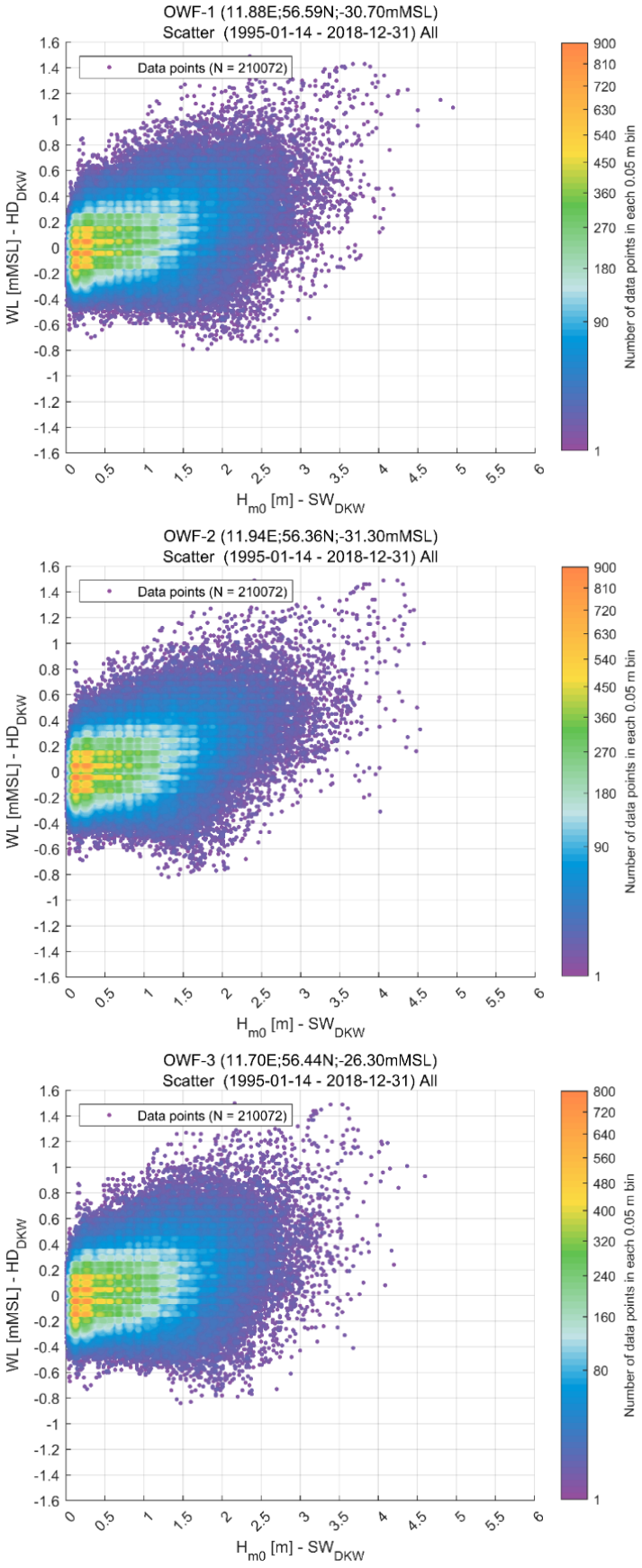

Figure 5.20 Density scatter plots of H_{m0} and WL at analysis points OWF-1, OWF-2, and OWF-3
All-year and omnidirectional

5.2.8 Wave spectral shape

This section concerns an assessment of how sea states at the Hesselø OWF may be described by parametric wave spectra, specifically the JONSWAP spectrum for developing wind wave sea-states.

As there were no available measurements of the wave energy spectra within the wind farm site, the assessment is based on the spectral output from the SW_{DKW} model.

According to Section 2.4.5.1 of [25], the spectral density of the sea elevation process may be represented by the JONSWAP spectrum:

$$S(f) = \frac{\alpha g^2}{(2\pi)^4} f^{-5} e^{\left(\frac{-5}{4}\left(\frac{f}{f_p}\right)^{-4}\right)} \gamma^{e^{(-0.5(f-f_p/\sigma f_p)^2)}} \qquad 5.3$$

Where f is the wave frequency, f_p is the spectral peak frequency, g is gravitation acceleration, α is Phillips' constant, σ is the spectral width parameter, and γ is the peak enhancement factor.

Representative parameterisations of the JONSWAP spectra were established for various discrete bins of H_{m0} (0.5 m) and T_{02} (1 second) for the total wave spectrum from the SW_{DKW} model. The parameterised spectra were fitted to the modelled frequency spectra averaged over all the sea states in each bin. The spectral peak frequency f_p was taken directly from the modelled wave energy spectra, while the quantities α and σ were determined from a least-squares fit. The spectral width parameter takes a different value for $f < f_p$ (σ_a) and $f > f_p$ (σ_b).

Examples of the spectral fits are provided for some of the most frequent sea states (i.e., 1.0 m ≤ H_{m0} < 3.0 m) at analysis point OWF-1 are shown in Figure 5.21 and Figure 5.22. Mean wave spectra for more severe sea-state conditions (i.e., 3.0 m ≤ H_{m0} ≤ 5.0 m) are provided in Figure 5.23 and Figure 5.24. For all sea-states, the fitted JONSWAP wave spectrum provides a very good fit to the mean modelled wave energy spectra.

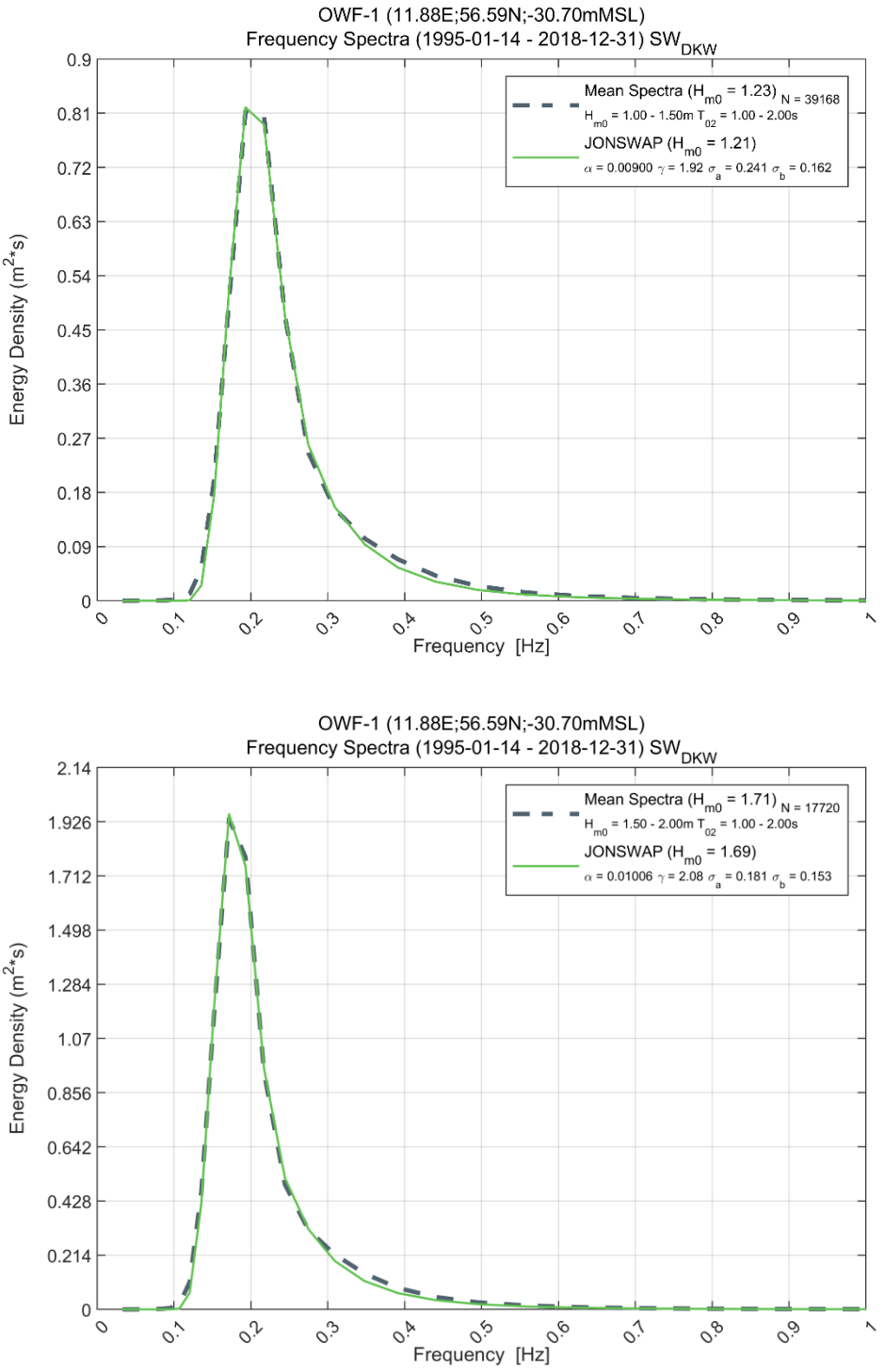

Figure 5.21 Mean wave energy density at analysis point OWF-1 (operational)

The plots show common sea-states at the site: 1.0 m ≤ H_{m0} < 1.5 m, 1.0 s ≤ T_{02} < 2.0 s (upper panel) and 1.5 m ≤ H_{m0} < 2.0 m, 1.0 s ≤ T_{02} < 2.0 s (lower panel). The dashed grey line shows the mean directional integrated model spectra, and the fitted JONSWAP spectrum is displayed in green. The value of N in the legend of the plot indicates the number of sea-states for the H_{m0}-T_{02} combination

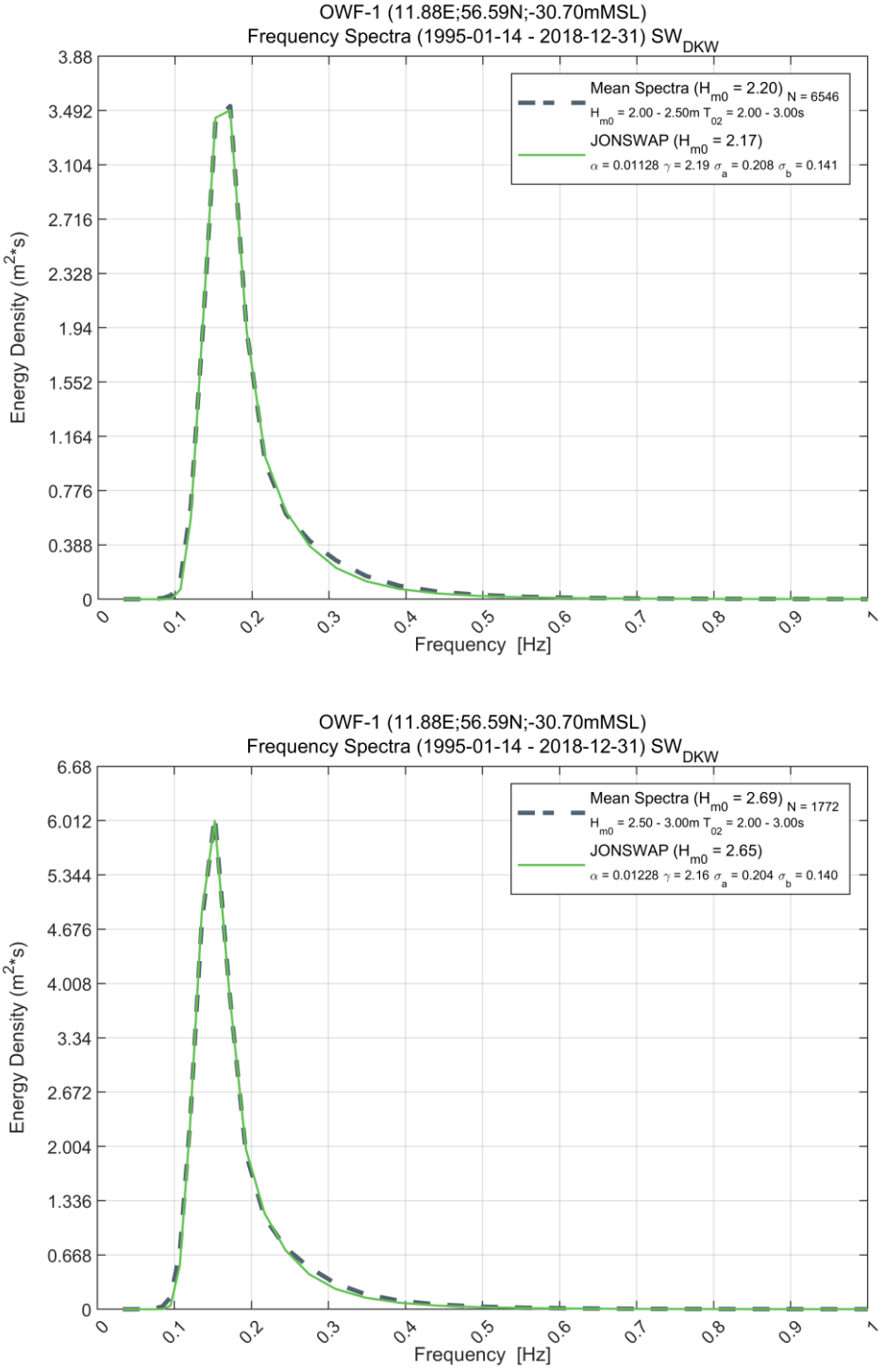

Figure 5.22 Mean wave energy density at analysis point OWF-1 (operational)
The plots show common sea-states at the site: 2.0 m ≤ H_{m0} < 2.5 m, 2.0 s ≤ T_{02} < 3.0 s (upper panel), 2.5 m ≤ H_{m0} < 3.0 m, 2.0 s ≤ T_{02} < 3.0 s (lower panel). The dashed grey line shows the mean directional integrated model spectra, and the fitted JONSWAP spectrum is displayed in green. The value of N in the legend of the plot indicates the number of sea-states for the H_{m0}-T_{02} combination

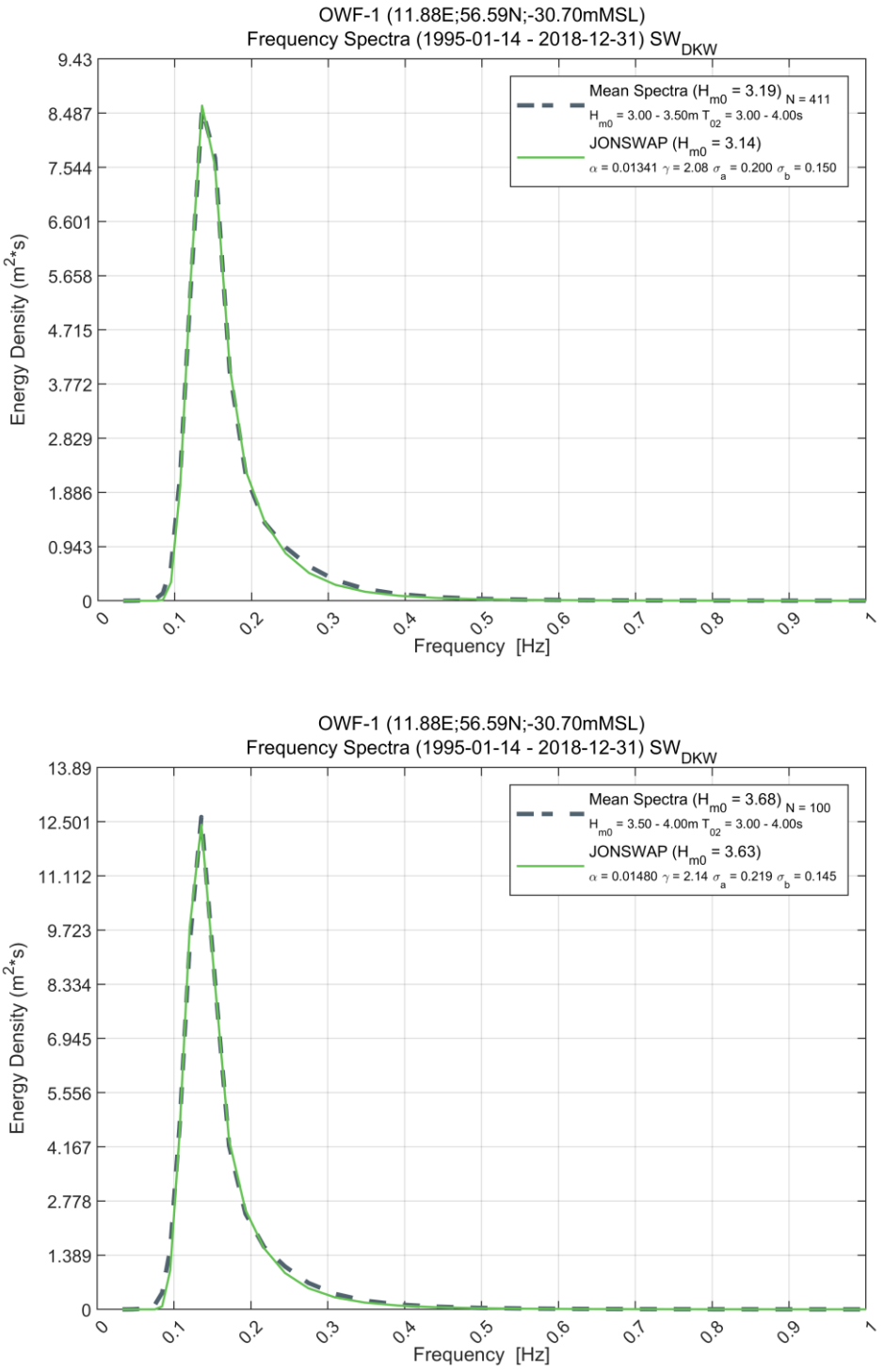

Figure 5.23 Mean wave energy density at analysis point OWF-1 (severe)
The plots show common sea-states at the site: 1.0 m ≤ H_{m0} < 1.5 m, 1.0 s ≤ T_{02} < 2.0 s (upper panel) and 1.5 m ≤ H_{m0} < 2.0 m, 1.0 s ≤ T_{02} < 2.0 s (lower panel). The dashed grey line shows the mean directional integrated model spectra, and the fitted JONSWAP spectrum is displayed in green. The value of N in the legend of the plot indicates the number of sea-states for the H_{m0}-T_{02} combination

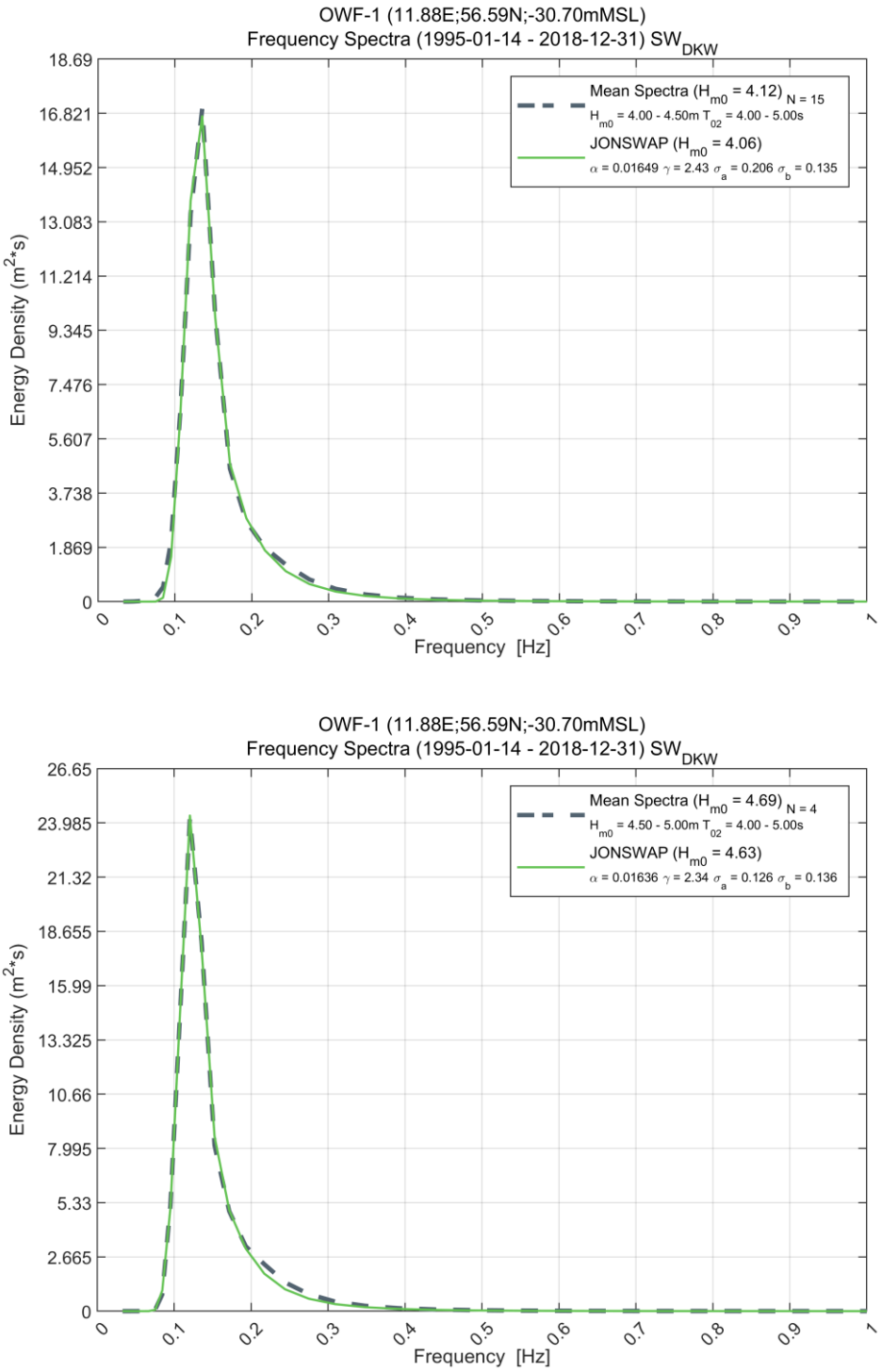

Figure 5.24 Mean wave energy density at analysis point OWF-1 (operational)
The plots show common sea-states at the site: 4.0 m ≤ H_{m0} < 4.5 m, 4.0 s ≤ T_{02} < 5.0 s (upper panel), 4.5 m ≤ H_{m0} < 5.0 m, 4.0 s ≤ T_{02} < 5.0 s (lower panel). The dashed grey line shows the mean directional integrated model spectra, and the fitted JONSWAP spectrum is displayed in green. The value of N in the legend of the plot indicates the number of sea-states for the H_{m0}-T_{02} combination

5.3 Current speed conditions

The operational current speeds at the Hesselø OWF are described below. The results are derived from the depth-averaged outputs from HD_{DKW} model as described in Section 2.3.2.

A multiplication factor of 1.5 has been applied to the total current speeds (see Section 3.3.2). It is noted that the depth averaged current speeds do not include any effects of stratification over the water depth.

5.3.1 Total current speed statistics

Figure 5.25 presents plots of the monthly and directional statistics (mean, min, max, and standard deviation) of the total depth-averaged current speed (CS_{Total}) at analysis point OWF-1. The statistics are summarised for all analysis points in Table 5.11 and Table 5.12 respectively.

The largest depth-averaged total current speeds occur between the months of November and February, while the smallest values from April to July. Directionally, the depth-average total current speeds exhibit a north-north-east to south-southwest orientation with noticeably stronger currents between 180°N and 210°N and between 0°N and 30°N whilst the remaining sectors show weaker flows.

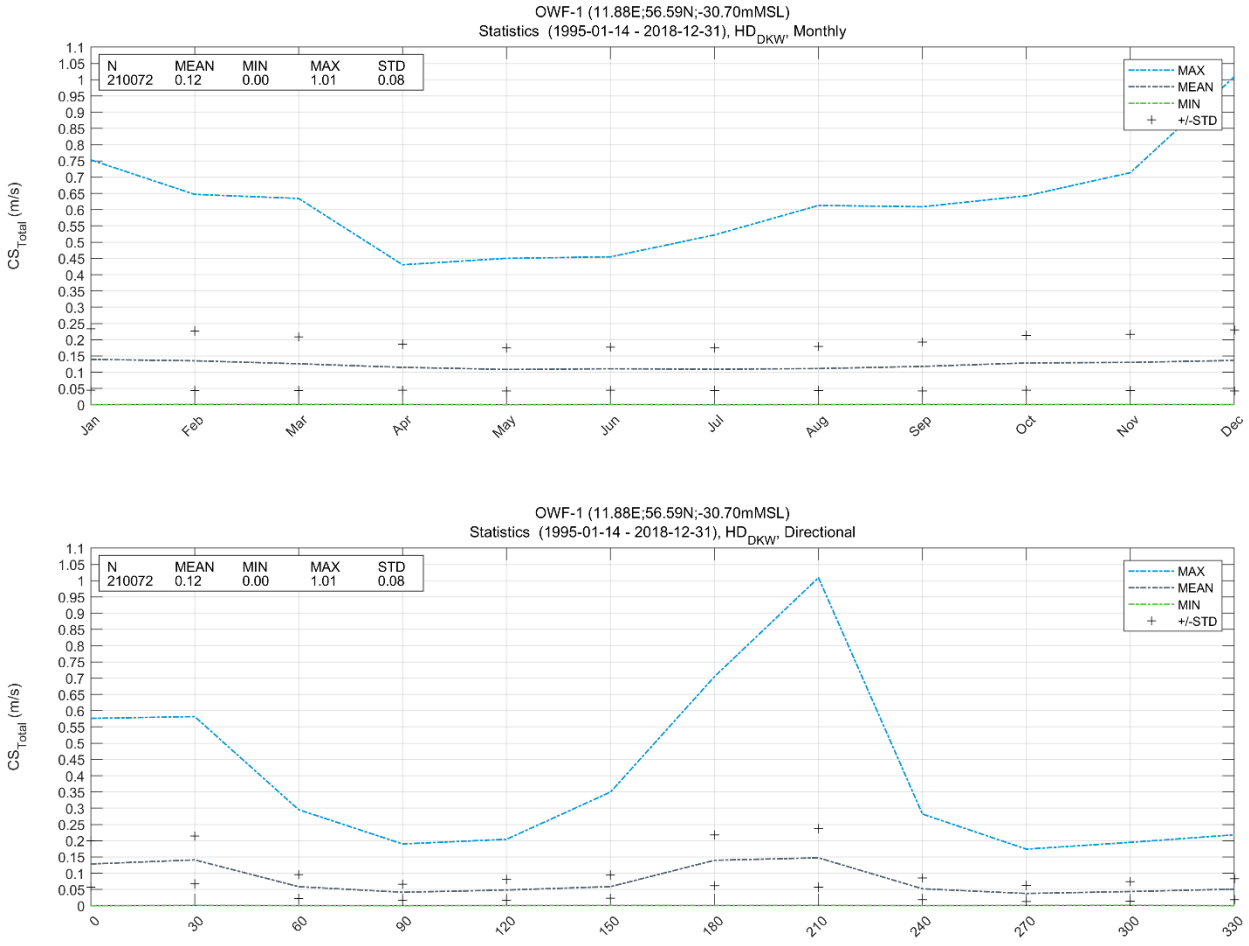

Figure 5.25 Plot of monthly and directional CS_{Total} statistics at analysis point OWF-1
Mean, min, max and standard deviation of CS_{Total} derived from the HD_{DKW} model

Table 5.11 All-year and monthly CS_{Total} statistics at Hesselø OWF

Mean, min, max and standard deviation of CS_{Total} derived from HD_{DKW} model (1995-01-14 to 2018-12-31)

Month	OWF-1				OWF-2				OWF-3			
	Mean [m/s]	Min. [m/s]	Max. [m/s]	STD [m/s]	Mean [m/s]	Min. [m/s]	Max. [m/s]	STD [m/s]	Mean [m/s]	Min. [m/s]	Max. [m/s]	STD [m/s]
All-year	0.12	0.00	1.01	0.08	0.08	0.00	0.54	0.05	0.12	0.00	0.85	0.07
Jan	0.14	0.00	0.75	0.09	0.09	0.00	0.43	0.06	0.14	0.00	0.60	0.08
Feb	0.14	0.00	0.65	0.09	0.09	0.00	0.42	0.06	0.13	0.00	0.59	0.08
Mar	0.13	0.00	0.63	0.08	0.08	0.00	0.36	0.05	0.12	0.00	0.51	0.07
Apr	0.12	0.00	0.43	0.07	0.08	0.00	0.27	0.05	0.11	0.00	0.38	0.06
May	0.11	0.00	0.45	0.07	0.07	0.00	0.31	0.04	0.10	0.00	0.39	0.06
Jun	0.11	0.00	0.46	0.07	0.07	0.00	0.30	0.04	0.10	0.00	0.42	0.06
Jul	0.11	0.00	0.52	0.07	0.07	0.00	0.26	0.04	0.10	0.00	0.43	0.06
Aug	0.11	0.00	0.61	0.07	0.07	0.00	0.39	0.04	0.10	0.00	0.57	0.06
Sep	0.12	0.00	0.61	0.08	0.08	0.00	0.36	0.05	0.11	0.00	0.53	0.06
Oct	0.13	0.00	0.64	0.08	0.09	0.00	0.38	0.05	0.13	0.00	0.53	0.07
Nov	0.13	0.00	0.71	0.09	0.09	0.00	0.47	0.05	0.13	0.00	0.61	0.07
Dec	0.14	0.00	1.01	0.09	0.09	0.00	0.54	0.05	0.13	0.00	0.85	0.08

Table 5.12 Omnidirectional and directional CS_{Total} statistics at Hesselø OWF

Mean, min, max and standard deviation of CS_{Total} derived from HD_{DKW} model (1995-01-14 to 2018-12-31)

Direction sector (°from)	OWF-1				OWF-2				OWF-3			
	Mean [m/s]	Min. [m/s]	Max. [m/s]	STD [m/s]	Mean [m/s]	Min. [m/s]	Max. [m/s]	STD [m/s]	Mean [m/s]	Min. [m/s]	Max. [m/s]	STD [m/s]
Omnidirectional	0.12	0.00	1.01	0.08	0.08	0.00	0.54	0.05	0.12	0.00	0.85	0.07
[345 – 015[	0.13	0.00	0.58	0.07	0.09	0.00	0.35	0.05	0.12	0.00	0.50	0.07
[015 - 045[	0.14	0.00	0.58	0.07	0.09	0.00	0.41	0.05	0.14	0.00	0.59	0.07
[045 - 075[	0.06	0.00	0.30	0.04	0.06	0.00	0.28	0.03	0.10	0.00	0.47	0.06
[075 – 105[	0.04	0.00	0.19	0.03	0.04	0.00	0.36	0.03	0.07	0.00	0.30	0.04
[105 – 135[	0.05	0.00	0.20	0.03	0.05	0.00	0.39	0.03	0.06	0.00	0.39	0.04
[135 – 165[	0.06	0.00	0.35	0.04	0.06	0.00	0.37	0.04	0.07	0.00	0.52	0.04
[165 – 195[	0.14	0.00	0.71	0.08	0.09	0.00	0.41	0.05	0.10	0.00	0.57	0.06
[195 – 225[	0.15	0.00	1.01	0.09	0.10	0.00	0.54	0.05	0.14	0.00	0.85	0.07
[225 – 255[	0.05	0.00	0.28	0.03	0.06	0.00	0.39	0.04	0.12	0.00	0.72	0.07
[255 – 285[	0.04	0.00	0.17	0.02	0.04	0.00	0.26	0.03	0.08	0.00	0.32	0.05
[285 – 315[	0.04	0.00	0.20	0.03	0.04	0.00	0.19	0.03	0.08	0.00	0.30	0.04
[315 – 345[	0.05	0.00	0.22	0.03	0.05	0.00	0.22	0.03	0.09	0.00	0.31	0.05

5.3.2 Residual current speed statistics

Figure 5.26 presents plots of the monthly and directional statistics (mean, min, max and standard deviation) of the depth-averaged residual current speed ($CS_{Residual}$) at analysis point OWF-1. The statistics are summarised for all analysis points in Table 5.13 and Table 5.14 respectively.

The largest depth-averaged residual current speeds occur between the months of December and February, while the smallest values occur between April to July. Directionally, the depth-average residual current speeds exhibit a north-north-east to south-south-west orientation with noticeably stronger currents between 180°N and 210°N with a secondary peak between 0°N and 30°N, whilst the remaining sectors show weaker flow speeds.

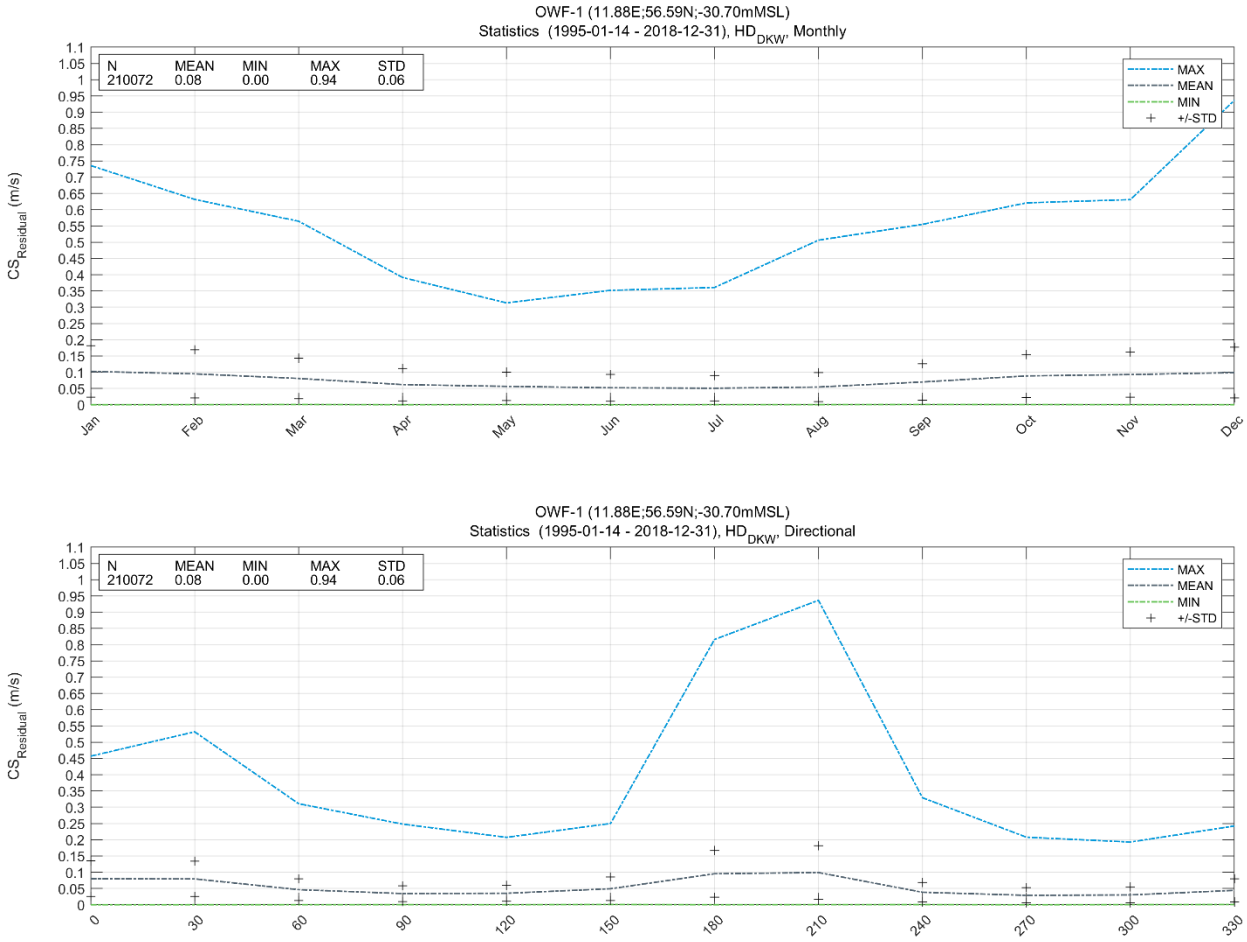

Figure 5.26 Plot of monthly and directional $CS_{Residual}$ statistics at analysis point OWF-1
Mean, min, max and standard deviation of $CS_{Residual}$ derived from the HD_{DKW} model

Table 5.13 All-year and monthly $CS_{Residual}$ statistics at Hesselø OWF

Mean, min, max and standard deviation of $CS_{Residual}$ derived from HD_{DKW} model (1995-01-14 to 2018-12-31)

Month	OWF-1				OWF-2				OWF-3			
	Mean [m/s]	Min. [m/s]	Max. [m/s]	STD [m/s]	Mean [m/s]	Min. [m/s]	Max. [m/s]	STD [m/s]	Mean [m/s]	Min. [m/s]	Max. [m/s]	STD [m/s]
All-year	0.08	0.00	0.94	0.06	0.05	0.00	0.51	0.04	0.07	0.00	0.82	0.06
Jan	0.10	0.00	0.74	0.08	0.07	0.00	0.43	0.05	0.10	0.00	0.62	0.07
Feb	0.10	0.00	0.63	0.07	0.07	0.00	0.35	0.04	0.09	0.00	0.50	0.07
Mar	0.08	0.00	0.56	0.06	0.06	0.00	0.32	0.04	0.08	0.00	0.50	0.05
Apr	0.06	0.00	0.39	0.05	0.05	0.00	0.25	0.03	0.06	0.00	0.34	0.04
May	0.06	0.00	0.31	0.04	0.04	0.00	0.21	0.03	0.05	0.00	0.26	0.04
Jun	0.05	0.00	0.35	0.04	0.04	0.00	0.30	0.03	0.05	0.00	0.34	0.04
Jul	0.05	0.00	0.36	0.04	0.04	0.00	0.20	0.03	0.05	0.00	0.29	0.03
Aug	0.05	0.00	0.51	0.04	0.04	0.00	0.39	0.03	0.05	0.00	0.53	0.04
Sep	0.07	0.00	0.55	0.06	0.05	0.00	0.31	0.03	0.07	0.00	0.53	0.05
Oct	0.09	0.00	0.62	0.07	0.06	0.00	0.33	0.04	0.09	0.00	0.55	0.06
Nov	0.09	0.00	0.63	0.07	0.07	0.00	0.39	0.04	0.09	0.00	0.55	0.06
Dec	0.10	0.00	0.94	0.08	0.07	0.00	0.51	0.04	0.10	0.00	0.82	0.07

Table 5.14 Omnidirectional and directional $CS_{Residual}$ statistics at Hesselø OWF

Mean, min, max and standard deviation of $CS_{Residual}$ derived from HD_{DKW} model (1995-01-14 to 2018-12-31)

Direction sector (°from)	OWF-1				OWF-2				OWF-3			
	Mean [m/s]	Min. [m/s]	Max. [m/s]	STD [m/s]	Mean [m/s]	Min. [m/s]	Max. [m/s]	STD [m/s]	Mean [m/s]	Min. [m/s]	Max. [m/s]	STD [m/s]
Omnidirectional	0.08	0.00	0.94	0.06	0.05	0.00	0.51	0.04	0.07	0.00	0.82	0.06
[345 – 015[	0.08	0.00	0.46	0.06	0.06	0.00	0.34	0.04	0.08	0.00	0.50	0.06
[015 - 045[	0.08	0.00	0.53	0.05	0.05	0.00	0.34	0.04	0.07	0.00	0.49	0.05
[045 - 075[	0.05	0.00	0.31	0.03	0.04	0.00	0.28	0.03	0.07	0.00	0.47	0.05
[075 – 105[	0.03	0.00	0.25	0.02	0.04	0.00	0.34	0.03	0.06	0.00	0.26	0.04
[105 – 135[	0.04	0.00	0.21	0.02	0.04	0.00	0.39	0.03	0.05	0.00	0.25	0.04
[135 – 165[	0.05	0.00	0.25	0.04	0.05	0.00	0.36	0.03	0.06	0.00	0.50	0.04
[165 – 195[	0.10	0.00	0.82	0.07	0.06	0.00	0.43	0.04	0.07	0.00	0.63	0.06
[195 – 225[	0.10	0.00	0.94	0.08	0.08	0.00	0.51	0.05	0.10	0.00	0.82	0.08
[225 – 255[	0.04	0.00	0.33	0.03	0.05	0.00	0.36	0.04	0.09	0.00	0.62	0.07
[255 – 285[	0.03	0.00	0.21	0.02	0.04	0.00	0.30	0.03	0.06	0.00	0.30	0.04
[285 – 315[	0.03	0.00	0.19	0.02	0.04	0.00	0.19	0.03	0.05	0.00	0.28	0.04
[315 – 345[	0.04	0.00	0.24	0.04	0.04	0.00	0.20	0.03	0.07	0.00	0.28	0.05

5.3.3 Tidal current speed statistics

Figure 5.27 presents plots of the monthly and directional statistics (mean, min, max and standard deviation) of the depth-averaged tidal current speed (CS_{Tide}) at analysis point OWF-1. The statistics are summarised for all analysis points in Table 5.15 and Table 5.16 respectively.

Tidal current speeds are weak and show consistent trends across all months with no period showing distinctly larger or lower depth-averaged tidal current speeds. Directionally there is a north-northeast to south-southwest orientation with the strongest current speeds towards 180°N and 210°N / 0°N and 30°N.

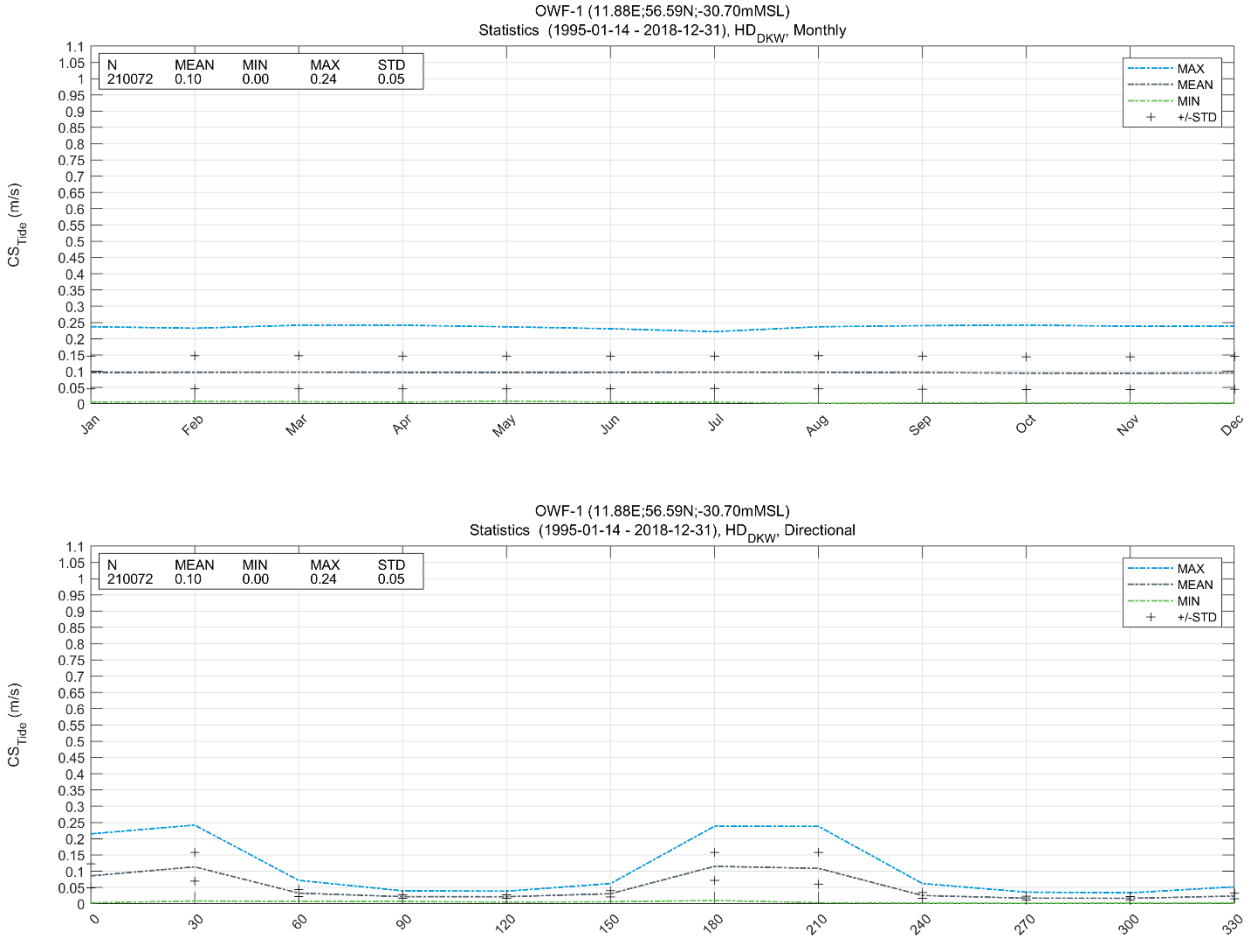

Figure 5.27 Plot of monthly and directional CS_{Tide} statistics at OWF-1
Mean, min, max and standard deviation of CS_{Tide} derived from the HD_{DKW} model

Table 5.15 All-year and monthly CS_{Tide} statistics at Hesselø OWF

Mean, min, max and standard deviation of CS_{Tide} derived from HD_{DKW} model (1995-01-14 to 2018-12-31)

Month	OWF-1				OWF-2				OWF-3			
	Mean [m/s]	Min. [m/s]	Max. [m/s]	STD [m/s]	Mean [m/s]	Min. [m/s]	Max. [m/s]	STD [m/s]	Mean [m/s]	Min. [m/s]	Max. [m/s]	STD [m/s]
All-year	0.10	0.00	0.24	0.05	0.06	0.00	0.15	0.03	0.09	0.00	0.23	0.04
Jan	0.10	0.00	0.24	0.05	0.06	0.00	0.14	0.03	0.09	0.00	0.21	0.04
Feb	0.10	0.01	0.23	0.05	0.06	0.00	0.15	0.03	0.09	0.00	0.22	0.04
Mar	0.10	0.01	0.24	0.05	0.06	0.00	0.15	0.03	0.09	0.00	0.22	0.05
Apr	0.10	0.00	0.24	0.05	0.06	0.00	0.15	0.03	0.09	0.00	0.22	0.05
May	0.10	0.01	0.24	0.05	0.06	0.00	0.15	0.03	0.09	0.00	0.22	0.05
Jun	0.10	0.01	0.23	0.05	0.06	0.00	0.14	0.03	0.09	0.00	0.21	0.05
Jul	0.10	0.00	0.22	0.05	0.06	0.00	0.14	0.03	0.09	0.00	0.20	0.05
Aug	0.10	0.00	0.24	0.05	0.06	0.00	0.15	0.03	0.09	0.00	0.21	0.05
Sep	0.10	0.00	0.24	0.05	0.06	0.00	0.15	0.03	0.09	0.00	0.22	0.04
Oct	0.09	0.00	0.24	0.05	0.06	0.00	0.15	0.03	0.09	0.00	0.23	0.04
Nov	0.09	0.00	0.24	0.05	0.06	0.00	0.15	0.03	0.09	0.00	0.23	0.04
Dec	0.09	0.00	0.24	0.05	0.06	0.00	0.14	0.03	0.09	0.00	0.22	0.04

Table 5.16 Omnidirectional and directional CS_{Tide} statistics at Hesselø OWF

Mean, min, max and standard deviation of CS_{Tide} derived from HD_{DKW} model (1995-01-14 to 2018-12-31)

Direction sector (°from)	OWF-1				OWF-2				OWF-3			
	Mean [m/s]	Min. [m/s]	Max. [m/s]	STD [m/s]	Mean [m/s]	Min. [m/s]	Max. [m/s]	STD [m/s]	Mean [m/s]	Min. [m/s]	Max. [m/s]	STD [m/s]
Omnidirectional	0.10	0.00	0.24	0.05	0.06	0.00	0.15	0.03	0.09	0.00	0.23	0.04
[345 – 015[	0.09	0.00	0.22	0.04	0.05	0.00	0.13	0.02	0.08	0.00	0.19	0.03
[015 - 045[	0.11	0.01	0.24	0.04	0.07	0.00	0.15	0.03	0.11	0.00	0.23	0.04
[045 - 075[	0.03	0.01	0.07	0.01	0.01	0.00	0.04	0.01	0.03	0.00	0.08	0.01
[075 – 105[	0.02	0.01	0.04	0.01	0.01	0.00	0.02	0.00	0.01	0.00	0.03	0.01
[105 – 135[	0.02	0.00	0.04	0.01	0.01	0.00	0.02	0.00	0.01	0.00	0.03	0.01
[135 – 165[	0.03	0.01	0.06	0.01	0.01	0.00	0.02	0.00	0.01	0.00	0.03	0.01
[165 – 195[	0.12	0.01	0.24	0.04	0.04	0.00	0.11	0.02	0.04	0.00	0.12	0.02
[195 – 225[	0.11	0.00	0.24	0.05	0.07	0.00	0.14	0.03	0.10	0.00	0.20	0.04
[225 – 255[	0.03	0.00	0.06	0.01	0.02	0.00	0.05	0.01	0.06	0.00	0.15	0.03
[255 – 285[	0.02	0.00	0.04	0.01	0.01	0.00	0.03	0.00	0.03	0.00	0.07	0.01
[285 – 315[	0.02	0.00	0.03	0.01	0.01	0.00	0.02	0.00	0.03	0.00	0.06	0.01
[315 – 345[	0.02	0.00	0.05	0.01	0.02	0.00	0.04	0.01	0.04	0.00	0.08	0.01

5.3.4 Total current speed all-year rose and scatter plots

Figure 5.28 and Figure 5.29 present the all-year rose plot and density scatter plot of CS_{Total} and CD_{Total} at analysis points OWF-1, OWF-2, and OWF-3.

Tables giving the frequency of occurrence [%] of total current speed and direction at all analysis points are provided in digital format (Microsoft Excel, .xlsx) accompanying this report (see Appendix C). The tables are provided for the following intervals:

- CS_{Total} intervals of 0.05 m/s
- CD_{Total} intervals of 30°, centred on 0°N, 30°N, 60°N, etc.
- All-year and for each calendar month

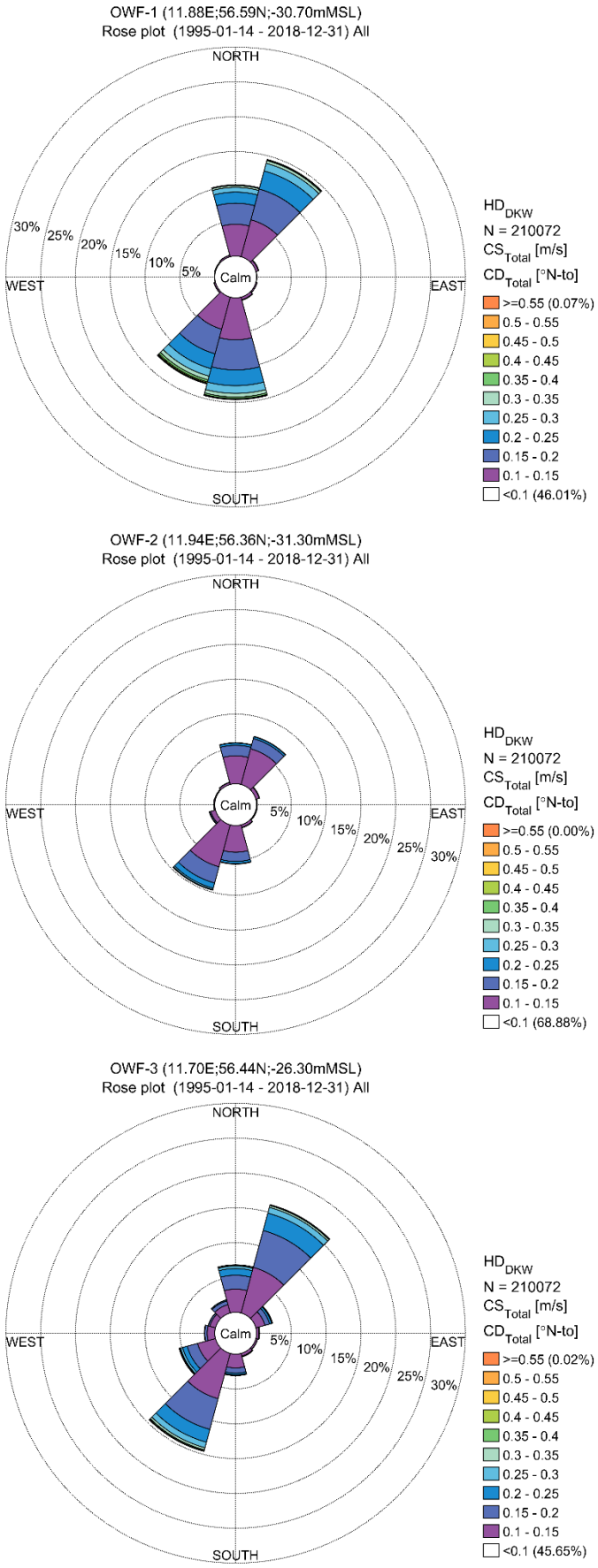

Figure 5.28 Rose plots of all-year CS_{Total} and CD_{Total} at analysis points OWF-1, OWF-2, and OWF-3

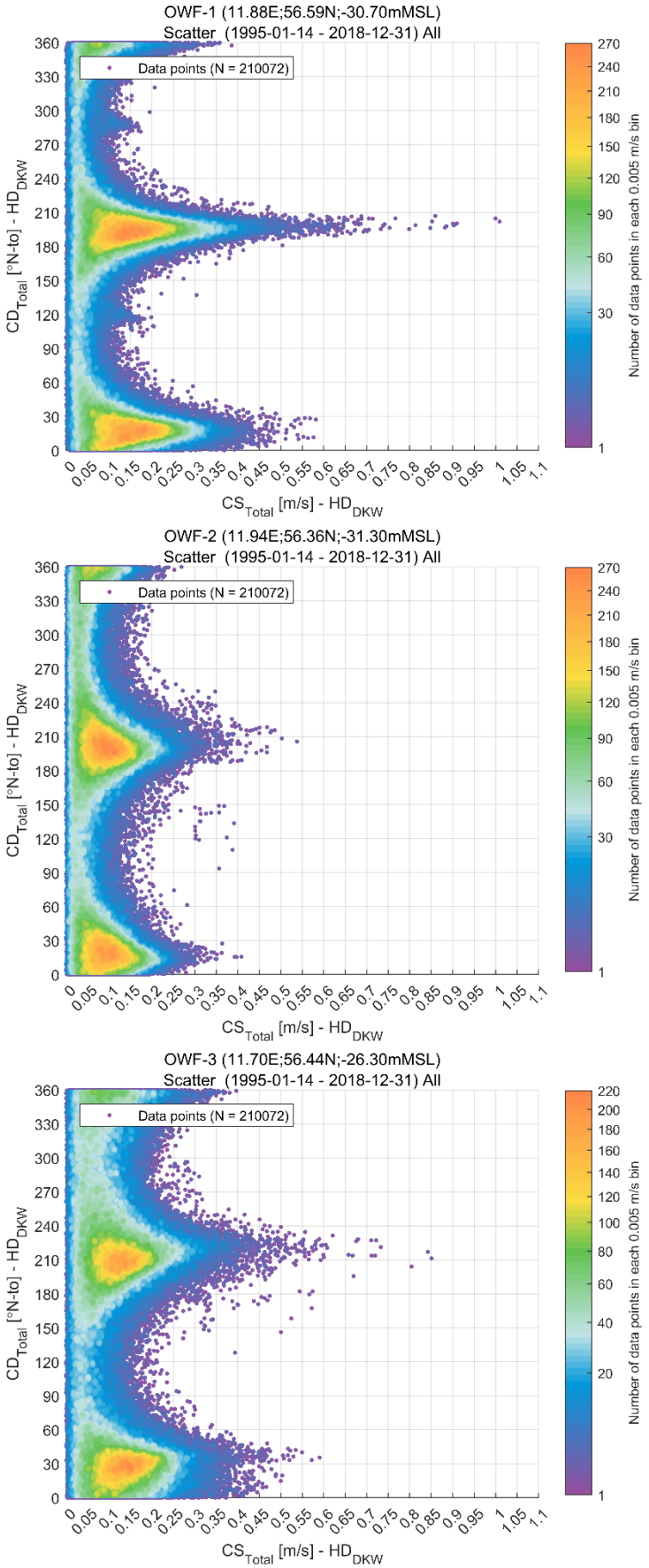

Figure 5.29 Density scatter plot of CS_{Total} and CD_{Total} at analysis points OWF-1, OWF-2, and OWF-3

5.3.5 Residual current speed all-year rose and scatter plots

Figure 5.30 and Figure 5.31 presents the all-year rose plots and density scatter plots of $CS_{Residual}$ and $CD_{Residual}$ at analysis points OWF-1, OWF-2, and OWF-3.

Tables giving the frequency of occurrence [%] of total current speed and direction at all analysis points are provided in digital format (Microsoft Excel, .xlsx) accompanying this report (see Appendix C). The tables are provided for the following intervals:

- $CS_{Residual}$ intervals of 0.05 m/s
- $CD_{Residual}$ intervals of 30°, centred on 0°N, 30°N, 60°N, etc.
- All-year and for each calendar month

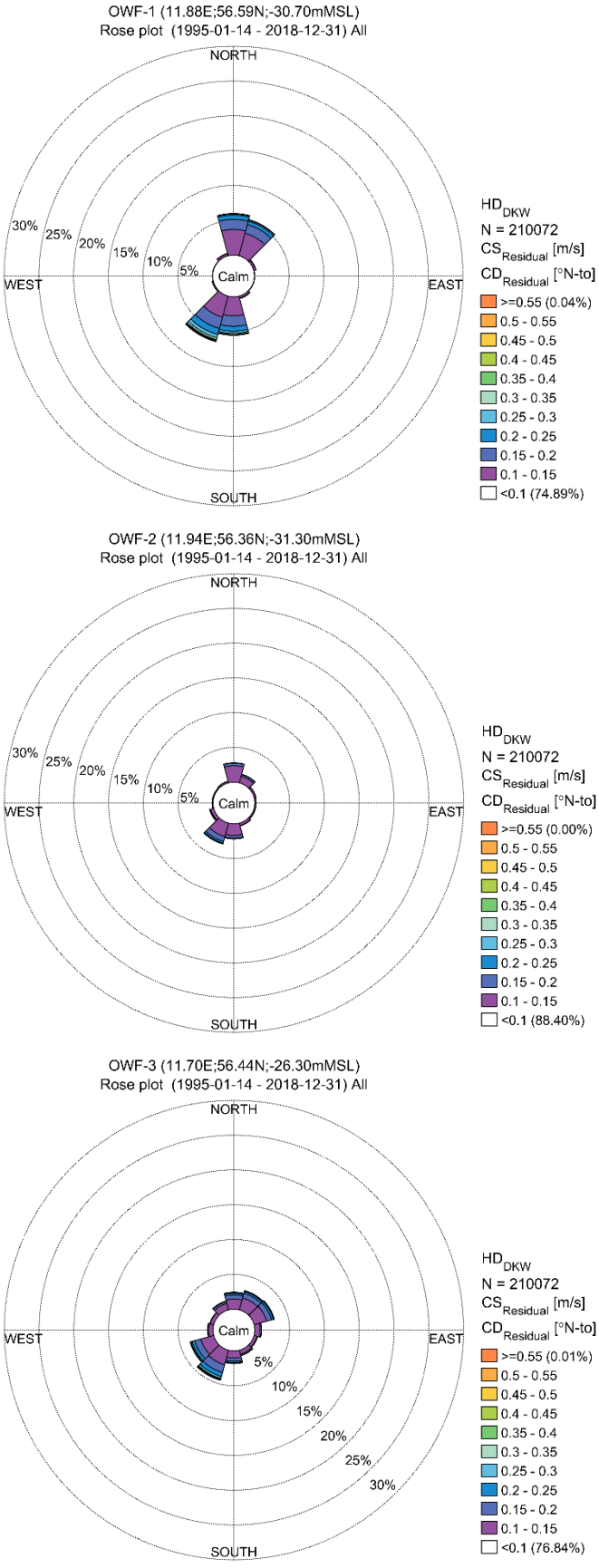

Figure 5.30 Rose plots of all-year $CS_{Residual}$ and $CD_{Residual}$ at analysis points OWF-1, OWF-2, and OWF-3

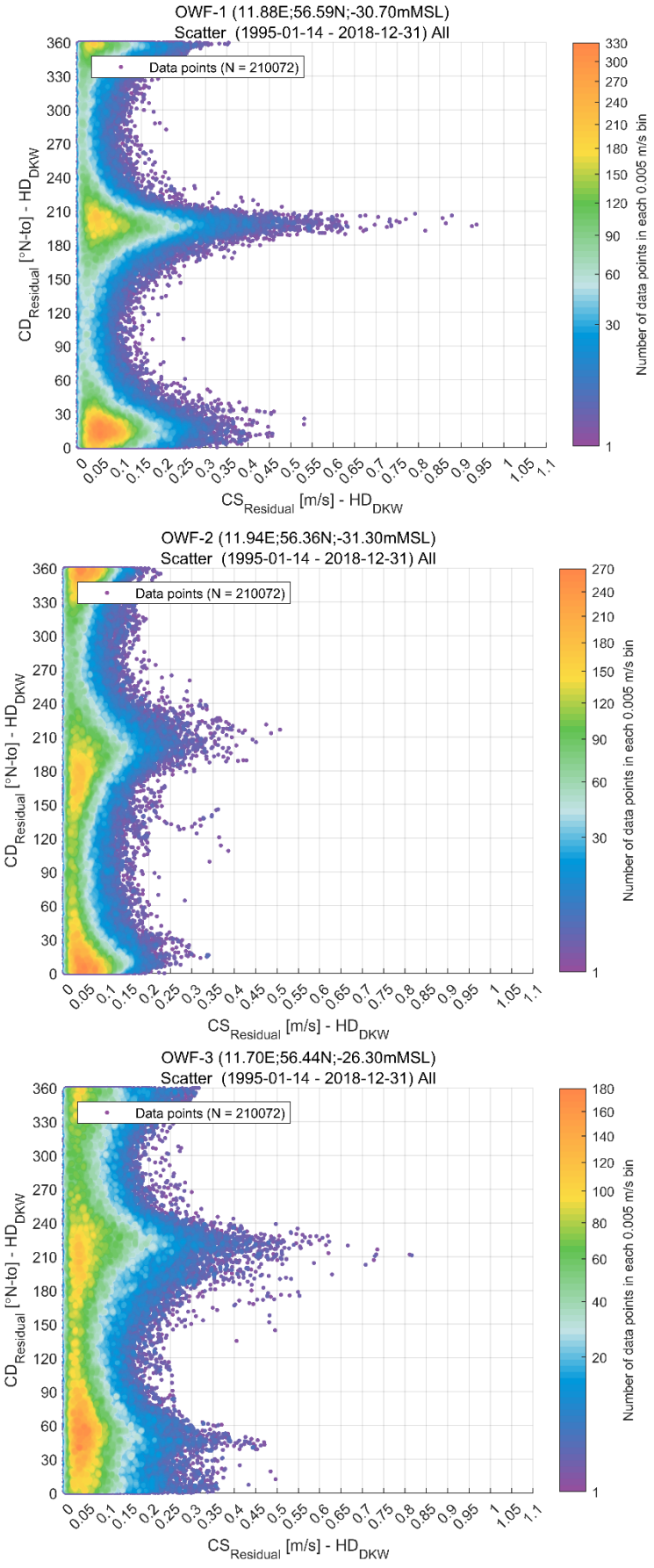

Figure 5.31 Density scatter plot of all-year $CS_{Residual}$ and $CD_{Residual}$ at analysis points OWF-1, OWF-2, and OWF-3

5.3.6 Tidal current speed all-year rose and scatter plots

Figure 5.32 and Figure 5.33 present the all-year rose plots and density scatter plots of CS_{Tide} and CD_{Tide} at analysis points OWF-1, OWF-2, and OWF-3.

Tables giving the frequency of occurrence [%] of total current speed and direction at all analysis points are provided in digital format (Microsoft Excel, .xlsx) accompanying this report (see Appendix C). The tables are provided for the following intervals:

- CS_{Tide} intervals of 0.05 m/s
- CD_{Tide} intervals of 30°, centred on 0°N, 30°N, 60°N, etc.
- All-year and for each calendar month

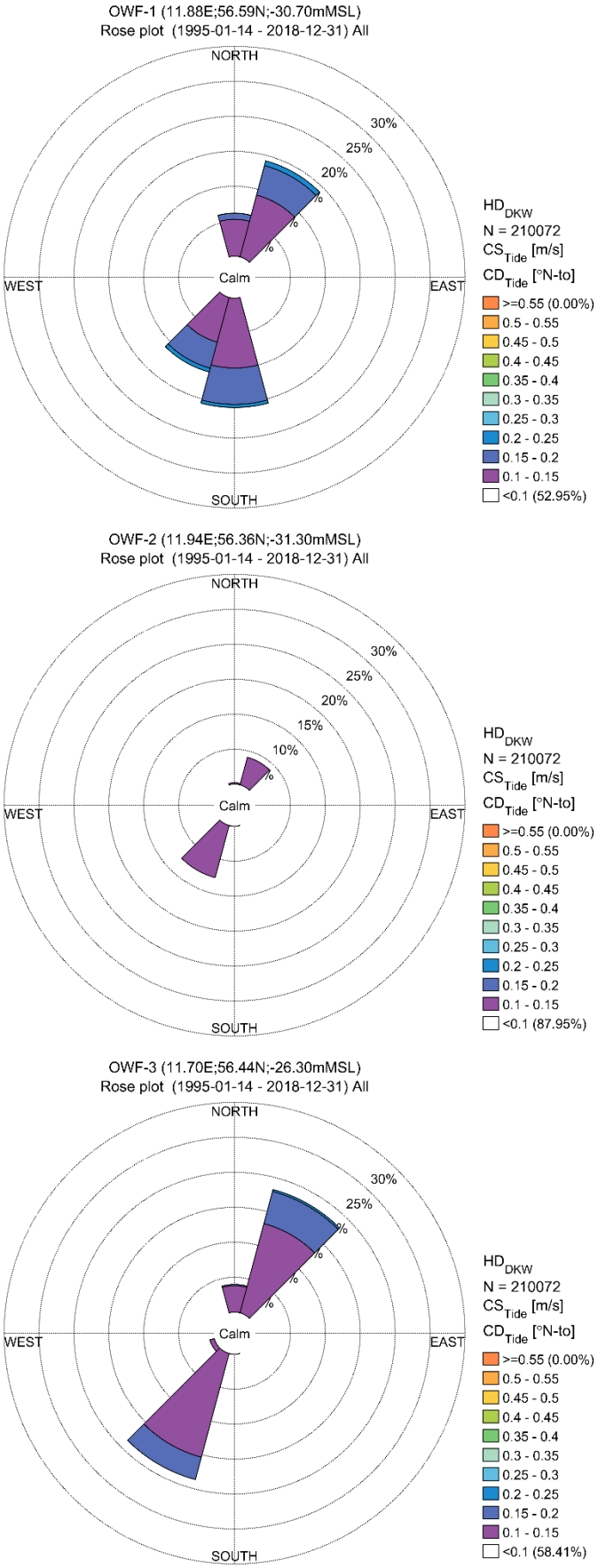

Figure 5.32 Rose plots of all-year CS_{Tide} and CD_{Tide} at analysis points OWF-1, OWF-2, and OWF-3

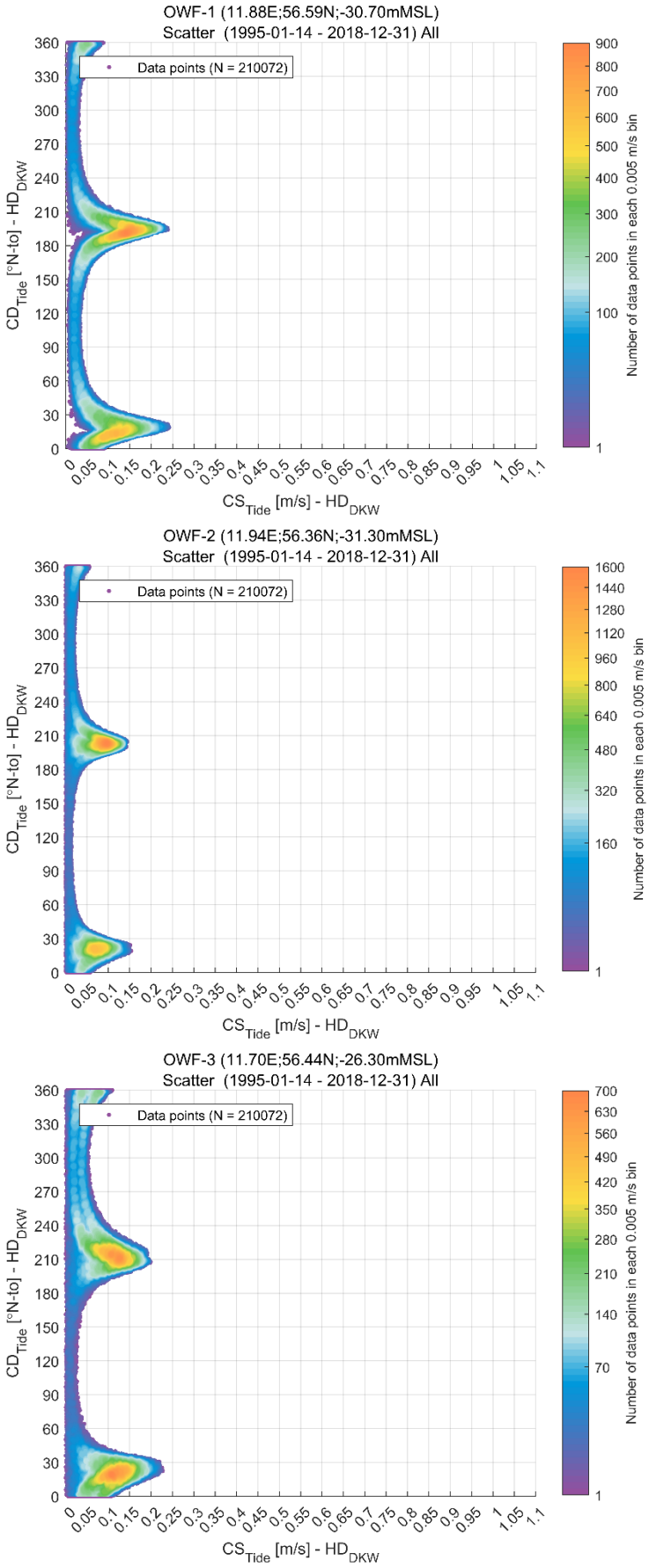

Figure 5.33 Density scatter plot of all-year CS_{Tide} and CD_{Tide} at analysis points OWF-1, OWF-2, and OWF-3

5.3.7 Vertical current profile

An investigation of the vertical variation in current speed and current direction over the water column was performed using the measurements at the Hesselø F-LiDAR. As mentioned previously (see Section 2.2.3) the instrumentation setup for this measurement station changed during the survey:

- 2021-03-01 to 2021-07-14, at 1.6 m intervals from 6.0 m to 39.6 m below sea surface
- 2021-07-17 to 2021-09-27, at 1.6 m intervals from 3.6 m to 37.2 m below sea surface

The analysis presented in the following treats these two periods individually.

Figure 5.34 shows examples of the measured vertical current speed profile at the Hesselø F-LiDAR for 12 randomly selected output times between 01 March 2021 and 14 July 2021. The vertical structure is not coherent, and the largest current speeds may occur at almost any position in the water column; hence, it may not be suitable to adopt a standard vertical current profile such as the $1/7^{th}$ power law for tidally dominant flows (e.g., as described by equation 2.31 in Section 2.4.8.3 of [25]).

Another way to illustrate the variation in the vertical current profile is by means of a statistical analysis of the measured current speed and direction relative to the depth-averaged values. Figure 5.35 and Figure 5.36 display normalised current profiles during normal conditions (herein represented by all profiles for which the depth-averaged current speed is larger than the 50% quantile). The following general set of characteristics were inferred:

- The ratio of the current speed at bin level to the depth-averaged current speed shows a large variation at all levels and is largest in the upper part of the water column
- In the upper part of the water column (i.e., from the near-surface layer to ~20 m below the surface) it is more likely that the current speed is larger than the depth-average current speed (U/CS > 1). At lower levels (i.e., from ~20 m below the surface to near-seafloor) the current speed is more likely to be less than the depth-averaged current speed (U/CS < 1).
- At all levels, the phase shift in the current direction relative to the depth-averaged current direction can be ±180°
- The most probable phase shift is close to 0° in the upper part of the water column (i.e., from near-surface to ~20 m below the surface) with more deviation from the depth-averaged current direction at lower levels (±30°)

Figure 5.37 and Figure 5.38 display normalised current profile plots conditioned on depth-averaged current speeds that are larger than the 99% quantile. The most probable values of the current speed ratio and the phase shift are similar to those presented in Figure 5.35 and Figure 5.36, however the variability of the values is markedly lower.

Figure 5.39 and Figure 5.40 display normalised of the current profiles conditioned on near-surface current speeds (i.e., the depth bin that is closest to the surface) that are larger than the 99% quantile. In the upper 10 m of the water column the ratio of the current speed at bin level to the depth-averaged current speed was, in all cases, larger than 1. The most probable value increased towards the surface, suggesting the presence of wind-generated surface currents (e.g., see equation 2.3.2 in Section 2.4.8.3 of [25]). The phase shift in current direction in the upper 10 m displayed less variability than at depth.

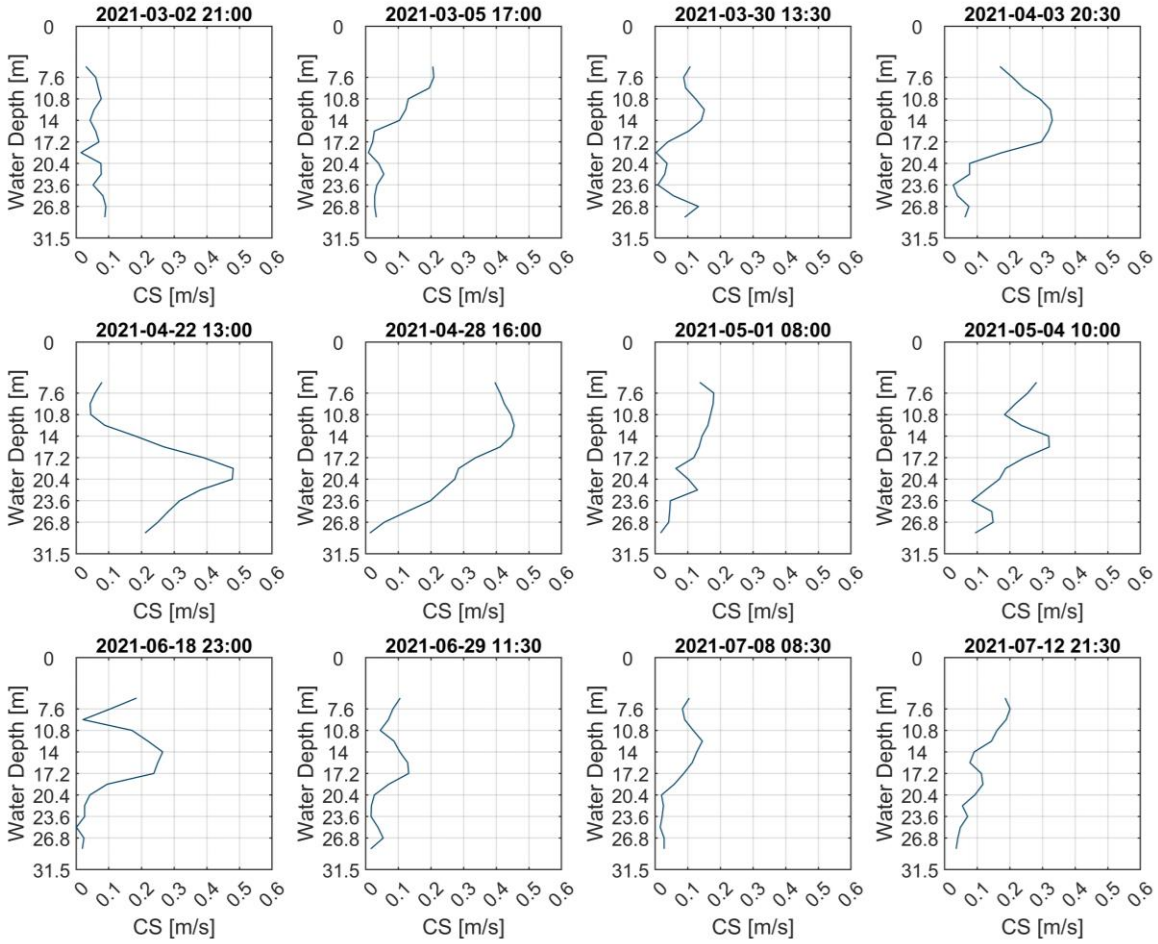

Figure 5.34 Measured current speed profile at Hesselø F-LiDAR
The images show 12 randomly selected profiles between 01 March 2021 and 14 July 2021

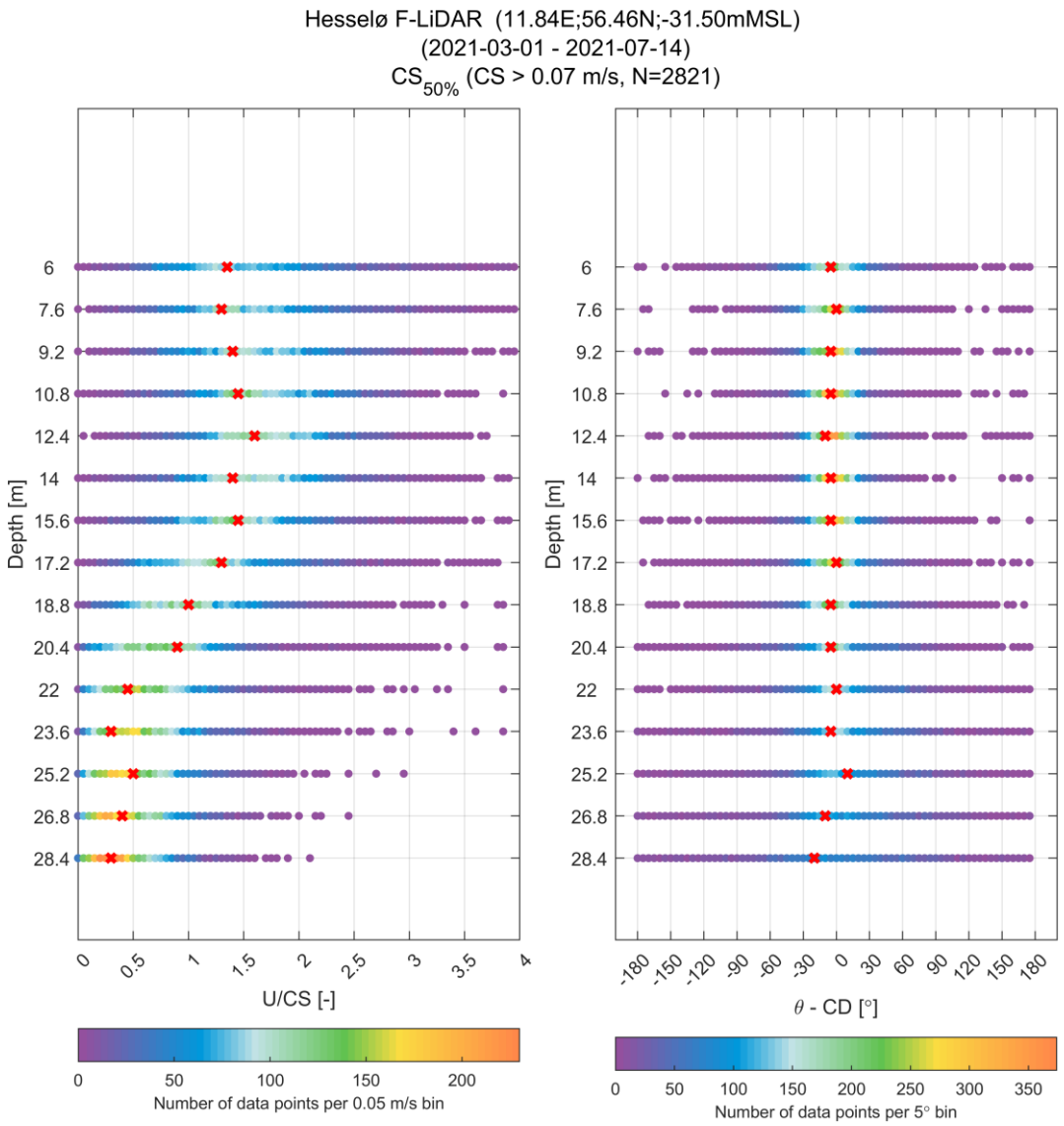

Figure 5.35 Normalised vertical current profiles (50% depth-averaged current exceedance) at Hesselø F-LiDAR (2021-03-01 to 2021-07-04)

Statistical representation of measured current profiles at the Hesselø F-LiDAR for the period 2021-03-01 to 2021-07-14, conditioned on depth-averaged current speeds larger than the 50% quantile value. Left hand panel: current speed at bin level (U) normalised by the depth-averaged current speed (CS). Right panel: the phase shift of the current direction at bin level (θ) to the depth-averaged current direction (CD). The red markers show the most probable value for each level

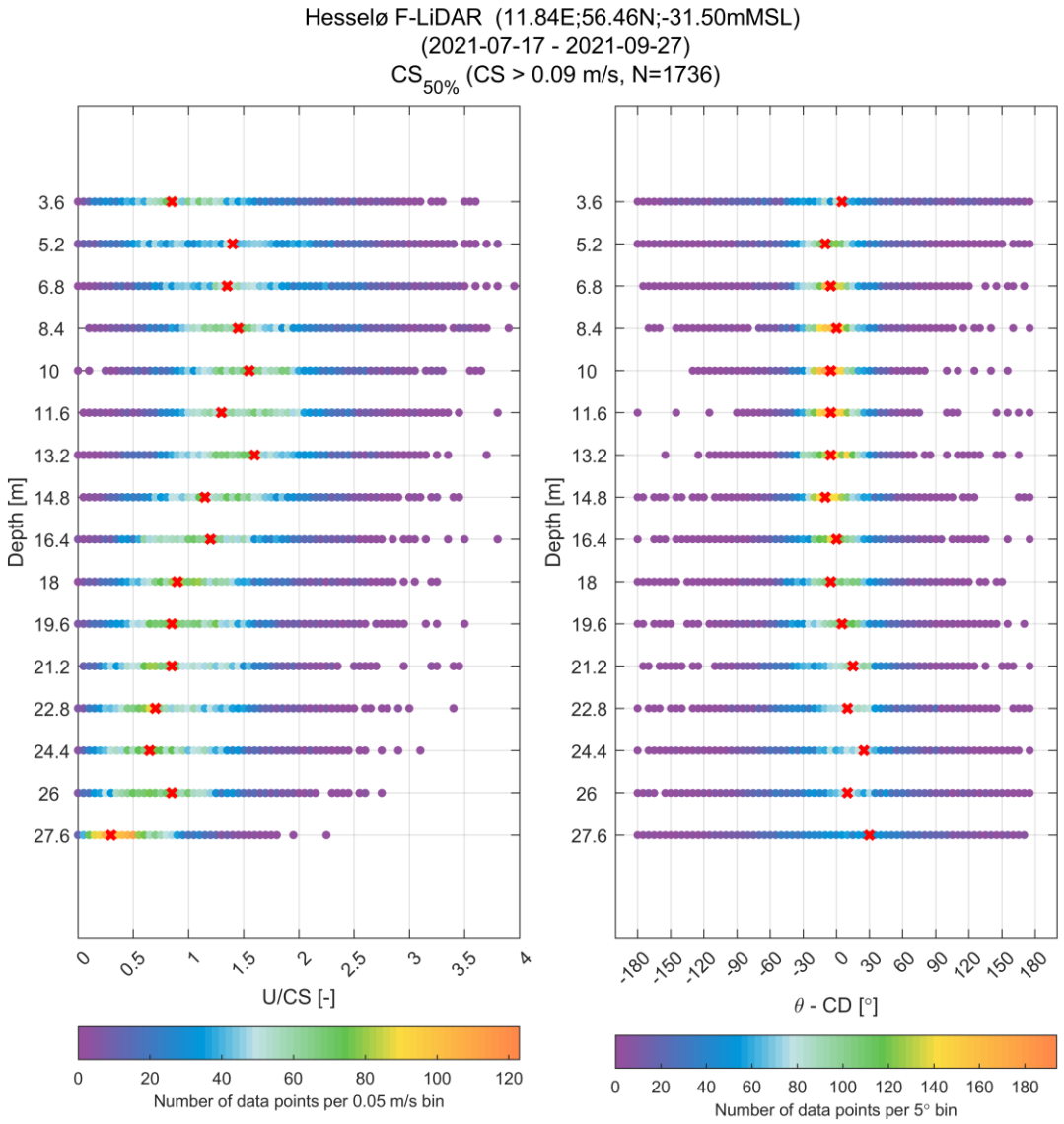

Figure 5.36 Normalised vertical current profiles (50% depth-averaged current exceedance) at Hesselø F-LiDAR (2021-07-17 to 2021-09-27)

Statistical representation of measured current profiles at the Hesselø F-LiDAR for the period 2021-07-17 to 2021-09-27, conditioned on depth-averaged current speeds larger than the 50% quantile value. Left hand panel: current speed at bin level (U) normalised by the depth-averaged current speed (CS). Right panel: the phase shift of the current direction at bin level (θ) to the depth-averaged current direction (CD). The red markers show the most probable value for each level

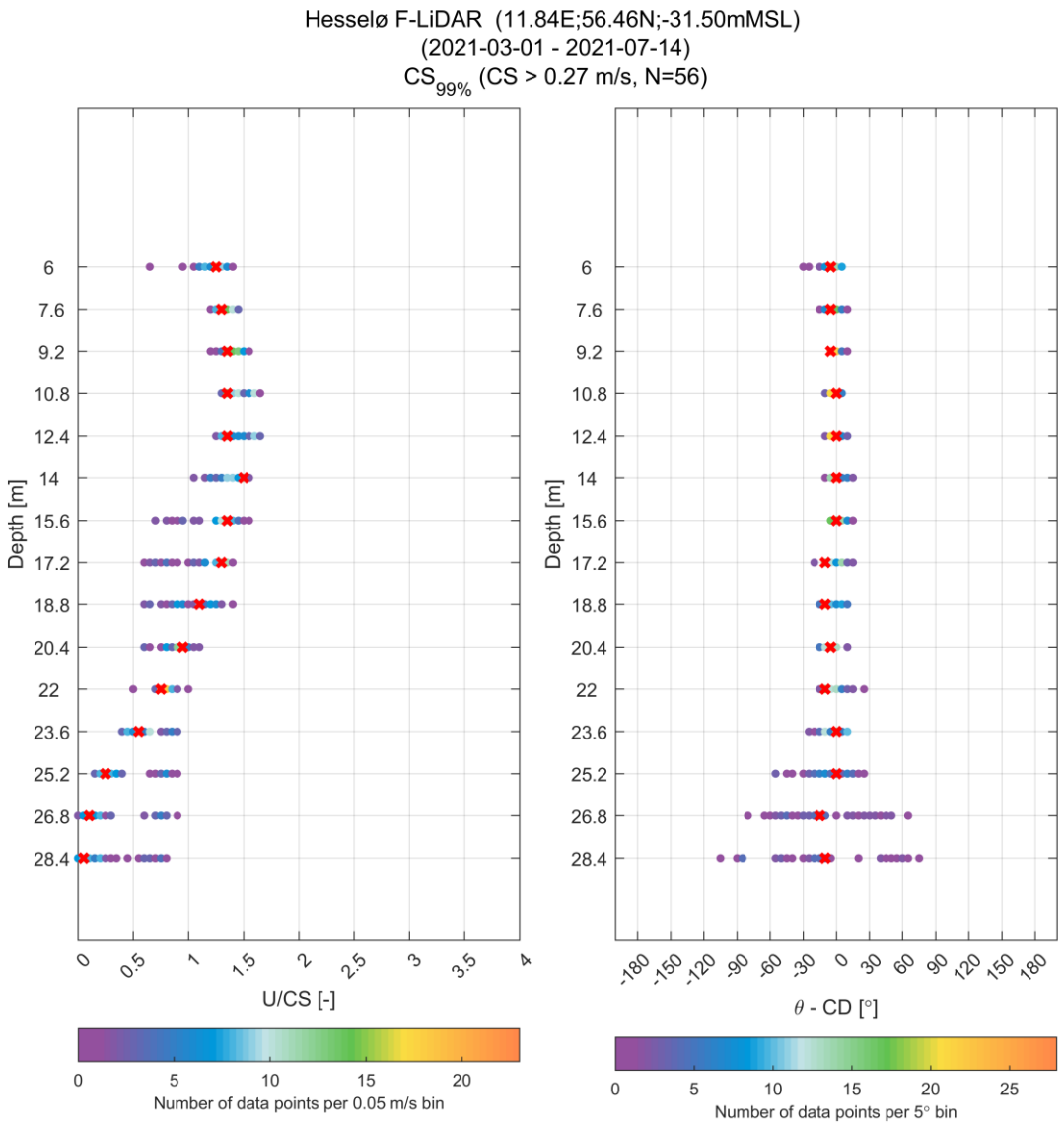

Figure 5.37 Normalised vertical current profiles (1% depth-averaged current exceedance) at Hesselø F-LiDAR (2021-03-01 to 2021-07-04)

Statistical representation of measured current profiles at the Hesselø F-LiDAR for the period 2021-03-01 to 2021-07-14, conditioned on depth-averaged current speeds larger than the 99% quantile value. Left hand panel: current speed at bin level (U) normalised by the depth-averaged current speed (CS). Right panel: the phase shift of the current direction at bin level (θ) to the depth-averaged current direction (CD). The red markers show the most probable value for each level

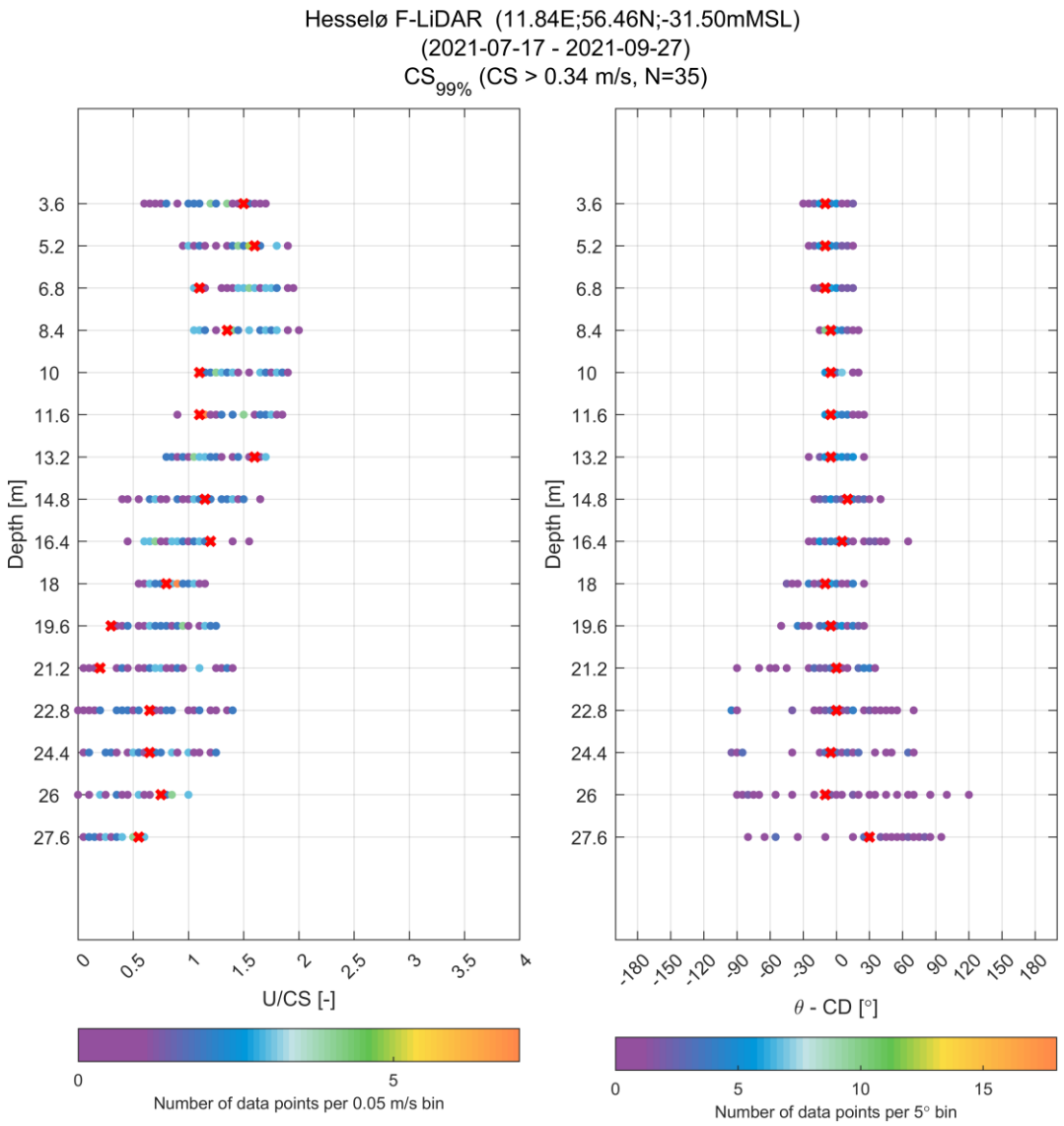

Figure 5.38 Normalised vertical current profiles (1% depth-averaged current exceedance) at Hesselø F-LiDAR (2021-07-17 to 2021-09-27)

Statistical representation of measured current profiles at the Hesselø F-LiDAR for the period 2021-07-17 to 2021-09-27, conditioned on depth-averaged current speeds larger than the 99% quantile value. Left hand panel: current speed at bin level (U) normalised by the depth-averaged current speed (CS). Right panel: the phase shift of the current direction at bin level (θ) to the depth-averaged current direction (CD). The red markers show the most probable value for each level

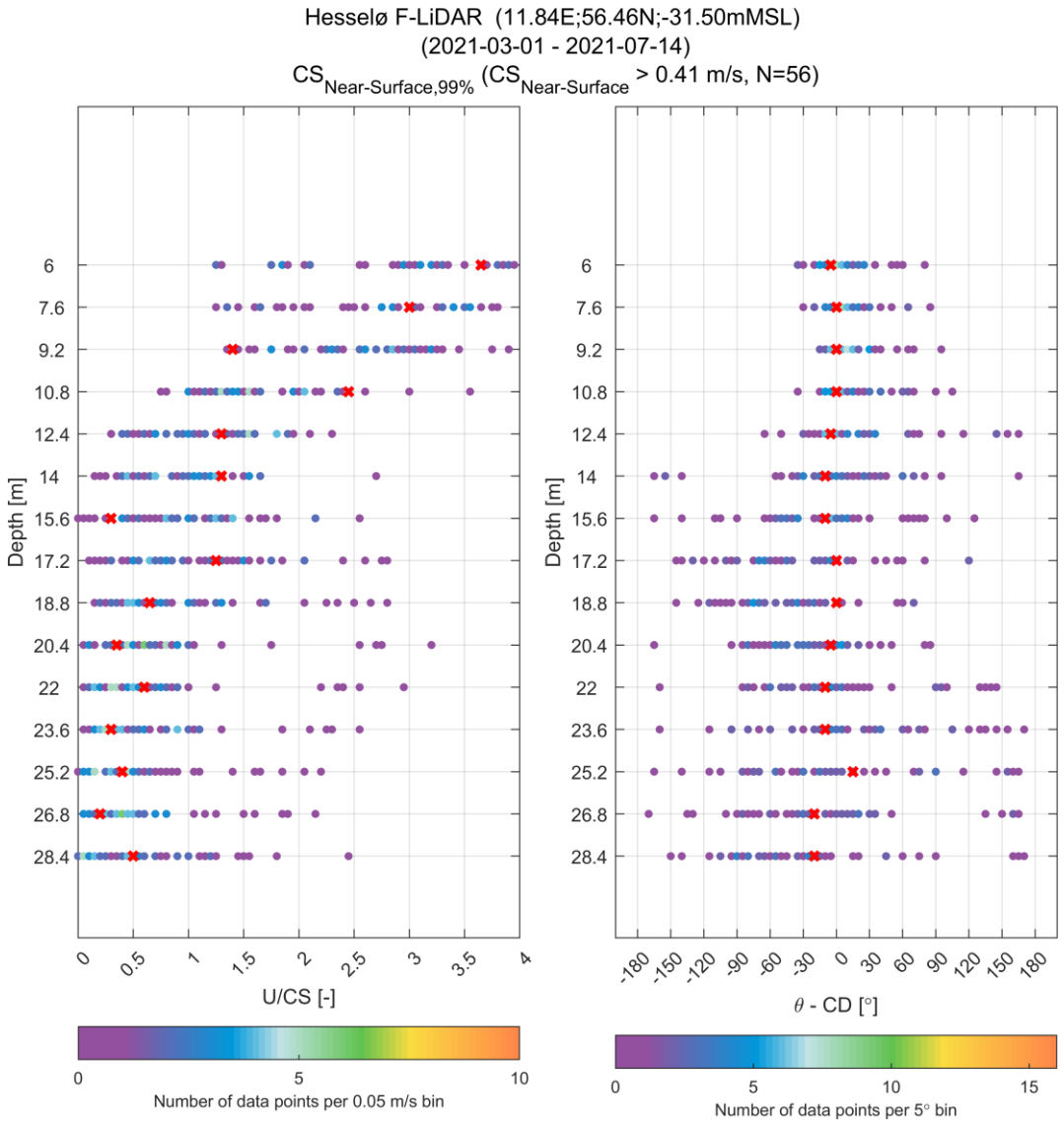

Figure 5.39 Normalised vertical current profiles (1% near-surface current exceedance) at Hesselø F-LiDAR (2021-03-01 to 2021-07-04)

Statistical representation of measured current profiles at the Hesselø F-LiDAR for the period 2021-03-01 to 2021-07-14, conditioned on near-surface current speeds larger than the 99% quantile value. Left hand panel: current speed at bin level (U) normalised by the depth-averaged current speed (CS). Right panel: the phase shift of the current direction at bin level (θ) to the depth-averaged current direction (CD). The red markers show the most probable value for each level

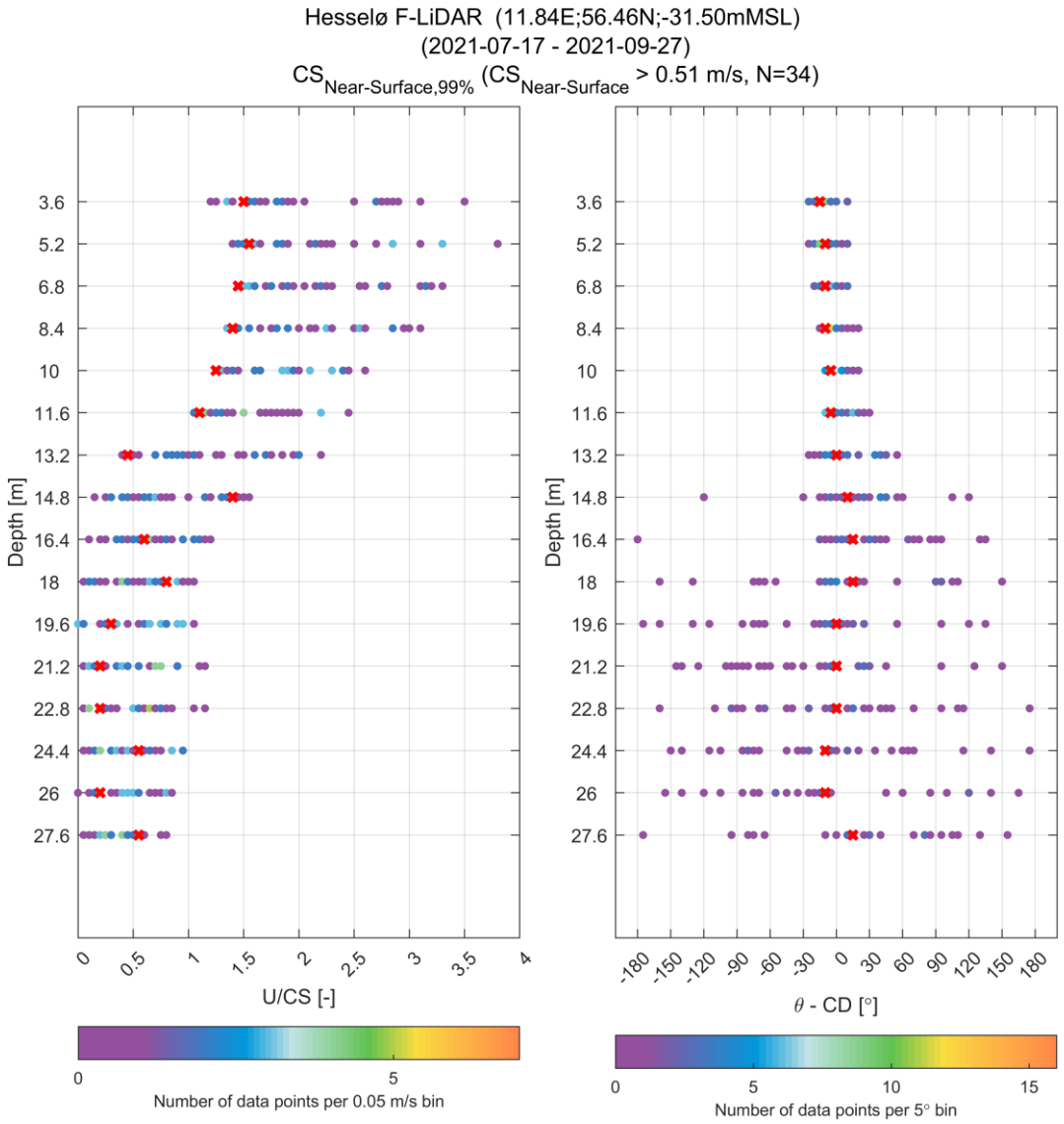

Figure 5.40 Normalised vertical current profiles (1% near-surface current exceedance) at Hesselø F-LiDAR (2021-07-17 to 2021-09-27)

Statistical representation of measured current profiles at the Hesselø F-LiDAR for the period 2021-07-17 to 2021-09-27, conditioned on near-surface current speeds larger than the 99% quantile value. Left hand panel: current speed at bin level (U) normalised by the depth-averaged current speed (CS). Right panel: the phase shift of the current direction at bin level (θ) to the depth-averaged current direction (CD). The red markers show the most probable value for each bin

5.4 Water level conditions

The operational water levels conditions at the Hesselø OWF are described below. This includes astronomical water levels (Section 5.4.1) and monthly statistics of high and low total water levels (Section 5.4.2).

5.4.1 Astronomical water levels

Astronomical water levels (tidal levels) were calculated using harmonic tidal analysis to separate the tidal and non-tidal (residual) components of the total water level time series.

The harmonic analysis was conducted using the U-tide toolbox, see [22], which is based on the IOS tidal analysis method as described by [23], and integrates the approaches defined in [26] and [27]. The residual water level was calculated by subtracting the tidal water level from the total water level. The astronomical water levels are defined as follows:

- Highest Astronomical Tide (HAT): the maximum tidal water level
- Mean High-Water Spring (MHWS): the average of the two successive high waters reached during the 24-hours when the tidal range is at its greatest (i.e., spring tide)
- Mean High-Water Neap (MHWN): the average of the two successive high waters reached during the 24-hours when the tidal range is at its lowest (i.e., neap tide)
- Mean Sea Level (MSL): the mean (average) of the tidal WL
- Mean Low-Water Neap (MLWN): the average of the two successive low waters reached during the 24-hours when the tidal range is at its lowest (neap tide)
- Mean Low-Water Springs (MLWS): the average of the two successive low waters reached during the 24 hours when the tidal range is at its greatest (spring tide)
- Lowest Astronomical Tide (LAT): the minimum tidal water level

Figure 5.41 presents a time series plot of the total (WL_{Total}), tidal (WL_{Tide}), and residual ($WL_{Residual}$) water levels at analysis point OWF-1. Table 5.17 summarises the astronomical tidal levels at all analysis points, which are given in metres relative to MSL.

Table 5.17 Astronomical water levels at Hesselø OWF analysis points

Tidal Descriptor	Water Level [m MSL]		
	OWF-1	OWF-2	OWF-3
HAT	0.31	0.32	0.33
MHWS	0.18	0.19	0.20
MHWN	0.13	0.13	0.14
MSL	0.00	0.00	0.00
MLWN	-0.13	-0.13	-0.14
MLWS	-0.17	-0.18	-0.19
LAT	-0.34	-0.35	-0.37

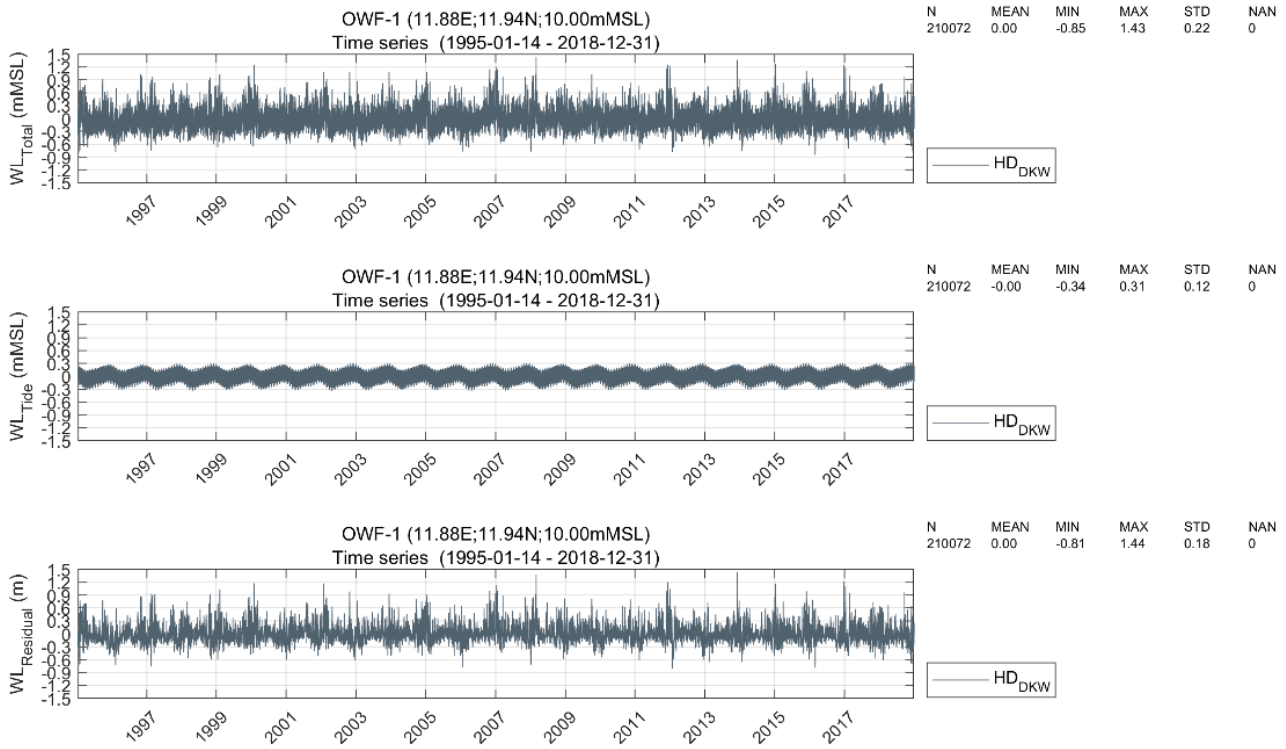

Figure 5.41 Time series of HD_{DKW} water levels at analysis point OWF-1
The graph shows the total (upper panel), tidal (central panel), and residual (lower panel) water levels

5.4.2 Operational water level statistics

Figure 5.42 present plots of the monthly statistics (mean, minimum, maximum, and standard deviation) of the total water level at analysis point OWF-1. The statistics are summarised for all analysis points in Table 5.18.

The largest positive water levels are associated with the months of November through to January, while the largest negative water levels occur between December and March.

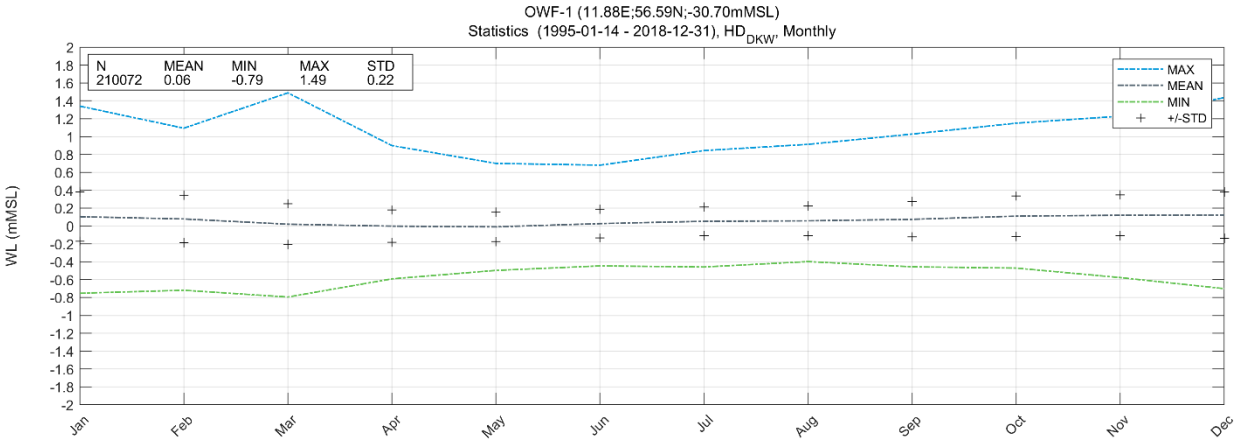

Figure 5.42 Monthly total water level statistics at analysis point OWF-1
Mean, min, max and standard deviation of WL_{Total} derived from HD_{DKW} model

Table 5.18 All-year and monthly WLTotal statistics at Hesselø OWF

Mean, min, max and standard deviation of total water level derived from HD_{DKW} model (1995-01-14 to 2018-12-31)

Month	OWF-1				OWF-2				OWF-3			
	Mean [mMSL]	Min. [mMSL]	Max. [mMSL]	STD [m]	Mean [mMSL]	Min. [mMSL]	Max. [mMSL]	STD [m]	Mean [mMSL]	Min. [mMSL]	Max. [mMSL]	STD [m]
All-year	0.06	-0.79	1.49	0.22	0.06	-0.82	1.49	0.22	0.06	-0.84	1.50	0.22
Jan	0.10	-0.75	1.34	0.28	0.10	-0.81	1.35	0.27	0.10	-0.81	1.35	0.28
Feb	0.08	-0.72	1.09	0.27	0.07	-0.74	1.11	0.26	0.07	-0.75	1.09	0.27
Mar	0.02	-0.79	1.49	0.23	0.02	-0.82	1.49	0.23	0.02	-0.84	1.50	0.23
Apr	0.00	-0.59	0.90	0.18	0.00	-0.59	0.90	0.18	0.00	-0.61	0.92	0.19
May	-0.01	-0.50	0.70	0.16	-0.01	-0.50	0.69	0.16	-0.01	-0.52	0.72	0.17
Jun	0.03	-0.45	0.68	0.16	0.03	-0.44	0.67	0.16	0.02	-0.47	0.68	0.17
Jul	0.05	-0.46	0.84	0.16	0.05	-0.46	0.85	0.16	0.05	-0.48	0.86	0.17
Aug	0.06	-0.40	0.91	0.17	0.06	-0.40	0.91	0.17	0.06	-0.42	0.92	0.17
Sep	0.07	-0.46	1.03	0.20	0.07	-0.46	1.00	0.20	0.07	-0.48	1.02	0.20
Oct	0.11	-0.47	1.15	0.23	0.11	-0.49	1.13	0.22	0.11	-0.51	1.14	0.23
Nov	0.12	-0.58	1.23	0.23	0.12	-0.62	1.26	0.23	0.12	-0.61	1.28	0.23
Dec	0.12	-0.70	1.44	0.26	0.12	-0.69	1.49	0.26	0.12	-0.73	1.49	0.26

6 Extreme Metocean Conditions

This section presents the analysis of the extreme sea-state conditions at the Hesselø OWF. This includes omnidirectional extreme wind speeds, wave conditions, depth-averaged current speeds, and residual water level for return periods of up to 50-years.

The extreme wind conditions presented in this section relate to the wind model used as input to hydrodynamic and spectral wave models. The reader is referred to the Hesselø Offshore Wind Farm Site Wind Condition Assessment [3] for reference to the recommended extreme wind speeds values for FEED.

6.1 Summary of results

The extreme metocean conditions were established based on the time series data extracted from the DHI's Danish Waters metocean hindcast database (see Section 2.3). Table 6.1 summarises the omnidirectional, all-year extreme metocean criteria at analysis points OWF-1, OWF-2, and OWF-3.

The distributions applied to estimate the extreme values were chosen based on sensitivity analyses comparing the extreme value estimates (and the corresponding fits to the data), obtained from various distribution types, thresholds (number of events per year, λ), and fitting methods. Additional technical information on the methodologies applied to determine extreme conditions are provided within Appendix D.

Further details on the methodology and analyses undertaken to derive these values are provided in Section 6.2.

Table 6.1 Summary of extreme metocean conditions at Hesselø OWF

Omnidirectional and all-year extreme wind, wave, total depth-averaged current speed, and residual water levels at analysis points OWF-1, OWF-2, and OWF-3. The table entries relating to extreme wind conditions are highlighted in grey are for information only (the reader is referred to the Hesselø Offshore Wind Farm Site Wind Condition Assessment [3] for reference to the recommended extreme wind speeds values for FEED)

Analysis point		OWF-1				OWF-2				OWF-3			
Return period, T_R [years]		1	5	10	50	1	5	10	50	1	5	10	50
30-minute average wind speed at 10 mMSL, WS_{10} [m/s]		22.3	25.4	26.7	29.5	22.0	25.5	27.0	30.6	22.3	25.3	26.6	29.4
30-minute average wind speed at 140 mMSL, WS_{140} [m/s]		29.1	33.5	35.3	39.3	28.8	33.4	35.3	39.7	29.1	33.2	34.9	38.7
10-minute average wind speed at 10 mMSL, WS_{10} [m/s]		23.0	26.2	27.5	30.4	22.7	26.3	27.8	31.5	23.0	26.1	27.4	30.3
10-minute average wind speed at 140 mMSL, WS_{140} [m/s]		30.0	34.5	36.4	40.5	29.7	34.4	36.4	41.0	30.0	34.2	36.0	40.0
Spectral significant wave height, 3-hour sea-state, H_{m0} [m]		3.6	4.1	4.3	5.0	3.6	4.2	4.4	5.0	3.4	3.9	4.1	4.7
Peak wave period associated with extreme H_{m0}, T_p [s]		7.3	7.6	7.8	8.2	7.2	7.7	7.8	8.2	7.0	7.3	7.4	7.8
Maximum individual wave height, H_{max} [m]		6.5	7.6	8.0	9.1	6.6	7.8	8.2	9.3	6.3	7.3	7.7	8.7
Wave period associated with extreme H_{max}, T_{Hmax} [s]	10%	5.9	6.3	6.4	6.8	5.9	6.4	6.5	7.0	5.8	6.2	6.4	6.8
	50%	6.4	6.9	7.1	7.5	6.5	7.0	7.2	7.6	6.3	6.8	7.0	7.4
	90%	7.1	7.6	7.8	8.2	7.1	7.7	7.8	8.3	6.9	7.4	7.6	8.1
Wave crest elevation above to mean sea level, $C_{max,MSL}$ [mMSL]		4.7	5.6	6.1	7.1	4.8	5.7	6.1	7.1	4.5	5.4	5.8	6.7
Wave crest elevation above to still wave level, $C_{max,SWL}$ [m]		4.0	4.8	5.1	5.8	4.1	4.9	5.2	5.9	3.9	4.6	4.9	5.5
Depth-averaged total current speed, CS_{Total} [m/s]		0.6	0.8	0.9	1.1	0.4	0.5	0.5	0.6	0.50	0.7	0.7	0.8
Positive residual water level, $WL_{Resid,High}$ [m]		0.9	1.2	1.3	1.5	0.9	1.2	1.3	1.6	1.0	1.2	1.3	1.5
Negative residual water level, $WL_{Resid,Low}$ [m]		-0.6	-0.8	-0.8	-0.9	-0.6	-0.8	-0.8	-0.9	-0.6	-0.8	-0.8	-0.9

6.2 Methodology

The following sections describe the methodology applied to derive the extreme metocean conditions at the Hesselø OWF.

- Section 6.2.1: extreme wind speeds (10 mMSL and 140 mMSL)
- Section 6.2.2: extreme high and low residual water level
- Section 6.2.3: extreme depth-averaged current speed
- Section 6.2.4: extreme spectral significant wave height and its associated peak wave period
- Section 6.2.5: extreme maximum wave height and its associated wave period
- Section 6.2.6: extreme wave crest elevation

6.2.1 Wind conditions

Extreme wind speeds (all-year and omnidirectional) at 10 m and 140 m above mean sea level were estimated from the CREA6 modelled wind data. The model data covered a ~24-year period (1995-01-14 to 2018-12-31) with a temporal resolution of 1-hour, and values are considered to represent a 30-minute average (see Section 2.3.1).

Sensitivity analyses comparing estimates of the 50-year omnidirectional extreme wind speed at analysis point OWF-1 are presented in Figure 6.1. The results show that the extreme wind speed estimates were approximately stable regarding the number of events per year for the truncated Weibull and 2-parameter Weibull distributions, when using a least-squares (LS) fitting method. A 2-parameter Weibull distribution with a least-squares (LS) estimation method using a threshold corresponding to an average of 3 annual peaks (λ=3) provided a good fit to the data and was selected for the extreme analysis of WS_{10} and WS_{140} at all analysis points.

The extreme distribution of WS_{10} and WS_{140} are shown for each analysis point in Figure 6.2 to Figure 6.4.

The results in Table 6.1 provide estimates of the extreme wind speed for an averaging period of 30-minutes. Factors for converting extreme wind speeds to different averaging periods were derived from the long-term record of wind speed measurements station at Anholt Havn. Figure 6.5 and Figure 6.6 show scatter plot comparisons of 10-minute average wind speeds at 10 mMSL, with wind speeds calculated using moving average windows of 30-minutes, 60-minutes, 120-minutes, and 180-minutes. The ratio between the magnitude of the 38 largest independent wind speeds events (based on an average of two annual peaks) were used to determine the conversion factors for extreme wind speeds (i.e., the peak ratio, PR). The results are summarised in Table 6.2. For example, to convert the 30-minute average wind speed to an equivalent 10-minute average wind speed, the return period estimates should be multiplied by a factor of $1/0.97 = 1.031$.

For comparison, the extreme wind speed conversion factors for 10-minute, 60-minute, and 180-minute averaging period provided in Section 6.4.3.1 of [16] are also included in Table 6.2.

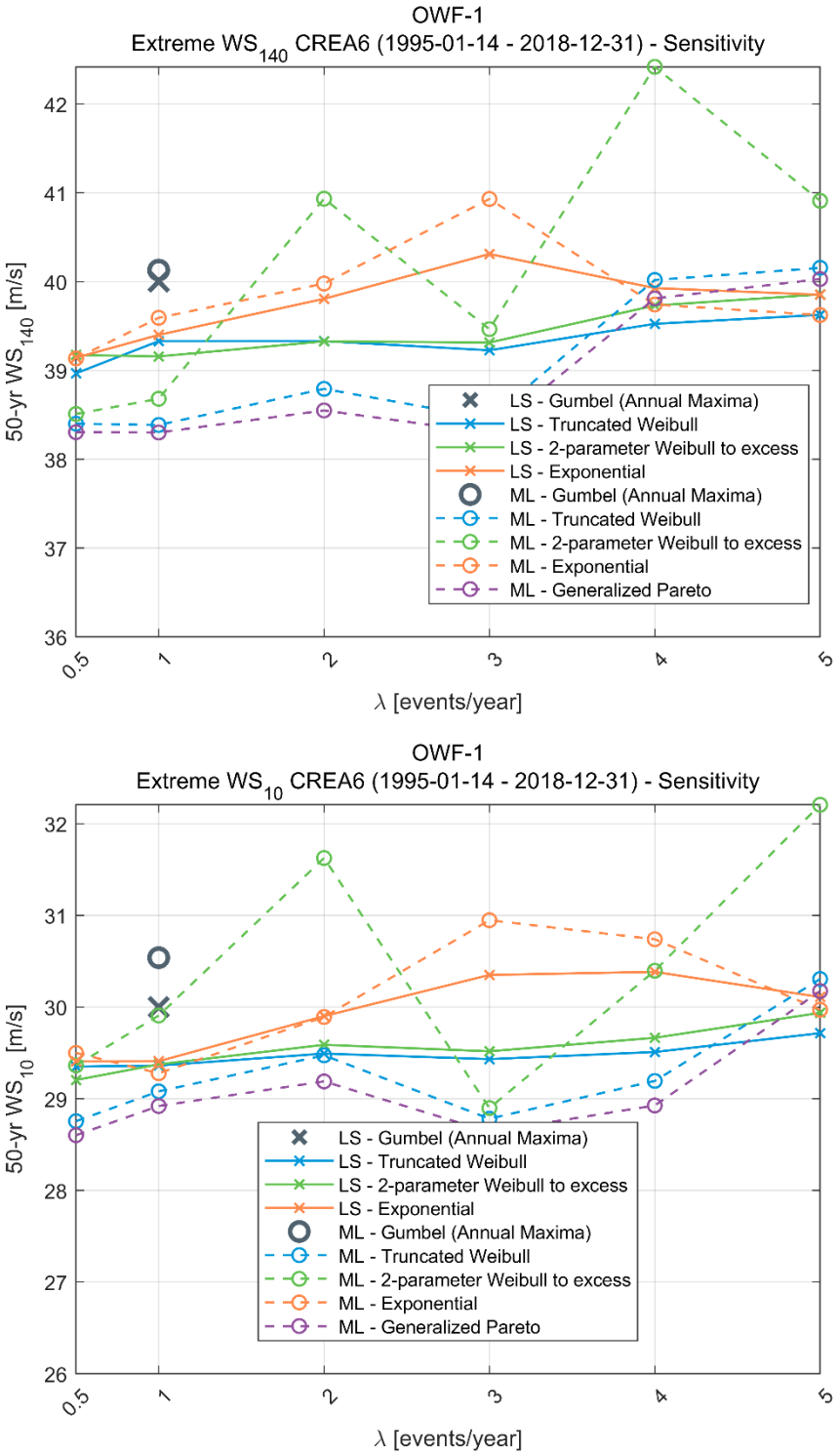

Figure 6.1 **Sensitivity analysis of extreme 30-minute wind speed at OWF-1**
The 50-year return period values at 140 m (upper panel) and 10 m (lower panel) are estimated from CREA6 modelled wind speeds, using different distributions, thresholds (number of events per year, λ), and fitting methods (ML and LS)

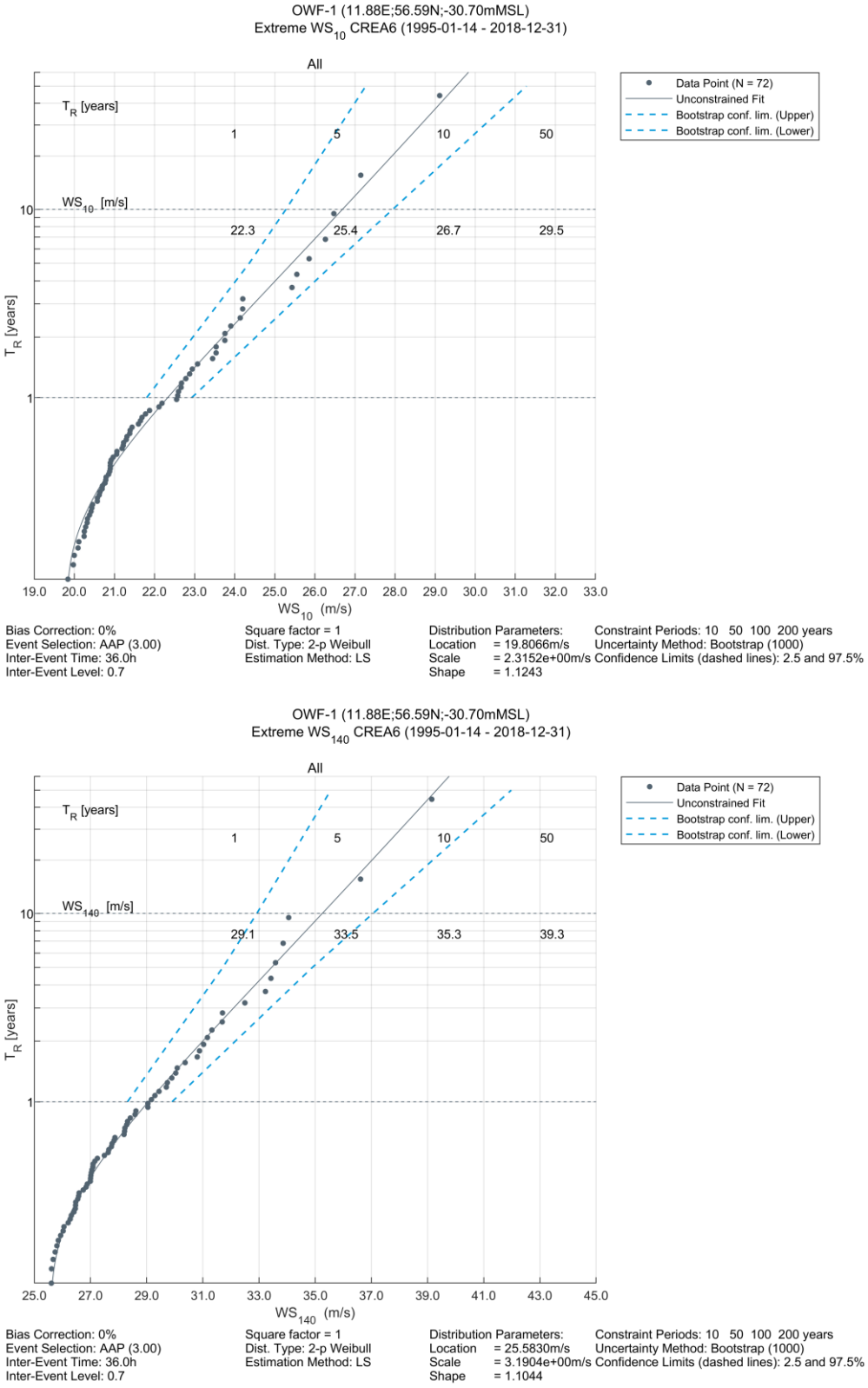

Figure 6.2 Omnidirectional extreme value distributions of wind speed at analysis point OWF-1
WS_{10} (upper panel) and WS_{140} (lower panel) according to a 2-parameter Weibull distribution fitted to an average of 3 annual peaks (λ=3) with a least-squares (LS) fitting method. The wind speeds represent an averaging period of 30 minutes

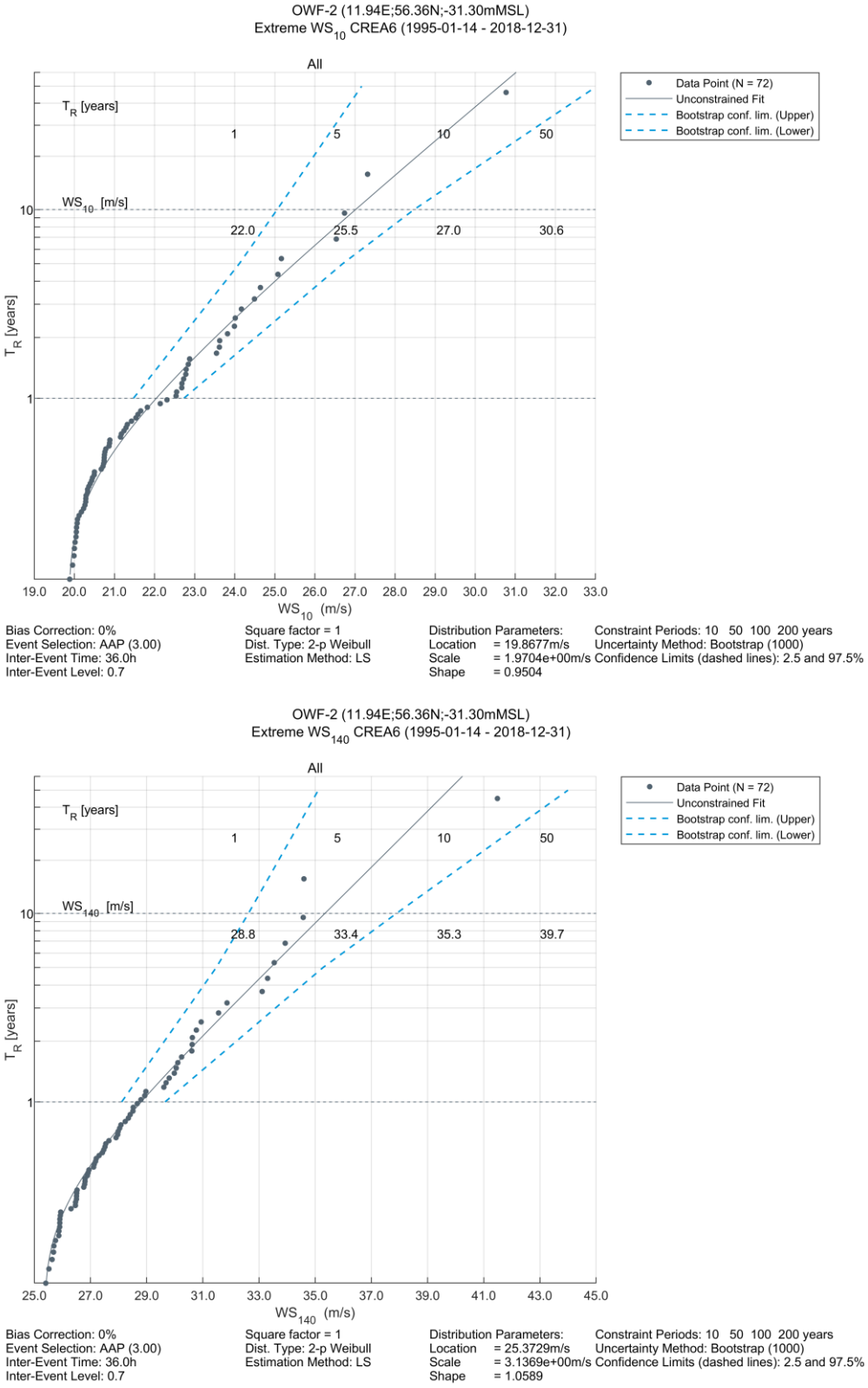

Figure 6.3 Omnidirectional extreme value distributions of wind speed at analysis point OWF-2
WS_{10} (upper panel) and WS_{140} (lower panel) according to a 2-parameter Weibull distribution fitted to an average of 3 annual peaks (λ=3) with a least-squares (LS) fitting method. The wind speeds represent an averaging period of 30 minutes

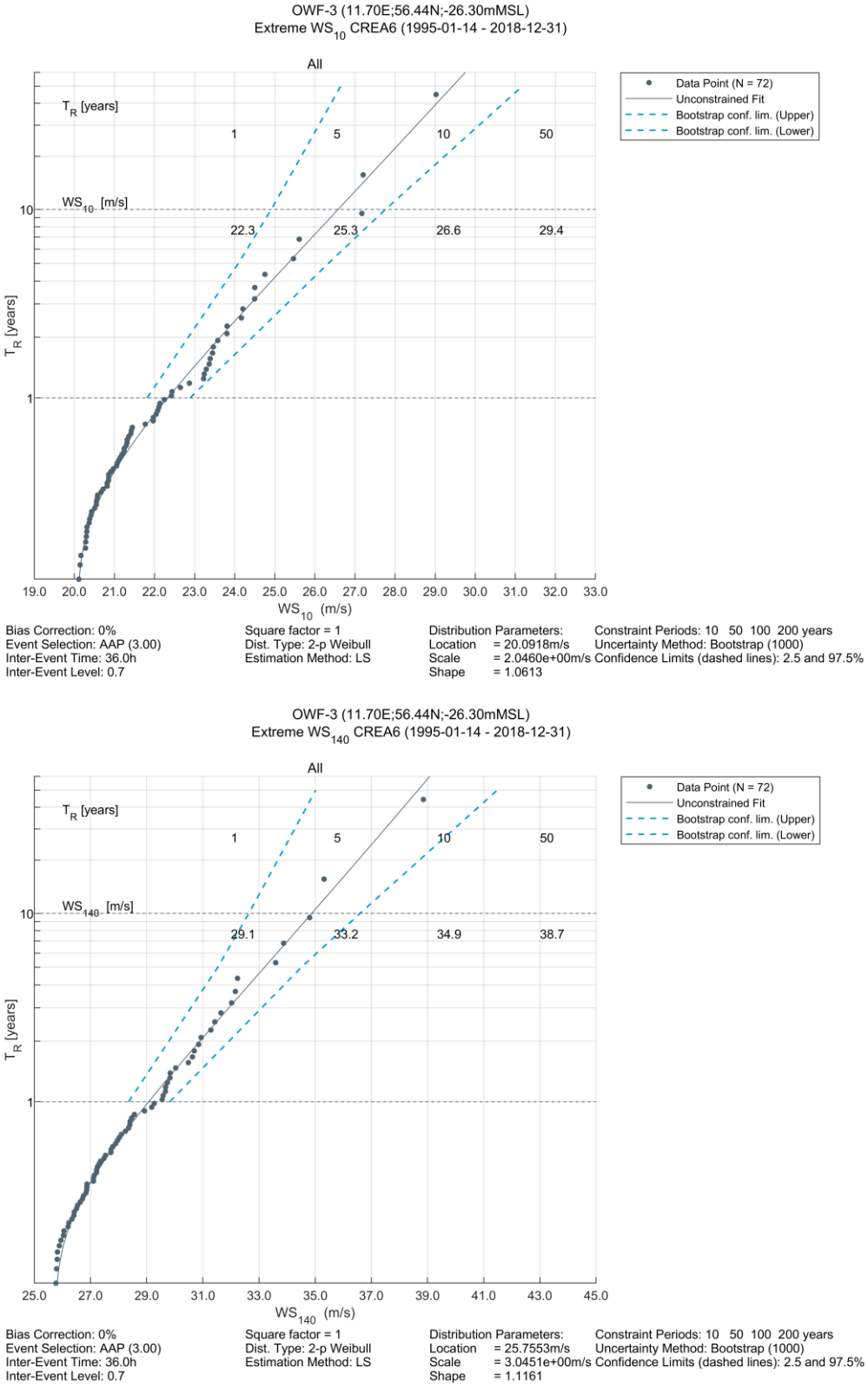

Figure 6.4 Omnidirectional extreme value distributions of wind speed at analysis point OWF-3
WS_{10} (upper panel) and WS_{140} (lower panel) according to a 2-parameter Weibull distribution fitted to an average of 3 annual peaks (λ=3) with a least-squares (LS) fitting method. The wind speeds represent an averaging period of 30 minutes

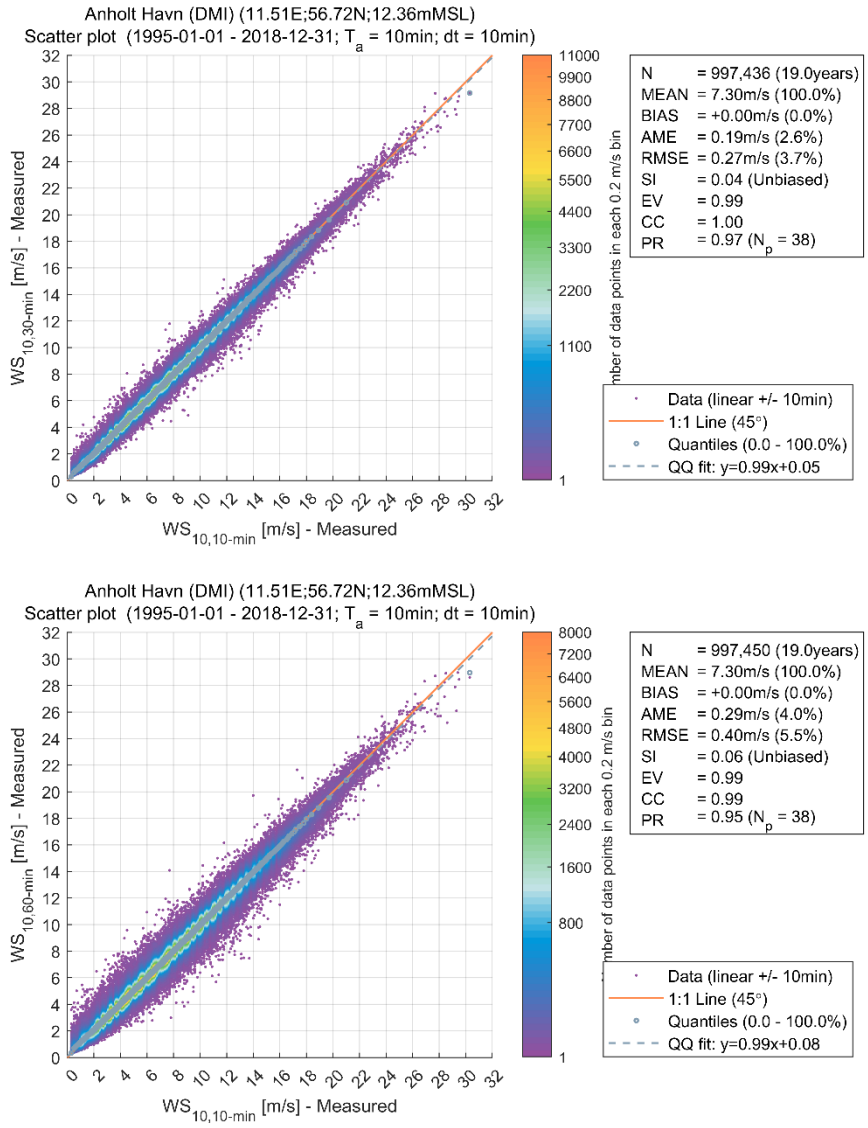

Figure 6.5 Comparison of measured wind speed at Anholt Havn for different averaging periods
The x-axis is the 10-minute average wind speed, while the y-axis is the wind speed averaged over a period of 30-minutes (upper panel), 60-minutes (lower panel)

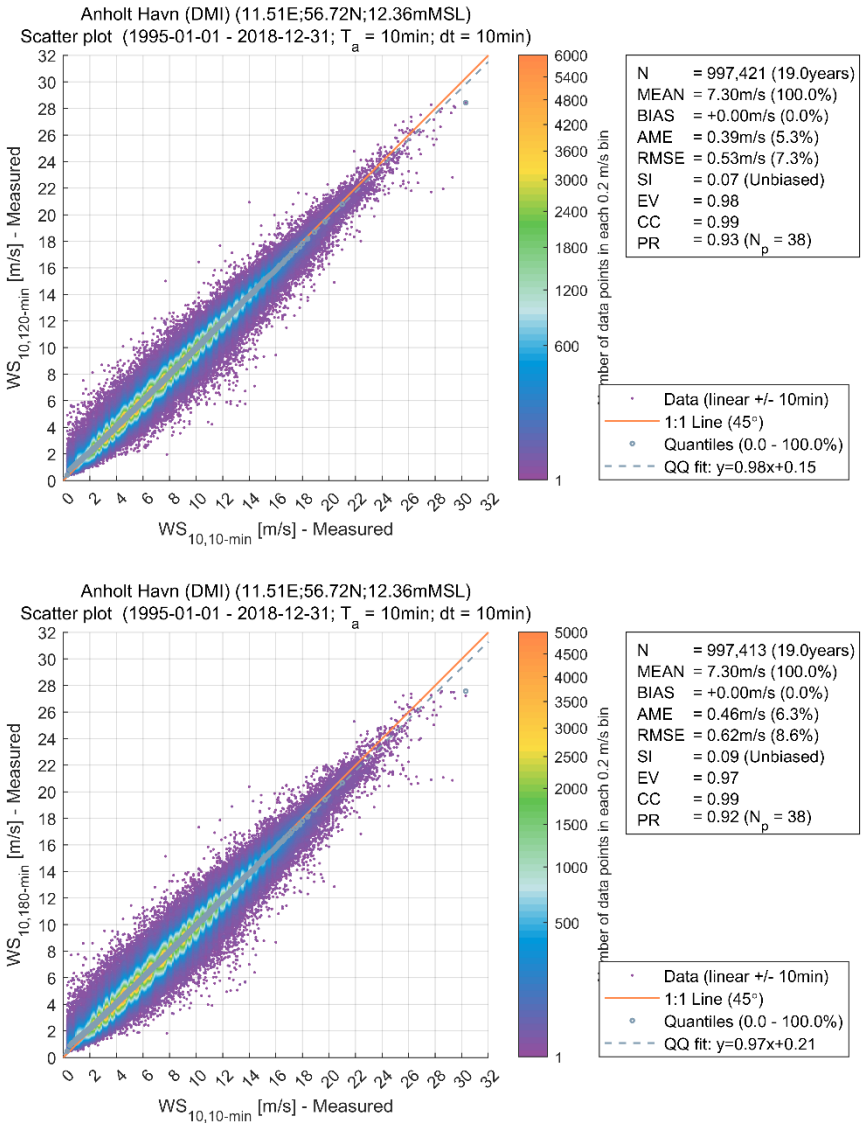

Figure 6.6 Comparison of measured wind speed at Anholt Havn for different averaging periods
The x-axis is the 10-minute average wind speed, while the y-axis is the wind speed averaged over a period of 120-minutes (upper panel), 180-minutes (lower panel)

Table 6.2 Conversion between 10-minute extreme wind speeds and longer averaging periods
Conversion factors are given from section 6.4.3.1 of IEC 61400-3--1 [16] and derived from DMI measured wind speeds at Anholt Havn

Averaging period	10-minute	30-minute	60-minute	120-minute	180-minutes
Anholt Havn	1.00	0.97	0.95	0.93	0.92
IEC 61400-3-1	1.00	-	0.95	-	0.90

6.2.2 Water levels

Extreme estimate of the high and low water level conditions was determined for the residual (i.e., surge) component. The residual water levels were calculated by de-tiding the total water level output from the HD_{DKW} model as described in Section 5.4.1.

Figure 6.7 summarises the results of the sensitivity analysis in terms of the 50-year residual high-water level and residual low-water level. The estimated extreme positive residual water level was approximately stable regarding the number of events per year when using a least-squares (LS) fitting method. It was decided to use a 2-parameters Weibull distribution fitted to an average of 3 annual peak events (λ=3) for all analysis points. The resulting extreme value distributions are shown in upper panel of Figure 6.8 to Figure 6.10.

For extreme negative residual water levels, it was decided to use the truncated Weibull distribution with a least-squares (LS) estimation method using a threshold corresponding to an average of 2 annual peaks (λ=2) at all sites. The resulting extreme value distributions are shown in lower panel of Figure 6.8 to Figure 6.10.

Extreme positive and negative total water levels (i.e., combined tide and residual) may be approximated by combining the extreme residual water levels with an appropriate astronomical water level (see Section 5.4.1)

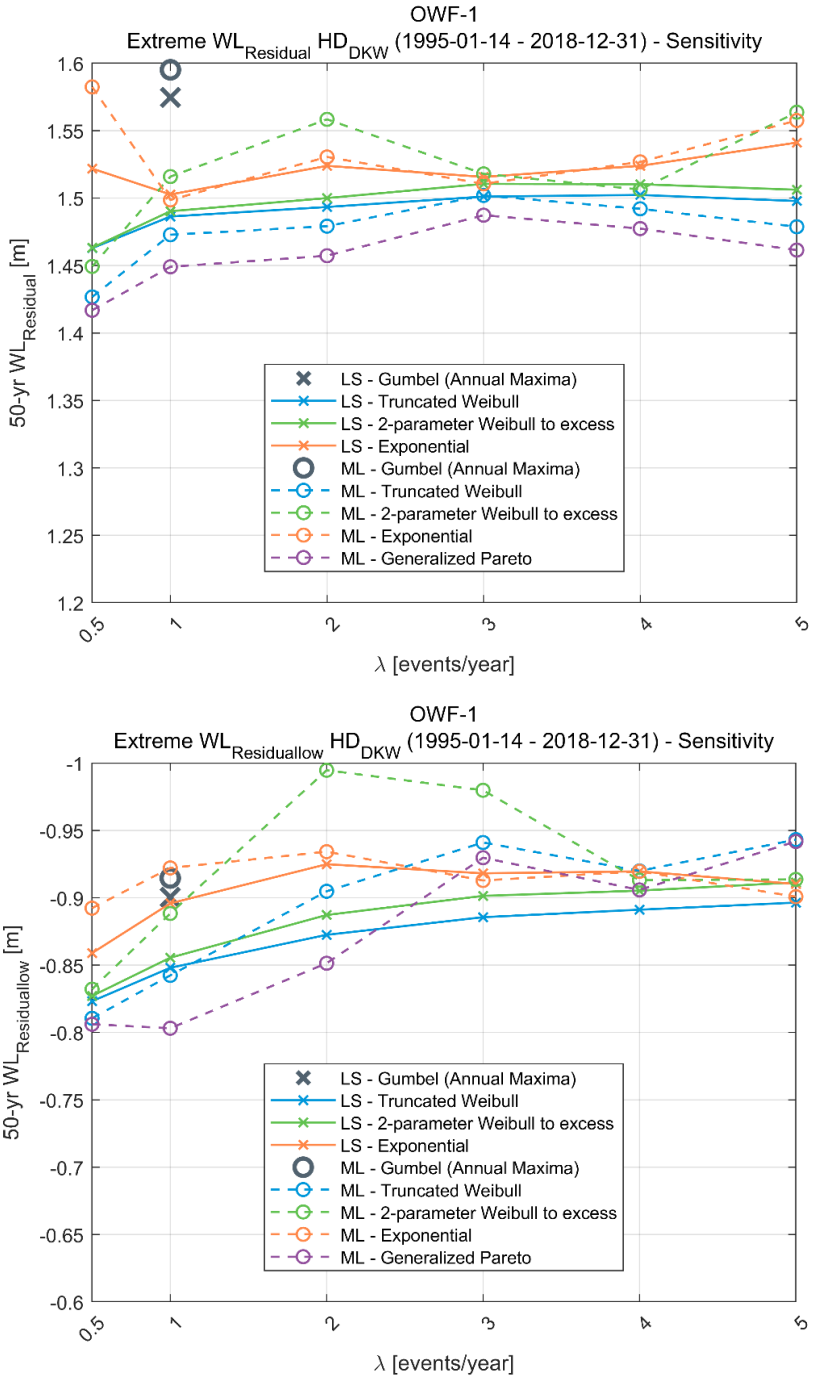

Figure 6.7 **Sensitivity analysis of extreme residual water level at OWF-1**
The 50-year return period values residual high-water level (upper panel) and residual low-water level (lower panel) estimated using different distributions, thresholds (number of events per year, λ), and fitting methods (ML and LS)

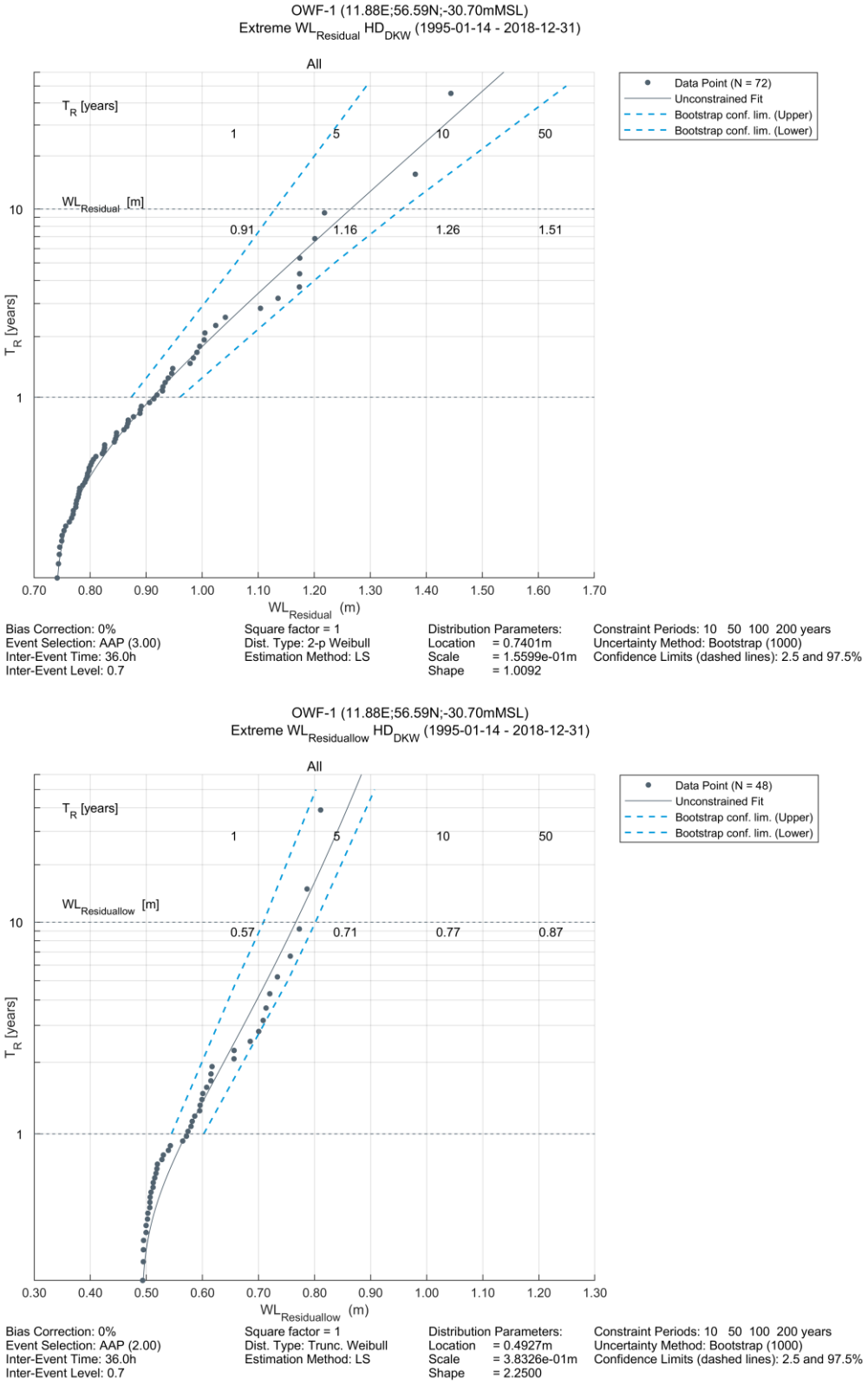

Figure 6.8 Extreme value distributions for $WL_{Residual}$ at analysis point OWF-1
$WL_{Residual,High}$ (upper panel) and $WL_{Residual,Low}$ (lower panel) according 2-parameter Weibull distribution fitted to an average of 3 annual peaks (λ=3) with a least-squares (LS) fitting method

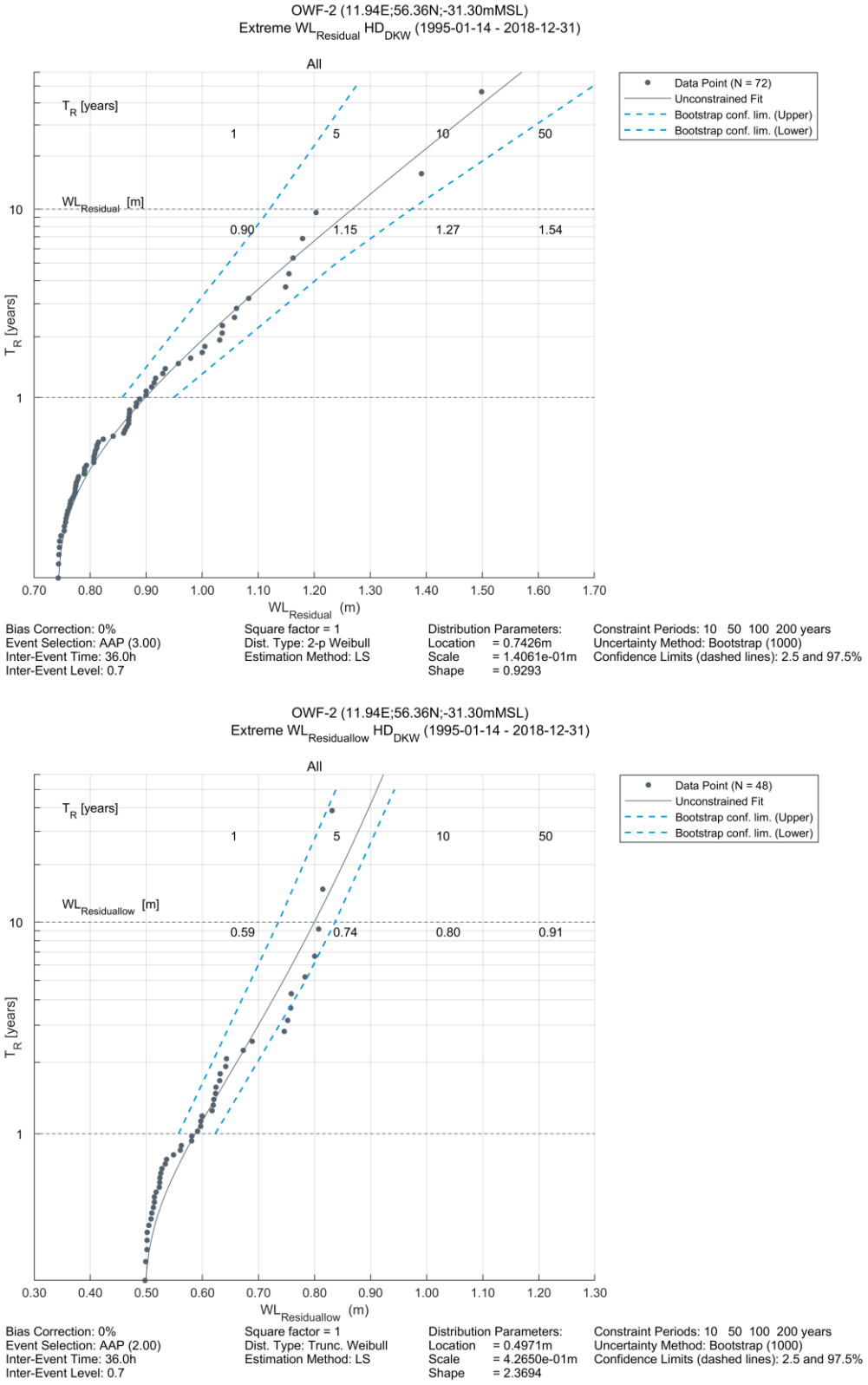

Figure 6.9 Extreme value distributions for $WL_{Residual}$ at analysis point OWF-2
$WL_{Residual,High}$ (upper panel) and $WL_{Residual,Low}$ (lower panel) according 2-parameter Weibull distribution fitted to an average of 3 annual peaks (λ=3) with a least-squares (LS) fitting method

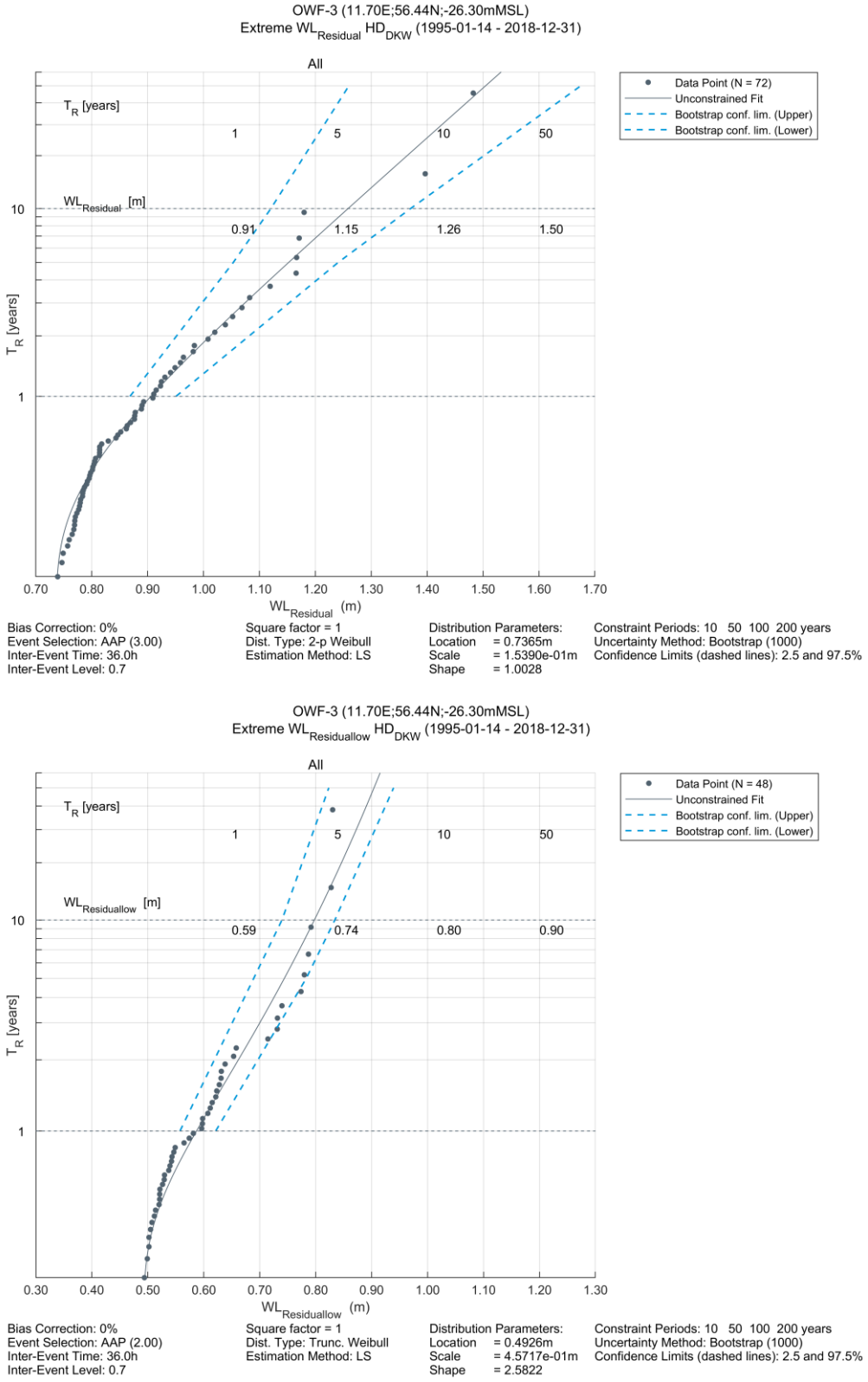

Figure 6.10 Extreme value distributions for $WL_{Residual}$ at analysis point OWF-3
$WL_{Residual,High}$ (upper panel) and $WL_{Residual,Low}$ (lower panel) according 2-parameter Weibull distribution fitted to an average of 3 annual peaks (λ=3) with a least-squares (LS) fitting method

6.2.3 Current speeds

Extreme depth-averaged total current speeds were estimated from the HD_{DKW} modelled current data. The model data covered a ~24-year period (1995-01-14 to 2018-12-31) with a temporal resolution of 1-hour.

A multiplication factor of 1.5 has been applied to the total current speeds (see Section 3.3.2). It is noted that the depth averaged current speeds do not include any effects of stratification over the water depth.

Sensitivity analyses comparing estimates of the 50-year omnidirectional extreme depth-averaged total current speed at analysis point OWF-1 are presented below in Figure 6.11. The results show that the extreme depth average total current speed estimates were approximately stable regarding the number of events per year when using either a Truncated Weibull or 2-parameter Weibull distribution when using a least-squares (LS) fitting method. It was decided to use a Truncated Weibull distribution with a least-squares (LS) estimation method using a threshold corresponding to an average of 2 annual peaks (λ=2) at all analysis points. The resulting extreme value distributions are shown in Figure 6.12 to Figure 6.14.

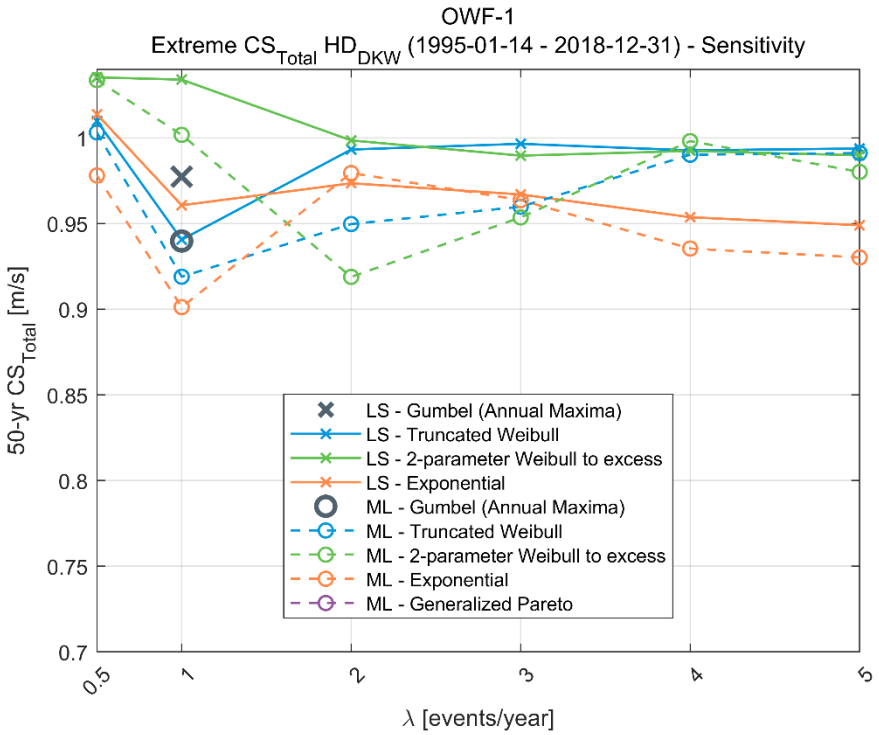

Figure 6.11 Sensitivity analysis of extreme CS_{Total} at analysis point OWF-1
The 50-year return period values depth-averaged total current peed estimated using different distributions, thresholds (number of events per year, λ), and fitting methods (ML and LS)

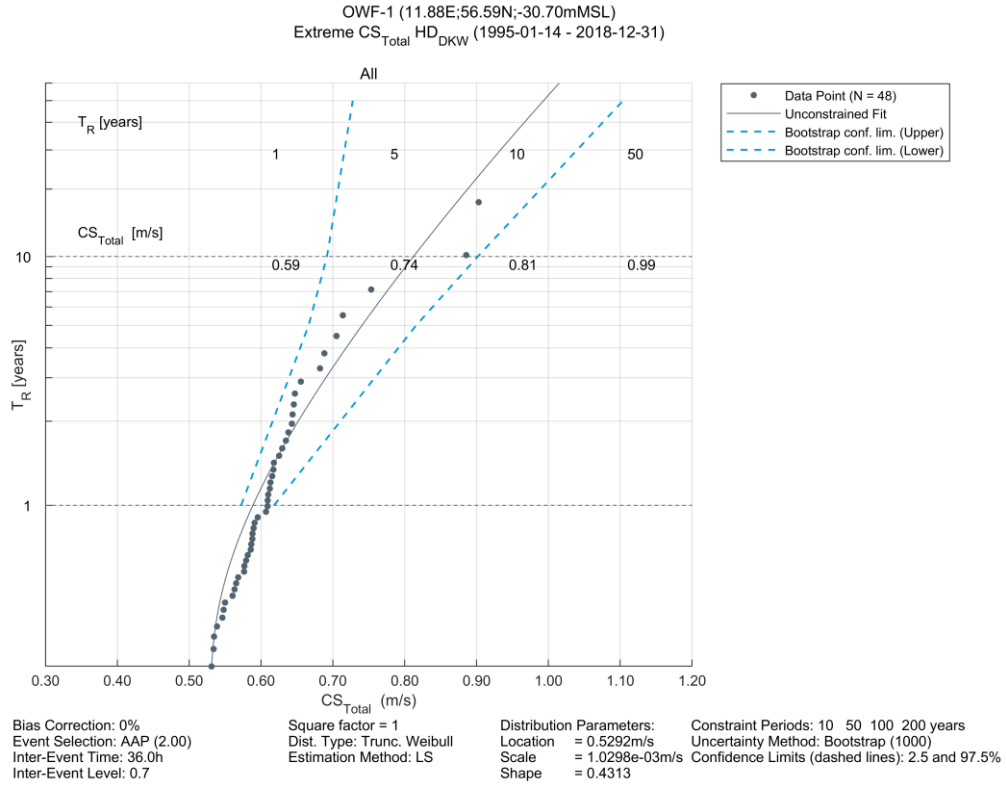

Figure 6.12 Extreme value distributions of CS_{Total} at analysis point OWF-1
Truncated Weibull distribution fitted to an average of 2 annual peaks (λ=2) with a least-squares (LS) fitting method

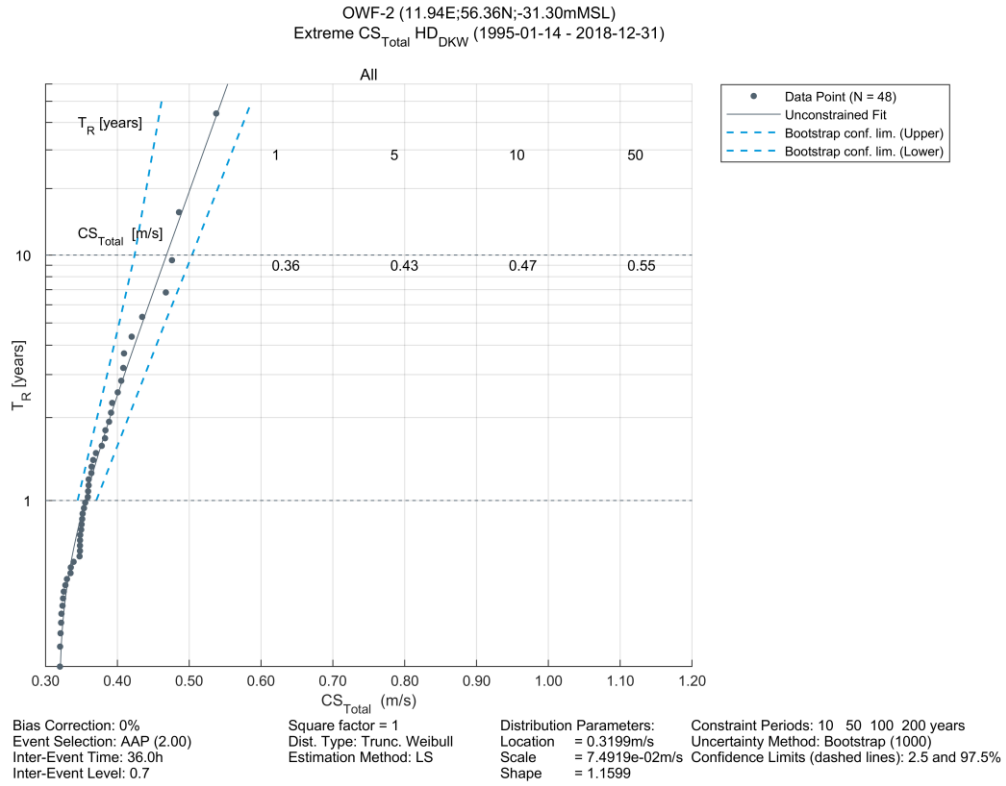

Figure 6.13 Extreme value distributions of CS_{Total} at analysis point OWF-2
Truncated Weibull distribution fitted to an average of 2 annual peaks (λ=2) with a least-squares (LS) fitting method

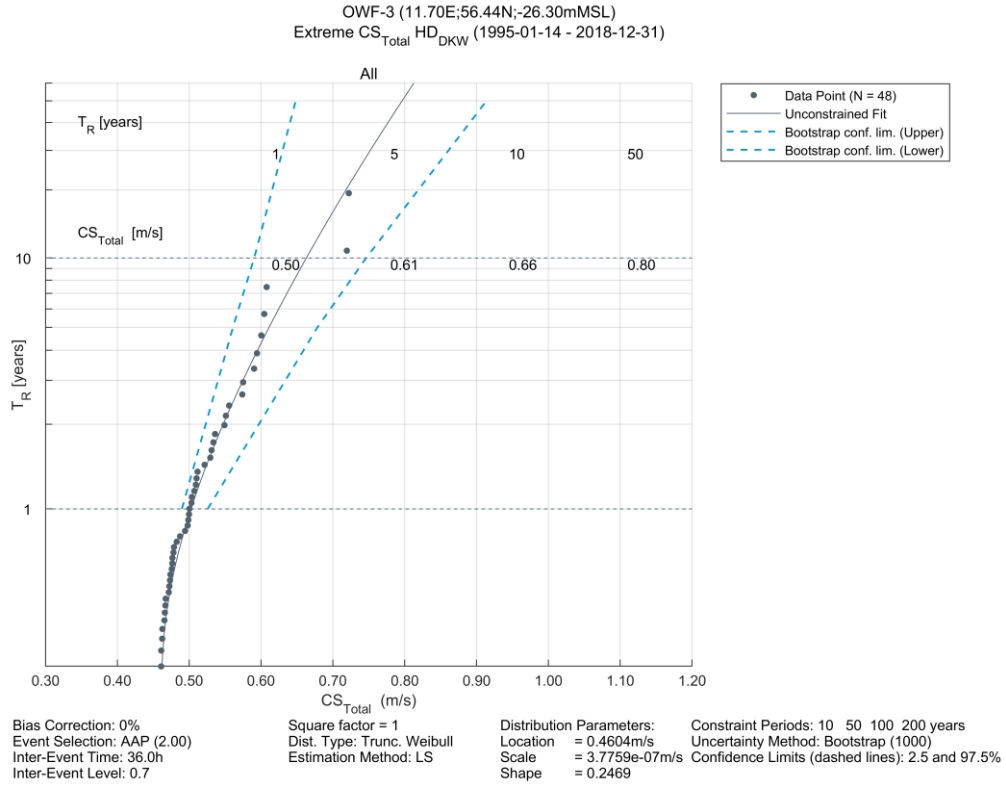

Figure 6.14 Extreme value distributions of CS_{Total} at analysis point OWF-3
Truncated Weibull distribution fitted to an average of 2 annual peaks (λ=2) with a least-squares (LS) fitting method

6.2.4 Significant wave height and associated peak wave period

Extreme significant wave heights (all-year and omnidirectional) were estimated from the SW_{DKW} modelled wave data. The model data covered a ~24-year period (1995-01-14 to 2018-12-31) with a temporal resolution of 1-hour, and values are considered to represent a 3-hour average (see Section 2.3.3).

Sensitivity analyses comparing estimates of the 50-year omnidirectional extreme significant wave height at analysis point OWF-1 are presented in Figure 6.15. The results show that the extreme significant wave height estimates were stable regarding the number of events per year, distribution type, and fitting method. A 2-parameter Weibull distribution with a least-squares (LS) estimation method using a threshold corresponding to an average of 3 annual peaks (λ=3) provided a good fit to the data and was selected for the extreme analysis of H_{m0} at all analysis points.

The extreme distribution of H_{m0} for analysis points are shown in Figure 6.16 (OWF-1), Figure 6.17 (OWF-2), and Figure 6.18 (OWF-3).

The peak wave period (T_p) associated with the extreme H_{m0} presented in Table 6.1 were derived by fitting a least-squares power function to the 50% quantile of the T_p data for each H_{m0} bin (conditioned on the top 10% of the H_{m0} data). The fitting of T_p to H_{m0} at analysis points OWF-1, OWF-2, and OWF-3 are shown in the scatter plots of in Figure 5.15, and the resulting equations are summarised in Table 6.3.

Table 6.3 Relationship between H_{m0} and T_p for extreme conditions
T_p is given in units of seconds, and H_{m0} is given in units of meters

Analysis point	Functional fit
OWF-1	$T_p = 4.518 \cdot {H_{m0}}^{0.370}$
OWF-2	$T_p = 4.545 \cdot {H_{m0}}^{0.364}$
OWF-3	$T_p = 4.508 \cdot {H_{m0}}^{0.354}$

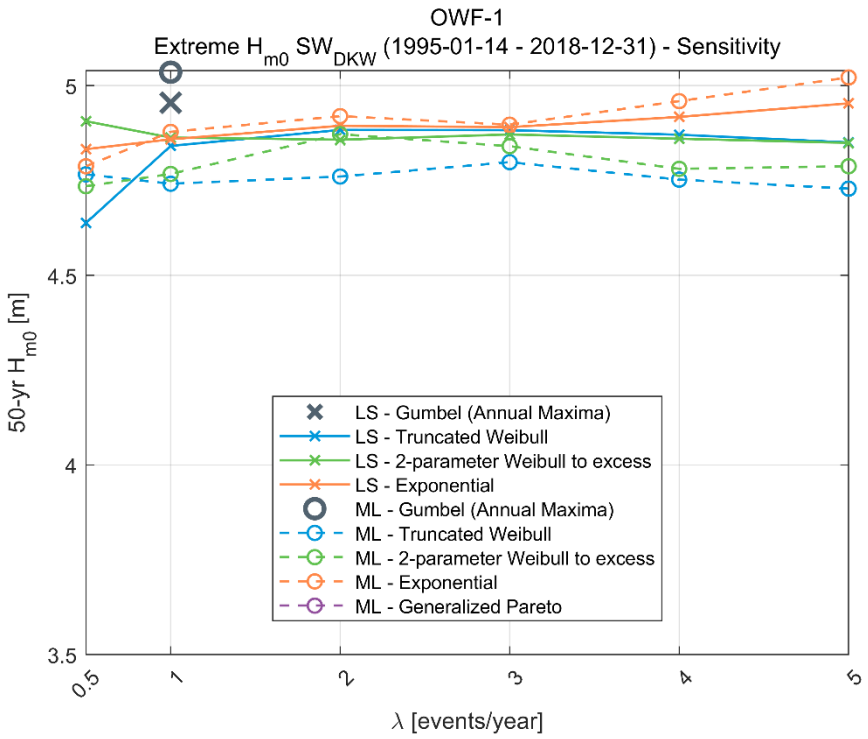

Figure 6.15 Sensitivity of extreme significant wave height at OWF-1
The 50-year return period values are estimated from SW_{DKW} modelled wave heights, using different distributions, thresholds (number of events per year, λ), and fitting methods (ML and LS)

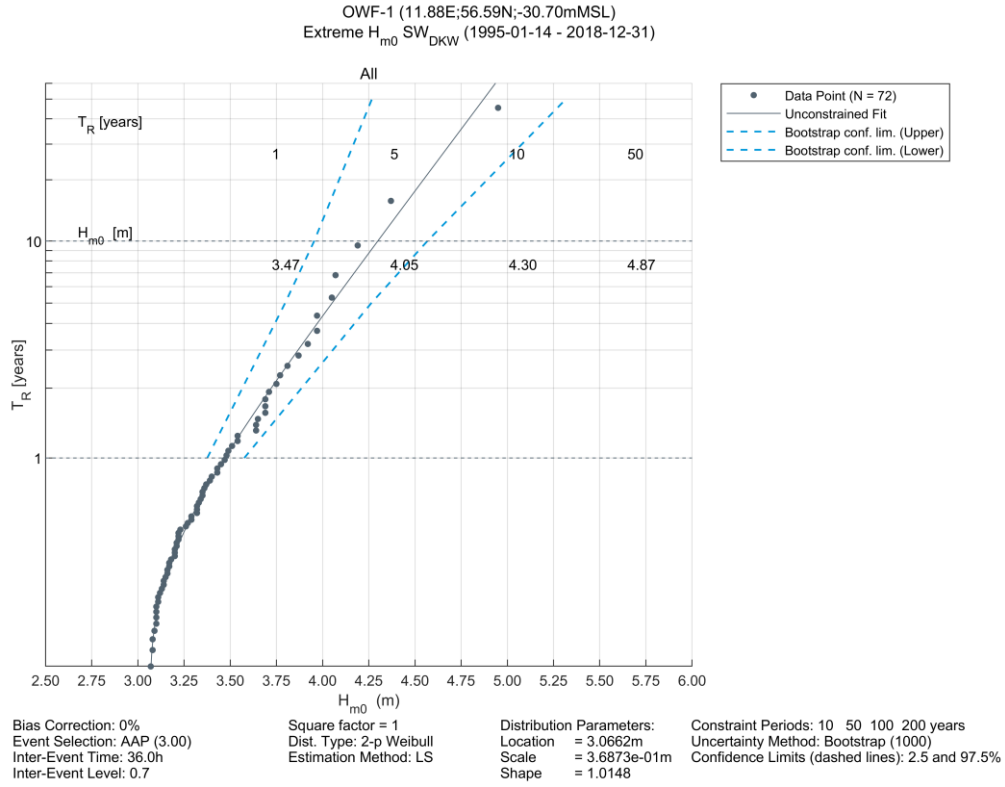

Figure 6.16 Extreme value distributions of H_{m0} at analysis point OWF-1
2-parameter Weibull distribution fitted to an average of 3 annual peaks (λ=3) with a least-squares (LS) fitting method

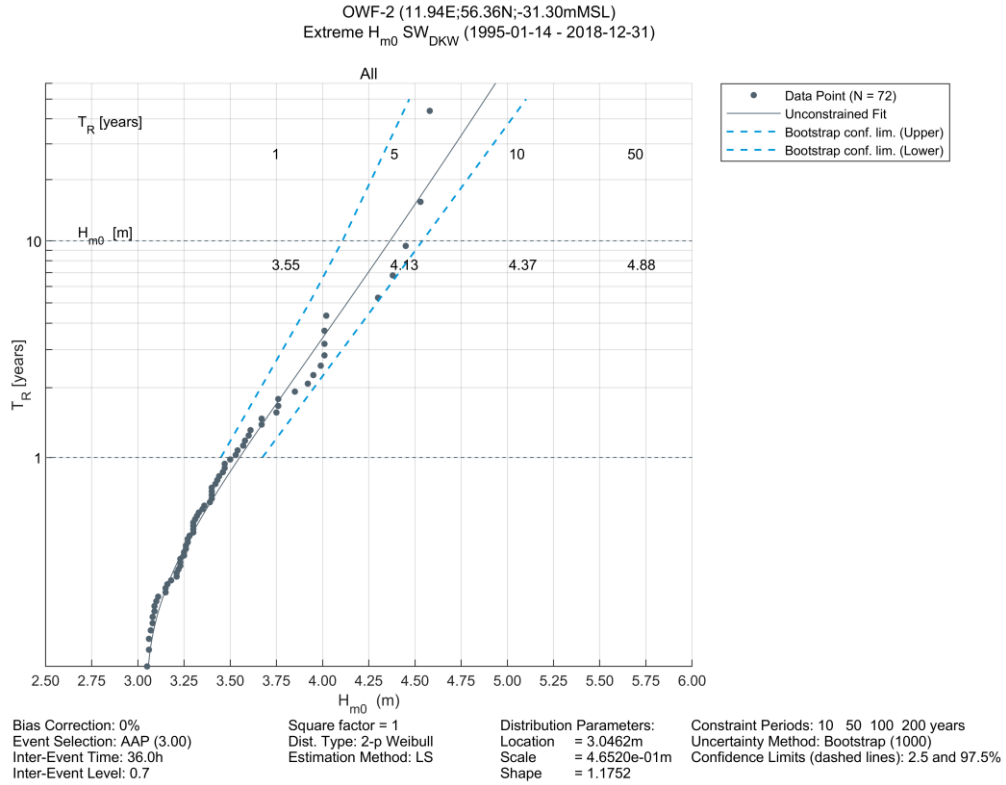

Figure 6.17 Extreme value distributions of H_{m0} at analysis point OWF-2
2-parameter Weibull distribution fitted to an average of 3 annual peaks (λ=3) with a least-squares (LS) fitting method

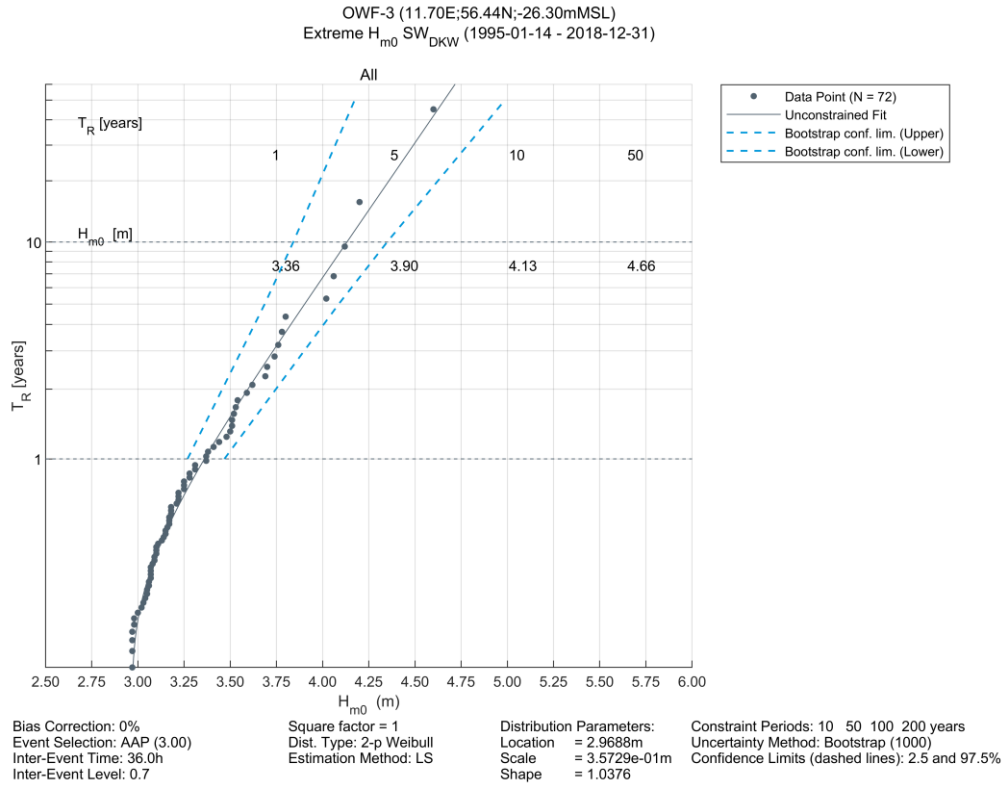

Figure 6.18 Extreme value distributions of H_{m0} at analysis point OWF-3
2-parameter Weibull distribution fitted to an average of 3 annual peaks (λ=3) with a least-squares (LS) fitting method

6.2.5 Individual wave height and associated wave period

For each sea state, the maximum individual wave height, H_{max}, was calculated through the convolution method by Tromans and Vanderschuren [28]. The short-term distribution of individual wave height conditional on H_{m0} was assumed to follow the distribution proposed by Forristall [29]. Additional technical information is included in Section D.3 of Appendix D.

The extreme values of H_{max} (all-year and omnidirectional) were estimated using the same method as applied to derive extreme H_{m0} in section 6.2.4 i.e., a 2-parameter Weibull distribution with a least-squares (LS) estimation method using a threshold corresponding to an average of 3 annual peaks (λ=3).

The all-year omnidirectional distributions of H_{max} are shown in Figure 6.19 (OWF-1), Figure 6.20 (OWF-2), and Figure 6.21(OWF-3). In these plots, the grey curve represents the unconstrained fit of H (the most probable maximum individual wave height of a storm), while the green curve is the convolution of the short-term distribution, H_{max} with the long-term distribution of H.

According to Section B.4 of [16], the breaking wave height in shallow water is approximately 78% of the local water depth. Taking the nominal water depth at the metocean analysis points from Table 4.1 the breaking wave heights at the Hesselø OWF according to this criterion are far larger than the estimated extreme individual wave heights for a return period of 50-years.

The range of wave period T_{Hmax} to be used in conjunction with extreme individual wave height H_{max} has been inferred from time series decomposition of the modelled wave energy spectra. Frequency wave spectral data from the SW_{DKW} model is available on 0.1° resolution grid (see Section 2.3.3) and has been used to derive the relationship between maximum wave height and the associated wave period for all analysis points.

The following stepwise calculation has been carried out to estimate the relationship between maximum wave height in a sea state and its associated period:

1. For all sea-states within the modelled period (1995-01-14 to 2018-12-31), a surface elevation time series of 1-hour duration was simulated from the modelled frequency spectrum, assuming a Gaussian process with random phase
2. A zero-crossing analysis was made on the time series, and the maximum wave and its period were extracted

After performing the above steps, scatter plots of maximum wave height in a sea-state (H_{max}) against its corresponding period (T_{Hmax}) were created (Figure 6.22 to Figure 6.24). Formulae for the mean and variance of the inverse log-normal distribution of T_{Hmax} as a function of H_{max} were established and these parameters were then used to calculate the 10%, 50%, and 90% quantiles of T_{Hmax} associated with the estimated extreme individual wave heights presented in Table 6.1.

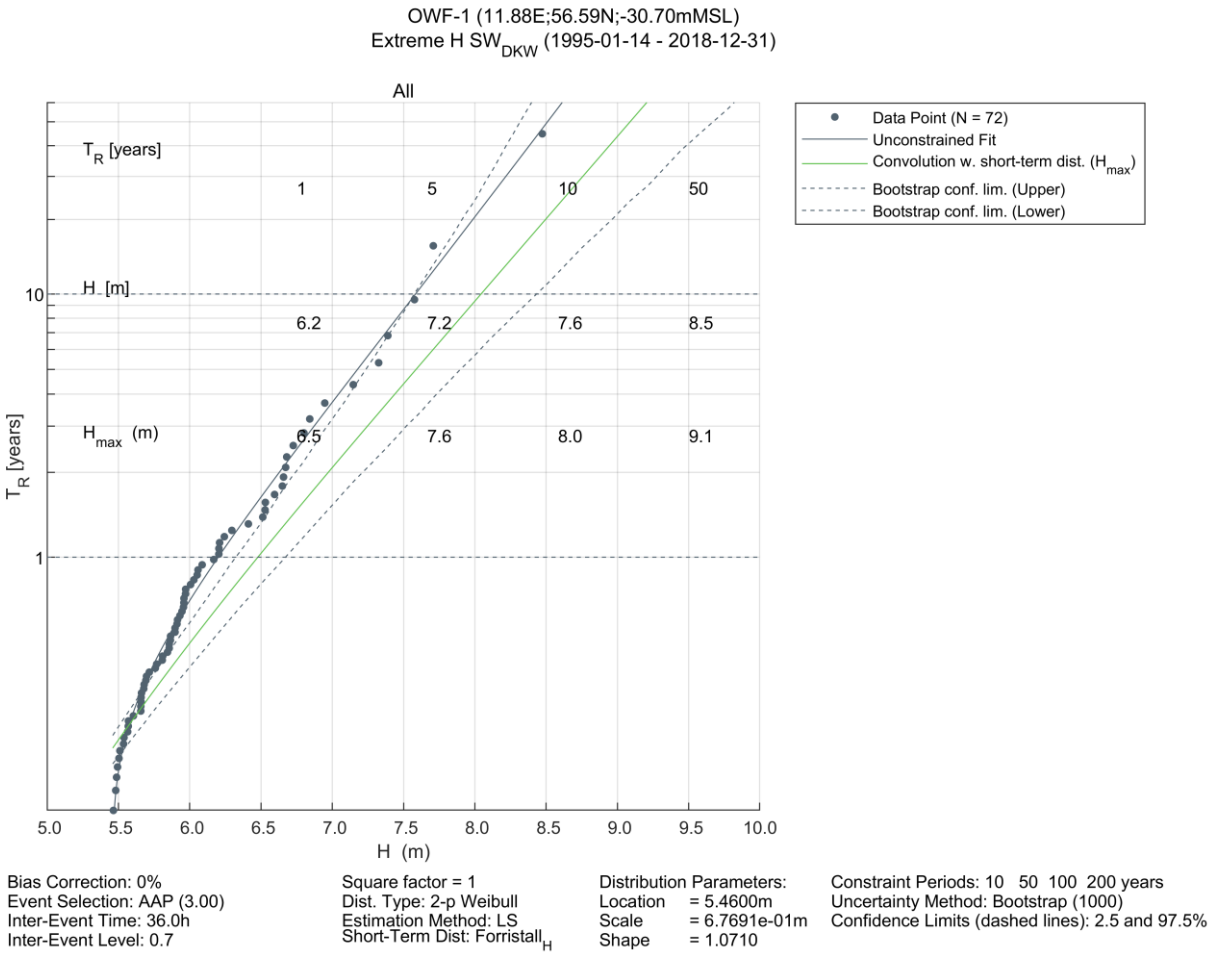

Figure 6.19 Extreme value distributions of H_{max} at analysis point OWF-1

2-parameter Weibull distribution fitted to an average of 3 annual peak (λ=3) individual wave heights (H) convolved with short term distribution (H_{max}). The dashed grey lines show the upper (97.5%) and lower (2.5%) confidence limits

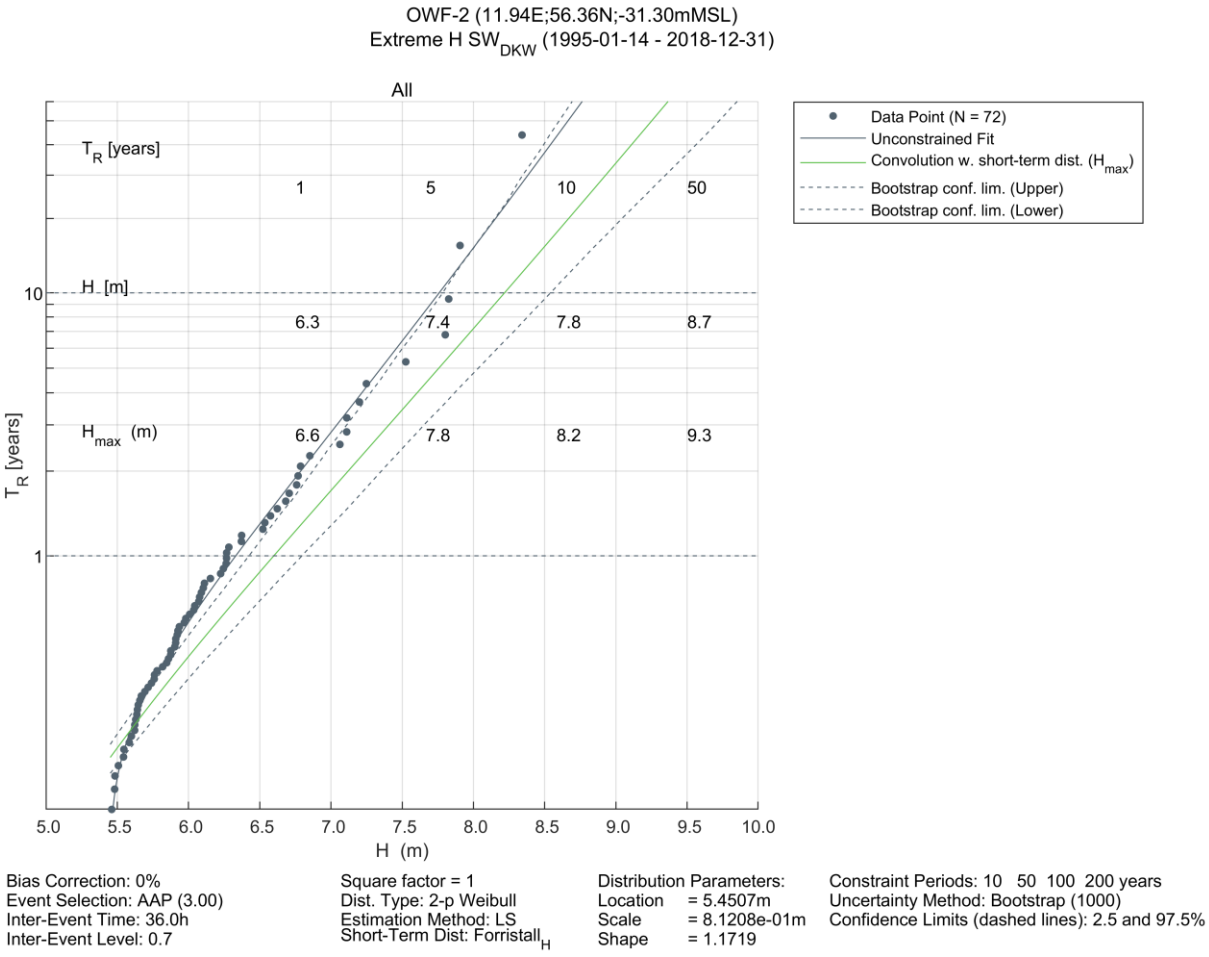

Figure 6.20 Extreme value distributions of H_{max} at analysis point OWF-2

2-parameter Weibull distribution fitted to an average of 3 annual peak (λ=3) individual wave heights (H) convolved with short term distribution (H_{max}). The dashed grey lines show the upper (97.5%) and lower (2.5%) confidence limits

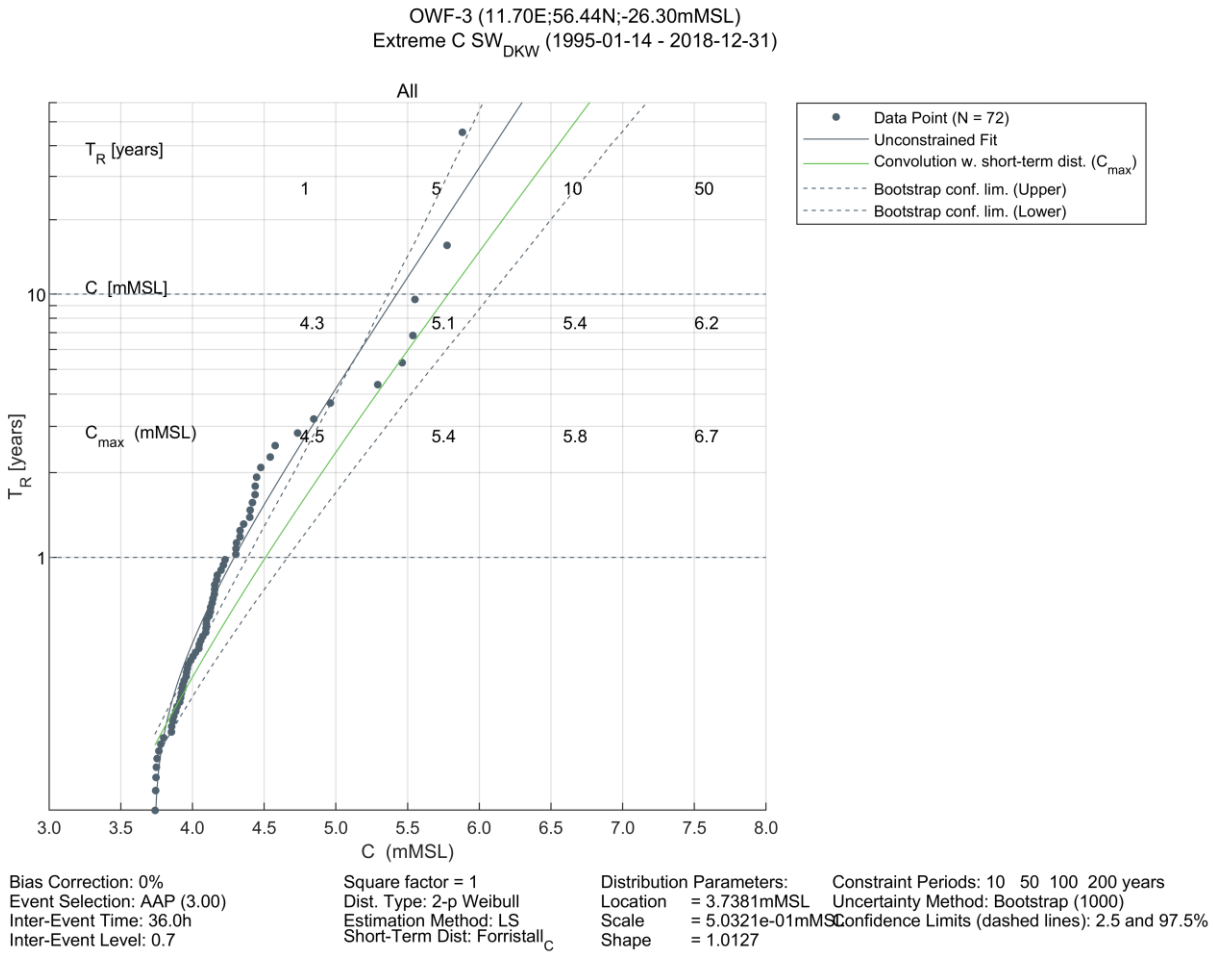

Figure 6.21 Extreme value distributions of H_{max} at analysis point OWF-3

2-parameter Weibull distribution fitted to an average of 3 annual peak (λ=3) individual wave heights (H) convolved with short term distribution (H_{max}). The dashed grey lines show the upper (97.5%) and lower (2.5%) confidence limits

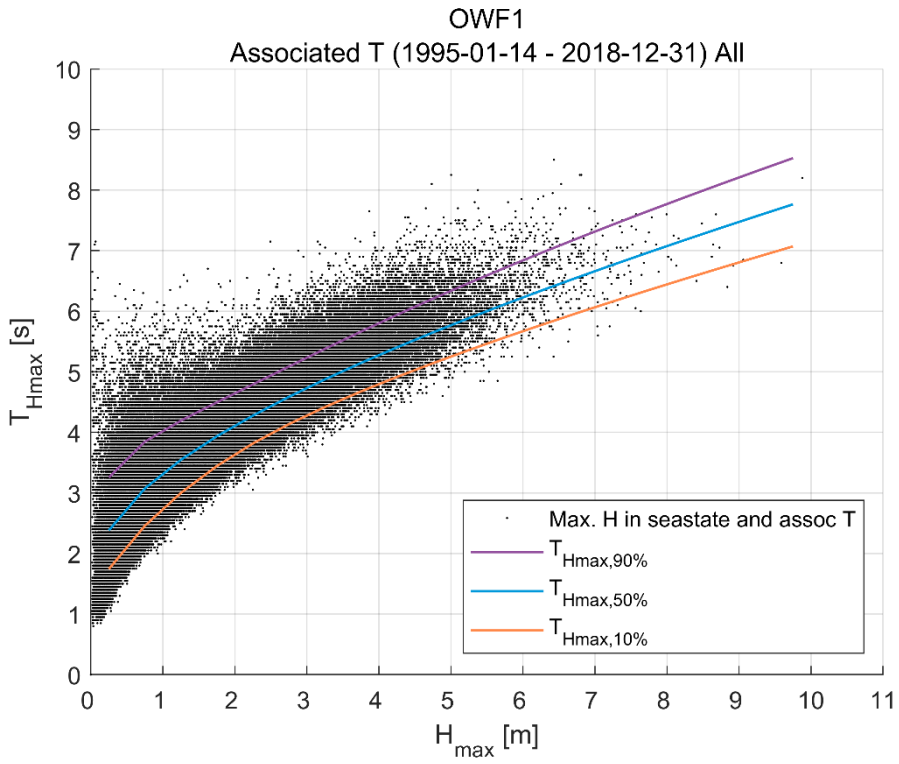

Figure 6.22 Scatter plots of T_{Hmax} against H_{max} at analysis point OWF-1
The fitted lines show the inverse log-normal relationship for T_{Hmax} based on H_{max}: 10% (orange), 50% (blue), and 90% (purple)

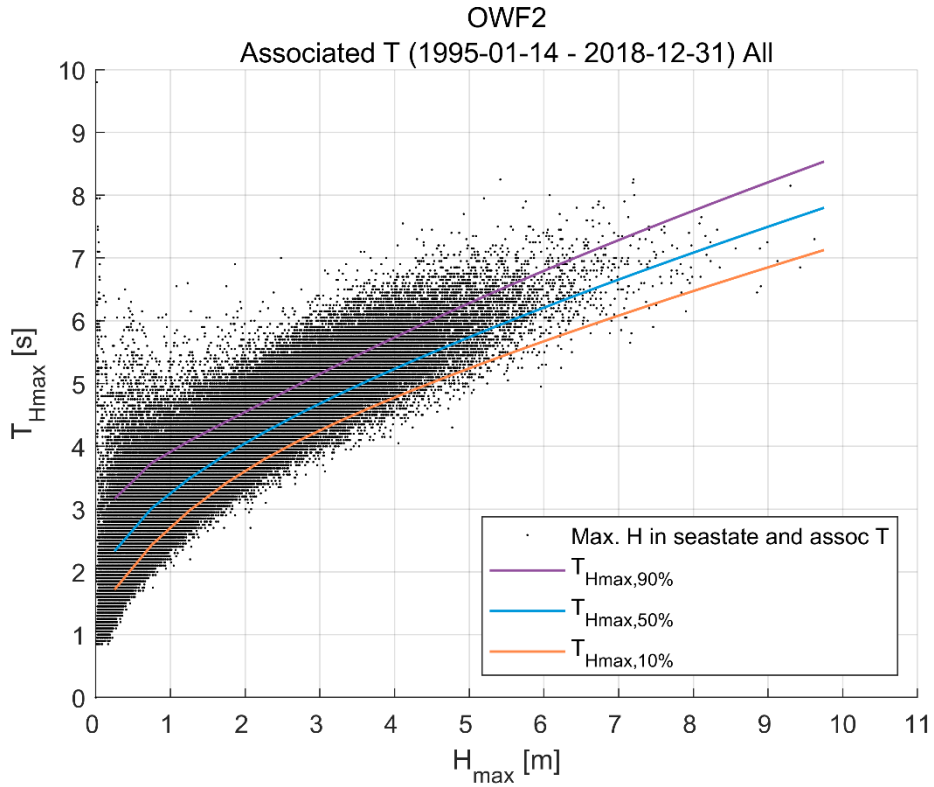

Figure 6.23 Scatter plots of T_{Hmax} against H_{max} at analysis point OWF-2
The fitted lines show the inverse log-normal relationship for T_{Hmax} based on H_{max}: 10% (orange), 50% (blue), and 90% (purple)

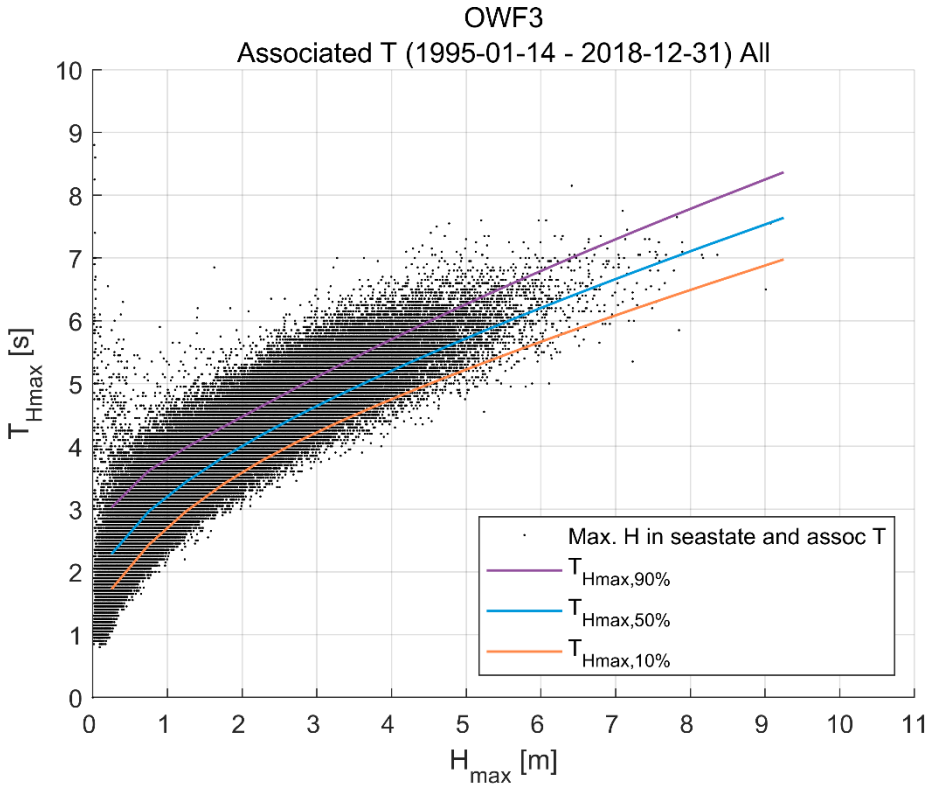

Figure 6.24 Scatter plots of T_{Hmax} against H_{max} at analysis point OWF-3
The fitted lines show the inverse log-normal relationship for T_{Hmax} based on H_{max}: 10% (orange), 50% (blue), and 90% (purple)

6.2.6 Wave crest elevation

For each sea state, the maximum wave crest elevation, $C_{max,}$ was estimated using the convolution method by Tromans and Vanderschuren [28]. The individual wave crest elevations were assumed to follow the distribution proposed by Forristall [30]. Additional technical information is included in Section D.3 of Appendix D.

The maximum wave crest elevations were calculated relative to both still water level ($C_{max,SWL}$) and mean sea level ($C_{max,MSL}$). For the latter, the link between water level and wave crest elevation was derived by adding the water level to the wave crest height distribution for each sea state during the integration of short-term distribution over the storms.

The extreme values of C_{max} (all-year and omnidirectional) were estimated using the same method as applied to derive extreme H_{m0} in Section 6.2.5, i.e., a 2-parameter Weibull distribution with a least-squares (LS) estimation method using a threshold corresponding to an average of 3 annual peaks (λ=3).

Figure 6.25, Figure 6.26 and Figure 6.27 present the omnidirectional distribution plots relative to SWL and MSL for analysis points OWF-1, OWF-2, and OWF-3, respectively. The distribution plots show the estimated most probable value of the wave crest elevation in a storm C_{mp} (grey curve), and the convolution of the short-term distribution C_{max} (green curve) conditional on C_{mp} (C_{max} | C_{mp}) with the long-term distribution of C_{mp} with reference to SWL and MSL, respectively.

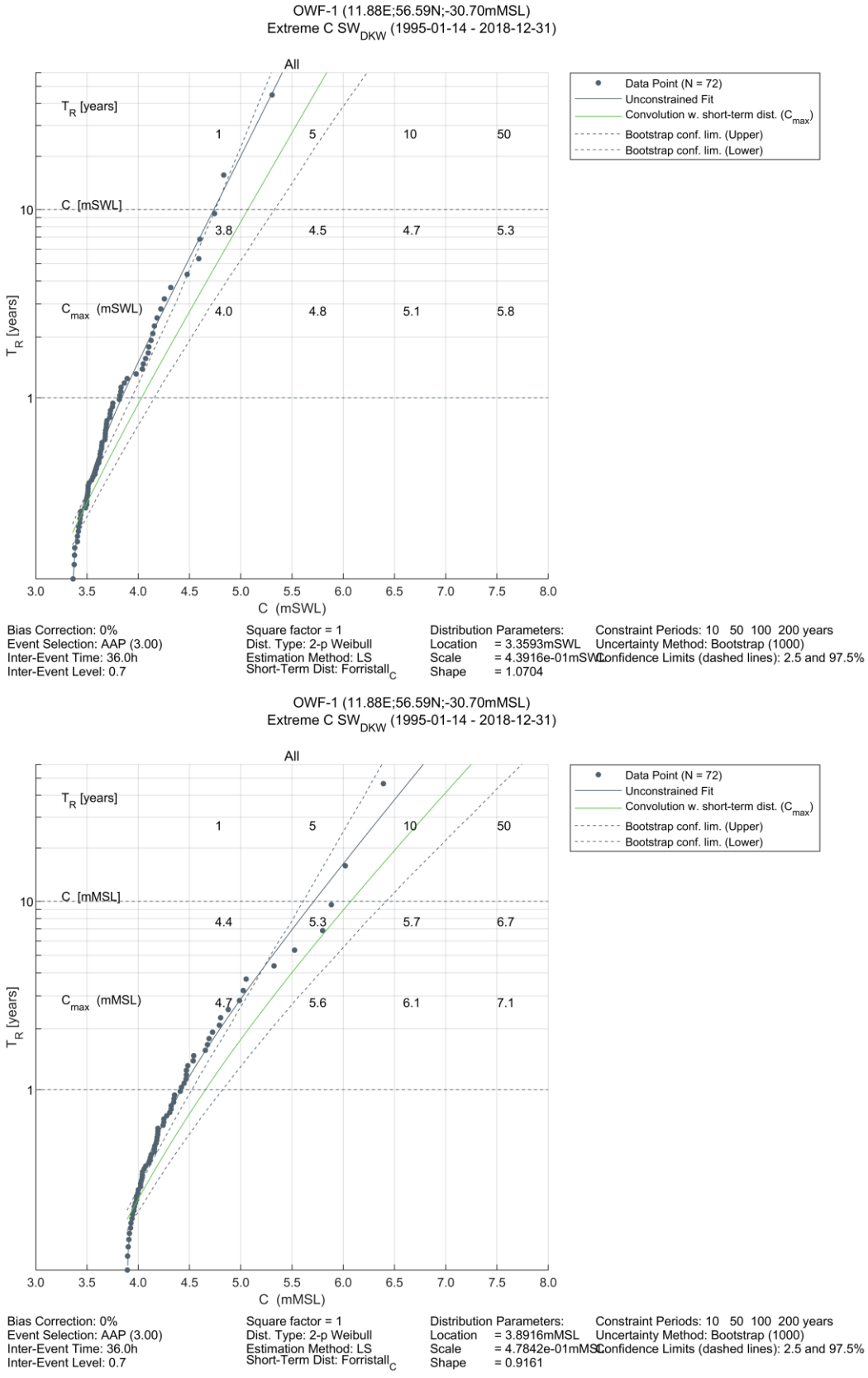

Figure 6.25 Extreme omnidirectional wave crest elevation at OWF-1

Long-term extreme values according to a 2-parameter Weibull distribution fitted to an average of 3 annual peak (λ=3) individual wave crests, C, convoluted with short term distribution (C_{max}). The upper panel shows crest elevations relative to still water level ($C_{max,SWL}$), and lower panel shows crest elevations relative to mean-sea-level ($C_{max,MSL}$). The dashed grey lines show the upper (97.5%) and lower (2.5%) confidence limits

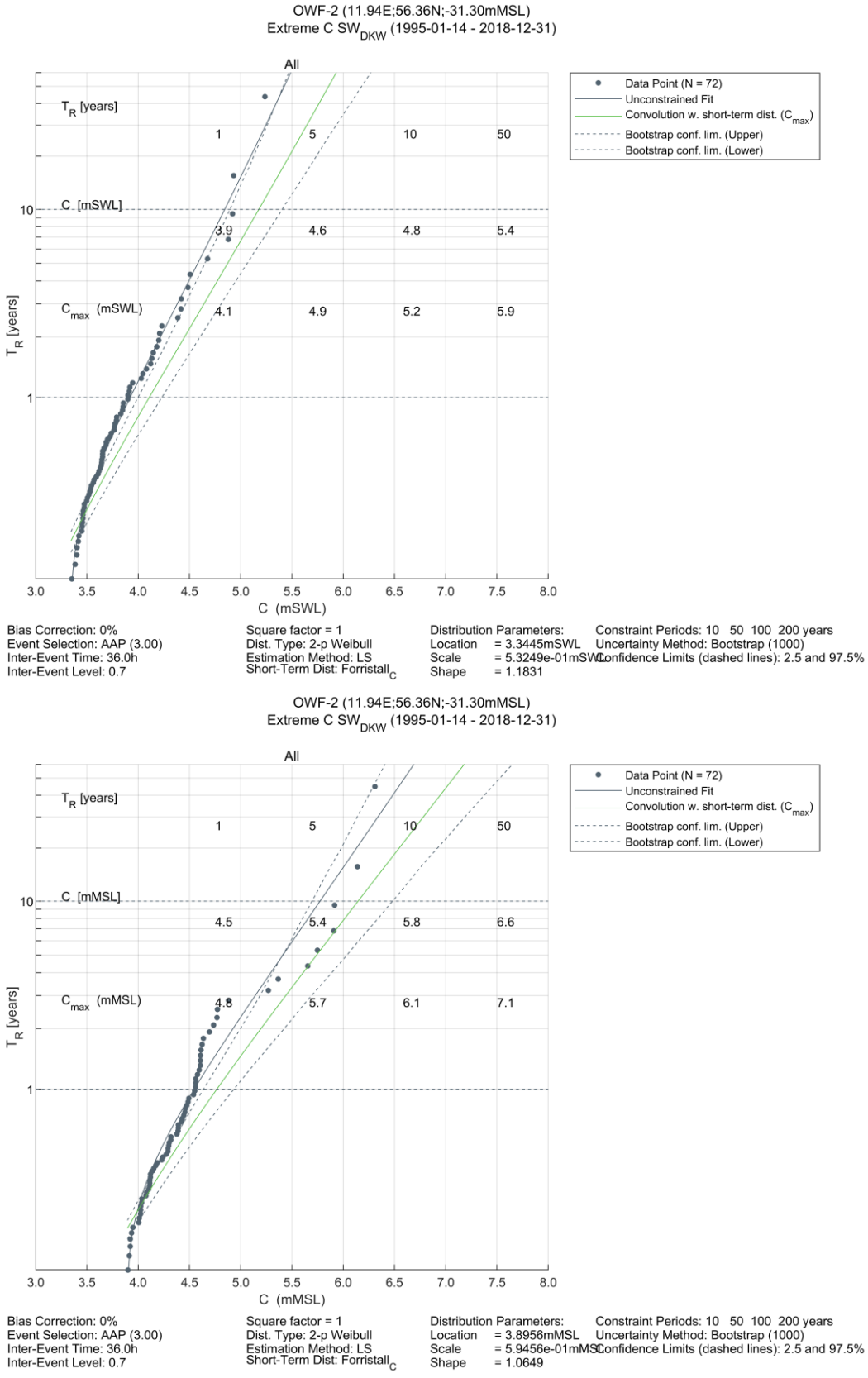

Figure 6.26 Extreme omnidirectional wave crest elevation at OWF-2

Long-term extreme values according to a 2-parameter Weibull distribution fitted to an average of 3 annual peak (λ=3) individual wave crests, C, convoluted with short term distribution (C_{max}). The upper panel shows crest elevations relative to still water level ($C_{max,SWL}$), and lower panel shows crest elevations relative to mean-sea-level ($C_{max,MSL}$). The dashed grey lines show the upper (97.5%) and lower (2.5%) confidence limits

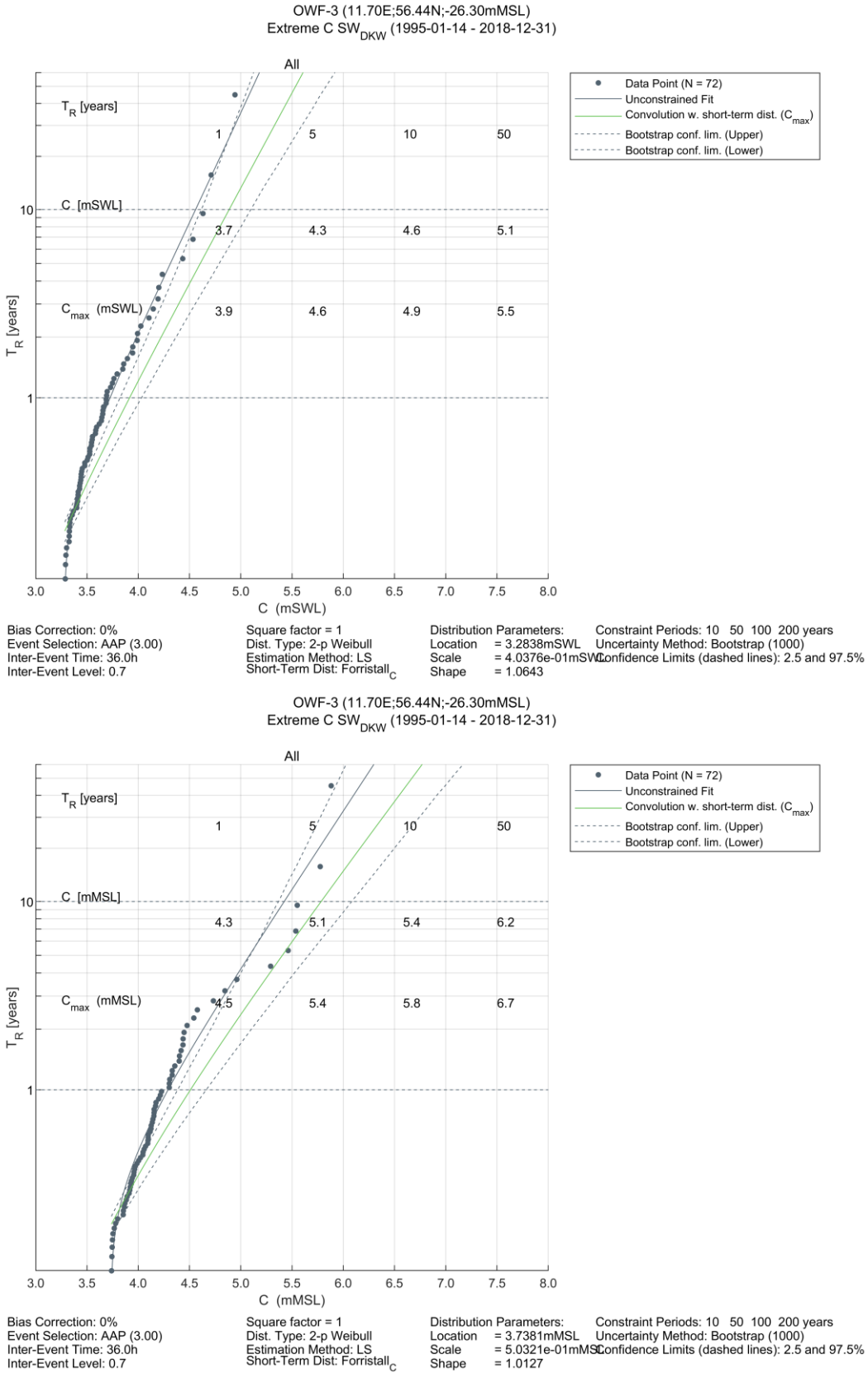

Figure 6.27 Extreme omnidirectional wave crest elevation at OWF-3

Long-term extreme values according to a 2-parameter Weibull distribution fitted to an average of 3 annual peak (λ=3) individual wave crests, *C*, convoluted with short term distribution (C_{max}). The upper panel shows crest elevations relative to still water level ($C_{max,SWL}$), and lower panel shows crest elevations relative to mean-sea-level ($C_{max,MSL}$). The dashed grey lines show the upper (97.5%) and lower (2.5%) confidence limits

7 Other Environmental Conditions

This section summarises an assessment of environmental conditions at the Hesselø OWF. This includes annual and monthly statistics relating to the properties of air and seawater, and information on marine growth.

Information on the properties of air and seawater, and marine growth, are all required to support the design of turbines and their related structures. These "other metocean conditions" can affect the integrity and safety of an offshore structure by thermal, chemical, and corrosive mechanical actions (or a combination of all these factors). In this section, information relating to several of these conditions are summarised based on a series of model data sets and information available in relevant industry guidance.

7.1 Atmospheric properties

Long-term information on the atmospheric properties at the Hesselø OWF site were determined from ~24 years (1995 to 2018, inclusive) of CREA6 model data (see Section 2.3.1), with a temporal resolution of 1 hour.

The atmospheric properties presented in this section relate to the wind model used as input to hydrodynamic and spectral wave models. The reader is referred to the Hesselø Offshore Wind Farm Site Wind Condition Assessment [3] for reference to the recommended values for be used for FEED.

7.1.1 Air temperature

Figure 7.1 present the monthly statistics (mean, minimum, maximum, and standard deviation) of air temperature at 2 mMSL at analysis point OWF-1. The statistics are summarised for all analysis points in Table 7.1.

The highest temperatures (mean and maximum) are associated with the months of June through to September, while the lowest temperatures (mean and minimum) occur from December to March.

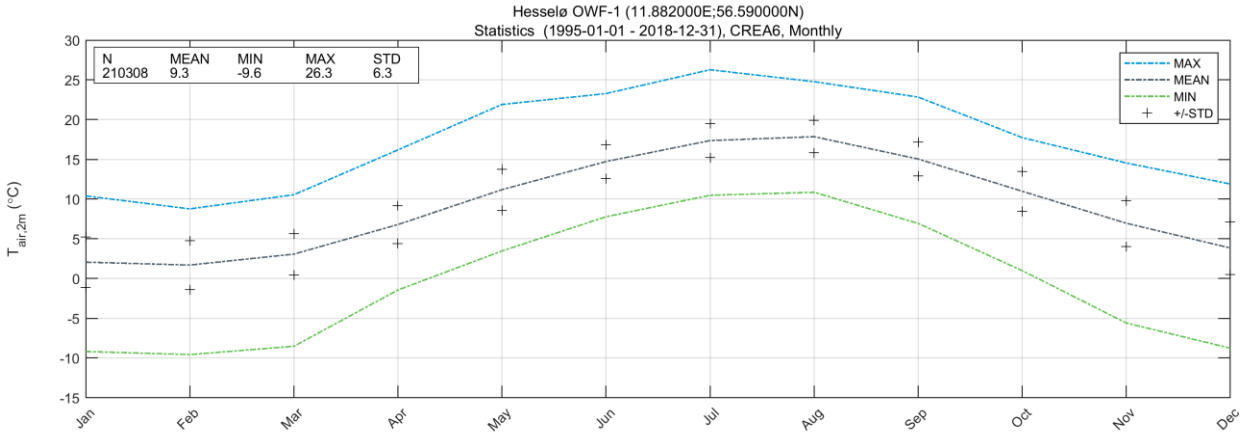

Figure 7.1 Monthly statistics of air temperature at analysis point OWF-1
Mean, minimum, maximum, and standard deviation of CREA6 model air temperature at 2 mMSL (1995-01-01 to 2018-12-31)

Table 7.1 All-year and monthly statistics of air temperature for Hesselø OWF

Mean, minimum, maximum, and standard deviation of CREA6 model air temperature at 2 mMSL (1995-01-01 to 2018-12-31)

Month	OWF-1				OWF-2				OWF-3			
	Mean [°C]	Min. [°C]	Max. [°C]	STD [°C]	Mean [°C]	Min. [°C]	Max. [°C]	STD [°C]	Mean [°C]	Min. [°C]	Max. [°C]	STD [°C]
All-year	9.3	-9.6	26.3	6.3	9.4	-9.1	26.9	6.3	9.4	-8.9	26.7	6.3
Jan	2.1	-9.2	10.4	3.2	2.1	-8.5	10.4	3.1	2.2	-8.3	10.4	3.1
Feb	1.7	-9.6	8.8	3.1	1.7	-9.1	8.8	3.1	1.8	-8.9	8.9	3.0
Mar	3.1	-8.5	10.6	2.6	3.1	-7.6	11.2	2.6	3.1	-7.9	11.3	2.5
Apr	6.8	-1.4	16.2	2.4	6.9	-1.2	16.8	2.4	6.8	-1.1	16.3	2.4
May	11.2	3.5	21.9	2.6	11.3	3.8	21.8	2.6	11.2	3.4	21.5	2.6
Jun	14.7	7.8	23.3	2.1	14.8	8.4	23.7	2.2	14.7	8.0	23.3	2.1
Jul	17.4	10.5	26.3	2.2	17.4	10.0	26.9	2.2	17.4	9.9	26.7	2.2
Aug	17.9	10.9	24.8	2.1	17.9	11.2	25.0	2.1	17.9	11.5	25.1	2.1
Sep	15.0	6.9	22.8	2.1	15.1	7.9	23.1	2.1	15.1	7.8	23.0	2.1
Oct	11.0	1.0	17.7	2.5	11.0	1.3	18.0	2.5	11.1	1.5	18.0	2.4
Nov	7.0	-5.6	14.6	2.9	7.0	-5.0	14.8	2.8	7.0	-5.1	14.9	2.8
Dec	3.8	-8.8	11.9	3.3	3.9	-8.4	12.1	3.2	3.9	-8.5	12.0	3.2

7.1.2 Relative humidity

Figure 7.2 present the monthly statistics (mean, minimum, maximum, and standard deviation) of relative humidity at analysis point OWF-1. The statistics are summarised for all analysis points in Table 7.2.

A small seasonal variation can be seen for the statistical mean as the relative humidity is highest during winter and lowest during summer.

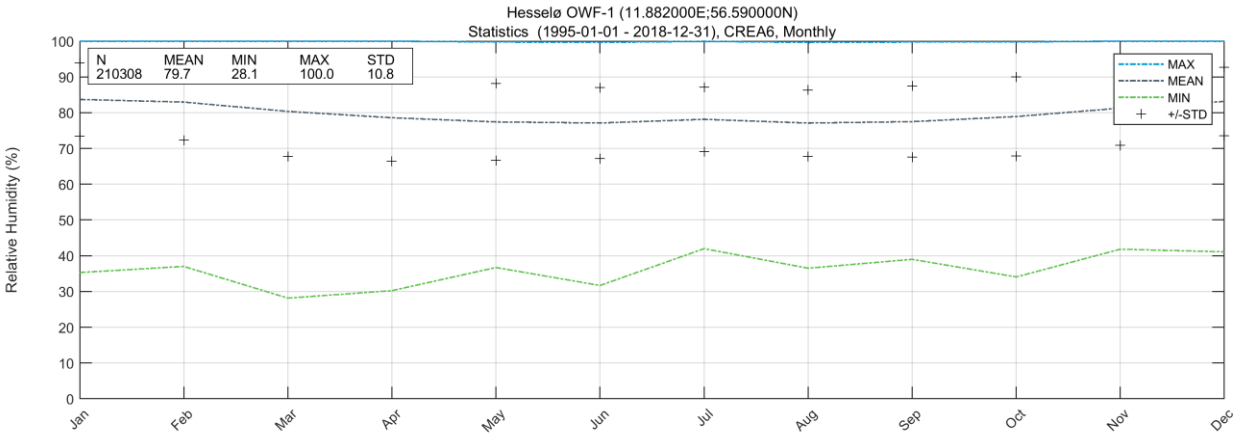

Figure 7.2 Monthly statistics of relative humidity at analysis point OWF-1
Mean, minimum, maximum, and standard deviation of CREA6 model relative humidity (1995-01-01 to 2018-12-31)

Table 7.2 All-year and monthly statistics of relative humidity for Hesselø OWF

Mean, minimum, maximum, and standard deviation of CREA6 model relative humidity (1995-01-01 to 2018-12-31)

Month	OWF-1				OWF-2				OWF-3			
	Mean [%]	Min. [%]	Max. [%]	STD [%]	Mean [%]	Min. [%]	Max. [%]	STD [%]	Mean [%]	Min. [%]	Max. [%]	STD [%]
All-year	79.7	28.1	100.0	10.8	79.7	26.6	100.0	10.8	79.7	27.6	100.0	79.7
Jan	83.7	35.3	100.0	10.3	83.8	35.0	100.0	10.2	83.7	35.1	100.0	83.7
Feb	83.0	37.0	100.0	10.7	83.2	39.1	100.0	10.7	83.0	35.6	100.0	83.0
Mar	80.4	28.1	100.0	12.6	80.4	26.6	100.0	12.5	80.4	27.6	100.0	80.4
Apr	78.6	30.2	100.0	12.2	78.5	32.2	100.0	12.1	78.7	33.0	100.0	78.7
May	77.4	36.7	99.8	10.8	77.3	31.5	99.8	10.9	77.5	33.0	99.8	77.5
Jun	77.1	31.7	99.7	10.0	77.0	31.9	99.7	9.9	77.1	31.6	99.7	77.1
Jul	78.1	42.0	99.7	9.1	78.0	44.7	99.9	9.1	78.2	40.2	100.0	78.2
Aug	77.1	36.5	99.9	9.3	76.9	45.1	99.7	9.4	77.2	43.2	99.7	77.2
Sep	77.5	39.0	99.6	10.0	77.3	39.3	99.7	10.1	77.5	37.0	99.8	77.5
Oct	78.9	34.1	99.8	11.1	79.1	32.5	99.8	11.0	79.1	35.4	99.8	79.1
Nov	81.3	41.8	100.0	10.4	81.6	40.5	100.0	10.4	81.4	40.9	100.0	81.4
Dec	83.1	41.1	100.0	9.6	83.4	40.7	100.0	9.6	83.2	39.0	100.0	83.2

7.2 Water properties

Long-term information on the properties on seawater (temperature and salinity) were obtained from the Baltic Sea physical reanalysis model (see Section 2.4). Time series of seawater temperature and seawater salinity were extracted for the sea surface layer and near bed layer at a single location in the centre of the Hesselø OWF area (11.8471°E; 56.4582°N). The data cover a ~24-year period (1995 to 2018, inclusive) with a temporal resolution of 1-day.

7.2.1 Seawater temperature

Figure 7.3 present the monthly statistics (mean, minimum, maximum, and standard deviation) of sea surface and seafloor temperature at the Hesselø OWF. The statistics are summarised for in Table 7.3.

The seasonal variation in seawater temperature is clear at the surface with largest temperatures occurring in summer and early autumn (June to September), and the lowest temperatures during the winter and early spring (January to March). The monthly mean seawater temperatures at the surface are higher than those at the seabed for half the year (April to September, inclusive).

The seasonal variation at the seabed is also clear but less pronounced. The highest temperatures occur during autumn and the lowest in spring, showing the delay in temperature changes over the depth.

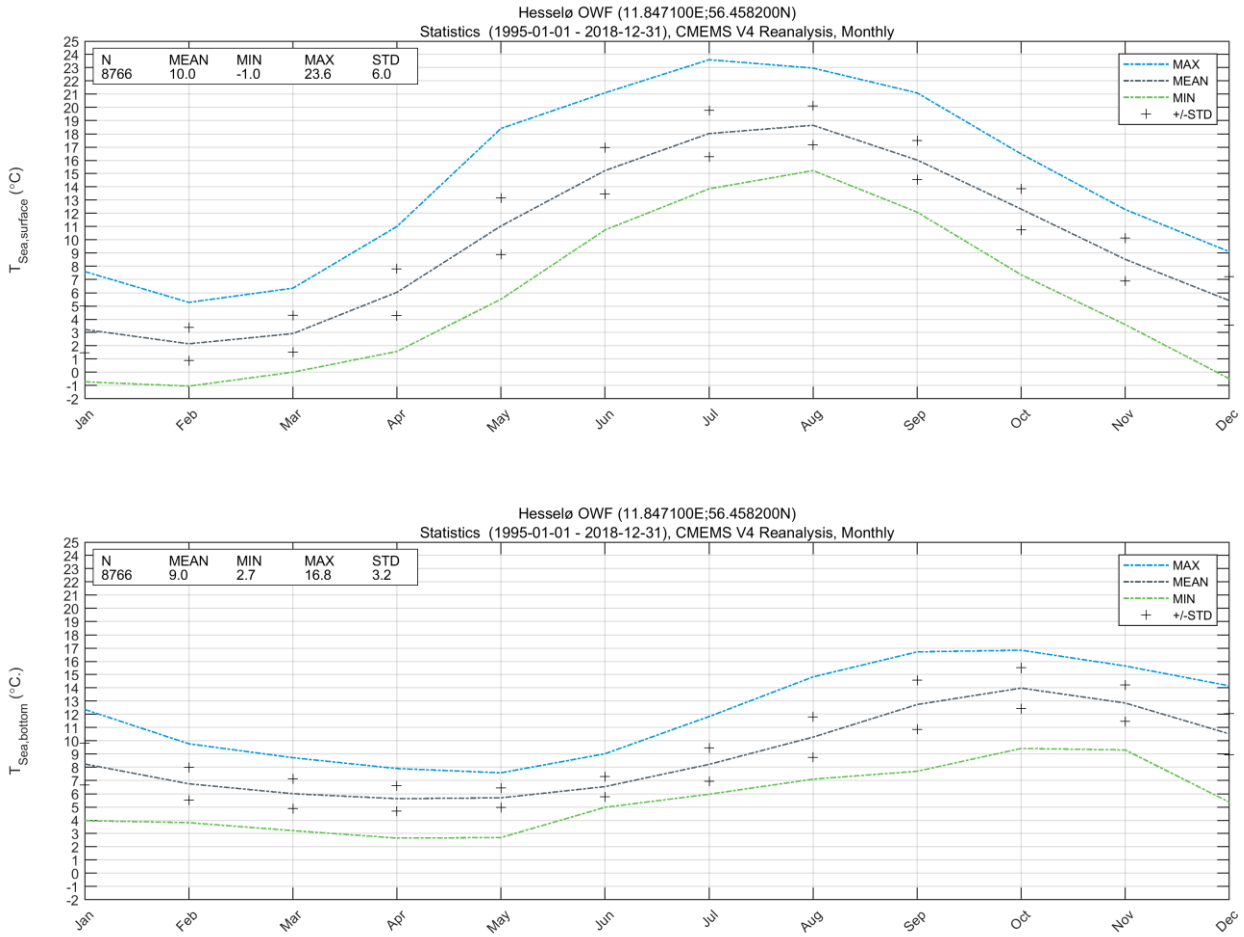

Figure 7.3 Monthly statistics of temperature at sea surface (upper panel) and seafloor (lower panel) at the Hesselø OWF

Mean, minimum, maximum, and standard deviation of seawater temperatures from CMEMS Baltic Sea physical reanalysis model (1995-01-01 to 2018-12-31)

Table 7.3 All-year and monthly statistics of temperature at sea surface and seafloor at the Hesselø OWF.
Mean, minimum, maximum, and standard deviation of seawater temperatures from CMEMS Baltic Sea physical reanalysis model (1995-01-01 to 2018-12-31)

Month	$T_{Sea,Surface}$				$T_{Sea\_seafloor}$			
	Mean [°C]	Min. [°C]	Max. [°C]	STD [°C]	Mean [°C]	Min. [°C]	Max. [°C]	STD [°C]
All-year	10.0	-1.0	23.6	6.0	9.0	2.7	16.8	3.2
Jan	3.2	-0.7	7.6	1.7	8.3	4.0	12.4	1.6
Feb	2.2	-1.0	5.3	1.2	6.8	3.8	9.8	1.3
Mar	2.9	0.0	6.4	1.4	6.0	3.2	8.7	1.1
Apr	6.0	1.6	11.0	1.8	5.6	2.7	7.9	1.0
May	11.0	5.5	18.4	2.1	5.7	2.7	7.6	0.7
Jun	15.2	10.7	21.1	1.7	6.5	5.0	9.0	0.8
Jul	18.0	13.9	23.6	1.8	8.2	6.0	11.8	1.3
Aug	18.6	15.2	23.0	1.5	10.3	7.1	14.8	1.5
Sep	16.0	12.1	21.1	1.4	12.7	7.7	16.7	1.9
Oct	12.3	7.4	16.5	1.6	14.0	9.4	16.8	1.5
Nov	8.5	3.6	12.3	1.6	12.9	9.3	15.7	1.4
Dec	5.4	-0.5	9.1	1.8	10.5	5.4	14.2	1.6

7.2.2 Seawater salinity

Figure 7.4 present the monthly statistics (mean, minimum, maximum, and standard deviation) of sea surface and seafloor salinity at the Hesselø OWF. The statistics are summarised in Table 7.4.

The seasonal variation in seawater salinity is clear at the surface with highest salinity occurring in winter (January and December) and the lowest salinity during early summer (May to July).

There is little seasonal variation at close to the seafloor, with the salinity being slightly higher in the summer. The mean salinity at the seafloor is larger than the maximum salinity at the surface.

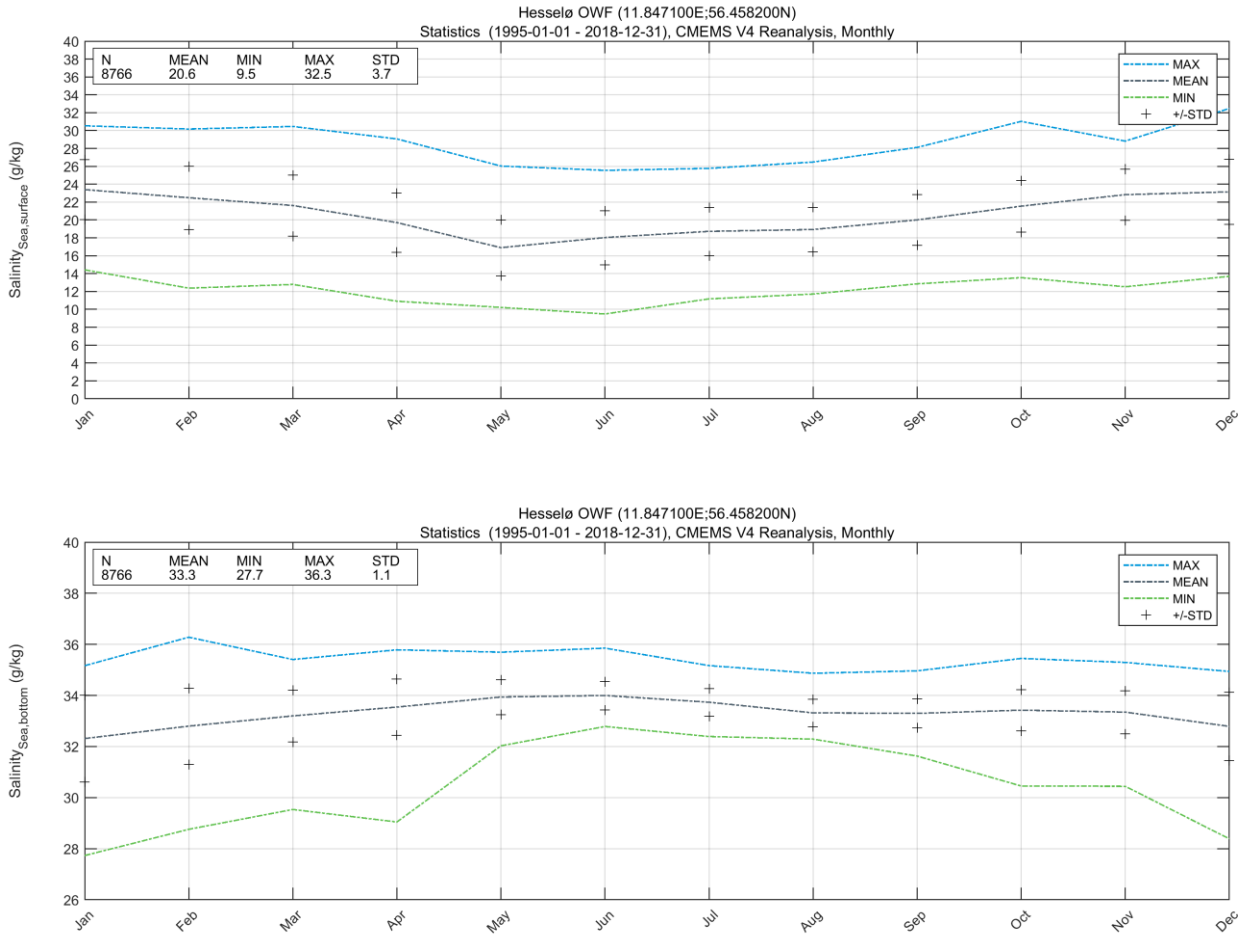

Figure 7.4 Monthly statistics of salinity at sea surface (upper panel) and seafloor (lower panel) at the Hesselø OWF

Mean, minimum, maximum, and standard deviation of seawater salinity from CMEMS Baltic Sea physical reanalysis model (1995-01-01 to 2018-12-31)

Table 7.4 All-year and monthly statistics of salinity at sea surface and seafloor at the Hesselø OWF.
Mean, minimum, maximum, and standard deviation of seawater salinity from CMEMS' Baltic Sea physical reanalysis model (1995-01-01 to 2018-12-31)

Month	Sea surface salinity				Sea bottom salinity			
	Mean [g/kg]	Min. [g/kg]	Max. [g/kg]	STD [g/kg]	Mean [g/kg]	Min. [g/kg]	Max. [g/kg]	STD [g/kg]
All-year	20.6	9.5	32.5	3.7	33.3	27.7	36.3	1.1
Jan	23.4	14.4	30.5	3.3	32.3	27.7	35.2	1.7
Feb	22.5	12.4	30.2	3.5	32.8	28.8	36.3	1.5
Mar	21.6	12.8	30.5	3.4	33.2	29.5	35.4	1.0
Apr	19.7	10.9	29.1	3.3	33.5	29.0	35.8	1.1
May	16.9	10.2	26.0	3.1	33.9	32.0	35.7	0.7
Jun	18.0	9.5	25.6	3.0	34.0	32.8	35.9	0.6
Jul	18.7	11.2	25.8	2.7	33.7	32.4	35.2	0.5
Aug	18.9	11.7	26.5	2.5	33.3	32.3	34.9	0.5
Sep	20.0	12.9	28.1	2.8	33.3	31.6	35.0	0.6
Oct	21.5	13.5	31.0	2.9	33.4	30.5	35.4	0.8
Nov	22.8	12.5	28.8	2.9	33.4	30.4	35.3	0.8
Dec	23.1	13.7	32.5	3.6	32.8	28.4	34.9	1.3

7.2.3 Seawater Density

The density of seawater [kgm^{-3}] was calculated using the standard Thermodynamic Equation of Seawater (TEOS-10) via the GSW Toolbox using the Gibbs function [31] and based on the daily modelled seawater temperature and seawater salinity from the CMEMS' Baltic Sea physical reanalysis model.

Figure 7.5 present the monthly statistics (mean, minimum, maximum, and standard deviation) of sea surface and seafloor water density at the Hesselø OWF. The statistics are summarised in Table 7.5.

The seasonal variation in seawater density is clear at the surface with the largest density occurring in winter (December to March) and the lowest salinity seen during summer (May to August).

There is little seasonal variation in seawater density at the seafloor.

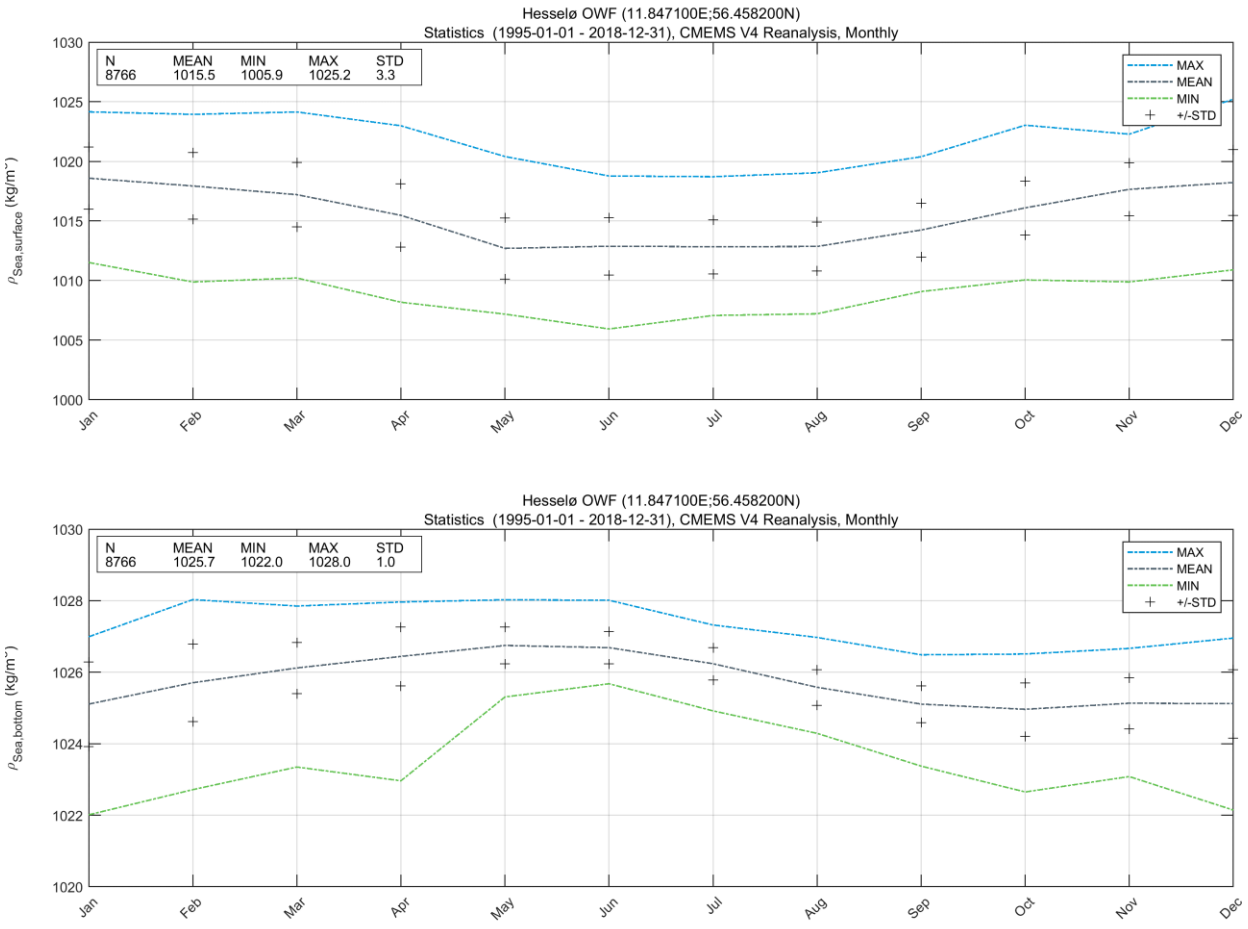

Figure 7.5 Monthly statistics of water density at sea surface (upper panel) and seafloor (lower panel) at Hesselø OWF

Mean, minimum, maximum, and standard deviation of seawater density calculated from CMEMS Baltic Sea physical reanalysis model data (1995-01-01 to 2018-12-31)

Table 7.5 All-year and monthly statistics of water density at sea surface and seafloor at the Hesselø OWF.
Mean, minimum, maximum, and standard deviation of seawater density calculated from CMEMS Baltic Sea physical reanalysis model data (1995-01-01 to 2018-12-31)

Month	Sea surface density				Sea bottom density			
	Mean [kg/m^3]	Min. [kg/m^3]	Max. [kg/m^3]	STD [kg/m^3]	Mean [kg/m^3]	Min. [kg/m^3]	Max. [kg/m^3]	STD [kg/m^3]
All-year	1015.5	1005.9	1025.2	3.3	1025.7	1022.0	1028.0	1.0
Jan	1018.6	1011.5	1024.2	2.6	1025.1	1022.0	1027.0	1.2
Feb	1017.9	1009.9	1023.9	2.8	1025.7	1022.0	1028.0	1.1
Mar	1017.2	1010.2	1024.1	2.7	1026.1	1023.3	1027.9	0.7
Apr	1015.5	1008.2	1023.0	2.7	1026.4	1023.0	1028.0	0.8
May	1012.7	1007.2	1020.4	2.6	1026.7	1025.3	1028.0	0.5
Jun	1012.9	1005.9	1018.8	2.4	1026.7	1025.7	1028.3	0.4
Jul	1012.8	1007.1	1018.7	2.3	1026.2	1024.9	1027.3	0.4
Aug	1012.9	1007.2	1019.0	2.1	1025.6	1024.3	1027.0	0.5
Sep	1014.2	1009.1	1020.4	2.2	1025.1	1023.4	1026.5	0.5
Oct	1016.1	1010.1	1023.0	2.3	1025.0	1022.7	1026.5	0.7
Nov	1017.7	1009.9	1022.3	2.2	1025.1	1023.1	1026.7	0.7
Dec	1018.2	1010.9	1025.2	2.8	1025.1	1022.1	1027.0	1.0

7.3 Marine growth

Marine growth includes the plants, animals, and bacteria, that form on structural components in seawater and in the splash zone. As well as adding weight to structural components, marine growth influences the geometry and roughness, with consequences for hydrodynamic loading, dynamic response, accessibility, and corrosion rates.

Specific guidance on marine growth in the Baltic Sea is provided in Section 2.4.11 of [25], which states that, unless data indicate otherwise, marine growth thickness of 100 mm should be considered from the seafloor to 2 m above mean sea level.

8 Conclusion

The aim of the report is to provide metocean data and analysis to serve as the basis for the Front-End Engineering Design (FEED) of offshore wind turbines and related project infrastructure at the Hesselø offshore wind farm.

Operational and extreme metocean criteria have been derived at three locations within the project area based on DHI's Danish Waters hindcast model database. This database provides long-term information on wind conditions, water levels, depth-averaged currents, and waves at hourly intervals over a period of 24-years (1995 – 2018, inclusive). The model database was validated at different measurement stations. Wind conditions, water levels, and waves showed that the model performs well compared to measurements. These results provided confidence in the quality of the data used for Hesselø OWF project area. DHI did not include any specific conservatism in the analyses as the data quality was judged to be suitable accurate and reliable basis for FEED design.

The currents conditions at the Hesselø OWF are governed by complex and seasonally varying exchanges of water masses between the Baltic Sea and North Sea. The depth-averaged representation of the hydrodynamics provided by the two-dimensional flow model does not describe the possible stratification of the water column. If the currents and a possible stratification are critical for more detailed structural design within the Hesselø OWF then analysis based on a three-dimensional hydrodynamic model coupled with long-term measurements should be considered.

Beyond FEED design, it is recommended to perform high resolution modelling at the wind farm site using local bathymetry data to lower the uncertainties for more detailed design. The model should be validated against long-term measurements with sufficient duration to capture the expected annual variability in conditions, including several storms events from various directions. In addition, it is recommended to apply more sophisticated extreme value analyses methodologies (and preferably non-stationary methods) to lower conservativism and reduce uncertainties for extreme values (i.e., for return period above 100-years).

Ahead of detailed design, DHI recommends that the below tasks are performed to meet certification criteria and provide more accurate metocean data to be used:

- Application of a validated 3D hydrodynamic model data to characterise the current conditions through the water column
- High resolution modelling of wave conditions is recommended. This will help to resolve the bathymetric features and reduce uncertainties. The wave model should include the effects of water level and currents. The forcing of the high-resolution model should be with spectral data or a validated model of the Kattegat (preferably using the CREA6 wind fields for consistency).
- DHI recommends that non-stationary extreme value analyses are performed to provide monthly and directional extreme values as well as accurate joint probabilities (see Section 9 of [32] as an example of such a method).

9 References

[1] Danish Ministry of Climate, Energy, and Utilities, “Energy Agreement,” 29 06 2018. [Online]. Available: https://en.kefm.dk/Media/C/5/Energy%20Agreement%202018%20a-webtilg%c3%a6ngelig.pdf. [Accessed 03 2022].

[2] Danish Ministry for Climate, Energy and Utilities, “Danish Climate Agreement for Energy and Industry 2020 – Overview,” 22 06 2020. [Online]. Available: https://en.kefm.dk/Media/C/B/faktaark-klimaaftale%20(English%20august%2014).pdf. [Accessed 03 2022].

[3] EMD International A/S, “Hesselø Offshore Wind Farm - Site Wind Conditions Assessment, Doc. no. 220114_21198_A_TS_1,” 24 February 2022.

[4] Fugro, “Geophysical Results Report, Energinet Denmark Hesselø Geophysical Survey, Denmark, Inner Danish Sea, F172145-REP-GEOP-001 02,” 13 08 2021. [Online]. Available: https://ens.dk/sites/ens.dk/files/Vindenergi/301_geophysical_survey_report.pdf. [Accessed 03 2022].

[5] DMI, “About meteorological observations,” 10 05 2021. [Online]. Available: https://confluence.govcloud.dk/display/FDAPI/About+meteorological+observations. [Accessed 03 2022].

[6] Energinet Eltransmission A/S, “Scope of Services Site Metocean Conditions Assessment, Hesselø offshore wind farm, 800-1200 MW, 21/07546-1,” October 2021.

[7] Tech Wise, “Wind Resources at Laesoe Syd, Report no.: D-160 950,” December 2002.

[8] Eolos, “Hesselø Measurement Plan, EIL-HSS07, Revision 05, 17 Febraury 2022”.

[9] DHI, “Anholt Offshore Wind Farm, Metocean Data for Design and Operational Conditions, Addendum: Validation of Wave and Flow Models against Measurements during the Spring of 2010, Report for Energinet.dk, revision Final 1.0,” August 2010.

[10] Teledyne RD Instruments, “Acousitc Doppler Current Profiler, Principles of Operations, A Practical Primer (P/N 951-6069-00),” 2011.

[11] DHI, “Measurement of currents and waves at four potential wind farm sites in inner Danish water, Measurement programme and results, Report for Energinet.dk, revision Final,” May 2014.

[12] DHI, “Wave and Water Level Hindcast of Danish Waters - Spectral wave and hydrodynamic modelling,” 05 2019. [Online]. Available: https://www.metocean-on-demand.com/fileshare/getfile.ashx?type=document&file_name=110910

04_Wave_and_Water_Level_Hindcast_of_Danish_Waters_08May2019.pdf. [Accessed 03 2022].

[13] C. Bollmeyer, J. D. Keller, C. Ohlwein, S. Wahl, S. Crewell, P. Friederichs, A. Hense, J. Keune, S. Kneifel, I. Pscheidt, S. Redl and S. Steinke, “Towards a high-resolution regional reanalysis for the European CORDEX domain,” *Q. J. R. Meteorol. Soc.,* vol. 141, pp. 1-15, 2015.

[14] D. P. Dee, S. M. Uppala, A. J. Simmons, P. Berrisford, P. Poli, S. Kobayashi, U. Andrae, M. A. Balmaseda, G. Balsamo, P. Bauer, P. Bechtold, A. C. Beljaars, L. van de Berg, J. Bidlot and N. Bormann, “The ERA-Interim reanalysis: configuration and performance of the data assimilation system,” *Q. J. R. Meteorol. Soc. ,* vol. 137, pp. 553-597, 2011.

[15] DHI, “Thor Offshore Wind Farm, Metocean Hindcast Data and Validation Report, Revision Final 2.0,” 11 2019. [Online]. Available: https://ens.dk/sites/ens.dk/files/Vindenergi/1_thor_owf_metocean_report.pdf. [Accessed 03 2022].

[16] IEC, “Wind energy generation systems - Part 3-1: Design requirements for fixed offshore wind turbines,” IEC 61400-3-1:2019.

[17] DHI, “MIKE 21 & MIKE 3 Flow Model FM. Hydrodynamic and Transport Module - Scientific Documentation,” 2021. [Online]. Available: https://manuals.mikepoweredbydhi.help//2021/Coast_and_Sea/MIKE_21_Flow_FM_Scientific_Doc.pdf. [Accessed 03 2022].

[18] DHI, “MIKE 21 Spectral Waves FM, Spectral Wave Module, User Guide,” 2021. [Online]. Available: https://manuals.mikepoweredbydhi.help//2021/Coast_and_Sea/MIKE21SW.pdf. [Accessed 03 2022].

[19] DHI, “MIKE 21, Spectral Waves Module, Scientific Documentation,” 2021. [Online]. Available: https://manuals.mikepoweredbydhi.help/2021/Coast_and_Sea/M21SW_Scientific_Doc.pdf. [Accessed 03 2022].

[20] Copernicus Marine Service, “Product user manual for Baltic Sea Physical Reanalysis Product, BALTICSEA_REANALYSIS_PHY_003_001, issue 2.1,” November 2021. [Online]. Available: https://catalogue.marine.copernicus.eu/documents/PUM/CMEMS-BAL-PUM-003-011.pdf. [Accessed 03 2022].

[21] CMEMS, “Quality Informaiton Document, Baltic Sea Production Centre, BALTICSEA_REANALYSIS_PHY_003_011,” 29 11 2019. [Online]. Available: https://catalogue.marine.copernicus.eu/documents/QUID/CMEMS-BAL-QUID-003-011.pdf. [Accessed 03 2022].

[22] D. L. Codiga, “Unified Tidal Analysis and Prediction Using the UTide Matlab Functions. Technical Report 2011-01,” Graduate School of Oceanography, University of Rhode Island, Narragansett, RI. 59pp, 2011.

[23] R. Pawlowicz, B. Beardsley and S. Lentz, “Classical tidal harmonic analysis including error estimates in MATLAB using T-TIDE,” *Computers & Geosciences 28,* pp. 929-937, 2002.

[24] IEC, “International Standard, Wind energy generation systems - Part 1: Design requirements. IEC 61400-1, ed. 4.0,” International Electrotechnical Commission, Geneva, Switzerland, 2019.

[25] DNV-GL, “Loads and site conditions for wind turbines, DNVGL-ST-0437, Edition 2016-11,” 2016.

[26] M. G. G. Foreman, J. Y. Cherniawsky and V. A. Ballantyne, “Versatile Harmonic Tidal Analysis: Improvements and Applications.,” *J. Atmos. Oceanic Tech. 26,* pp. 806-817. DOI: 810.1175/2008JTECHO1615.1171, 2009.

[27] K. E. Leffler and D. A. Jay, “Enhancing tidal harmonic analysis: Robust (hybrid L-1/L-2) solutions,” *Cont. Shelf Res. 29,* pp. 78-88. DOI: 10.1016/j.csr.2008.1004.1011, 2009.

[28] Tromans, P.S. and Vanderschuren, L., “Response Based Design Conditions in the North Sea: Application of a New Method,” in *Offshore Technology Conference Texas, USA May 1995.*, Texas, USA, 1995.

[29] G. Z. Forristall, “On the Statistical Distribution of Wave Heights in a Storm,” *Journal of Geophysical Research,* vol. 83, no. C5, pp. 2353-2358, 1978.

[30] G. Z. Forristall, “Wave Crest Distributions: Observations and Second-Order Theory,” *Journal of Geophysical Research,* vol. 30, no. 8, pp. 1931-1943, 2000.

[31] IOC, SCOR and IAPSO, “The international thermodynamic equation of seawater – 2010: Calculation and use of thermodynamic properties,” Intergovernmental Oceanographic Commission, Manuals and Guides No. 56, UNESCO (English), 196 pp., 2010.

[32] DHI, “Metocean desk study and database for Dutch Offshore Wind Farm Zones - Hollandse Kust (west),” RVO.nl, 2020.

[33] Ø. Hagen, “Estimation of long term extreme waves from storm statistics and initial distribution approach,” May 31 - June 5, 2009, Honolulu, Hawaii, USA, 2009.

Appendix A Definition of Model Quality Indices

To obtain an objective and quantitative measure of how well the model data compared to the observed data, a number of statistical parameters so-called quality indices (QI's) are calculated.

Prior to the comparisons, the model data are synchronised to the time stamps of the observations so that both time series had equal length and overlapping time stamps. For each valid observation, measured at time t, the corresponding model value is found using linear interpolation between the model time steps before and after t. Only observed values that had model values within ± the representative sampling or averaging period of the observations are included (e.g., for 10-min observed wind speeds measured every 10 min compared to modelled values every hour, only the observed value every hour is included in the comparison).

The comparisons of the synchronized observed and modelled data are illustrated in (some of) the following figures:

- Time series plot including general statistics
- Scatter plot including quantiles, QQ-fit and QI's (dots coloured according to the density)
- Histogram of occurrence vs. magnitude or direction
- Histogram of bias vs. magnitude
- Histogram of bias vs. direction
- Dual rose plot (overlapping roses)
- Peak event plot including joint (coinciding) individual peaks

The quality indices are described below, and their definitions are listed in Table A.1. Most of the quality indices are based on the entire dataset, and hence the quality indices should be considered averaged measures and may not be representative of the accuracy during rare conditions.

The MEAN represents the mean of modelled data, while the BIAS is the mean difference between the modelled and observed data. AME is the mean of the absolute difference, and RMSE is the root mean square of the difference. The MEAN, BIAS, AME and RMSE are given as absolute values and relative to the average of the observed data in percent in the scatter plot.

The scatter index (SI) is a non-dimensional measure of the difference calculated as the unbiased root-mean-square difference relative to the mean absolute value of the observations. In open water, an SI below 0.2 is usually considered a small difference (excellent agreement) for significant wave heights. In confined areas or during calm conditions, where mean significant wave heights are generally lower, a slightly higher SI may be acceptable (the definition of SI implies that it is negatively biased (lower) for time series with high mean values compared to time series with lower mean values (and same scatter/spreading), although it is normalised).

EV is the explained variation and measures the proportion [0 - 1] to which the model accounts for the variation (dispersion) of the observations.

The correlation coefficient (CC) is a non-dimensional measure reflecting the degree to which the variation of the first variable is reflected linearly in the variation of the second variable. A value close to 0 indicates very limited or no (linear) correlation between the two datasets, while a value close to 1 indicates a very high or perfect correlation. Typically, a CC above 0.9 is considered a high correlation (good agreement) for wave heights. It is noted that CC is 1 (or -1) for any two fully linearly correlated variables, even if they are not 1:1. However, the slope and intercept of the linear relation may be different from 1 and 0, respectively, despite CC of 1 (or -1).

The Q-Q line slope and intercept are found from a linear fit to the data quantiles in a least-squares sense. The lower and uppermost quantiles are not included on the fit. A regression line slope different from 1 may indicate a trend in the difference.

The peak ratio (PR) is the average of the Npeak highest model values divided by the average of the Npeak highest observations. The peaks are found individually for each dataset through the Peak-Over-Threshold (POT) method applying an average annual number of exceedances of 4 and an inter-event time of 36 hours. A general underestimation of the modelled peak events results in PR below 1, while an overestimation results in a PR above 1.

An example of a peak plot is shown in Figure A.1. 'X' represents the observed peaks (x-axis), while 'Y' represents the modelled peaks (y-axis), based on the POT methodology, both represented by circles ('o') in the plot. The joint (coinciding) peaks, defined as any X and Y peaks within ±36 hours of each other (i.e., less than or equal to the number of individual peaks), are represented by crosses ('x'). Hence, the joint peaks ('x') overlap with the individual peaks ('o') only if they occur at the same time exactly. Otherwise, the joint peaks ('x') represent an additional point in the plot, which may be associated with the observed and modelled individual peaks ('o') by searching in the respective X and Y-axis directions, see example in Figure A.1. It is seen that the 'X' peaks are often underneath the 1:1 line (orange), while the 'Y' peaks are often above the 1:1 line.

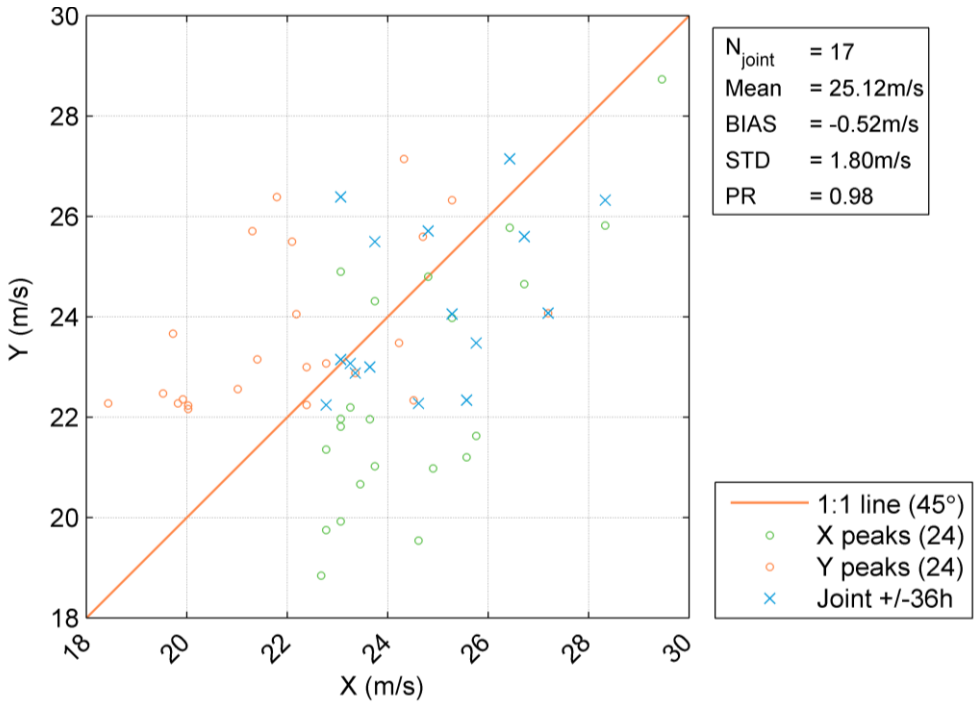

Figure A.1 Example of peak event plot (wind speed)

Table A.1 Definition of model quality indices (X = Observation, Y = Model)

Abbreviation	Description	Definition
N	Number of data (synchronized)	–
MEAN	Mean of Y data, Mean of X data	$\frac{1}{N}\sum_{i=1}^{N} Y_i \equiv \overline{Y}$, $\frac{1}{N}\sum_{i=1}^{N} X_i \equiv \overline{X}$
STD	Standard deviation of Y data Standard deviation of X data	$\sqrt{\frac{1}{N-1}\sum_{i=1}^{N}(Y-\overline{Y})^2}$, $\sqrt{\frac{1}{N-1}\sum_{i=1}^{N}(X-\overline{X})^2}$
BIAS	Mean difference	$\frac{1}{N}\sum_{i=1}^{N}(Y-X)_i = \overline{Y}-\overline{X}$
AME	Absolute mean difference	$\frac{1}{N}\sum_{i=1}^{N}(\lvert Y-X\rvert)_i$
RMSE	Root mean square error	$\sqrt{\frac{1}{N}\sum_{i=1}^{N}(Y-X)_i^{\,2}}$
SI	Scatter index (unbiased)	$\frac{\sqrt{\frac{1}{N}\sum_{i=1}^{N}(Y-X-\mathrm{BIAS})_i^{\,2}}}{\frac{1}{N}\sum_{i=1}^{N}\lvert X_i\rvert}$
EV	Explained variance	$\frac{\sum_{i=1}^{N}(X_i-\overline{X})^2-\sum_{i=1}^{N}[(X_i-\overline{X})-(Y_i-\overline{Y})]^2}{\sum_{i=1}^{N}(X_i-\overline{X})^2}$
CC	Correlation coefficient	$\frac{\sum_{i=1}^{N}(X_i-\overline{X})(Y_i-\overline{Y})}{\sqrt{\sum_{i=1}^{N}(X_i-\overline{X})^2\sum_{i=1}^{N}(Y_i-\overline{Y})^2}}$
QQ	Quantile-Quantile (line slope and intercept)	Linear least-squares fit to quantiles
PR	Peak ratio (of N_{peak} highest events)	$PR=\frac{\sum_{i=1}^{N_{peak}} Y_i}{\sum_{i=1}^{N_{peak}} X_i}$

Appendix B Validation DHI Danish Waters Metocean Hindcast Database

Appendix B.1 CREA6

Appendix B.1.1 Anholt Havn

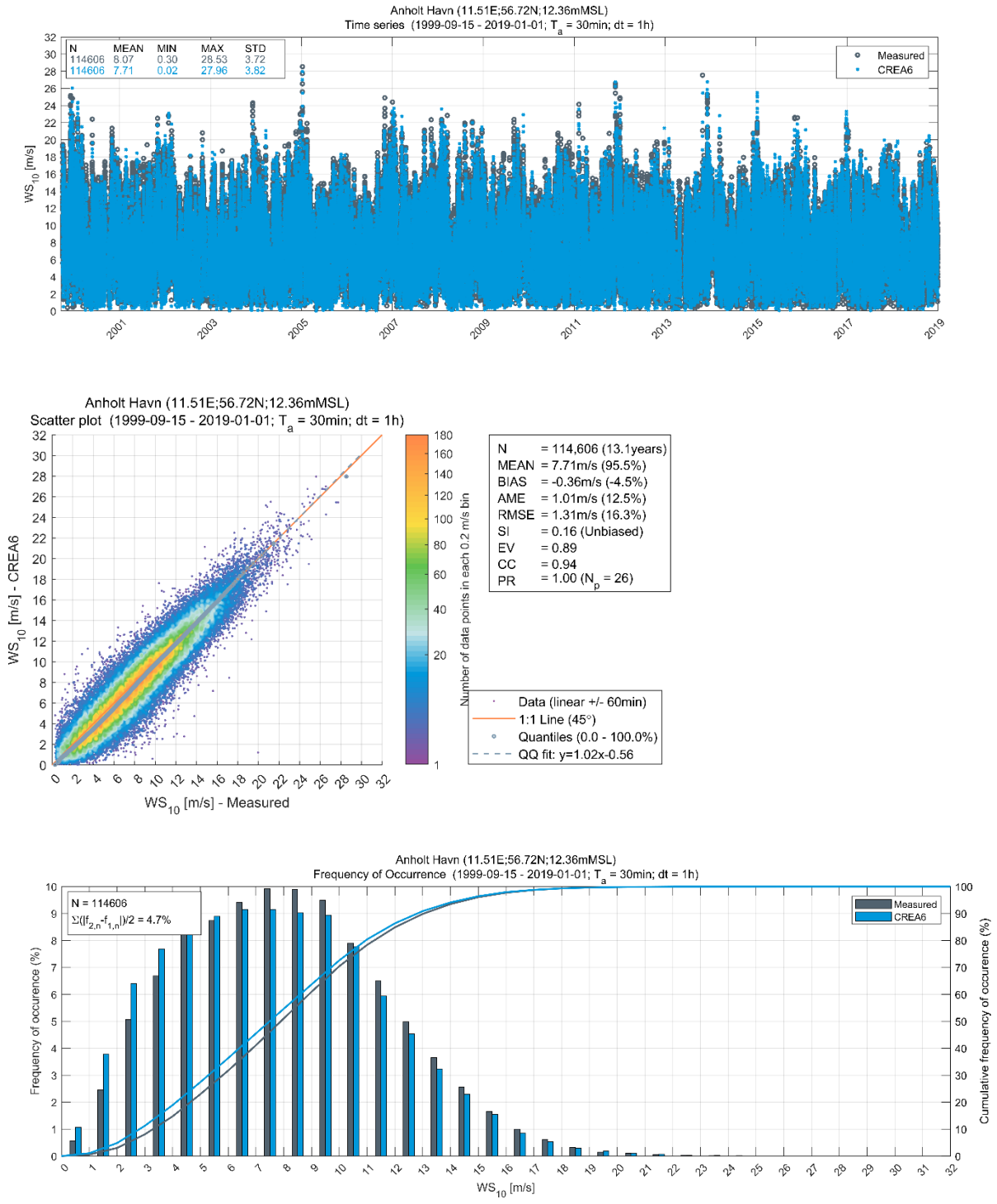

Figure B.01 Validation of CREA6 wind speeds at Anholt Havn (10 m)

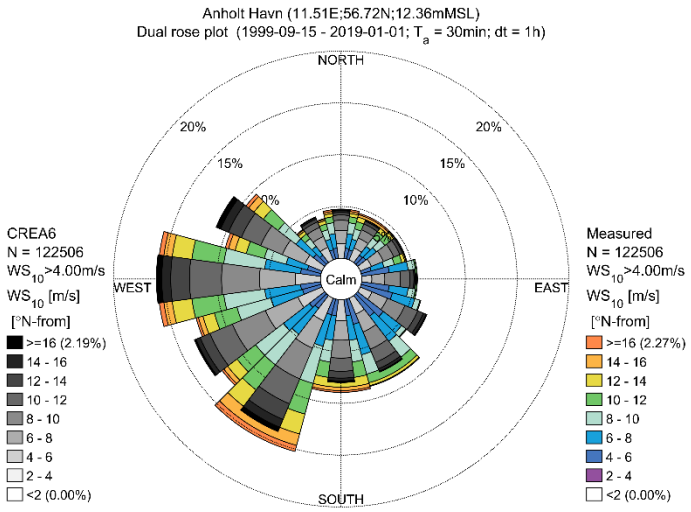

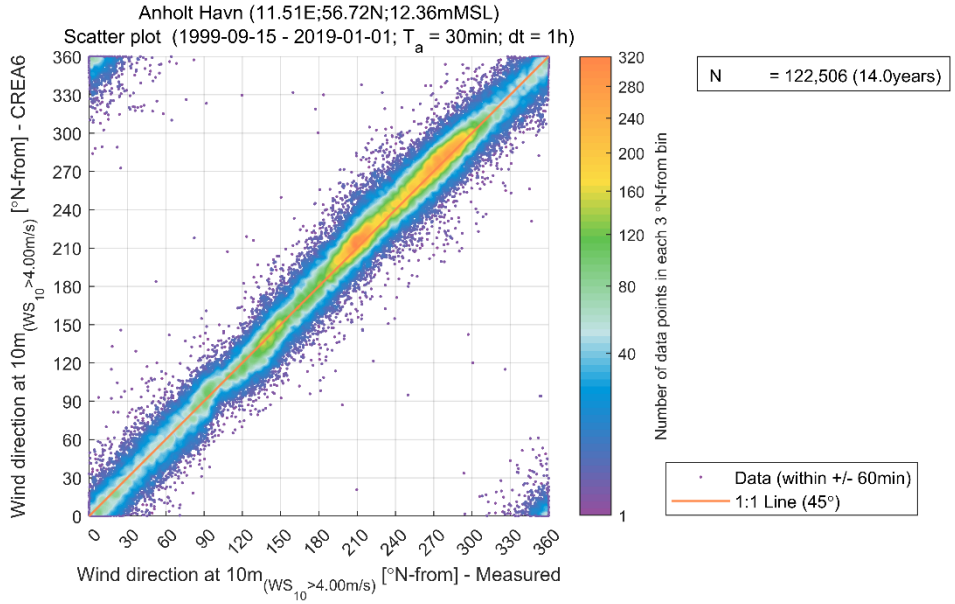

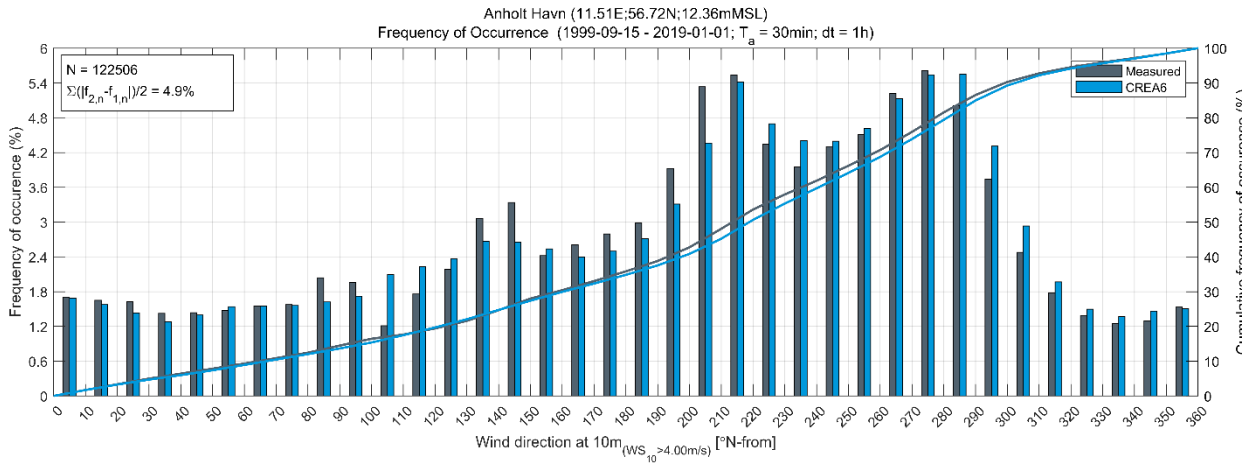

Figure B.02 Validation of CREA6 wind direction at Anholt Havn (10 m)

Appendix B.1.2 Gniben

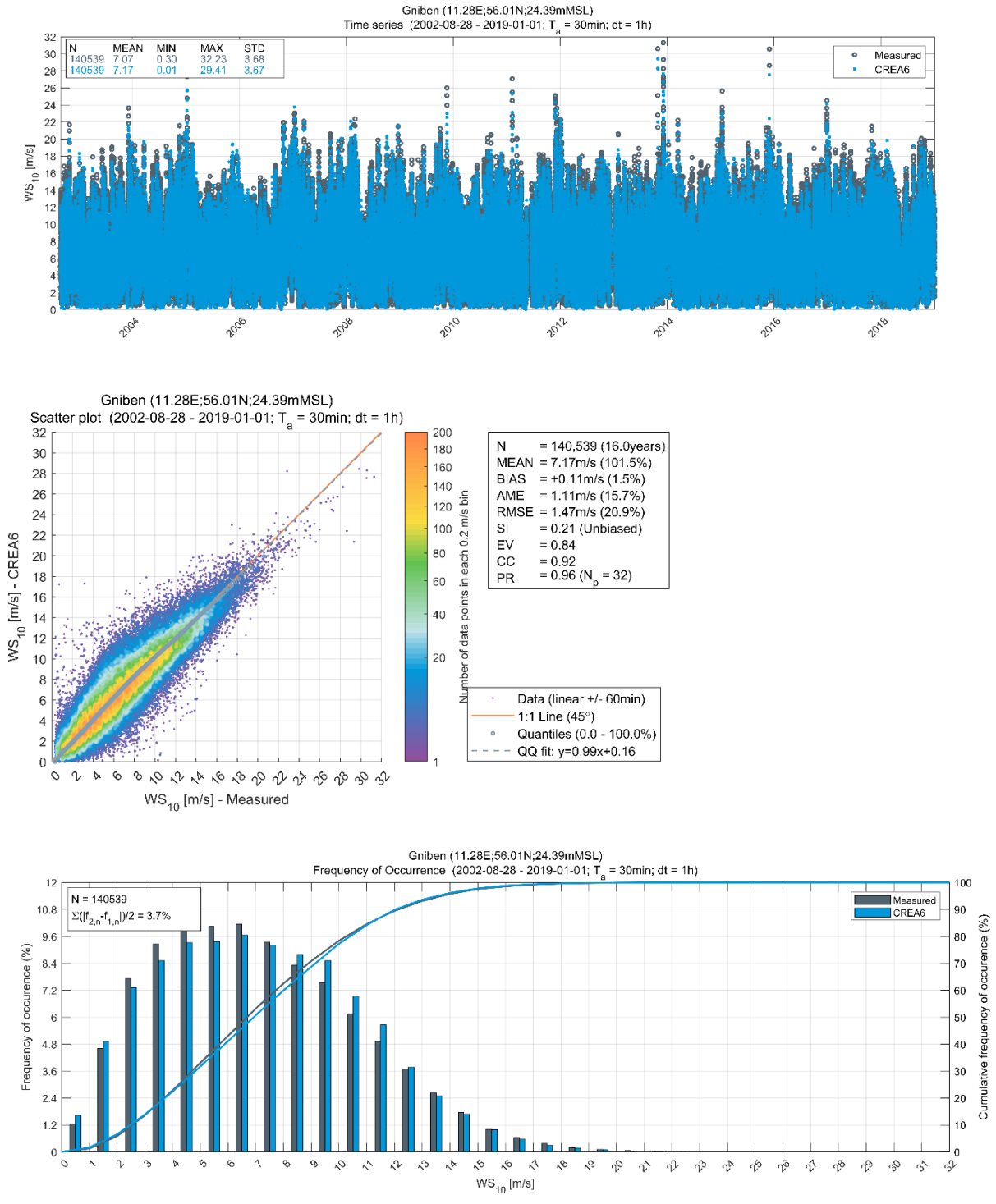

Figure B.03 Validation of CREA6 wind speeds at Gniben (10 m)

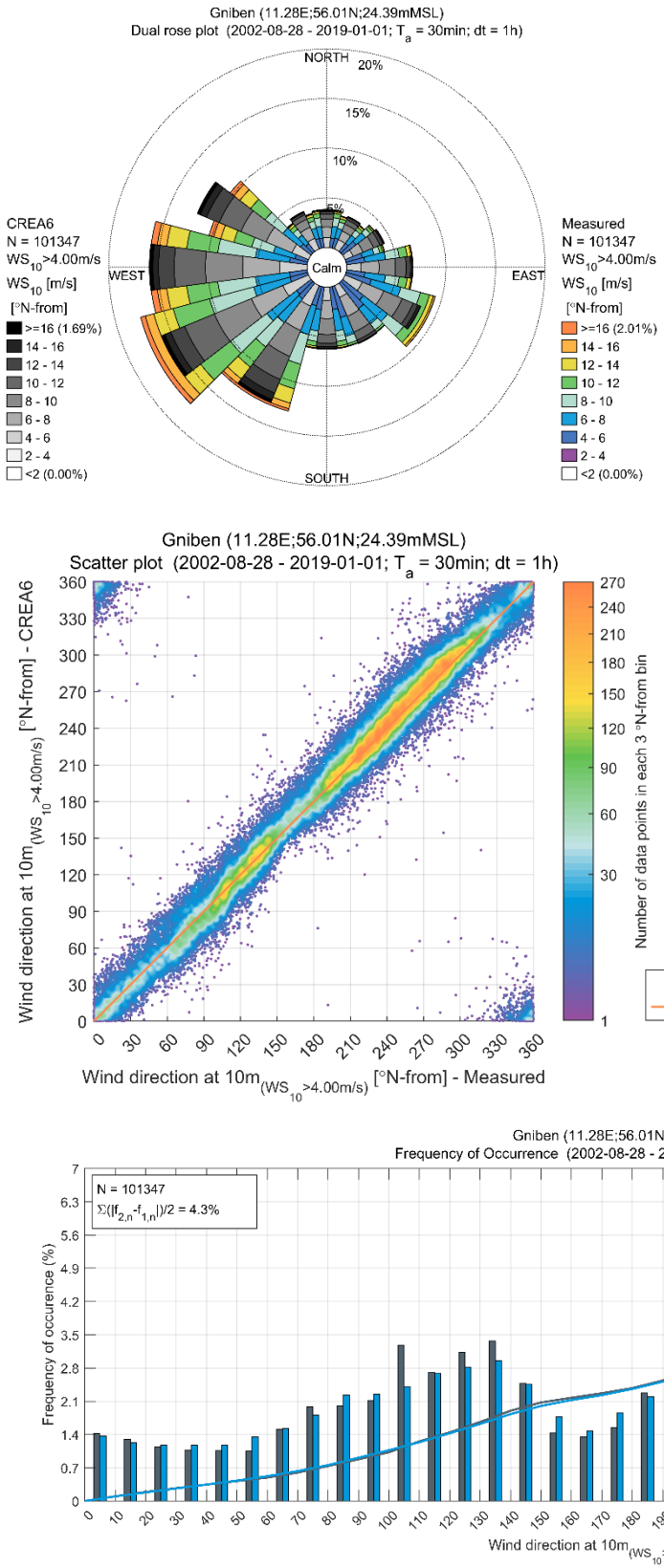

Figure B.04 Validation of CREA6 wind direction at Gniben (10 m)

Appendix B.1.3 Nakkehoved Fyr

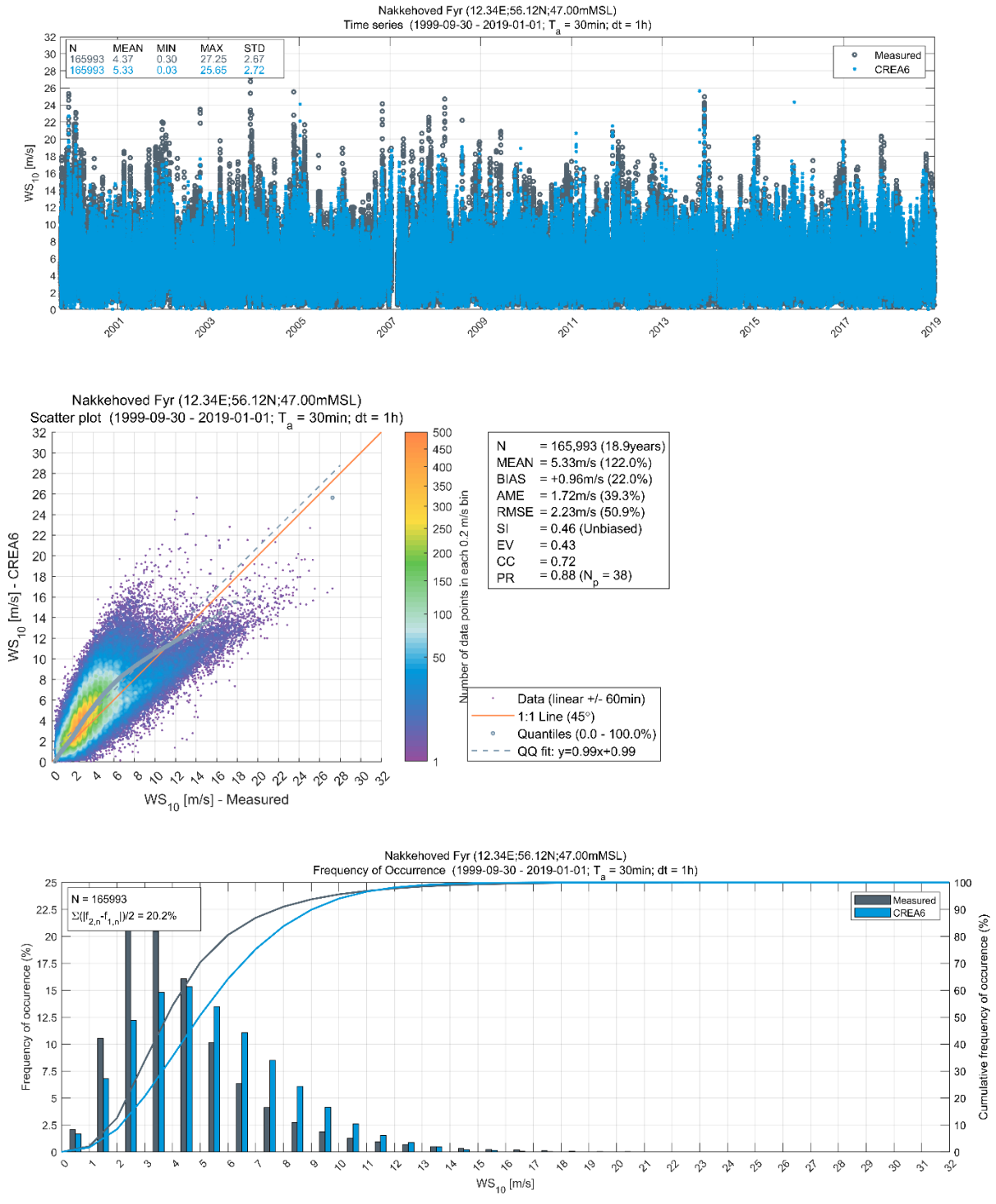

Figure B.05 Validation of CREA6 wind speeds at Nakkedhoved Fyr (10 m)

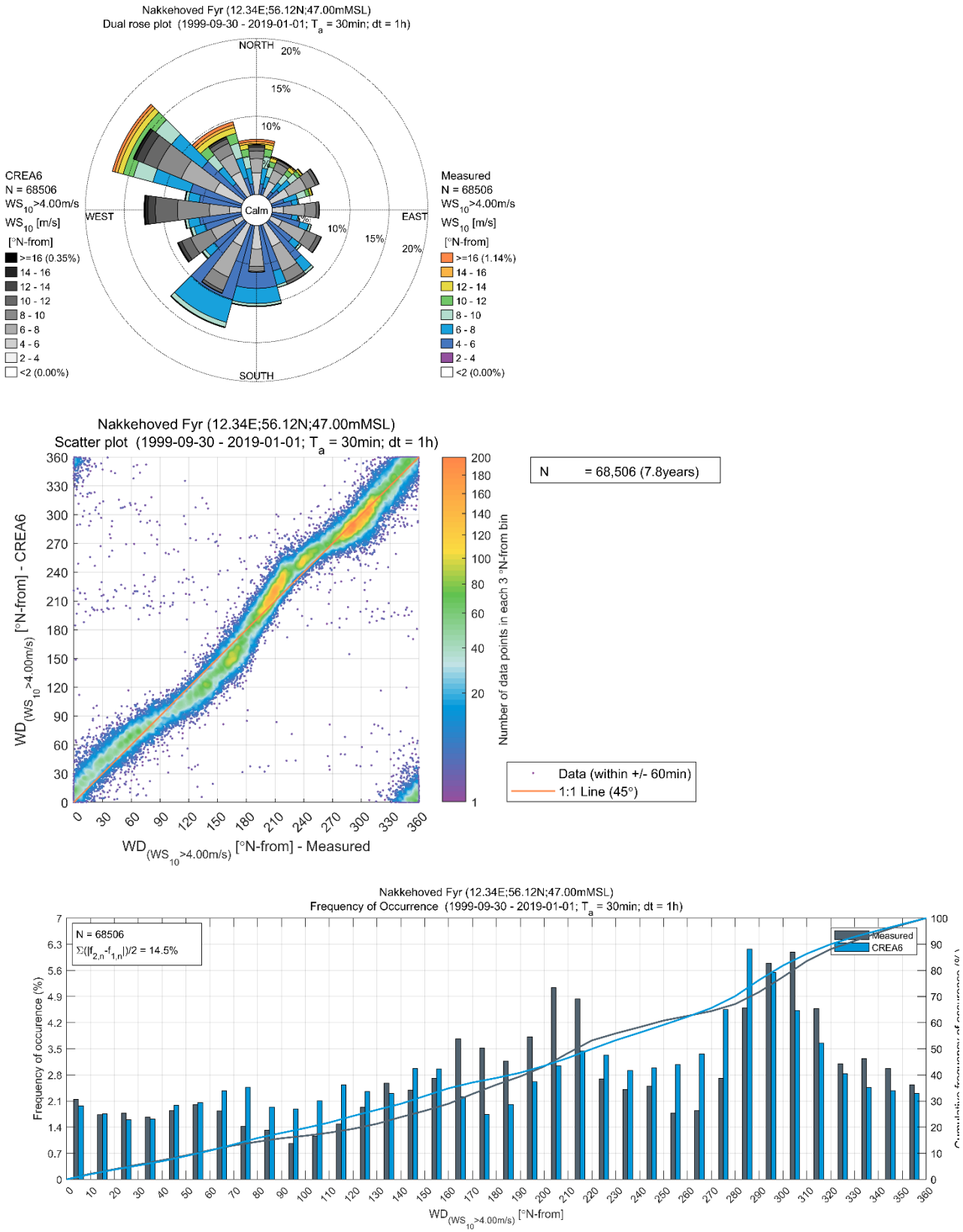

Figure B.06 Validation of CREA6 wind direction at Nakkedhoved Fyr (10 m)

Appendix B.1.4 Läsö Ost A

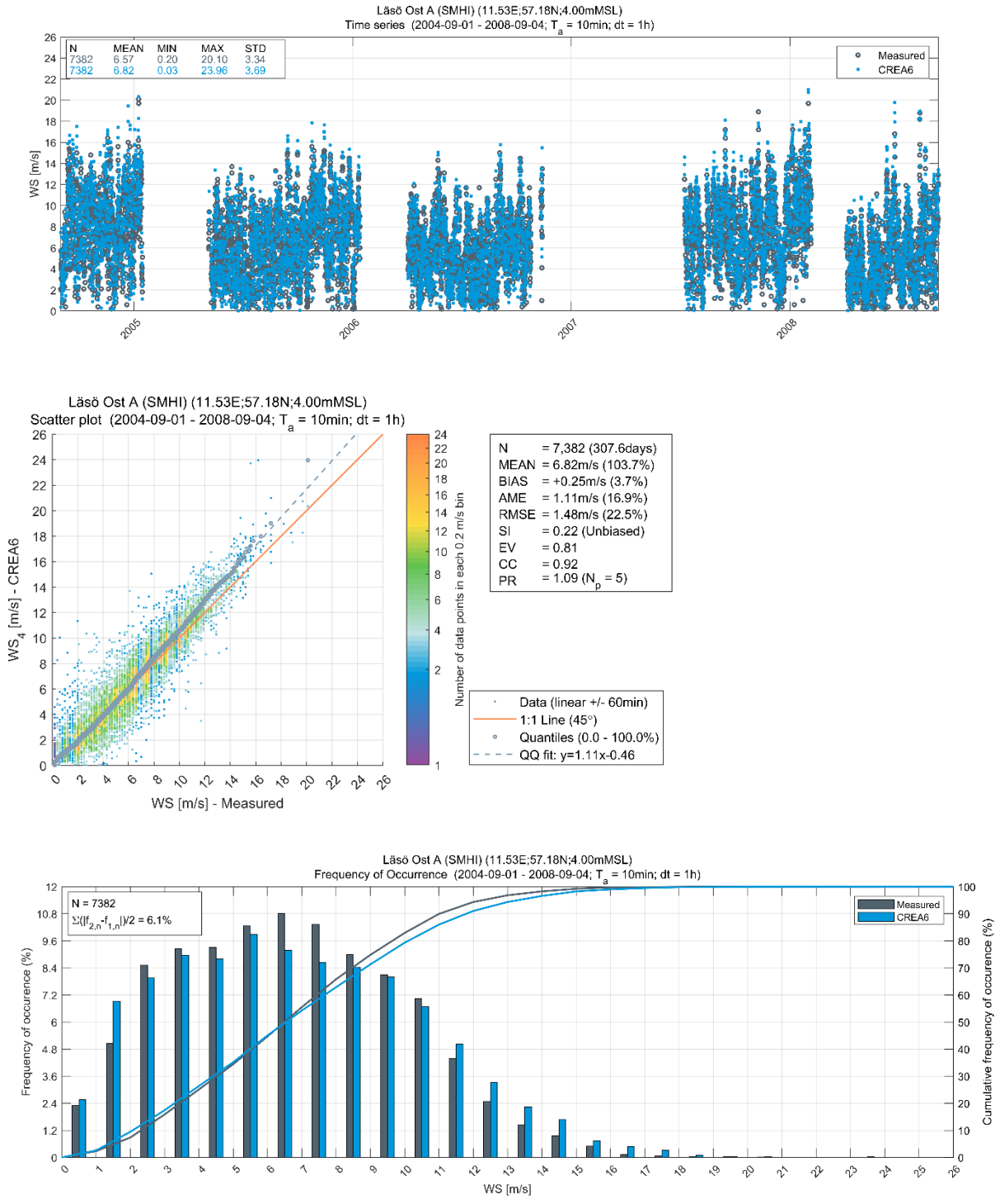

Figure B.07 Validation of CREA6 wind speeds at Laesø Ost A (4 m)

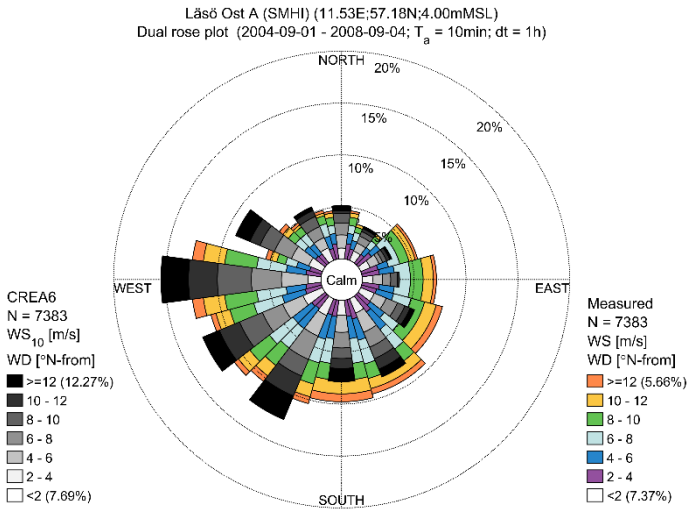

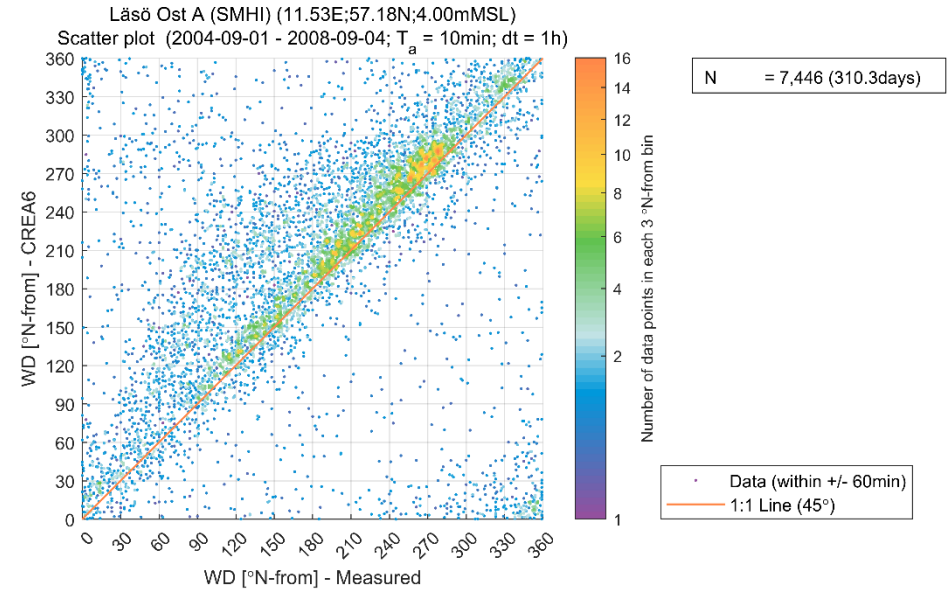

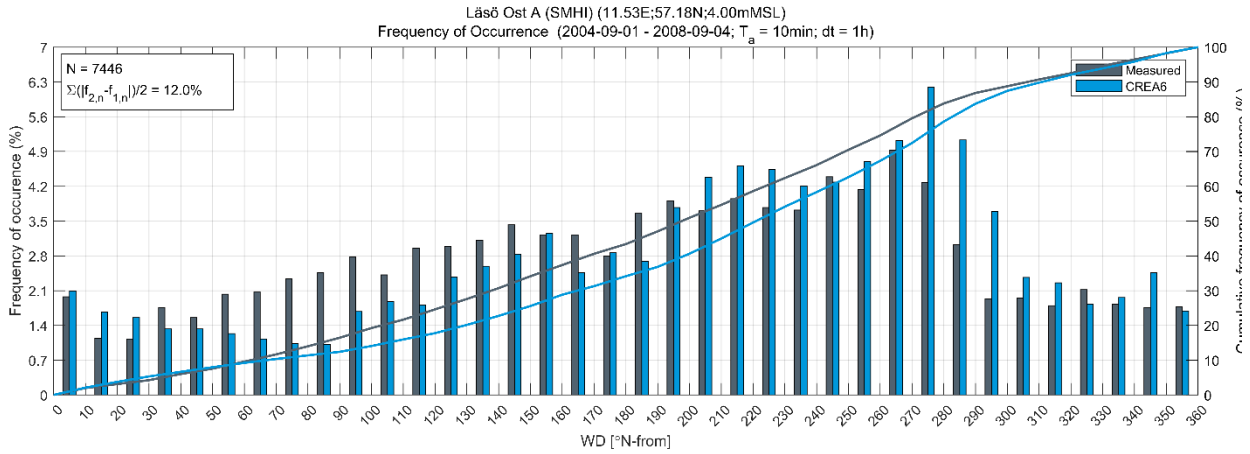

Figure B.08 Validation of CREA6 wind direction at Laesø Ost A (4 m)

Appendix B.1.5 Hallands Väderö

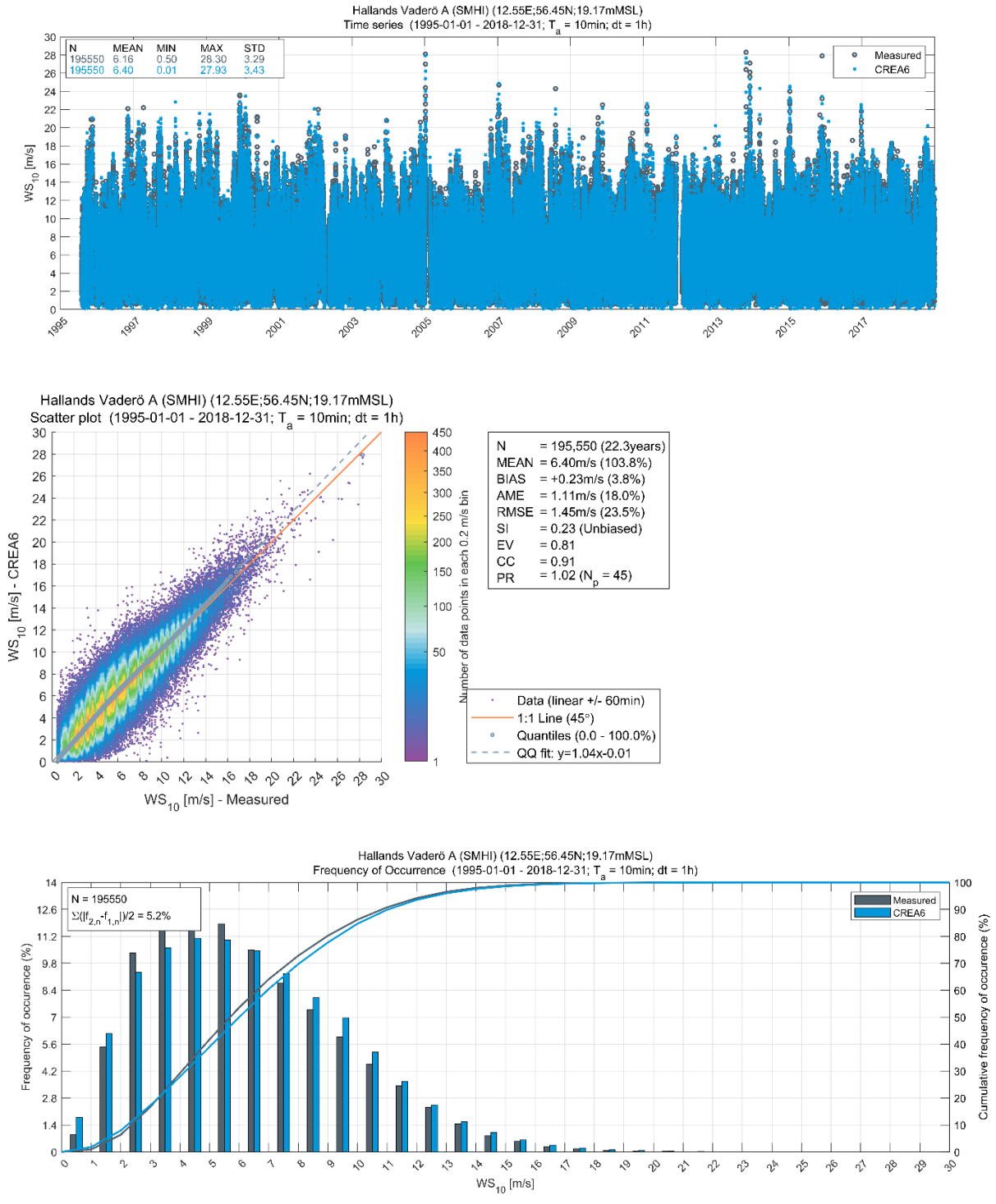

Figure B.09 Validation of CREA6 wind speeds at Hallands Väderö Ost A (10 m)

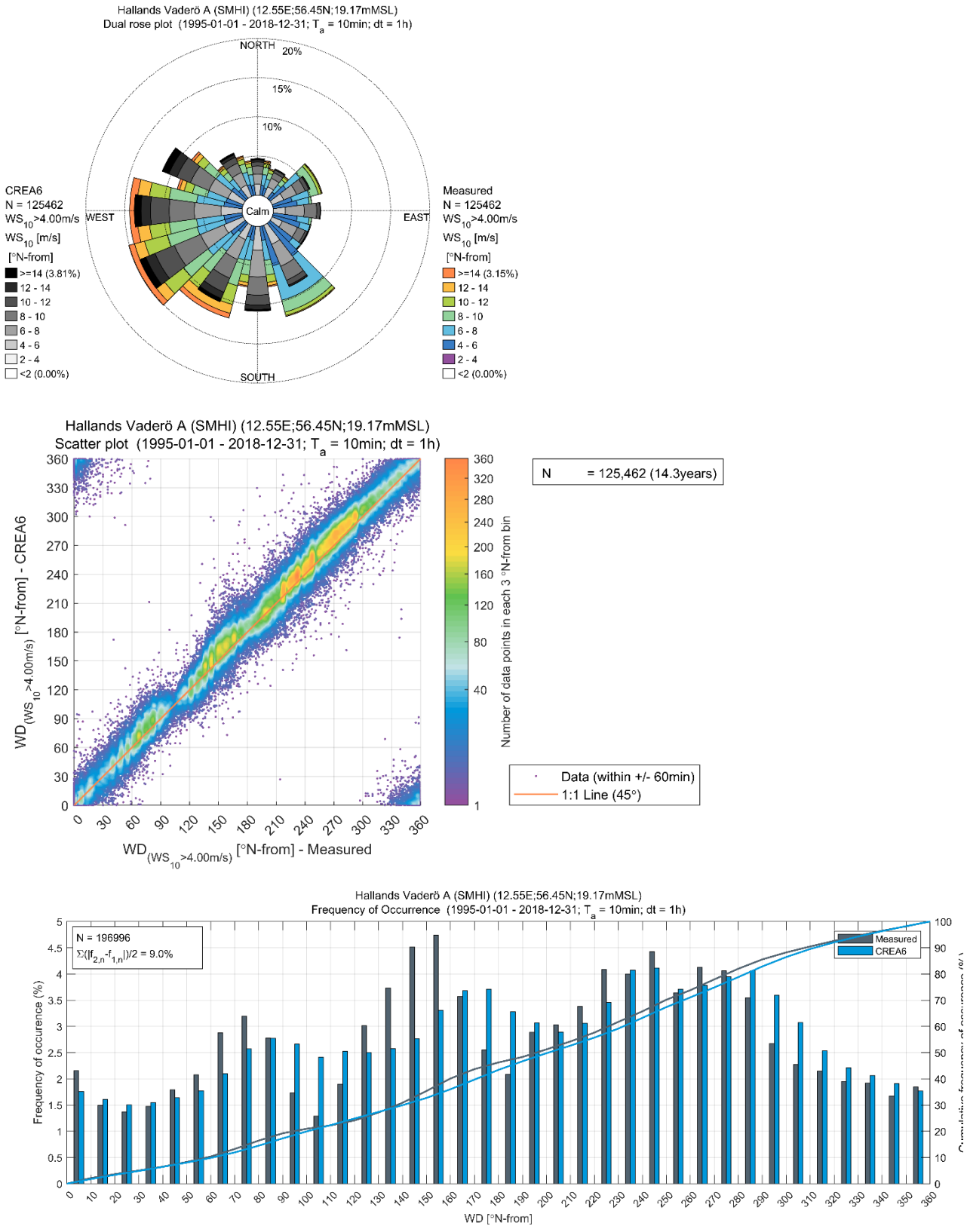

Figure B.10 Validation of CREA6 wind direction at Hallands Väderö Ost A (10 m)

Appendix B.1.6 Læsø Syd

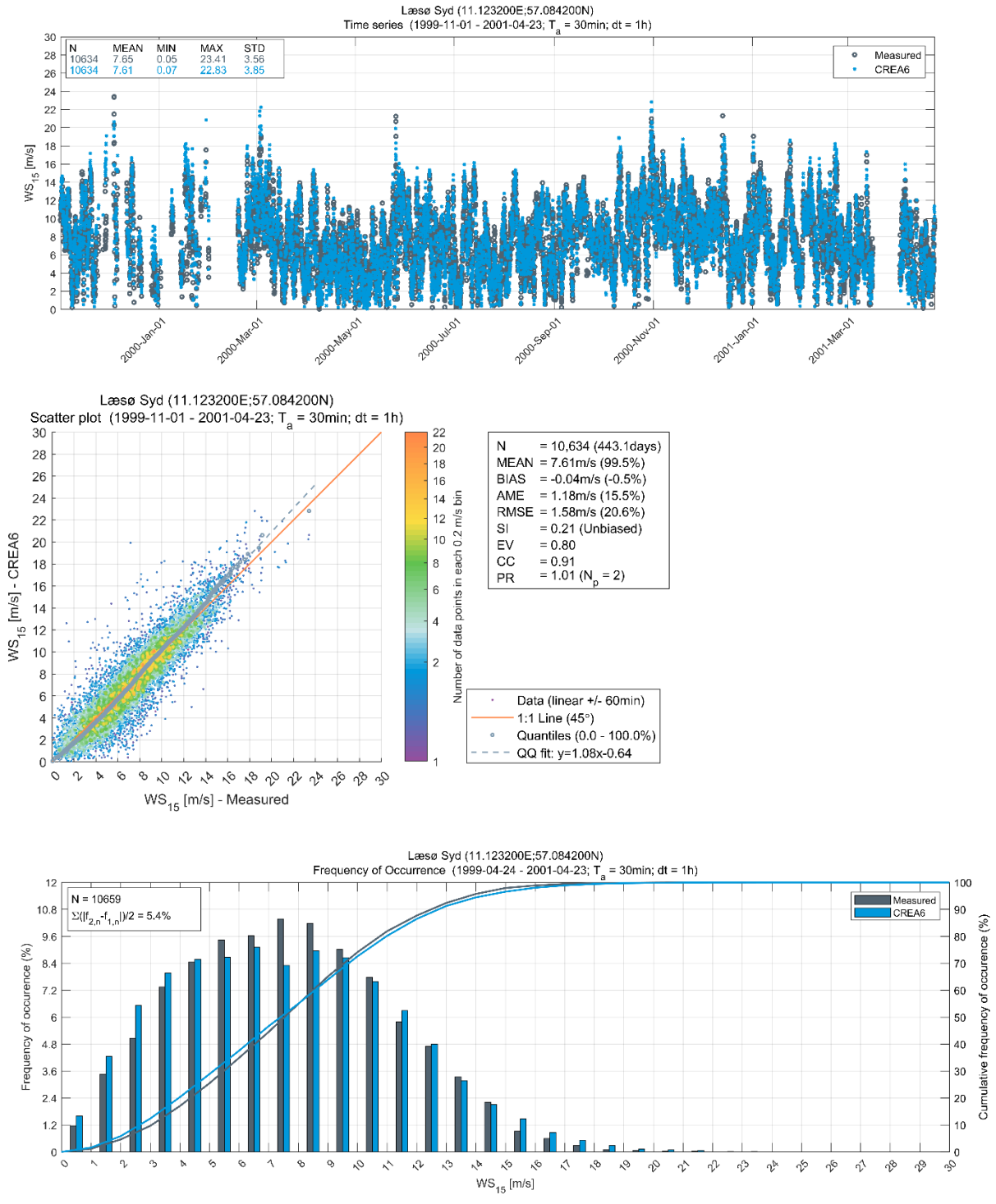

Figure B.11 Validation of CREA6 wind speeds at Laesø Syd (15 m)

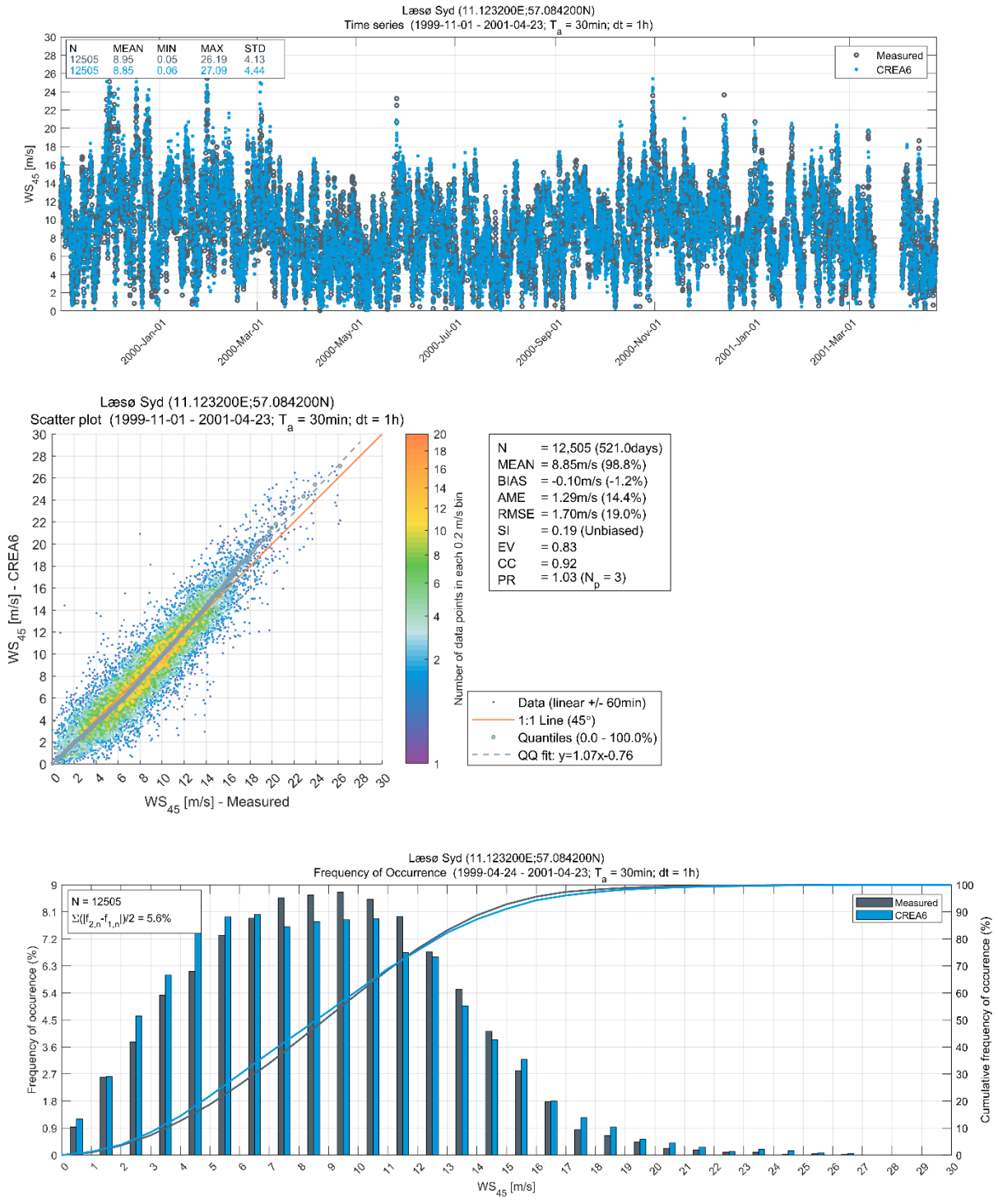

Figure B.12 Validation of CREA6 wind speeds at Laesø Syd (45 m)

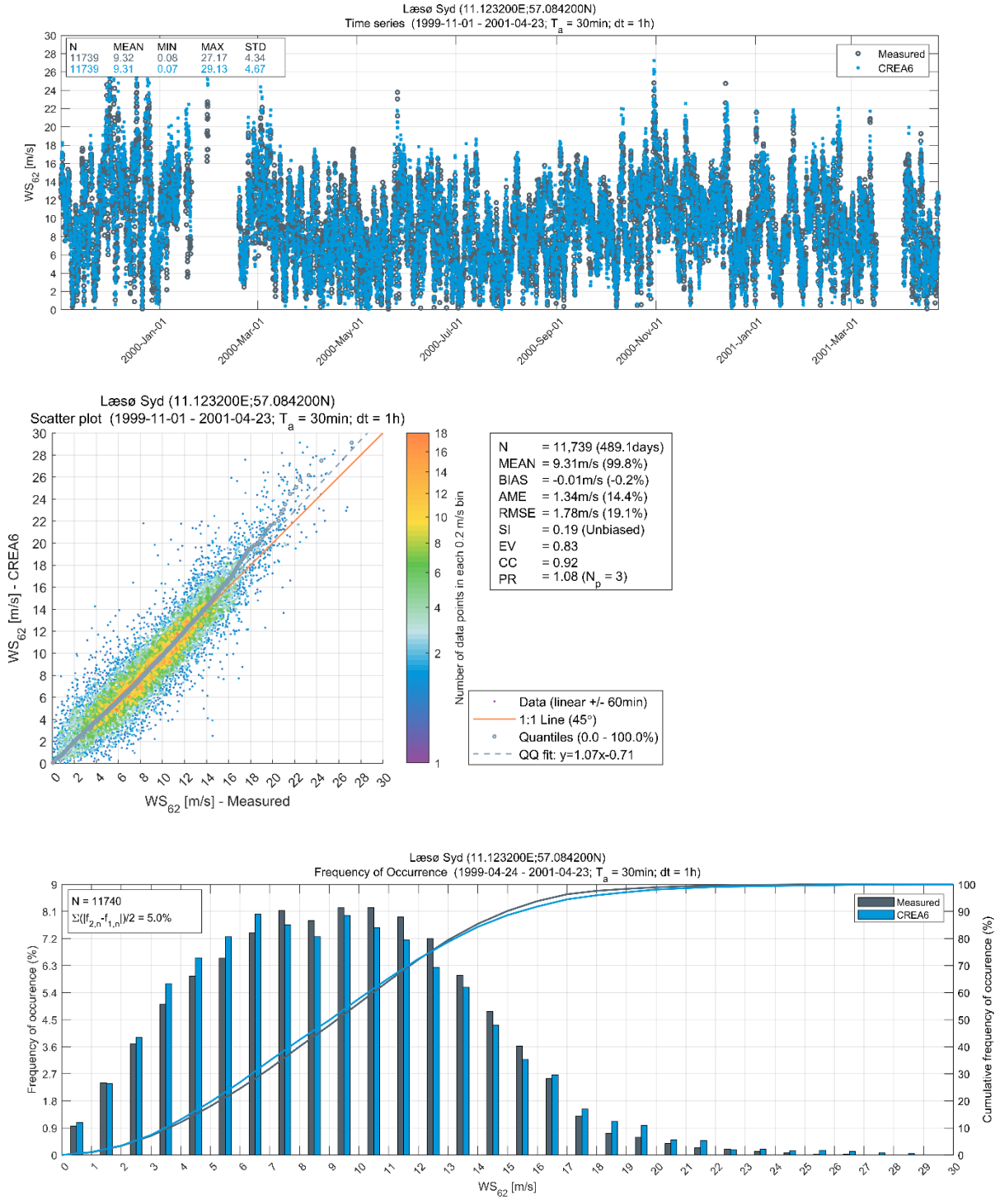

Figure B.13 Validation of CREA6 wind speeds at Laesø Syd (62 m)

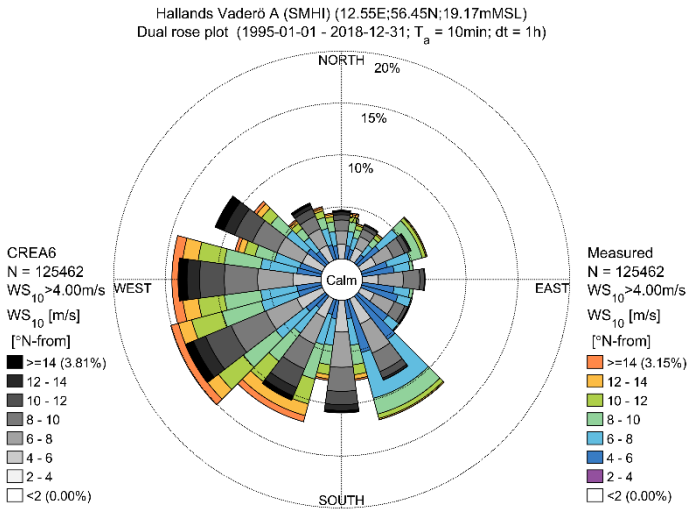

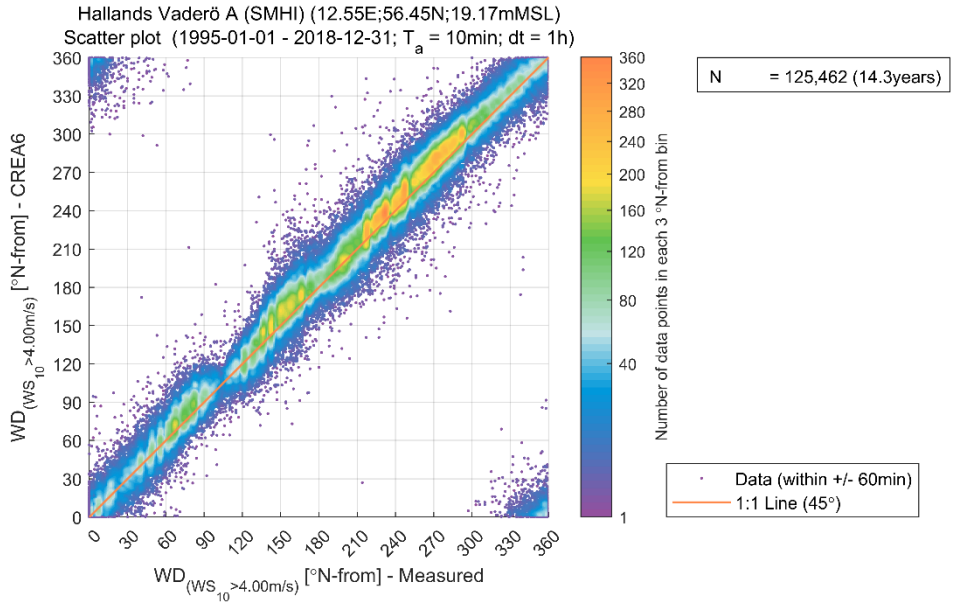

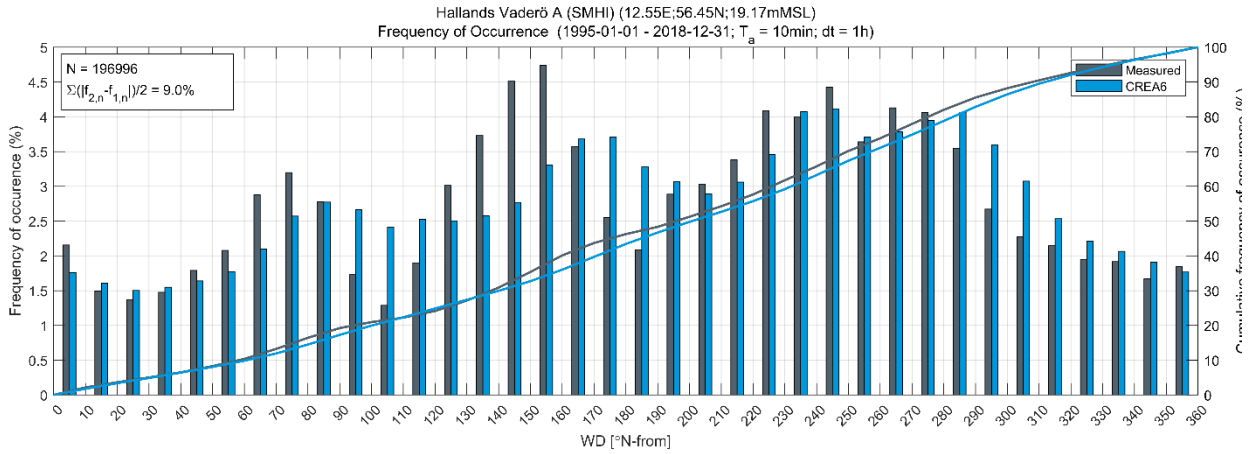

Figure B.14 Validation of CREA6 wind direction at Hallands Vaderö Ost A (10 m)

Appendix B.2 Danish waters hydrodynamic model (HD_{DKW})

Appendix B.2.1 Grenaa Havn residual water levels

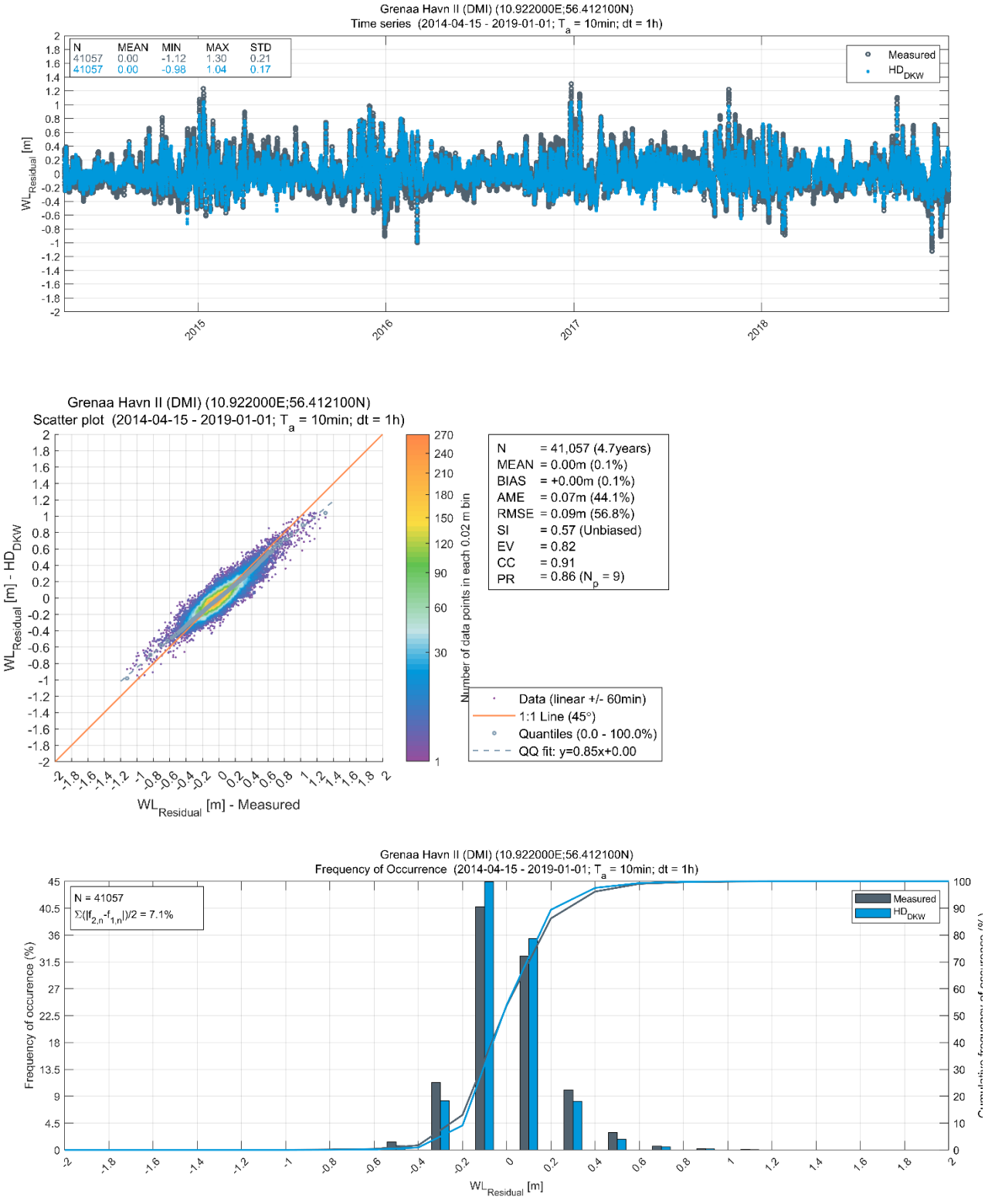

Figure B.15 Validation of HD_{DKW} residual water level at Grenaa Havn

Appendix B.2.2 Havnebyen Sjællands Odde residual water levels

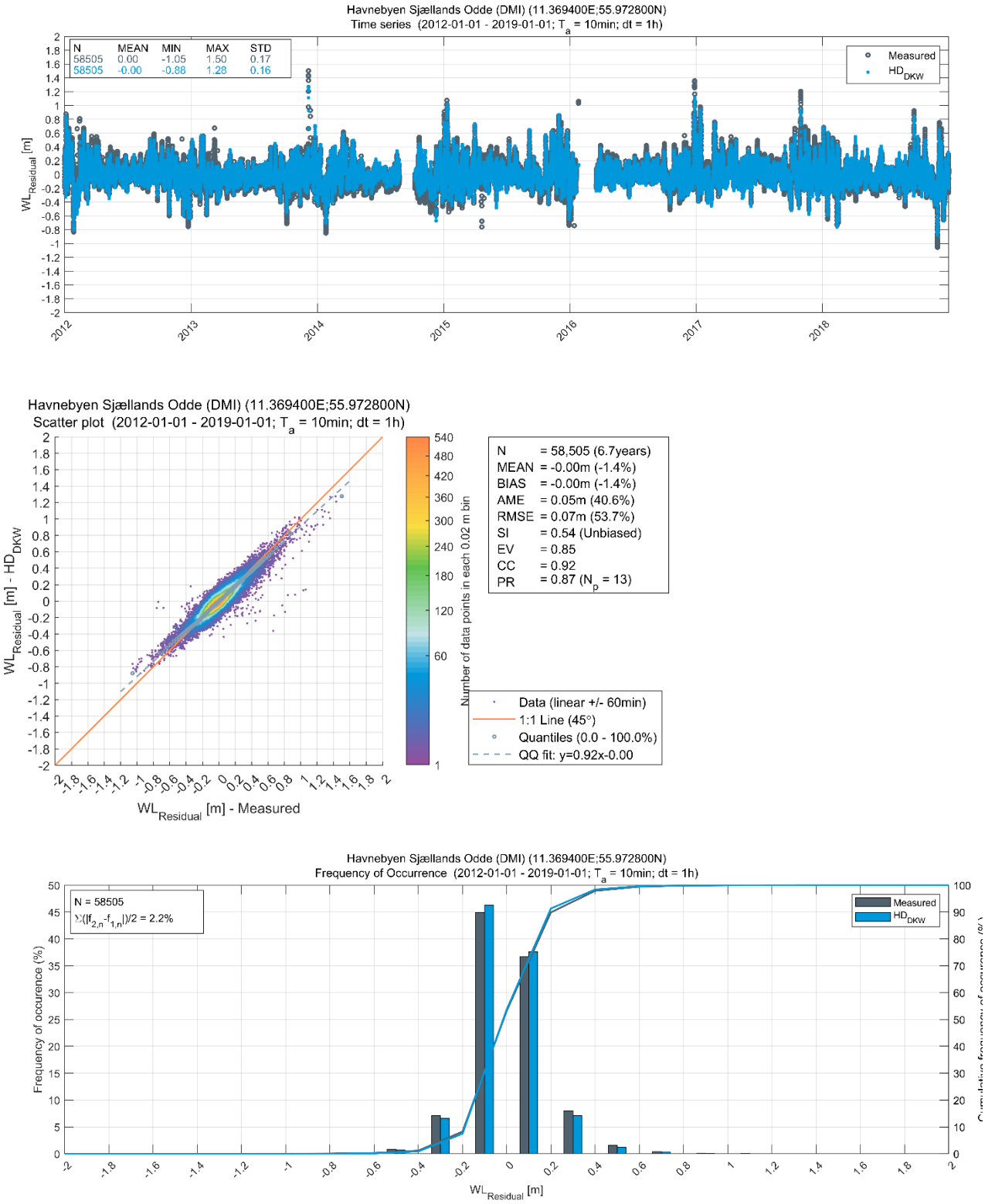

Figure B.16 Validation of HD_{DKW} residual water level at Havnebyen Sjællands Odde

Appendix B.2.3 Viken residual water levels

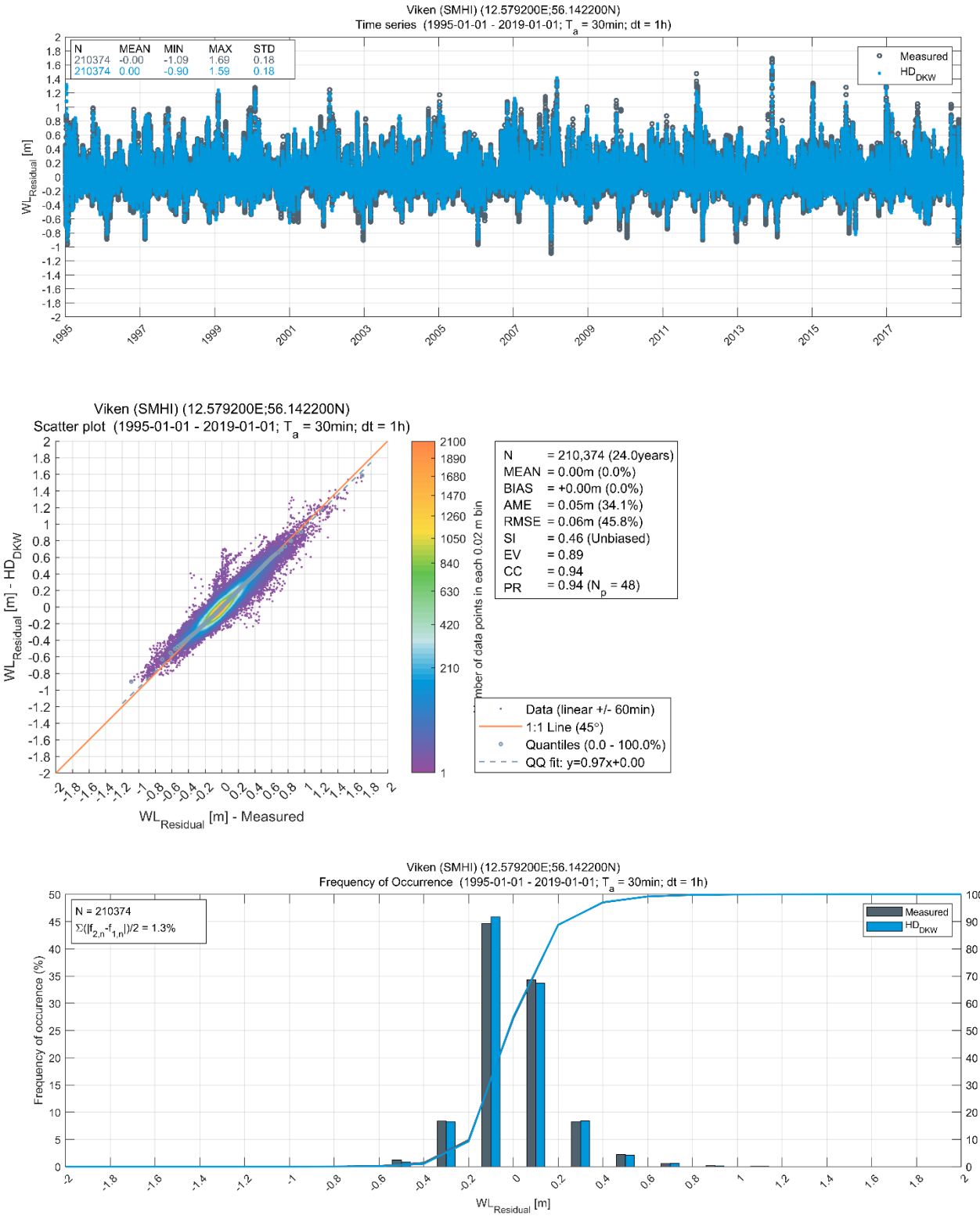

Figure B.17 Validation of HD_{DKW} residual water level at Viken

Appendix B.2.4 Halmstad Sjöv residual water levels

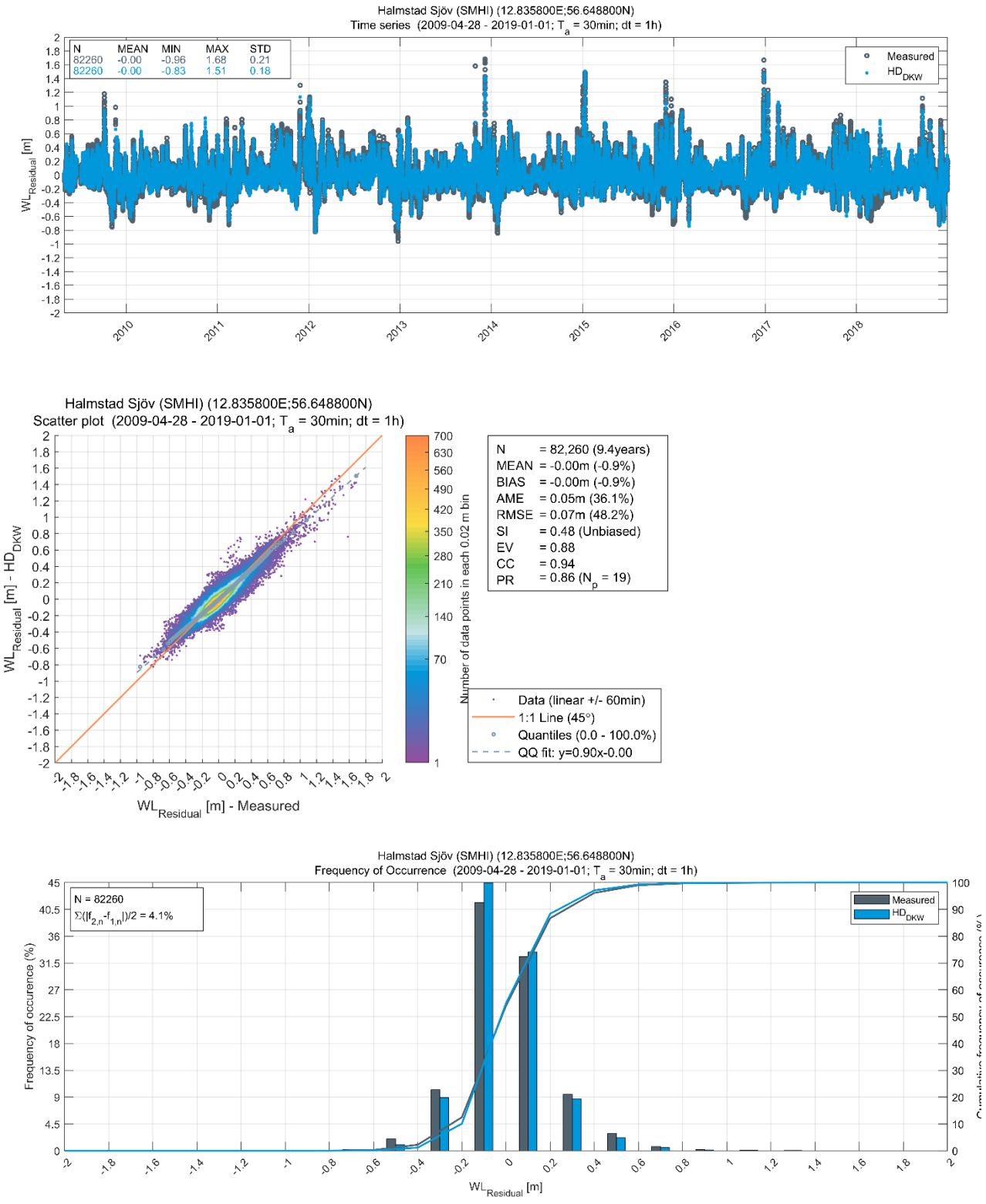

Figure B.18 Validation of HD_{DKW} residual water level at Halmstad Sjöv

Appendix B.2.5 Ringhals residual water levels

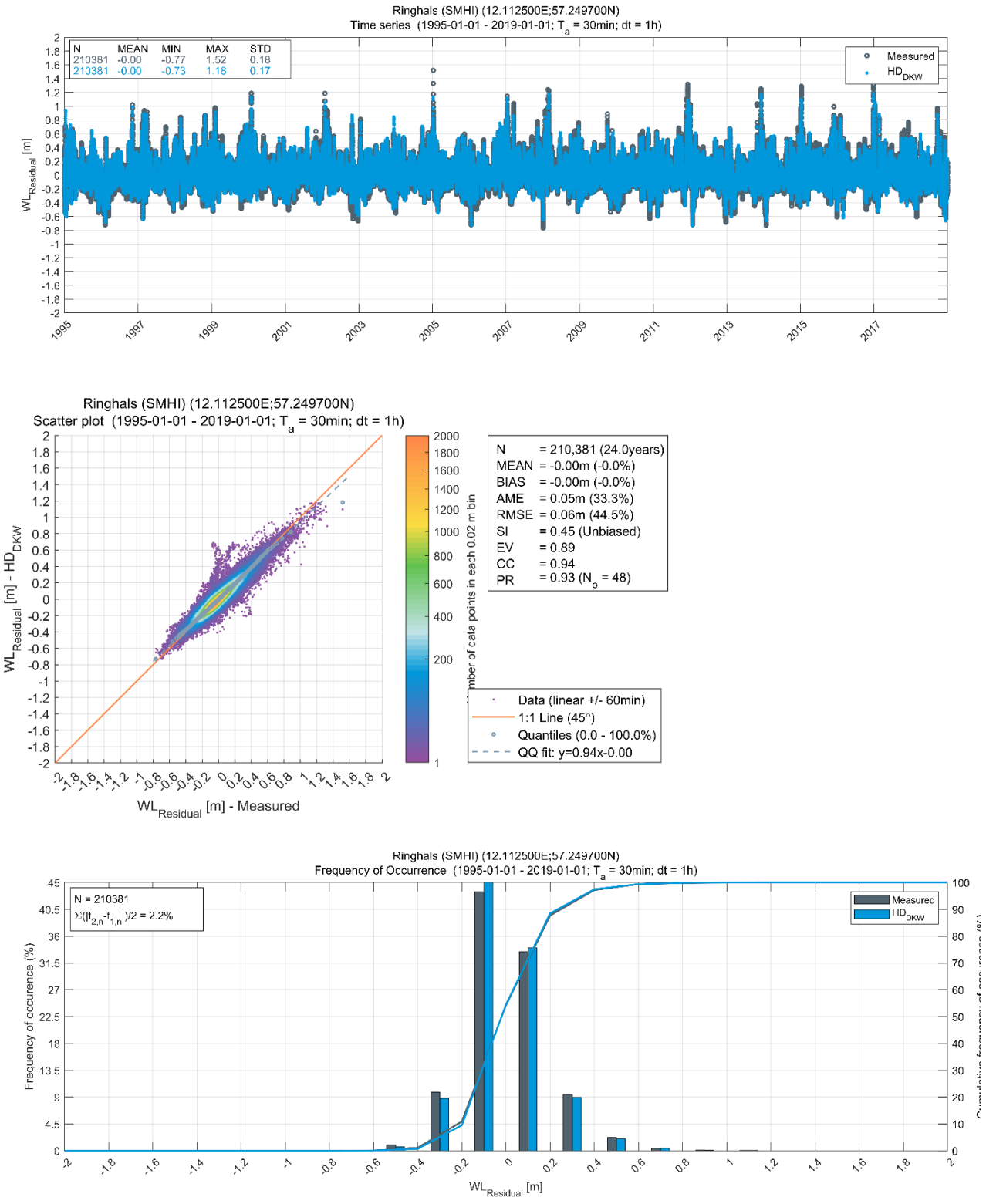

Figure B.19 Validation of HD_{DKW} residual water level at Ringhals

Appendix B.3 Danish waters spectral wave model (SW_{DKW})

Appendix B.3.1 Læsø Syd significant wave height and direction

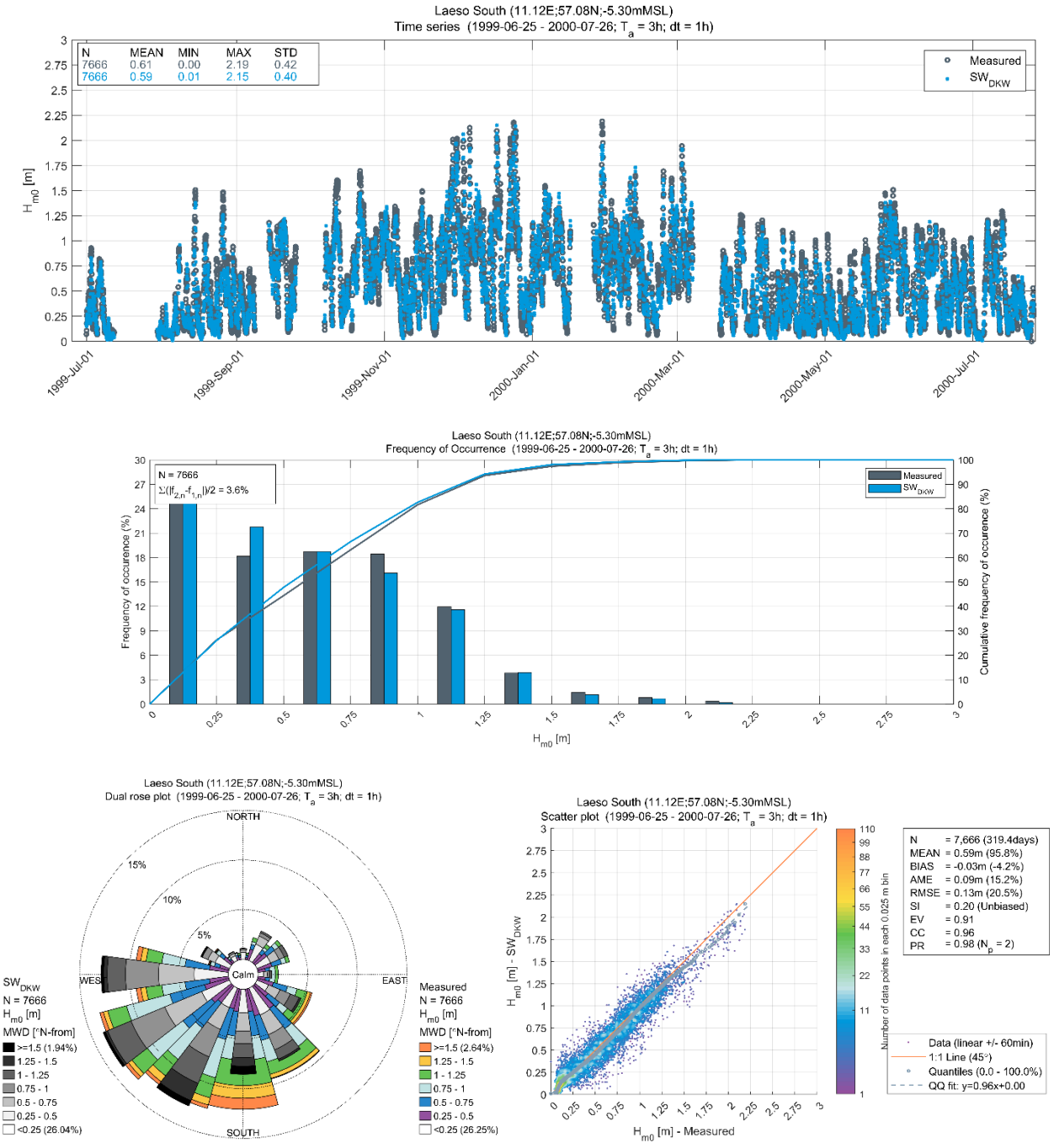

Figure B.20 Validation of SW_{DKW} Significant wave height and direction at Laesø South

Appendix B.3.2 Sejero Bugt significant wave height, direction, and periods

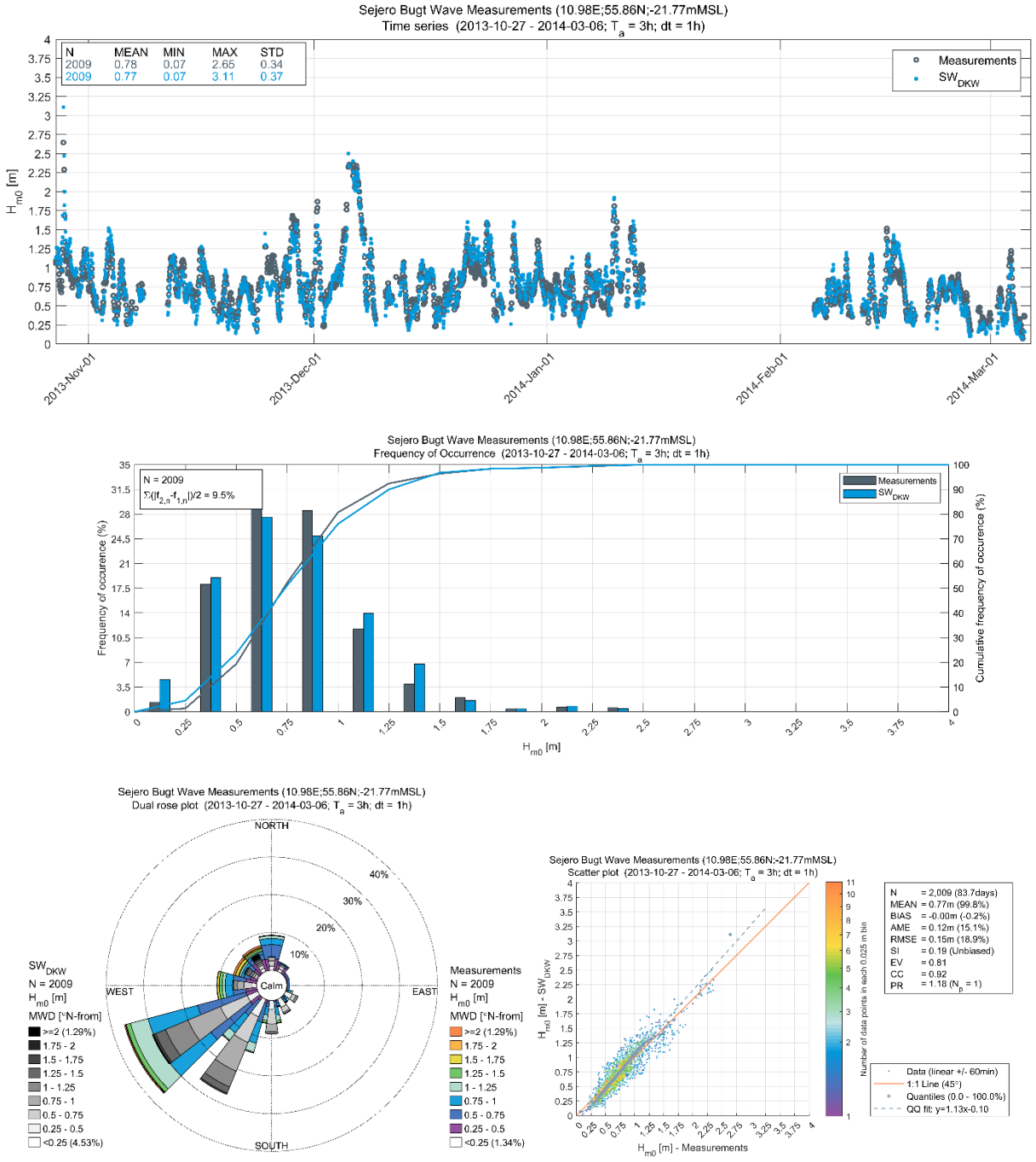

Figure B.21 Validation of SW_{DKW} Significant wave height and direction at Sejero Bugt

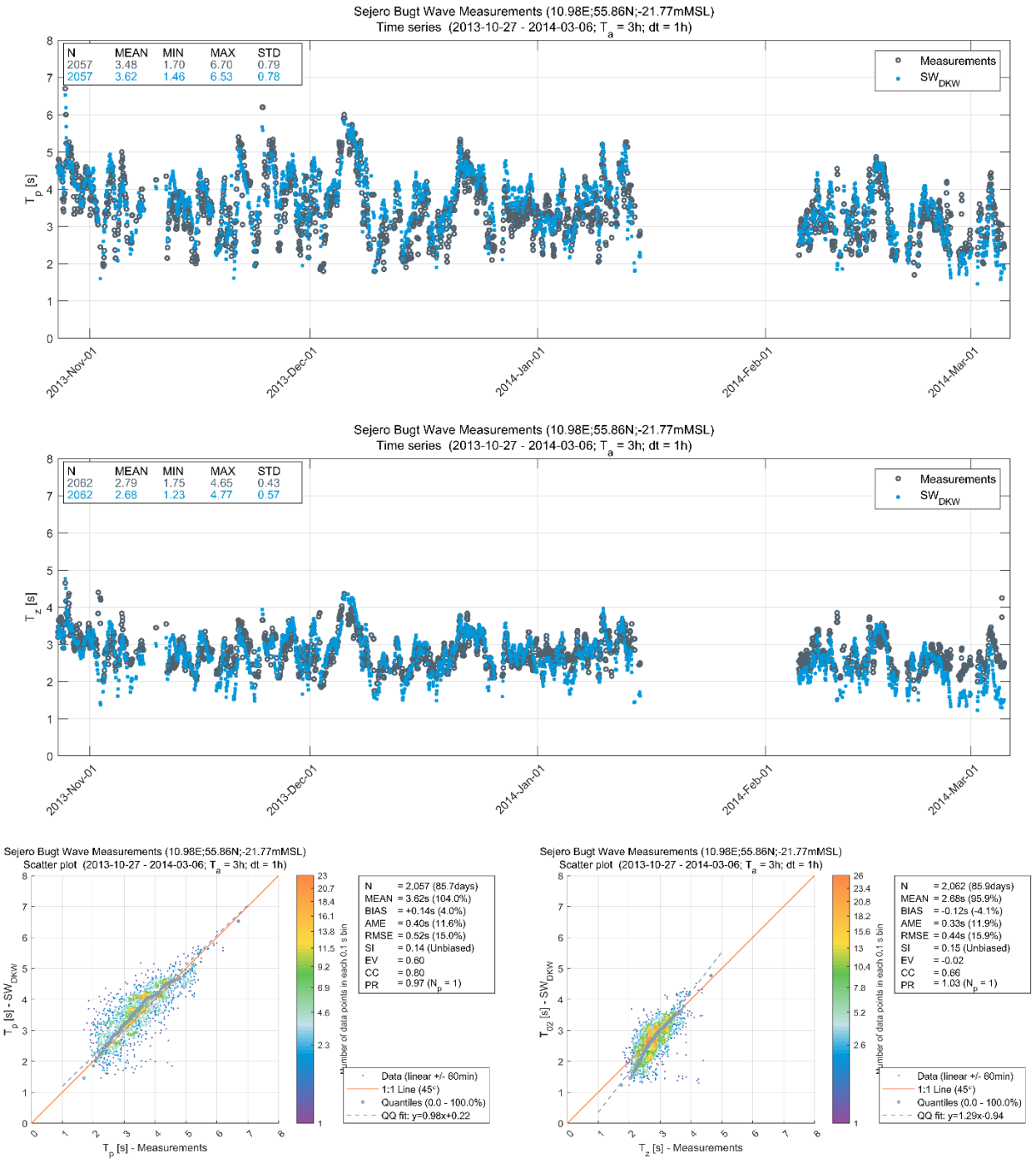

Figure B.22 Validation of SW_{DKW} peak and zero-crossing period at Sejero Bugt

Appendix B.3.3 Fladen Boj significant wave height and mean wave period

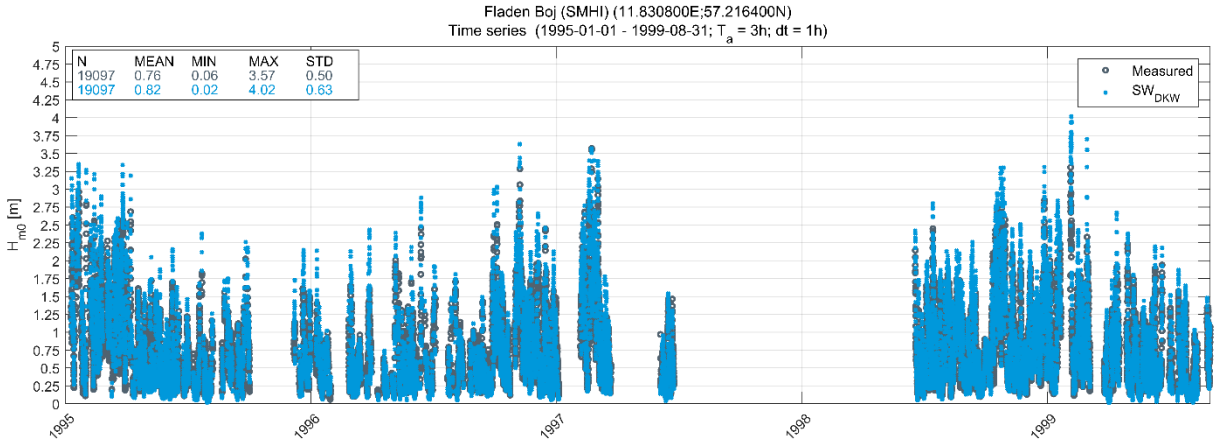

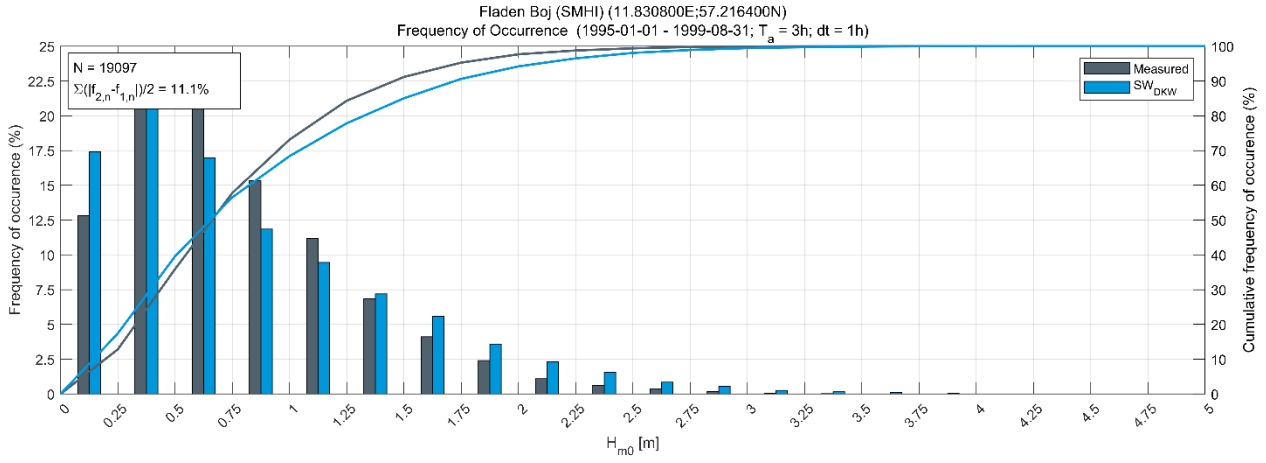

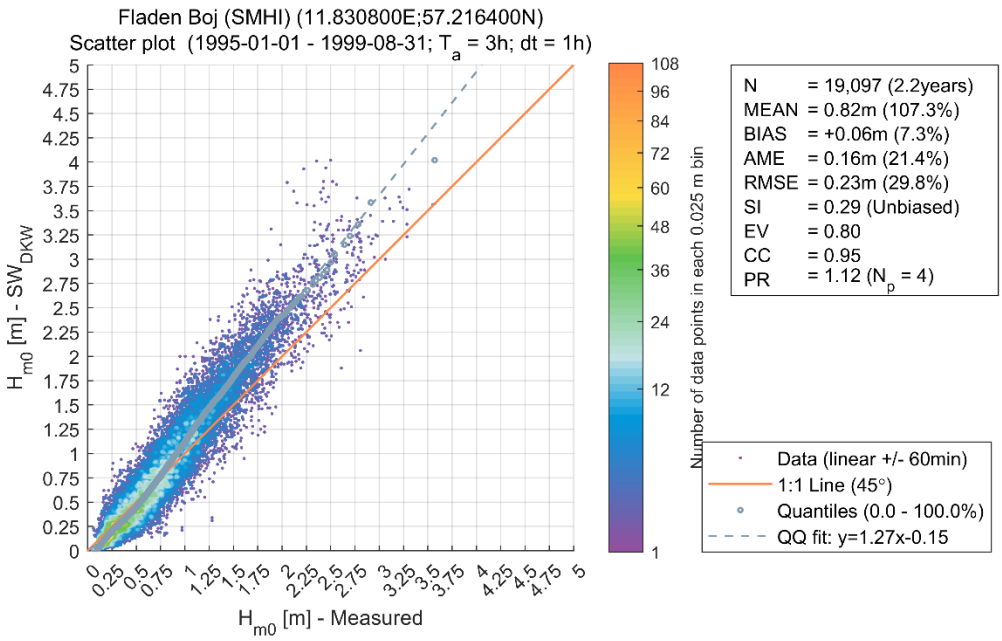

Figure B.23 Validation of SW_{DKW} significant wave height at Fladen

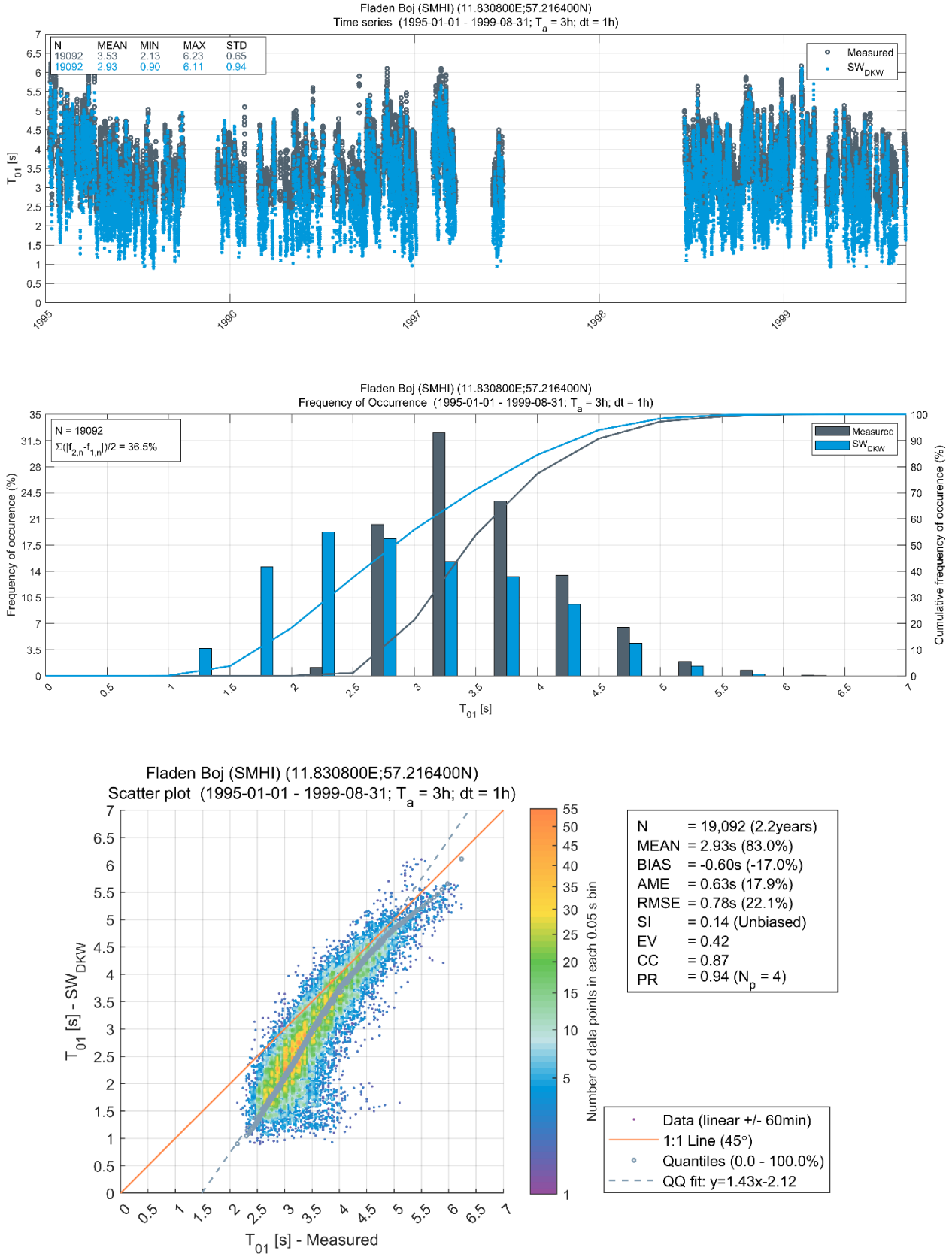

Figure B.24 Validation of SW_{DKW} mean wave period at Fladen

Appendix C Frequency of Occurrence Tables (digital files)

The table on the following page summarises the digital frequency of occurrence tables that are provided alongside this metocean report.

Analysis Point	Filename	Description
OWF-1	OWF-1_Scatter_WS10_CREA6_WD10_CREA6_(1995-01-14_-_2018-12-31).xlsx	Wind speed and wind direction at 10 mMSL (all-year and monthly)
	OWF-1_Scatter_WS140_CREA6_WD140_CREA6_(1995-01-14_-_2018-12-31).xlsx	Wind speed and wind direction at 140 mMSL (all-year and monthly)
	OWF-1_Scatter_MWD_SW_{DKW}_Hm0_SW_{DKW}_(1995-01-14_-_2018-12-31).xlsx	Total sea-state spectral significant wave height and mean wave direction (all-year and monthly)
	OWF-1_Scatter_Tp_SW_{DKW}_Hm0_SW_{DKW}_(1995-01-14_-_2018-12-31).xlsx	Total sea-state spectral significant wave height and spectral peak wave period (omnidirectional and for 12 x 30° sectors based on mean wave direction)
	OWF-1_Scatter_T02_SW_{DKW}_Hm0_SW_{DKW}_(1995-01-14_-_2018-12-31).xlsx	Total sea-state spectral significant wave height and spectral mean zero-crossing wave period (omnidirectional and for 12 x 30° sectors based on mean wave direction)
	OWF-1_Scatter_MWD_SW_{DKW}_WD10_CREA6_(1995-01-14_-_2018-12-31).xlsx	Wind directional at 10 mMSL and mean wave direction (all-year and monthly)
	OWF-1_Scatter_CS_HD_{DKW}_CD_Total_HD_{DKW}_(1995-01-14_-_2018-12-31).xlsx	Total depth-averaged current speed and total depth-averaged current direction (all-year and monthly)
	OWF-1_Scatter_CS_Tide_HD_{DKW}_CD_Tide_HD_{DKW}_(1995-01-14_-_2018-12-31).xlsx	Tidal depth-averaged current speed and tidal depth-averaged current direction (all-year and monthly)
	OWF-1_Scatter_CS_Resid_HD_{DKW}_CD_Resid_HD_{DKW}_(1995-01-14_-_2018-12-31).xlsx	Residual depth-averaged current speed and residual depth-averaged current direction (all-year and monthly)
OWF-2	OWF-2_Scatter_WS10_CREA6_WD10_CREA6_(1995-01-14_-_2018-12-31).xlsx	Wind speed and wind direction at 10 mMSL (all-year and monthly)
	OWF-2_Scatter_WS140_CREA6_WD140_CREA6_(1995-01-14_-_2018-12-31).xlsx	Wind speed and wind direction at 140 mMSL (all-year and monthly)
	OWF-2_Scatter_MWD_SW_{DKW}_Hm0_SW_{DKW}_(1995-01-14_-_2018-12-31).xlsx	Total sea-state spectral significant wave height and mean wave direction (all-year and monthly)
	OWF-2_Scatter_Tp_SW_{DKW}_Hm0_SW_{DKW}_(1995-01-14_-_2018-12-31).xlsx	Total sea-state spectral significant wave height and spectral peak wave period (omnidirectional and for 12 x 30° sectors based on mean wave direction)
	OWF-2_Scatter_T02_SW_{DKW}_Hm0_SW_{DKW}_(1995-01-14_-_2018-12-31).xlsx	Total sea-state spectral significant wave height and spectral mean zero-crossing wave period (omnidirectional and for 12 x 30° sectors based on mean wave direction)

Analysis Point	Filename	Description
	OWF-2_Scatter_MWD_SW_{DKW}_WD10_CREA6_(1995-01-14_-_2018-12-31).xlsx	Wind directional at 10 mMSL and mean wave direction (all-year and monthly)
	OWF-2_Scatter_CS_HD_{DKW}_CD_Total_HD_{DKW}_(1995-01-14_-_2018-12-31).xlsx	Total depth-averaged current speed and total depth-averaged current direction (all-year and monthly)
	OWF-2_Scatter_CS_Tide_HD_{DKW}_CD_Tide_HD_{DKW}_(1995-01-14_-_2018-12-31).xlsx	Tidal depth-averaged current speed and tidal depth-averaged current direction (all-year and monthly)
	OWF-2_Scatter_CS_Resid_HD_{DKW}_CD_Resid_HD_{DKW}_(1995-01-14_-_2018-12-31).xlsx	Residual depth-averaged current speed and residual depth-averaged current direction (all-year and monthly)
OWF-3	OWF-3_Scatter_WS10_CREA6_WD10_CREA6_(1995-01-14_-_2018-12-31).xlsx	Wind speed and wind direction at 10 mMSL (all-year and monthly)
	OWF-3_Scatter_WS140_CREA6_WD140_CREA6_(1995-01-14_-_2018-12-31).xlsx	Wind speed and wind direction at 140 mMSL (all-year and monthly)
	OWF-3_Scatter_MWD_SW_{DKW}_Hm0_SW_{DKW}_(1995-01-14_-_2018-12-31).xlsx	Total sea-state spectral significant wave height and mean wave direction (all-year and monthly)
	OWF-3_Scatter_Tp_SW_{DKW}_Hm0_SW_{DKW}_(1995-01-14_-_2018-12-31).xlsx	Total sea-state spectral significant wave height and spectral peak wave period (omnidirectional and for 12 x 30° sectors based on mean wave direction)
	OWF-3_Scatter_T02_SW_{DKW}_Hm0_SW_{DKW}_(1995-01-14_-_2018-12-31).xlsx	Total sea-state spectral significant wave height and spectral mean zero-crossing wave period (omnidirectional and for 12 x 30° sectors based on mean wave direction)
	OWF-3_Scatter_MWD_SW_{DKW}_WD10_CREA6_(1995-01-14_-_2018-12-31).xlsx	Wind directional at 10 mMSL and mean wave direction (all-year and monthly)
	OWF-3_Scatter_CS_HD_{DKW}_CD_Total_HD_{DKW}_(1995-01-14_-_2018-12-31).xlsx	Total depth-averaged current speed and total depth-averaged current direction (all-year and monthly)
	OWF-3_Scatter_CS_Tide_HD_{DKW}_CD_Tide_HD_{DKW}_(1995-01-14_-_2018-12-31).xlsx	Tidal depth-averaged current speed and tidal depth-averaged current direction (all-year and monthly)
	OWF-3_Scatter_CS_Resid_HD_{DKW}_CD_Resid_HD_{DKW}_(1995-01-14_-_2018-12-31).xlsx	Residual depth-averaged current speed and residual depth-averaged current direction (all-year and monthly)

Appendix D Extreme Value Analysis Methodology

Appendix D.1 General

Extreme values with associated long return periods are estimated by fitting a probability distribution to historical data. A number of distributions, data selection and fitting techniques are available for estimation of extremes, and the estimated extremes are often rather sensitive to the choice of method. However, it is not possible to choose a preferred method only on its superior theoretical support or widespread acceptance within the industry. Hence, it is common practice to test a number of approaches and make the final decision based on the quality of the fit.

The typical extreme value analyses involved the following steps:

1. Extraction of independent identically distributed events by requiring that events are separated by at least 36 hours, and that the value between events had dropped to below 70% of the minor of two consecutive events.
2. Fitting of extreme value distribution to the extracted events, both omni/all-year and directional/seasonal subsets. Distribution parameters are estimated either by maximum likelihood or least-square methods. The following analysis approaches are used (see Section C.2 for details):

   A) Fitting the Gumbel distribution to annual maxima.

   B) Fitting a distribution to all events above a certain threshold (the Peak-Over-Threshold method). The distribution type can be exponential, truncated Weibull or 2-parameter Weibull to excess.
3. Constraining of subseries to ensure consistency with the omni/all-year distribution; see Section D.5 for details.
4. Bootstrapping to estimate the uncertainty due to sampling error; see Section D.6 for details.

Appendix D.2 Long term distributions

The following probability distributions are often used in connection with extreme value estimation:

- 2-parameter Weibull distribution
- Truncated Weibull distribution
- Exponential distribution
- Gumbel distribution

The 2-parameter Weibull distribution is given by:

$$P(X < x) = 1 - \exp\left(-\left(\frac{x}{\beta}\right)^{\alpha}\right) \quad \text{(D.1)}$$

With distribution parameters α (shape) and β (scale). The 2-parameter Weibull distribution used in connection with Peak-Over-Threshold (POT) analysis is fitted to the excess of data above the threshold, i.e. the threshold value is subtracted from data prior to fitting.

The 2-parameter truncated Weibull distribution is given by:

$$P(X < x) = 1 - \frac{1}{P_0}\exp\left(-\left(\frac{x}{\beta}\right)^{\alpha}\right) \quad \text{(D.2)}$$

With distribution parameters α (shape) and β (scale) and the exceedance probability, P_0, at the threshold level, γ, given by:

$$P_0 = \exp\left(-\left(\frac{\gamma}{\beta}\right)^{\alpha}\right) \quad \text{(D.3)}$$

The 2-parameter truncated Weibull distribution is used in connection with Peak-Over-Threshold analysis, and as opposed to the non-truncated 2-p Weibull, it is fitted directly to data, i.e. the threshold value is **not** subtracted from data prior to fitting.

The exponential distribution is given by:

$$P(X < x) = 1 - \exp\left(-\left(\frac{x-\mu}{\beta}\right)\right), \quad x \geq \mu \quad \text{(D.4)}$$

With distribution parameters β (scale) and μ (location). Finally, the Gumbel distribution is given by:

$$P(X < x) = \exp\left(-\exp\left(\frac{\mu - x}{\beta}\right)\right) \quad \text{(D.5)}$$

With distribution parameters β (scale) and μ (location).

Appendix D.3 Individual wave and crest elevation

Appendix D.3.1 Short-term distributions

The short-term distributions of individual wave heights and crests conditional on Hm0 are assumed to follow the distributions proposed by Forristall [29, 30].

The Forristall wave height distribution is based on Gulf of Mexico measurements, but experience from the North Sea has shown that these distributions may have a more general applicability. The Forristall wave and crest elevation distributions are given by:

$$P(X > x \mid H_{m0}) = \exp\left(-\left(\frac{x}{\alpha H_{m0}}\right)^{\beta}\right) \quad \text{(D.6)}$$

Where the distribution parameters, α and β, are as follows:

- Forristall wave height: α = 0.681, β = 2.126
- Forristall crest elevation (3D): α = 0.3536 + 0.2568·S1 + 0.0800·Ur

  β = 2 – 1.7912·S1 – 0.5302·Ur + 0.284·Ur2

  $S_1 = \frac{2\pi}{g}\frac{H_{m0}}{T_{01}^2}$ and $U_r = \frac{H \cdot L^2}{d^3}$

For this type of distribution, the distribution of the extremes of a given number of events, N, (waves or crests) converges towards the Gumbel distribution conditional on the most probable value of the extreme event, H_{mp} (or C_{mp} for crests):

$$P\left(h_{\max} \mid H_{mp}\right) = \exp\left(-\exp\left(-\ln N\left(\left(\frac{h_{\max}}{H_{mp}}\right)^{\beta} - 1\right)\right)\right) \tag{D.7}$$

Appendix D.3.2 Individual waves (modes)

The extreme individual wave and crest elevations are derived using the storm mode approach [28]. The storm modes, or most probable values of the maximum wave or crest in the storm (H_{mp} or C_{mp}), are obtained by integrating the short-term distribution of wave heights conditional on H_{m0} over the entire number of sea states making up the storm. In practice, this is done by following these steps:

1. Storms are identified by peak extraction from the time series of significant wave height. Individual storms are taken as portions of the time series with H_{m0} above 0.7 times the storm peak, H_{m0}.

2. The wave (or crest) height distribution is calculated for each sea state above the threshold in each individual storm. The short-term distribution of H (or C) conditional on H_{m0}, $P(h|H_{m0})$, is assumed to follow the empirical distributions by Forristall (see Section D.3.1). The wave height probability distribution is then given by the following product over the n sea states making up the storm:

$$P\left(H_{\max} < h\right) = \prod_{j=1}^{n_{seastates}} P\left(h \mid H_{m0,j}\right)^{N_{waves,j}} \tag{D.8}$$

With the number of waves in each sea state, N_{waves}, being estimated by deriving the mean zero-crossing period of the sea state. The most probable maximum wave height (or mode), H_{mp}, of the storm is given by:

$$P\left(H_{\max} < h\right) = \frac{1}{e} \tag{D.9}$$

This produces a database of historical storms each characterised by its most probable maximum individual wave height which is used for further extreme value analysis.

Appendix D.3.3 Convolution of short-term variability with long-term storm density

The long-term distribution of individual waves and crests is found by convolution of the long-term distribution of the modes (subscript $_{mp}$ for most probable value) with the distribution of the maximum conditional on the mode given by:

$$P(H_{\max}) = \int_0^{\infty} P(h_{\max} \mid H_{mp}) \cdot p(H_{mp}) dH_{mp}$$
$$= \int_0^{\infty} \exp\left(-\exp\left(-\ln N \left(\left(\frac{h}{H_{mp}} \right)^{\beta} - 1 \right) \right) \right) \cdot p(H_{mp}) dH_{mp} \quad \text{(D.10)}$$

The value of *N*, which goes into this equation, is determined by defining equivalent storm properties for each individual storm. The equivalent storms have constant H_{m0} and a duration such that their probability density function of H_{max} or C_{max} matches that of the actual storm. The density functions of the maximum wave in the equivalent storms are given by:

$$p(H_{\max} \mid H_{m0,eq}, N_{eq}) = \frac{d}{dH} \left[1 - \exp\left(-\left(\frac{H_{\max}}{\alpha \cdot H_{m0,eq}} \right)^{\beta} \right) \right]^{N_{eq}} \quad \text{(D.11)}$$

The β parameter in eq. (D.10) comes from the short-term distribution of individual crests, eq. (D.6), and is a function of wave height and wave period. Based on previous studies, it has been assessed that the maximum crest elevations are not sensitive to β_C for a constant value of 1.88; hence, it is decided to apply β_C = 1.88. The number of waves in a storm, *N*, was conservatively calculated from a linear fit to the modes minus one standard deviation.

Appendix D.3.4 Plotting positions

In plotting the extreme distributions, the return period associated with the extracted peak events (plotting positions) are determined via the recommendations within [33].

For the Gumbel distributions, the un-biased plotting position used is the Gringorten plotting position. For the Weibull distribution, the un-biased plotting position for the Weibull distribution depends on the distribution shape parameter.

These plotting position formulas give the “expected probability of the i^{th} ordered variate in a population of sample size n” [33]. In other words, these plotting positions tell us that the largest observation in *N* years has an expected probability corresponding to a return period > *N* years.

Appendix D.4 Subset extremes

Estimates of subset (e.g., directional and monthly) extremes are required for a number of parameters. In order to establish these extremes, it is common practice to fit extreme value distributions to data sampled from the population (i.e., the model database) that fulfils the specific requirement e.g., to direction, i.e. the extremes from each direction are extracted and distributions fitted to each set of directional data in turn. By sampling an often relatively small number of values from the data set, each of these directional distributions is subject to uncertainty due to sampling error. This will often lead to the directional distributions being inconsistent with the omnidirectional distribution fitted to the maxima of the entire (omnidirectional) data set. Consistency between directional and omnidirectional distributions is ensured by requiring that the product of the n directional annual non-exceedance probabilities equals the omnidirectional, i.e.:

$$\prod_{i=1}^{n} F_i\left(x,\hat{\theta}_i\right)^{N_i} = F_{omni}\left(x,\hat{\theta}_{omni}\right)^{N_{omni}} \tag{B12}$$

Where N_i is the number of sea states or events for the i'th direction and $\hat{\theta}_i$, the estimated distribution parameter. This is ensured by estimating the distribution parameters for the individual distributions and then minimizing the deviation:

$$\delta = \sum_{x_j}\left[-\ln\left(-N_{omni}\ln F_{omni}\left(x,\hat{\theta}_{omni}\right)\right) + \ln\left(-\sum_{i=1}^{n} N_i \ln F_i\left(x_j,\hat{\theta}_i\right)\right)\right]^2 \tag{D.13}$$

Here x_j are extreme values of the parameter for which the optimization is carried out, i.e., the product of the directional non-exceedance probabilities is forced to match the omnidirectional for these values of the parameter in question.

The directional extremes are derived from fits to each subseries data and will be given without scaling; that is, a T_{yr} event from direction *i* will be exceeded once every *T* year on average. As a first order approximation, having e.g., 12 directions this means that **one** of the directions will be exceeded once every T_R/12 years on average. A 100-year event would thus be exceeded once every 100/12 = 8⅓ years (on average) from **one** of the directions. The same applies for monthly extremes. A T_{yr} monthly event corresponds to the event that is exceeded once (in that month) every T years, which is the same as saying that it is exceeded once every *T*/12 years (on average) of the climate for that particular month.

Appendix D.5 Uncertainty assessment

Appendix D.5.1 Sources of uncertainty

The extreme values presented in this report are estimated quantities and therefore all associated with uncertainty. The uncertainty arises from a number of sources:

Measurement/model uncertainty: The contents of the database for the extreme value analysis are associated with uncertainty. This type of uncertainty is preferably mitigated at the source – e.g., by correction of biased model data and removal of obvious outliers in data series. The model uncertainty can be quantified if simultaneous good quality measurements are available for a reasonably long overlapping period.

True extreme value distribution is unknown: The distribution of extremes is theoretically unknown for levels above the levels contained in the extreme value database. There is no justification for the assumption that a parametric extreme value distribution fitted to observed/modelled data can be extrapolated beyond the observed levels. However, it is common practice to do so, and this obviously is a source of uncertainty in the derived extreme value estimates. This uncertainty, increasing with decreasing occurrence probability of the event in question, is not quantifiable but the metocean expert may minimize it by using experience and knowledge when deciding on an appropriate extreme

value analysis approach. Proper inclusion of other information than direct measurements and model results may also help to minimize this type of uncertainty.

Uncertainty due to sampling error: The number of observed/modelled extreme events is limited. This gives rise to sampling error which can be quantified by statistical methods such as Monte Carlo simulations or bootstrap resampling. The results of such an analysis are termed the confidence limits. The confidence limits should not be mistaken for the total uncertainty in the extreme value estimate.

Appendix D.5.2 Confidence limits

The confidence limits of extreme estimates are established from a bootstrap analysis or a Monte Carlo simulation.

The bootstrap analysis estimates the uncertainty due to sampling error. The bootstrap consists of the following steps:

1. Construct a new set of extreme events by sampling randomly with replacement from the original data set of extremes
2. Carry out an extreme value analysis on the new set to estimate T-year events

An empirical distribution of the T-year event is obtained by looping steps 1 and 2 many times. The percentiles are read from the resulting distribution.

In the Monte Carlo simulation, the uncertainty is estimated by randomly generating a large number of samples that have the same statistical distribution as the observed sample.

The Monte Carlo simulation can be summarised in the following steps:

1. Randomly generating a sample consisting of N data points, using the estimated parameters of the original distribution. If the event selection is based on a fixed number of events, N is set equal to the size of original data set of extremes. If the event selection is based on a fixed threshold, the sample size *N* is assumed to be Poisson distributed.
2. From the generated sample, the parameters of the distribution are estimated, and the *T*-year return estimates are established.

Steps 1 and 2 are looped a large number of times, whereby an empirical distribution of the *T*-year event is obtained. The quartiles are read from the resulting distribution.